Chemical Synthesis and Characterization of Nanostructured TiO_2 Based Composites: Studies on their Potential Biomedical Applications

THESIS

Submitted in partial fulfilment
of the requirements for the degree of
DOCTOR OF PHILOSOPHY

By
NAIK KSHIPRA SUDHAKAR

Under the Supervision of
Prof. Meenal Kowshik

BITS Pilani
Pilani | Dubai | Goa | Hyderabad

BIRLA INSTITUTE OF TECHNOLOGY AND SCIENCE, PILANI
2015

BIRLA INSTITUTE OF TECHNOLOGY AND SCIENCE, PILANI

CERTIFICATE

This is to certify that the thesis entitled **"Chemical Synthesis and Characterization of Nanostructured TiO_2 Based Composites: Studies on their Potential Biomedical Applications"** submitted by **Ms. Naik Kshipra Sudhakar** ID No **2009PHXF417G** for award of Ph.D. of the Institute embodies original work done by her under my supervision.

Signature of the Supervisor

Prof. Meenal Kowshik

Associate Professor (HOD)

Date: 13/04/2015

Acknowledgements

Thank you God !!!

Work described in this thesis titled ***"Chemical Synthesis and Characterization of Nanostructured TiO_2 Based Composites: Studies on their Potential Biomedical Applications"*** *was started in the Department of Biological Sciences, BITS Pilani K K Birla Goa Campus in 2010 and would not have been what it is today without the support and advice of members of this department. Though the following thesis is an individual work, I could never have reached the heights or explored the depths without the support, guidance and efforts of a lot of people.*

I am grateful to Prof. Bijendra Nath Jain, Vice Chancellor, BITS Pilani and Prof. K. E. Raman, Director, BITS Pilani K K Birla Goa Campus for providing me the opportunity to pursue my doctoral studies successfully by providing necessary facilities and financial support.

Prior to everything, I would like to express my deep gratitude towards Prof. Meenal Kowshik (Head, Department of Biological Sciences), for being my Supervisor and for granting me the opportunity to work in her research group. I thank you ma'am for believing in me since day one. You have reinforced in me the values of independence and perseverance and you were never too busy to meet or to discuss. I truly feel I have become a better scientist under your supervision. Your infectious enthusiasm and unlimited support have been major driving forces throughout my graduate career at BITS. Prof. Meenal Kowshik has always been an excellent mentor who genuinely cares for her students and is more than just an advisor for scientific and academic growth. It is a great motivation as a researcher when your supervisors are so engaged and interested in your work. She promotes more than an academic role within the laboratory; she maintains her group like a family. I always enjoyed the chance for independent thinking that Meenal ma'am has given me over the years. I am highly indebted to her for all the support.

I express heartiest thanks to Prof. Judith M. Braganca, Convenor, Doctoral Research Committee (DRC) and other DRC members for their guidance and co-operation. I would also like to thank Prof. Utpal Roy and Prof. Halan Prakash, members of my Doctoral Advisory Committee (DAC) for teaching, guidance and great cooperation in refining my thesis.

I am grateful to my family and loved ones who put up with me through the long hours and less than pleasant responses to any questions regarding completion of this work. My very special thanks to Shri. Sudhakar Naik, my father, Smt. Meeta Naik, my mother and my Late Grandparents to whom I owe everything I am today. Thank you for your whole hearted support, love and encouragement for my studies. Thank you for everything. I would also like to thank my sister Ms. Netra for helping me with Scientific Drawings and for her whole hearted support, love and encouragement.

There have been a number of people who have helped me during these five years and I would like to thank them for all their help. My first thanks must go to my "amigos" Vidhya, Kabilan, Bhakti and Priya for the laughs and banter and for sharing the Ph.D. experience; we have all gone through it together! Thank you for always providing a torch and lots of batteries when there was no light at the end of *that* tunnel throughout my thesis work. Thank you for sharing the good times and being a part of the agony and ecstasy of graduate education. In particular I would like to give special thanks to Bhakti for providing the much needed fun distractions and just being there for me. I find your philosophy on life and your sense of humour very refreshing! I also thank you all for the weekends spent at hostel or outdoors, exploring the most remote corners of Goa and elsewhere. It has been a constant reminder of how much more there is to life than lab bench tops and evenings spent in the less stimulating company of cell cultures. I will definitely miss our everyday tea and coffee trips to the mess, cafeteria and Monginis and will always remember all those memorable movie weekend nights. I am also thankful to Yogesh, Meghnath, Arun, Archana, Rajesh, Nupoor, Bhanudas, Zubeida, Ramya, Ajay, Shivaraman, Chandrashekhar, Poornima and Shruti for being wonderful friends over the years and being there for me whenever I needed your help.

I thank all the members, past and present, of my research group – Vilas, Celisa, Sushma, Pallavee, Monsoor and Ketaki; all of whom were always supportive. Thank you to all of my labmates for their help, friendship, good humour, and valuable infotainment. Good luck to you all in the future, whatever it may bring!

I would also like to thank the staff of Department of Biological Sciences, Kamana Madam, Mahadev Bhaiya and Mahalinga Bhaiya and all others who make graduate student's life easier.

I would like to acknowledge Council of Scientific and Industrial Research (CSIR), India for the Research Fellowship (File No. 09/919(0008)/2010-EMR-1). I would like to thank Department of Science and Technology (DST), India (Commitment letter no.: SR/ITS/00127/2013 –2014), Indian Council of Medical Research (ICMR), India (Sanction no.: 3/2/TG-37/HRD-2013) and Department of Biotechnology (DBT), India (Proposal code: DBT/CTEP/02/201300084) for the travel grant for presenting a poster at Nanomedicine 2013, Barcelona, Spain. I would like to thank Indo-French Center for the Promotion of Advanced Research (CEFIPRA) for 2014 Cefipra - Esonn Fellowship for participation in the European School on Nanoscience and Nanotechnologies (ESONN) training programme held at Grenoble, France.

I would like to thank National Centre for Antarctic and Ocean Research (NCAOR), Goa for their assistance with EDX analysis and Dr. C. S. Harendranath and Sophisticated Analytical Instrument Facility (SAIF), Indian Institutes of Technology (IIT) BOMBAY for their assistance with HR TEM and TEM analysis.

I am thankful to Prof. Srinivasan B. R. of Goa University for the help with DRS and FTIR studies and Prof. N. N. Ghosh, Department of Chemistry, BITS Pilani K K Birla Goa Campus for the help with surface area and porosity measurements. I also thank Department of Chemistry, BITS Pilani K K Birla Goa Campus for allowing me to use the FTIR spectrophotometer for analysis.

I would like to thank Dr. K. M. Paknikar, Agarkar Research Institute, Pune for the help with AAS analysis. I am very grateful to Mr. Areef Sardar (SEM Incharge), National Institute of Oceanography (NIO), Goa for assistance with SEM analysis and for giving me the time and carrying out my analysis very patiently. I am very thankful to Dr. Swati Pund, STES's Sinhgad Institute of Pharmacy for help with Zeta potential analysis.

I would like to thank Dr. Lisette D' Souza from National Institute of Oceanography (NIO), Goa for allowing me to use the lyophilizer. I am very thankful to Dr. Sachin Waigaonkar and Mr. Girish Chandran V. for their valuable time, guidance and help with Dynamic mechanical analysis.

Naik Kshipra Sudhakar

Dedication

To My Beloved Parents

Shri. Sudhakar Naik and Smt. Meeta Naik

I will be eternally grateful for your love, support and encouragement and for making it possible and easy for me to pursue my ambitions.

Thank you for being my source of inspiration and strength and for making my dreams come true.

Abstract

Mesoporous AgCl–TiO_2 nanoparticles (ATNPs) with Titanium dioxide (TiO_2) as the homogenous anatase crystalline phase were synthesized using a one–pot sol–gel method. The sample was calcined at 100 °C and characterized by X–ray diffraction, High resolution transmission electron microscopy, Energy dispersive X–ray spectroscopy, Fourier transform infrared spectroscopy, Diffuse reflection spectroscopy, N_2 adsorption–desorption isotherm and Brunauer–Emmett–Teller (BET) analysis. The BET surface area and crystallite size of ATNPs were determined to be 266 m^2/g and 3.76 nm respectively. The ATNPs exhibited excellent antimicrobial activity against representative Gram–positive and Gram–negative bacterial cultures and *Candida albicans*. Complete inhibition of microorganisms was achieved at a very low ATNP concentration, in the range of 1.0 to 20 µg/mL (effective Ag concentrations were 11.7 to 234 ppb) in less than 2 h under ambient conditions. Silver ion release studies showed that about 18 % of total silver incorporated in TiO_2 was present as silver ions in solution, indicating that the antimicrobial activity is due to silver ions released from the TiO_2 matrix.

As most microorganisms are present as biofilms, these ATNPs were further tested for their anti-biofilm activity. Sol–gel coatings of ATNPs presented as potential anti-biofilm agents, wherein TiO_2 acted as a good supporting matrix to prevent aggregation of silver and facilitated its controlled release. Low–temperature processed ATNP coatings inhibited biofilm formation by *Escherichia coli*, *Staphylococcus epidermidis* and *Pseudomonas aeruginosa*. *In vitro* biofilm assay experiments demonstrated that ATNP coated surfaces, inhibited the development of biofilms over a period of 10 days as confirmed by Scanning electron microscopy (SEM). The silver release kinetics exhibited an initial high release, followed by a slow and sustained release. The anti–biofilm efficacy of the coatings could be attributed to the release of silver ions, which prevents the initial bacterial adhesion required for biofilm formation.

The anti–quorum sensing activity of ATNPs and its mechanism was evaluated using *Chromobacterium violaceum* as the bacterial model. Silver present in ATNPs significantly reduced violacein production in a concentration dependent manner, indicating inhibition of quorum sensing. Anti–quorum sensing activity was confirmed by the absence of signalling molecule, Oxo–octanoyl homoserine lactone during growth in the presence of ATNPs. TiO_2 acted as a good supporting matrix facilitating controlled release of silver ions with prolonged residual activity. Hence these ATNPs are proposed as quorum sensing inhibitors with potential for use as an anti-pathogenic but nontoxic bioactive material. Although silver is well known for its bioactive potential of antibacterial, antifungal and antiviral properties, this study adds further note on its anti–quorum sensing activity and its potential use in food packaging industry. Anti–quorum sensing activity of ATNP is proposed as an efficient model for controlling food spoilage.

Furthermore, the potential of TiO_2 nanoparticles in the field of tissue engineering was assessed. Nanocomposite scaffold using a mixture of nanoparticles TiO_2 and hydroxyapatite (HAp) and Alginate was developed using the technique of freeze drying, with an intended use towards biomedical applications such as bone tissue engineering and drug delivery. TiO_2–HAp nanocomposites were prepared with variable ratios of TiO_2 and HAp and characterized using X–ray diffraction, Fourier transform infrared spectroscopy and Transmission electron microscopy. TiO_2–HAp (50:50) was selected for further studies based on biocompatibility studies. TiO_2–HAp–Alginate scaffolds were prepared and studied for mechanical properties, biocompatibility and drug loading and release kinetics. The mechanical properties of the scaffolds were investigated using dynamic mechanical analysis and the cell viability of osteosarcoma cells (MG–63) on these scaffolds was evaluated using 3–(4,5–dimethylthiazol–2–yl)–2,5 diphenyltetrazolium bromide (MTT) assay.

Brief contents

Table of Contents

Chapter 2: Synthesis and Physico–chemical Characterization of Silver Incorporated Titanium dioxide Nanoparticles

List of Tables

List of Figures

List of Abbreviations/Symbols

ρ – Density of water

3D – Three dimensional

3–Oxo–C_8–HSL – 3–Oxo–Octanoyl homoserine lactone

AAM – Anodic alumina membrane

AAS – Atomic absorption spectroscopy

ADP – Adenosine diphosphate

Ag – Silver

AgCl – Silver chloride

$AgNO_3$ – Silver nitrate

AgNPs – Silver nanoparticles

AgSH – Silver sulfhydrate

AHL – *N*–acyl homoserine lactone

AI–2s – Autoinducer–2

AIPs – Autoinducing peptides

Al_2O_3 – Aluminium oxide

Alg – Alginate

Anti–QS – Anti–quorum sensing

ATCC – American Type Culture Collection

ATNP – AgCl–TiO_2 nanoparticles

ATP – Adenosine triphosphate

ATR – Attenuated total reflection

ATSDR – Agency for Toxic Substances and Disease Registry

a u – Arbitrary unit

$BaSO_4$ – Barium sulphate

BET – Brunauer–Emmett–Teller

BJH – Barret–Joyner–Halenda

BT–20 – Human breast cancer cells

$CaCl_2 \cdot 2H_2O$ – Calcium chloride dihydrate

CaP – Calcium phosphate

CC_{50} 50% – Cytostatic concentration

CMC – Critical micelle concentration

CO_2 – Carbon dioxide

cps – Counts per second

CVD – Chemical vapour deposition

DCF – 2', 7'– dichlorofluorescein

DCFH–DA – 2', 7'–dichlorofluorescin–diacetate

DI – Deionized

DMA – Dynamic mechanical analysis

DMEM – Dulbecco's Modified Eagle's medium

DMSO – Dimethyl sulfoxide

DNA – Deoxyribonucleic acid

DRS – Diffuse reflection spectroscopy

E′ – Storage modulus

EDL – Electrostatic double layer

EDX – Energy dispersive X–ray spectroscopy

EPA – Environmental Protection Agency

EPS – Exopolysaccharide

ESBL – Extended spectrum β–lactamase

FBS – Fetal bovine serum

FDA – Food and Drug Administration

Fe_3O_4 – Iron oxide

FTIR – Fourier transform infrared spectroscopy

GSH – Glutathione

H_2O – Water

H_2O_2 – Hydrogen peroxide

HaCaT – Human epidermal keratinocyte

HAp – Hydroxyapatite

HBV – Hepatitis B virus

HCl - Hydrochloric acid

HepAD38 – Human hepatoma cell line

HHL – N–hexanoyl–L–homoserine lactone

HIV – Human immunodeficiency virus

hMSC – Human mesenchymal stem cells

HPLC – High performance liquid chromatography

HR TEM – High resolution transmission electron microscopy

Hut/CCR5 – Cells derived from Hut 78 cells, a human T cell line which expresses the chemokine receptor CCR5

IR – Infrared

JCPDS – Joint Committee on Powder Diffraction Standards

K562 – Leukemia cells

KBr – Potassium bromide

KCl – Potassium chloride

m/z – Mass–to–charge ratio

MDCK – Madin–Darby canine kidney cells

MG–63 – Human osteosarcoma cells

$MgCl_2 \cdot 6H_2O$ – Magnesium chloride hexahydrate

MH – Muller Hinton

MIC – Minimum inhibitory concentration

MRSA – Methicillin resistant *Staphylococus aureus*

MRSE – Methicillin resistant *Staphylococus epidermidis*

MTCC – Microbial Type Culture Collection

MTT – 3– (4, 5–dimethylthiazol–2–yl) –2, 5–diphenyltetrazolium bromide

MTX – Methotrexate

Na_2SO_4 – Sodium sulfate

NAC – N–acetylcysteine

NaCl – Sodium chloride

NADH – Nicotinamide adenine dinucleotide (reduced form)

NaH_2PO_4 – Sodium dihydrogen phosphate

$NaHCO_3$ – Sodium bicarbonate

NaOH – Sodium hydroxide

NB – Nutrient broth

NCCS – National Centre for Cell Science

NCIM – National Collection of Industrial Microorganisms

NNI – National Nanotechnology Initiative

PBS – Phosphate buffered saline

PC – Polycarbonate

PCL – Polycaprolactone

PCLm – Polycaprolactam

PHBV – Polyhydroxybutyrate–co–hydroxyvalerate

PLGA – Polylactide–co–glycolide

PLLA – Poly–L–lactic acid

PMMA – Polymethylmethaacrylate

ppb – parts per billion

ppm – parts per million

Pt – Platinum

PU – Polyurethane

PVD – Physical vapour deposition

QS - Quorum sensing

RF – Radio frequency

RNA – Ribonucleic acid

ROS – Reactive oxygen species

rpm – revolutions per minute

rps – Revolutions per Second

SAED – Selected area electron diffraction

SBF – Simulated body fluid

SDS – Sodium dodecyl sulfate

SEM – Scanning electron microscopy

SiO_2 – Silicon dioxide

SMMC–7721 – Human hepatocarcinoma cells

SNW – Silver nanowires

–S–S – Disulfide bridge

Ti – Titanium

$TiCl_4$ – Titanium tetrachloride

TiO_2 – Titanium dioxide

UV – Ultraviolet

VRE – Vancomycin–resistant *Enterococcus*

WHO – World Health Organization

XRD – X–ray Diffraction

YES – Yeast Extract with supplements

ZrO_2 – Zirconium dioxide

CHAPTER 1

Chapter 1: Introduction and Literature Review

1.1 Nanotechnology

Nanotechnology is the production and application of devices and systems at the nanometer scale, which is of the order of 10^{-9} m. The prefix 'nano–' is derived from the Greek word *nannos*, meaning "very short man". Nanotechnology has great potential for producing improvements and innovations in many areas of life, such as new and improved health treatments; cleaner, safer and faster manufacturing; quicker and smaller devices; increased life cycle of products and improvements to existing products; reduced use of some harmful or scarce resources (Allhoff *et al.* 2010).

Nanotechnology involves research and technology development at 1 nm to 100 nm range and creates and uses structures that have novel properties because of their small size. It builds on the ability to control or manipulate at atomic scale. Nanoparticles are microscopic particles with at least one dimension less than 100 nm and are of great scientific interest as they effectively bridge the gap between bulk materials and atomic or molecular structures.

National Nanotechnology Initiative (NNI) defines nanotechnology as: "The understanding and control of matter at dimensions of roughly 1 to 100 nm, where unique phenomena enable novel applications". A more complete definition includes the formation and use of materials, structures, devices, and systems that have unique properties because of their small size. Also, nanotechnology includes the technologies that enable the control of materials at the nanoscale (NNI 2011).

The reason why nanotechnology is so innovative and revolutionary lies in quantum mechanics. When particles are created with dimensions of about 1–100 nanometers, the material properties change significantly from their conventional, bulk counterparts. The two main reasons for this are increased relative surface area and new quantum effects (Chaturvedi *et al.* 2012). Nanomaterials have a much greater surface area to volume ratio than their conventional forms, which can lead to greater chemical reactivity and affect their strength. Also at the nano scale, quantum effects can become much more important in determining the materials properties and characteristics, leading to novel physical, chemical, mechanical, optical, electrical and magnetic behaviours. Classical physics can no longer control the behaviour of the material which is now under the control of quantum laws (Zettili 2009). This fact gives the nanostructured material new abilities and properties that may be more favourable than the ones of the bulk material (Uskokovic 2007; Andrievski and Glezer 2001). A good example is that some polymers which are insulators in the bulk form, behave as semiconductors at the nanoscale. Thus, when particle size is in nanoscale, properties such as melting point, fluorescence, electrical conductivity, magnetic permeability, and chemical reactivity change as a function of the size of the particle.

Growing interest in the medical applications of nanotechnology has led to the emergence of a new field called nanomedicine or more generally, 'bionanotechnology'. (Freitas 1999; Emerich and Thanos 2003). Nanomedicine can be very broadly defined as a technology that uses molecular tools, nanoscale or nanostructured materials and knowledge of the human body for medical diagnosis and treatment (Wagner 2006; Duncan 2004). It utilizes extremely small materials like particles, surfaces and instruments that are often barely larger than a few molecules in scale to interface with human cells and tissues in a therapeutic mode. Nanomedicine promises to be very useful in areas like diagnosis, regenerative medicine, tissue engineering and targeted drug delivery. Currently, nanomedical technologies are in their infancy, but many physicians and medical scientists believe that nanomedicine will revolutionize medical care as dramatically as the development of antibiotics did in the 1930s and 1940s.

The first scientist to voice the possibilities of manipulating and controlling things on a small scale was the late Nobel physicist Richard P. Feynman. In his 1959 prescient talk, "There's Plenty of Room at the Bottom," Feynman proposed using machine tools to make smaller machine tools, these to be used in turn to make still smaller machine tools, and so on all the way down to the atomic level (Feynman 1960). Feynman was clearly aware of the potential medical applications of the new technology that he was proposing. The idea that tiny nanorobots and related machines could be designed, manufactured, and introduced into the human body to perform cellular repairs at the molecular level was also championed in the popular writings of Drexler (Drexler 1986; Drexler *et al.* 1991) in the 1980s and1990s, and in the technical writings of Freitas (Freitas 1999; Freitas 2003) in the 1990s and 2000s.

Without losing sight of Feynman's original long–term vision of medical nanorobotics, nanomedicine today has branched out in numerous different directions, each of them embodying the key insight that the ability to structure materials and devices at the molecular scale can bring enormous immediate benefits in the research and practice of medicine (Freitas 2005).

1.2 The World of Metal Oxide Nanomaterials

Metal elements are able to form a large diversity of oxide compounds which play a very important role in many areas of chemistry, physics and materials science (Noguera 1996; Henrich and Cox 1994). Metal oxide nanoparticles can exhibit unique physical and chemical properties due to their limited size and a high density of corner or edge surface sites. (Klabunde *et al.* 1996). Metal oxides are used in various technological applications such as the fabrication of microelectronic circuits, sensors, piezoelectric devices, fuel cells, coatings for the passivation of surfaces against corrosion, and as catalysts. (Gleiter 1995; Valden *et al.* 1998; Rodriguez *et al.* 2002; Baumer and Freund 1999; Trudeau and Ying 1996). Metal oxide nanoparticles have a unique structure, interesting and unusual redox and catalytic properties, high surface area, good mechanical stability and are biocompatible. For these reasons, metal oxide nanoparticles have attracted considerable interest in the field of biomedical therapeutics, bio–imaging and bio–sensing. These materials have become important components in medical implants, cancer diagnosis and therapy and in neurochemical monitoring. For example titania is the material of choice in medical implants as it provides an excellent biocompatible surface for cell attachment and proliferation. Several other metal oxides have been used as gas sensing nanoprobes for cell labelling and separation, as contrast agents for magnetic resonance imaging and as carriers for targeted drug delivery (Andreescu *et al.* 2012).

1.2.1 Titanium dioxide (TiO_2) as a multifunctional nanomaterial

Multifunctional nanomaterials can be defined as nanomaterials that integrate more than one kind of function to accomplish a wide range of applications. For example, nanoparticles that integrate more than one kind of imaging or therapeutic agents, makes them potential multifunctional nanoplatforms for both diagnosis and therapy. Among these, titanium dioxide (TiO_2) is of primary interest for its unusual electronic properties, non–toxicity, structural stability and low cost. Moreover, it is already present in many different commercial products such as paints, cosmetics, ceramics, coatings, etc. Its potential applications range from photocatalysis in environmental remediation (Gayaa and Abdullaha 2008), water splitting (Fujishima and Honda 1972; Tang *et al.* 2008; Kudo and Miseki 2009; Osterloh 2008), solar cells (e.g. dye–sensitized solar cells (O'Regan and Graetzel 1991; Sauvage *et al.* 2010), hybrid solar cells (Lancelle–Beltran *et al.* 2006), quantum dots solar cells (Kongkanand *et al.* 2008), and gas sensors, to biomedical applications in tissue engineering (Naldoni *et al.* 2011), magnetic resonance imaging (Endres *et al.* 2007), and drug/gene therapy (Paunesku *et al.* 2007; Paunesku *et al.* 2003).

TiO_2 materials are expected to play an important role in helping solve many serious environmental and pollution challenges. TiO_2 also bears tremendous potential in addressing the energy crisis through effective utilization of solar energy based on photovoltaic and water–splitting devices (Chen and Mao 2007)

1.2.2 Synthesis of Nano Titanium dioxide

The synthesis of nanoparticles with controlled size, crystalline structure and shape has been very profoundly inspired by the world of nanochemistry. In general the synthesis methods for nanoparticles can be classified into two categories viz. the top down approach and the bottom up approach. The top down approach involves the division of a solid into smaller portions. This method could involve the process of milling or attrition, chemical methods, and volatilization of a solid followed by condensation of the volatilized components. The second which is the bottom up approach of nanoparticle fabrication involves the condensation of atoms or molecular units in a gas phase or in solution. This method is widely used in the synthesis of nanoparticles.

In recent years, there has been a great deal of research on the preparation of nanostructured titania due to its extensive applications. There is much literature on the synthesis of anatase TiO_2 particles in the size range of 5 nm to several microns and with a variety of shapes (Zhang and Gao 2003; Matsuda *et al.* 2000; Parala *et al.* 2002; Trentler *et al.* 1999; Zaban *et al.* 2000; Bersani *et al.* 1998).

Sol–gel method for synthesis of TiO_2 nanomaterials involves hydrolysis of a titanium precursor (Bessekhouad *et al.* 2003; Kuznetsova *et al.* 2005; Lee and Yang 2005; Zhang and Banfield 2005; Sugimoto *et al.* 2003). It is a versatile process used in making various ceramic materials. In a typical sol–gel process, a colloidal suspension, or a sol, is formed from the hydrolysis and polymerization reactions of the precursors, which are usually inorganic metal salts or metal organic compounds such as metal alkoxides. Complete polymerization and loss of solvent leads to the transition from the liquid sol into a solid gel phase (Chen and Mao 2007).

Sol method refers to the non–hydrolytic sol–gel process and usually involves the reaction of titanium salt with a variety of different oxygen donor molecules, e.g., a metal alkoxide or organic ether (Niederberger *et al.* 2002; Parala *et al.* 2002; Tang *et al.* 2005). Even though aqueous sol–gel methods were highly successful in the synthesis of bulk metal oxides, they exhibit certain limitations while preparing their nanoscale counterparts. Aqueous sol–gel chemistry is quite complex, mainly due to the high reactivity of the metal oxide precursors and the double role of water as ligand and solvent. In many cases, the three reaction types (hydrolysis, condensation, and aggregation) occur almost simultaneously and are difficult to control individually, therefore slight changes in experimental conditions result in altered particle morphologies which is a serious issue regarding the reproducibility of a synthesis protocol. Moreover, the as synthesized metal oxides are often amorphous and require an additional annealing step for crystallization (Niederberger 2007). Nonaqueous/non–hydrolytic sol–gel processes in organic solvents, generally under exclusion of water, are able to overcome these limitations of aqueous systems, and thus represent a powerful and versatile alternative (Vioux 1977; Chen and Mao 2007).

Micelles and inverse micelles are commonly employed to synthesize TiO_2 nanomaterials with amorphous structure (Hong *et al.* 2003; Kim *et al.* 2005a; Li *et al.* 2004; Lim *et al.* 2004a; Lim *et al.* 2004b). In this method, calcination is usually necessary to induce high crystallinity which can lead to the growth and agglomeration of TiO_2 nanoparticles. Aggregates of surfactant molecules dispersed in a liquid colloid are called micelles when the surfactant concentration exceeds the critical micelle concentration (CMC). In micelles, the hydrophobic hydrocarbon chains of the surfactants are oriented toward the interior of the micelle, and the hydrophilic groups of the surfactants are oriented toward the surrounding aqueous medium. The lipids form a single layer on the liquid surface and are dispersed in solution below the CMC. The lipids organize in spherical micelles at the first CMC (CMC–I), into elongated pipes at the second CMC (CMC–II), and into stacked lamellae of pipes at the lamellar point (LM or CMC–III) (Kangarlou Rafizadeh 2012). The CMC depends on the chemical composition, mainly on the ratio of the head area and the tail length. Reverse micelles are formed in non–aqueous media, and the hydrophilic head groups are directed toward the core of the micelles while the hydrophobic groups are directed outward toward the non–aqueous media. There is no obvious CMC for reverse micelles, because the number of aggregates is usually small and they are not sensitive to the surfactant concentration (Chen and Mao 2007).

Hydrothermal method is a "soft solution chemical processing" technique, which provides an easier way to control particle size, particle morphology, microstructures, phase composition, and surface chemical properties with adjustments in experimental parameters such as temperature, pressure, duration of process, and solution pH (Chang *et al.* 2012). It is an easy route to prepare well–crystalline and phase–pure oxides in one step. It is normally conducted in steel pressure vessels called autoclaves with or without Teflon liners under controlled temperature and/or pressure. The temperature can be elevated above the boiling point of water, reaching the pressure of vapour saturation. The temperature and the amount of solution added to the autoclave largely determine the internal pressure produced. It is a method that is widely used for the production of small particles in the ceramics industry (Chen and Mao 2007). Hydrothermal method has been used by many groups to prepare TiO_2 nanoparticles (Yang *et al.* 2000; Yang *et al.* 2001a; Yang *et al.* 2002; Yang *et al.* 2004a; Yang *et al.* 2004b). For example, TiO_2 nanoparticles can be obtained by hydrothermal treatment of peptized precipitates of a titanium precursor with water (Yang *et al.* 2001a).

Solvothermal method has been found to be a versatile method for the synthesis of a variety of nanoparticles with narrow size distribution and dispersity (Li *et al.* 2006; Xu and Li 2006; Wang *et al.* 2005b). The solvothermal method is almost identical to the hydrothermal method except that the solvent used here is non–aqueous. However, the temperature can be elevated much higher than that in hydrothermal method, as a variety of organic solvents with high boiling points can be used. In case of TiO_2 nanoparticles, the solvothermal method is generally observed to provide better control of the size and shape distributions and crystallinity than hydrothermal methods with/without the aid of surfactants (Chen and Mao 2007; Wen *et al.* 2005a; Wen *et al.* 2005b; Kim *et al.* 2003a; Kim *et al.* 2003b; Yang and Gao 2006).

Direct oxidation method facilitates synthesis of TiO_2 nanomaterials by oxidation of titanium metal using oxidants or under anodization. Crystalline TiO_2 nanorods have been obtained by direct oxidation of a titanium metal plate with hydrogen peroxide (Wu *et al.* 2005a; Wu *et al.* 2002; Wu and Zhang 2004). Anodic oxidation of titanium foil has been used to synthesize TiO_2 nanotubes (Mor *et al.* 2006; Paulose *et al.* 2006; Varghese *et al.* 2008; Ruan *et al.* 2005; Shankar *et al.* 2005).

Vapour deposition refers to any process in which materials in a vapour state are condensed to form a solid–phase material. These processes are normally used to form coatings to alter the mechanical, electrical, thermal, optical, corrosion resistance, and wear resistance properties of various substrates. They are also used to form free–standing bodies, films, and fibres and to infiltrate fabric to form composite materials. Recently, they have been widely explored to fabricate various nanomaterials. Vapour deposition processes usually take place within a vacuum chamber. If no chemical reaction occurs, this process is called physical vapour deposition (PVD); otherwise, it is called chemical vapour deposition (CVD). (Chen and Mao 2007). In CVD processes, thermal energy heats the gases in the coating chamber and drives the deposition reaction. In PVD, materials are first evaporated and then condensed to form a solid material. The primary PVD methods include thermal deposition, ion plating, ion implantation, sputtering, laser vaporization, and laser surface alloying. TiO_2 nanowire arrays have been fabricated by a simple PVD method or thermal deposition (Wu *et al.* 2005b; Wu *et al.* 2005c; Xiang *et al.* 2005). The following CVD approaches are used in preparing TiO_2 nanomaterials (i) electrostatic spray hydrolysis: a method in which a metal alkoxide in an organic solvent is transformed into an aerosol by the electrostatic "atomization" technique (electrospray). Charged droplets in the aerosol form unaggregated nanoparticles during their flight from the spray nozzle to the collector (Park and Burlitch 1992), (ii) diffusion flame pyrolysis is widely used in production of ultrafine TiO_2 and many other materials. In this process flame heat is used to initiate the chemical reactions. The disadvantage of this method is that it usually yields agglomerated particles. (Gurav *et al.* 1993; Jang and Kim 2001), (iii) thermal plasma pyrolysis involves the use of thermal plasma to deliver the energy necessary to cause vaporization of small micrometer size particles. The temperature of thermal plasma is in the order of 10,000 K to facilitate easy evaporation of solid powder. Nanoparticles are formed upon cooling while exiting the plasma region. The thermal plasma torches used to produce nanoparticles are dc plasma jet, dc arc plasma, and radio frequency (RF) induction plasmas. (Oh *et al.* 2005a; Wang *et al.* 2005a), (iv) ultrasonic spray pyrolysis consists of the precursor solution which is ultrasonically nebulized into microdroplets, which are carried by a gas flow into a furnace where solvent evaporation and precursor decomposition occurs, producing nanoparticles. Ultrasonic spray pyrolysis may be employed to generate an aerosol from a dilute aqueous metal salt solution, resulting in the production of particles with a narrow size distribution. (Nedeljkovic *et al.* 1997; Skrabalak and Suslick 2005; Pingali *et al.* 2005), (v) laser–induced pyrolysis is a well established method of obtaining particle sizes smaller than 10 nm wherein the infra–red laser is used to rapidly heat a flowing reacting gas. The source molecules are heated selectively by absorption of the laser energy whereas the carrier gas is not. Heating leads to decomposition of the precursors and super saturation is created resulting in nanoparticle formation (Grujic–Brojcin, M, 2005; Scepanovic *et al.* 2005).

Electrodeposition is commonly employed to produce a coating, usually metallic, on a surface by the action of reduction at the cathode. The substrate to be coated is used as cathode and immersed into a solution which contains a salt of the metal to be deposited. The metallic ions are attracted to the cathode and reduced to metallic form. TiO_2 nanowires were obtained by electrodeposition with the use of the template of an anodic alumina membrane (AAM) (Lei *et al.* 2001; Liu and Huang 2005).

Sonochemical method enables the use of ultrasound in the synthesis of a wide range of nanostructured materials, including high surface area transition metals, alloys, carbides, oxides, and colloids. The chemical effects of ultrasound do not come from a direct interaction with molecular species. Instead, sonochemistry arises from acoustic cavitation: the formation, growth, and implosive collapse of bubbles in a liquid. Cavitational collapse produces intense local heating (~5000 K), high pressures (~1000 atm), and enormous heating and cooling rates (>10^9 K/s). The sonochemical method has been applied to prepare various TiO_2 nanomaterials by different groups (Blesic *et al.* 2002; Guo *et al.* 2003; Huang *et al.* 2000; Jokanovic *et al.* 2004).

Microwave synthesis is relatively new and an interesting technique for the synthesis of oxide materials (Rao *et al.* 1999; Corradi *et al.* 2005; Gressel–Michel *et al.* 2005; Ma *et al.* 2005; Szabo *et al.* 2001; Uchida *et al.* 2004). Various nanomaterials have been synthesized in remarkably short time under microwave irradiation (Bhat *et al.* 2000; Subramanian *et al.* 2001). Microwave techniques eliminate the use of high temperature calcination for extended periods of time and allow for fast, reproducible synthesis of crystalline metal oxide nanomaterials. Utilizing microwave energy for the thermal treatment generally leads to a very fine particle in the nanocrystalline regime because of the shorter synthesis time and a highly focused local heating.

In conclusion, the tremendous effort put into nanostructured TiO_2 in the recent years, has resulted in a rich database for their synthesis, properties, modifications, and applications. The continuing progress in the synthesis and modifications of nanostructured TiO_2 has brought new properties and applications with improved performance. Accompanied by the progress in the synthesis of TiO_2 nanostructures are new findings in the synthesis of TiO_2 nanorods, nanotubes, nanowires, as well as mesoporous structures.

1.2.3 Applications of Titanium dioxide

1.2.3.1 Titanium dioxide for drug delivery

Titanium dioxide is used in biomedical field for its stability and non–toxicity. It is one of the most promising nanomaterials capable of a wide variety of applications in medicine and life science. The biocompatibility of TiO_2 makes it a promising candidate for drug eluting schemes. On the other hand, it is frequently included in many biomedical studies because of its resistance to photoinduced corrosion in addition to its ease of handling and relatively low manufacturing cost. TiO_2 nanoporous films were studied for loading of therapeutic amounts of drug dexamethasone on its surface (Ayon *et al.* 2006).

Surface defects present in TiO_2 nanoparticles smaller than 20 nm makes them reactive such that binding with a variety of ligands on the surface is possible. This property is extremely useful for attaching drugs for improved drug delivery systems, enabling the use of TiO_2 as a drug surface carrier in addition to a drug encapsulating agent (Zhang *et al.* 2012). So far, daunorubicin and doxorubicin are the two anticancer drugs that have been loaded on to the TiO_2 nanoparticles to form the nanocomposites for the drug delivery systems. The cytotoxic effects, drug release behaviour and anticancer efficacy of doxorubicin–TiO_2 and daunorubicin–TiO_2 nanocomposites were investigated in human SMMC–7721 hepatocarcinoma cells and K562 leukemia cells respectively (Chen *et al.* 2011; Zhang *et al.* 2012). Both these studies concluded that these drugs when conjugated with TiO_2 nanoparticles hold promising approach as a drug delivery system for clinical practice.

Mesoporous, nanostructured TiO_2 reservoir implanted in the temporal lobe of the brain was reported to be capable of prolonged release of anticonvulsant drugs at a constant rate and a promising candidate for the treatment of epilepsy (Peterson *et. al.* 2007; López *et al.* 2007; López *et al.* 2006). In addition, TiO_2 nanoparticles were recently used to conjugate DNA for intracellular delivery of DNA oligonucleotides (Paunesku *et al.* 2007). The system was further labelled with magnetic resonance contrast agents for MRI application (Endres *et al.* 2007). The synthesis of highly biocompatible mesoporous titania nanoparticles as an anticancer drug vehicle with fluorescence cell tag was reported. In this study, mesoporous titania nanoparticles with excellent biocompatibility and a large surface area were functionalized with a phosphate–containing fluorescent molecule (flavin mononucleotide) and loaded with an anticancer drug (Doxorubicin) for successful intracellular bio–imaging and drug delivery in human breast cancer cells BT–20 (Wu *et al.* 2011).

1.2.3.2 Titanium dioxide in tissue engineering

Tissue engineering is defined as ‘‘an interdisciplinary field of research that applies the principles of engineering and the life sciences towards the development of biological substitutes that restore, maintain, or improve tissue function’’ (Langer and Vacanti 1993). It is based on the understanding of tissue formation and regeneration, and aims to induce new functional tissues, rather than just to implant new spare parts (Kneser *et al.* 2002). The fundamental concept behind tissue engineering is to utilize the body’s natural biological response to tissue damage in conjunction with engineering principles.

TiO_2 is a highly biocompatible ceramic material with good osteoconductive properties (Forsgren *et al.* 2007; Uchida *et al.* 2003; Tsukimura *et al.* 2008). Osteoconductivity is an important feature for scaffolds that are intended to integrate with bone as this property promotes direct contact between bone tissue and scaffold material (Ducheyne Qiu 1999; Albrektsson and Johansson 2001). TiO_2 has also been reported to have bioactive properties and a certain degree of bacteriostatic effect (Fostad *et al.* 2009; Nygren *et al.* 1997; Rincon *et al.* 2005). Therefore, ceramic TiO_2 has been studied as a material for bone tissue engineering purposes (Fostad *et al.* 2009; Sabetrasekh *et al.* 2010; Tiainen *et al.* 2010). Rutile TiO_2 is a promising scaffolding material for inducing bone formation from the surrounding tissue in the restoration of large bone defects (Haugen *et al.* 2004; Fostad *et al.* 2009; Sabetrasekh *et al.* 2010; Tiainen *et al.* 2010). The fabrication of non–resorbable ceramic TiO_2 scaffolds with pore architectural properties well matched for those required for a bone scaffold, namely high porosity, appropriate pore size distribution and well–interconnected pore volume have been reported (Fostad *et al.* 2009; Tiainen *et al.* 2010). These scaffolds were also shown to be biocompatible and to promote adhesion onto the entire scaffold surface during *in vitro* studies of murine osteoblasts and human mesenchymal stem cells (hMSC) (Haugen *et al.* 2004; Fostad *et al.* 2009; Sabetrasekh *et al.* 2011).

However, increased porosity and pore size are known to have a detrimental effect on the mechanical strength and consequently reduce the mechanical integrity of the scaffold structure. Due to the inherently higher compressive strength of ceramic TiO_2 in comparison to other common osteoconductive scaffold materials, such as calcium phosphate ceramics (CaP), bioactive glass and CaP/polymer composites, TiO_2 can be expected to provide better mechanical strength to the scaffold structure at high interconnected porosities. Moreover for complete utilization of bioactive hydroxyapatite (HAp) based implants, improvements in mechanical properties are required. TiO_2 has been incorporated with HAp materials in order to achieve the necessary mechanical strength and bioactive properties, and at the same time overcome the weaknesses such as poor toughness and low–bending strength. (Jonásová *et al.* 2004; Li *et al.* 2003). High porous and well–interconnected TiO_2 scaffolds with high mechanical strength achieving values of 90% of porosity and of 1.63–2.67 MPa of compressive strength have been recently developed (Tiainen *et al.* 2010) and their biocompatibility and osteoconductive properties have been demonstrated in *in vitro* (Gomez–Florit *et al.* 2012) and *in vivo* (Haugen *et al.* 2012; Tiainen *et al.* 2012) studies. These scaffolds provide a suitable surface for osteoblast cell attachment and cell differentiation and cells were well–distributed through the entire 3D structure over time (Gomez–Florit *et al.* 2012). *In vivo* studies have demonstrated the formation of new mineralized bone tissue and vascularization of the ingrowth tissue (Haugen *et al.* 2012; Tiainen *et al.* 2012). Ceramic TiO_2 scaffolds with good compressive strength and an overall porosity of ~85% were obtained (Tiainen *et al.* 2010), and this strength was also reported to be retained after implantation due to the non–resorbable nature of TiO_2.

1.2.3.3 Titanium dioxide as a photocatalyst

Photocatalytic activity is the ability of a material to create an electron hole pair as a result of exposure to ultraviolet radiation. The resulting free radicals efficiently oxidize organic matter. Photocatalysis has recently become a common word and various products using photocatalytic functions have been commercialized. Among many candidates as photocatalysts, TiO_2 is currently the most popular material for industrial applications owing to its highly efficient photocatalytic activity, high stability and low cost. Moreover, it has a lot of potential for novel applications in the future. There are two types of photochemical reactions occurring on a TiO_2 surface when irradiated with ultraviolet light. One includes the photo–induced redox reaction of adsorbed substances, and the other is the photo–induced hydrophilic conversion of TiO_2 itself. The former type has been known since the early part of the 20th century, but the latter was found only at the end of the century (Hashimoto *et al.* 2005).

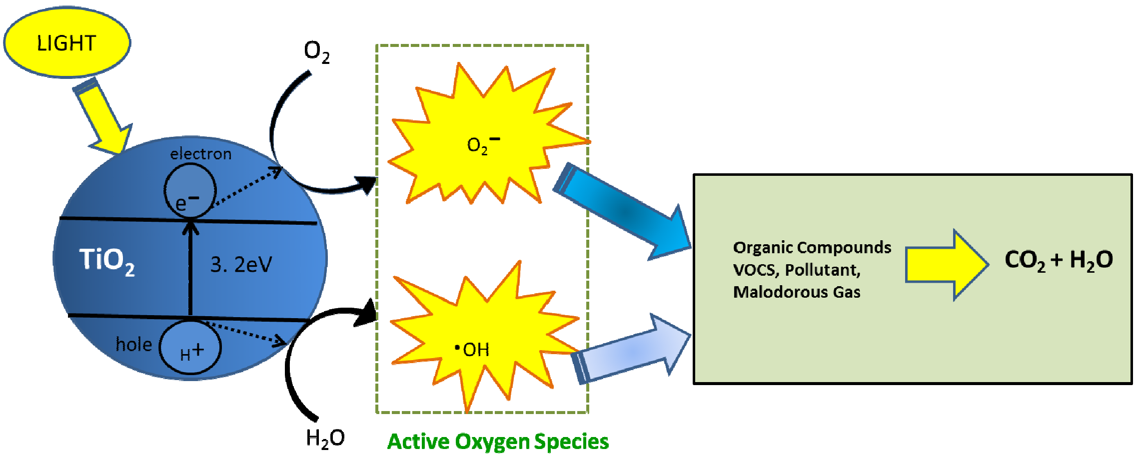

Figure 1.1 Photocatalytic process on TiO_2 semiconductor.

(Adapted from: http://www.overship.com.au/pest_control/pestrol_outdoor_exterminator)

The photocatalytic biocidal effect of TiO_2 was first reported by Matsunaga and coworkers. They observed that when TiO_2–Pt catalyst in contact with the microbial cell was exposed to near–ultraviolet light, the microbial cells in water were killed (Matsunaga *et al.* 1985; Banerjee *et al.* 2006). It is now well known that TiO_2 is one of the most superior materials for decomposing organic matter due to its strong photocatalytic property. It has become the most important photocatalyst in environmental bio–decontamination for a large variety of organics, bacteria, viruses, fungi and cancer cells, which can be totally degenerated and converted to CO_2, H_2O and harmless inorganic anions (Blake *et al.* 1999; Banerjee *et al.* 2006).

Photocatalytic activity in TiO_2 has been extensively studied because of its potential use in sterilization, sanitation, and remediation applications. Titanium dioxide as a photocatalyst has various applications such as anti–fogging, self–cleaning, anti–soiling, deodorizing, air purification, water treatment and purification. Antimicrobial coatings of titania result in the material exhibiting self–cleaning and disinfecting properties under exposure to UV radiation. These properties make the material a candidate for applications such as medical devices, food preparation surfaces, air conditioning filters, and sanitary ware surfaces (Fujishima *et al.* 2000).

1.3 Silver and Other Silver Based Compounds

1.3.1 Historical overview

Silver (Ag) metal came into use even before Neolithic revolution (Vaidyanathan *et al.* 2009) and has since been widely used across civilizations for different purposes. There are anecdotal reports of many societies using silver as jewellery, ornamentation and fine cutlery as it was considered to impart health benefits to the users. The first recorded medicinal use of silver was reported during 8^{th} century (Moyer 1965). Silver has been described as therapeutic agent for many diseases in ancient Indian medical system called Ayurveda (Lara *et al.* 2011). Hippocrates, the father of modern medicine advocated silver powder to have beneficial healing and anti–disease properties and listed it as a treatment for ulcers (Hippocrates and Adams 400 B.C.E.). Silver compounds were major weapons against wound infections during World War I until the advent of antibiotics (Vaidyanathan *et al.* 2009). Pencils or sticks of hardened silver nitrate were considered essential items in a surgeon's chest as early as the 1600s and silver nitrate solutions were used to treat burn victims of the Hindenberg disaster (Klasen 2000; Duncan 2011).

The rise of nanosilver as an antimicrobial agent is part of the larger emergence of nanotechnology as a ubiquitous force in our lives and the increased bacterial resistance to antibiotics. (Vaidyanathan *et al.* 2009). Nanosilver in the form of colloidal silver, has been used for more than 150 years for treatment of wounds and infections and has been registered as a biocidal material in the United States since 1954 (Nowack *et al.* 2011; Reidy *et al.* 2013). The first report of nanosilver was over 120 years ago, stating the synthesis of a citrate–stabilized silver colloid (Lea 1889). Such a kind of nanosilver has been manufactured commercially since 1897 under the name "Collargol" and since has been used for medical applications (Nowack *et al.* 2011).

1.3.2 Different forms of silver

Silver can be present in four different oxidation states such as Ag^0, Ag^+, Ag^{2+} and Ag^{3+}, former two being the most abundant ones and the latter two unstable in the aquatic environment (Smith and Carson 1977). In the natural environment, silver is found as a monovalent ion complexed with sulphide, sulphate, bicarbonate or chlorides and sulphates adsorbed onto particulate matter in the aqueous phase (ATSDR 1990). Metallic silver itself is insoluble in water, but metallic salts such as silver nitrate ($AgNO_3$) and silver chloride (AgCl) are soluble in water (WHO 2002). Silver at low concentrations in aqueous phase exist as silver sulfhydrate (AgSH) or as HS–Ag–S–Ag–SG, a simple polymer. When silver is present in high concentrations in this phase, it is found as colloidal silver sulphide or polysulfide complexes (Wijnhoven *et al.* 2009).

Different forms of silver based compounds have been developed to serve diverse range of applications. Commonly manufactured silver products range from additives that store and release discrete silver ions held within a ceramic or glass matrix to products that store silver ions as silver salts or elemental silver (Nowack *et al.* 2011). Kulinowski, has provided an excellent review of different forms of silver and some of their characteristics (Table 1). Silver containing products may contain silver in ionic, colloidal or nanoparticulate form, and further these may either be in free or bound form (Kulinowski 2008).

Table 1.1 Forms of silver and their approximate size and characteristics.

Type of Silver	Approximate Size	Attributes
Elemental/metallic (a single atom)	0.288 nm	Not found as single atom in nature, normally found as an aggregate. Elemental silver has no oxidation state.
Silver ion (Ionic)	0.258 nm	Toxic, may dissolve in water, may have positive or negative charge.
Nanosilver	1–100 nm	May release ions and/or be toxic inherently
Colloidal	1–1000 nm	A mixture of different sized particles, suspended in fluid, may contain nano particulate silver or silver ions or both.
Inorganic silver compounds/silver salts e.g. silver chloride, silver oxide	Depends	Not easily dissolved, can be nano–sized.
Organic silver compounds e.g. silver proteins	Depends	Covalent, almost impossible to dissolve.

(Adapted from: Kulinowski 2008; http://cohesion.rice.edu/centersandinst/icon/emplibrary/ICON-Backgrounder_NanoSilver-in-the-Environment-v4.pdf)

One of the fundamental issues in all biological studies on the environmental or biological impacts of silver nanoparticles is to distinguish the impact of nanoparticles from the impact of silver ions and other forms of silver present in the solution. The main differences between bulk, nanoparticulate and ionic silver are summarized below. The bulk form of silver has small surface area and slow dissolution rate with limited oxidative capacity. It is not taken up by cells and exhibits limited binding of biomolecules. However in contrast to bulk silver, nanoparticulate form of silver is highly reactive and has a large surface area and capacity for rapid dissolution. It has oxidative potential and can bind to biomolecules. It is taken up by cells via active processes. Nanosilver, due to its small particle size and enormous specific surface area, facilitates more rapid dissolution of ions than the equivalent bulk material; potentially leading to increased bioactivity of nanosilver. The ionic form of silver has no surface area and is highly reactive. It precipitates and can form complexes with inorganic and organic compounds. It can easily get inside cells through the process of equilibrium partitioning (Reidy *et al.* 2013).

1.3.3 Silver as a broad spectrum antimicrobial agent

Silver has attracted a lot of attention as broad spectrum antimicrobial agent because of its non–toxic nature to the human body at low concentrations. It is a well–known fact that silver ions and Ag–based compounds possess strong biocidal effects on microorganisms including bacteria, fungi, yeasts and viruses. Nanosilver is a potent bactericidal agent against wide range of Gram–positive and Gram–negative bacteria (at least 12 species) such as *E. coli*, *Enterococcus faecalis*, *Staphylococcus* (*aureus* and *epidermidis*), *Vibrio cholerae*, *Pseudomonas* (*aeruginosa*, *putida*, *fluorescens* and *oleovorans*), *Shigella flexneri*, *Bacillus* (*anthracis*, *subtilis* and *cereus*), *Acinetobacter, Proteus mirabilis*, *Salmonella enterica* Typhimurium, *Micrococcus luteus*, *Listeria monocytogenes*, *Klebsiella pneumoniae Clostridium*, *Listeria* and *Streptococcus* (Duncan 2011; Wijnhoven *et al.* 2009). Nanosilver and silver nanoparticles are also effective against strains of organisms that are resistant to potent chemical antimicrobials including multi–resistant bacteria like methicillin resistant *Staphylococus aureus* (MRSA), methicillin resistant *Staphylococus epidermidis* (MRSE), vancomycin–resistant *Enterococcus* (VRE), extended spectrum β–lactamase (ESBL) producing *Klebsiella*, multidrug–resistant *Pseudomonas aeruginosa*, ampicillin–resistant *E. coli* O157:H7 and erythromycin–resistant *S. pyogenes* (Duncan 2011; Lara *et al.* 2011). Silver nanoparticles have been shown to enhance the antibacterial activity of various antibiotics due to synergistic effect between them. The antibacterial activities of penicillin G, amoxicillin, erythromycin, clindamycin, and vancomycin against *Staphylococcus aureus* and *Escherichia coli* increased in the presence of silver nanoparticles (Shahverdi *et al.* 2007).

Broad spectrum antifungal activity of nanosilver has been reported against common fungal genera such as *Aspergillus*, *Candida*, and *Saccharomyces* (Wright *et al.* 1999; Kim *et al.* 2007). Significant antifungal activity of nanosilver was demonstrated against *T. mentagrophytes, Candida albicans*, *C. tropicalis* and *T. rubrum* in the range of 2 µg/mL to 0.84 mg/L (Kim *et al.* 2008; Kim *et al.* 2009; Noorbakhsh 2011). In some cases, the antifungal effects of certain drugs like fluconazole and griseofulvin was observed to increase in the presence of AgNPs (Noorbakhsh 2011). In addition, AgNPs were reported to be toxic to algae (e.g., *Chlamydomonas reinhardtii*) and phytoplankton (e.g., *Thalassiosira weissflogii*) (Duncan 2011).

Antimicrobial activity of nanosilver is not limited to only bacteria, fungi and algae as nanostructured silver has also been reported to exhibit anti–viral activity. However, the interaction of AgNPs with viruses is an unexplored field and the few studies on antiviral activity of nanosilver have demonstrated activity against HIV, monkeypox and several enveloped viruses (Duncan 2011). In another study, AgNPs were shown to be superior to gold nanoparticles for cytoprotective activities towards Hut/CCR5 cells infected with HIV–1 (Sun *et al.* 2005). In addition, size–dependent antiviral activity of silver nanoparticles against HIV–1 virus has been shown. Interaction of silver nanoparticles with HIV–1 was exclusively within the range of 1–10 nm (Elechiguerra *et al.* 2005). The antiviral effects of AgNPs on the hepatitis B virus (HBV) were studied using HepAD38 human hepatoma cell line. These nanoparticles had high binding affinity for HBV DNA and also could inhibit the production of HBV RNA and extracellular virions *in vitro* (Lu *et al.* 2008). The CC_{50} (50 % cytostatic concentration) value of nanosilver against influenza virus using MDCK cell culture was 1 µg/ml by MTT method and the effective minimal cytotoxic concentration with least cytopathic effects on the cells was 0.5 µg/ml (Mehrbod *et al.* 2009). Other studies also showed that AgNPs effectively inhibited arenavirus replication during early phases of viral replication at non–toxic concentrations (Speshock *et al.* 2010).

1.3.4 Mode of action of silver

Although the antimicrobial activity of nanosilver has been studied extensively, its effects on microorganisms and the microbicidal mechanism are only partially understood. The actual mechanism of toxicity of nanosilver is proposed to be the sum of various mechanisms and hence termed as multimodal action. Silver is known to react with nucleophilic amino acid residues in proteins, and attach to sulphydryl, amino, imidazole, phosphate and carboxyl groups. It causes bacterial cell wall damage and disruption of cytoplasmic membrane leading to leaching of metabolites, interferes with DNA synthesis, denatures proteins and enzymes (dehydrogenases), binds to ribosome and inhibits protein synthesis, interferes with electron transport in cytochrome system and is involved in the production of ROS (reactive oxygen species).

The primary mode of silver and nanosilver toxicity is their potential to release silver ions. Irrespective of the form of the silver used, a major characteristic that will affect the microbicidal effect of the silver is the concentration of silver ions released. The nano form with its large surface area to volume ratio has high potential for release of silver ions (Sotiriou *et al.* 2010). All forms of silver including silver compounds and silver salts have potential to release silver ions. Even the biocidal effect of elemental silver is due to formation of silver ions at low concentration on its surface. The biocidal effect and reactivity of silver depends on and is directly proportional to the concentration of available silver ions. In a study using stress–specific bioluminescent bacteria it has been shown that the synergistic action of AgNPs and silver ions released by these nanoparticles resulted in enhanced toxicity (Hwang *et al.* 2008). Furthermore, silver nanoparticles damage the cell membranes leading to disruption in the ion efflux system. Therefore, the cells cannot effectively extrude the silver ions released by AgNPs further contributing towards cell damage (Morones *et al.* 2005). In addition, nanosilver may increase the impact of the toxicity of ionic silver and/or be toxic on its own. Several mechanisms for this have been proposed, including silver nanoparticles acting as Trojan horses to enter the cell and then release silver ions to destroy cell content, or nanosilver particles clumping on the outside surface of cells and disrupting cell behaviour (Lubick 2008; Navarro *et al.* 2008).

1.3.4.1 Destruction of cell wall and cell membrane: Nanostructured silver targets the bacterial cell wall and cell membrane which serves several functions and is a protective barrier against some substances. It is well known that nanoparticles less than 10 nm in diameter can bind to bacterial cell wall to cause its perforation which finally leads to cell death. Nanosilver with average particle size ca.12 nm is reported to cause specific damage to *E. coli* cells by formation of irregular shaped pits in the bacterial cell membrane. According to a study, silver ions can also make the cell membrane detach from the cell wall but the mechanism of this operation has still been unknown (Feng *et al.* 2000). Nanosilver accumulation within the cell membrane leads to rapidly increased cell permeability and ultimately, cell death (Sondi and Salopek–Sondi 2004) The destructive effect of nanosilver on cell membrane is due to binding through electrostatic interaction of silver ions with membrane proteins (Holt and Bard 2005), or damage to its structure by generating free radicals (Choi and Hu 2008). Nanosilver can also interact with sulfur–containing proteins present in the membranes and inhibit their function (Wong and Liu 2010).

1.3.4.2 Inhibition of respiratory chain: Silver (nanoparticles or silver ions) can attack the respiratory chain in bacterial mitochondria and lead to cell death (Sondi and Salopek–Sondi 2004). Respiration is the critical point in bacterial cell metabolic activity and the mechanism of obtaining energy to perform all the energy–demanding life processes. Energy generation relies on the respiratory enzyme complexes associated with the respiratory chain and it was found that silver ions likely disturb its function. Investigations on the interaction between silver ions and respiratory chain enzymes in *E. coli* concluded that silver ions bind to functional groups of amino acids making up enzymes and that activity inhibits the efficient electron transport via the respiratory chain. The final effect is the complete stoppage of electron transport and blockage of phosphorylation of ADP to ATP. NADH dehydrogenase complex is a potential target for silver ions activity (Holt and Bard 2005). Proton depleted regions were reported to form around silver nanoparticles due to micro–galvanic effect causing proton consumption which may further lead to disruption of electrochemical gradient (Cao *et al.* 2011). Another study supported a similar hypothesis where proteomic analysis results indicated that silver nanoparticles of average diameter 9.3 nm may accumulate in the protein precursors leading to depleted intracellular ATP levels (Lok *et al.* 2006).

1.3.4.3 Production of reactive oxygen species: The creation of free radicals and induction of oxidative stress also contributes towards toxicity of silver nanoparticles/ions (Wong and Liu 2010; Cao and Liu 2010). Production of reactive oxygen species is dependent to some extent on the catalytic activity of nanoscale silver. ROS generation is initiated mainly as an outcome of the respiratory enzymes and respiratory chain dysfunction (Choi and Hu 2008). Reactive Oxygen Species (ROS) are generated within or outside of the cell, as a consequence of cell damage/disruption (Liu *et al.* 2010; Thannickal and Fanburg VJ, 2000). The studies on nitrifying bacteria revealed that silver nanoparticles sized 15 nm produced the increase in intracellular ROS level and the concentration was correlated to bacterial growth inhibition rate (Choi and Hu 2008). Sustained release of silver ions by AgNPs inside the bacterial cells (in an environment with lower pH) may create free radicals and induce oxidative stress, thus further enhancing their bactericidal activity (Morones *et al.* 2005; Song *et al.* 2006). Yeast and *E. coli* cells were inhibited at a low concentration of AgNPs in a study which revealed that free radicals and oxidative stress were responsible for the antibacterial activities (Kim *et al.* 2007).

1.3.4.4 DNA damage: Inside the microbial cells, silver nanoparticles can result in DNA damage as the genetic material is one of the target sites for nanostructured silver (Feng *et al.* 2000; Kim *et al.* 2010). DNA loses its replication ability once the bacteria are treated by nanoscale silver, due to the capacity of silver ions to bind phosphorane residues of DNA molecules (Morones *et al.* 2005; Hatchett and White 1996). This interaction may prevent cell division, and may ultimately lead to cell death. Furthermore, silver ions are also reported to affect gene expression. Nanosilver was observed to stop S2 protein expression, a component of 30S ribosomal subunit and resulted in denaturation in *E. coli*. Additionally, the expression of genes encoding other proteins and enzymes involved in energy reactions in ATP synthesis were inhibited (Gogoi *et al.* 2006).

1.3.4.5 Inactivation of proteins: The release of silver ions also leads to inactivation of proteins. Silver ions can interact with sulphur containing proteins and thiol group of vital enzymes in bacterial cell and result in their impaired function or inactivation (Cao and Liu 2010; Hatchett and White 1996). Exchange of silver ions between inorganic sulphur complexes has also been proposed (Pal *et al.* 2007; Adams and Kramer 1999). Silver exhibits catalytic behaviour by binding with functional groups of amino acids and forming –S–S bonds between the –SH groups of neighbouring protein amino acids. This formation of additional –S–S bonds than normal may induce molecular changes that lead to protein inactivation and in the case of enzymes, to their deactivation (Wzorek and Konopka 2007). In another study it was reported that silver nanoparticles may modulate the phosphotyrosine profile of putative bacterial peptides that could affect cellular signalling and therefore inhibit the growth of bacteria (Shrivastava *et al.* 2007).

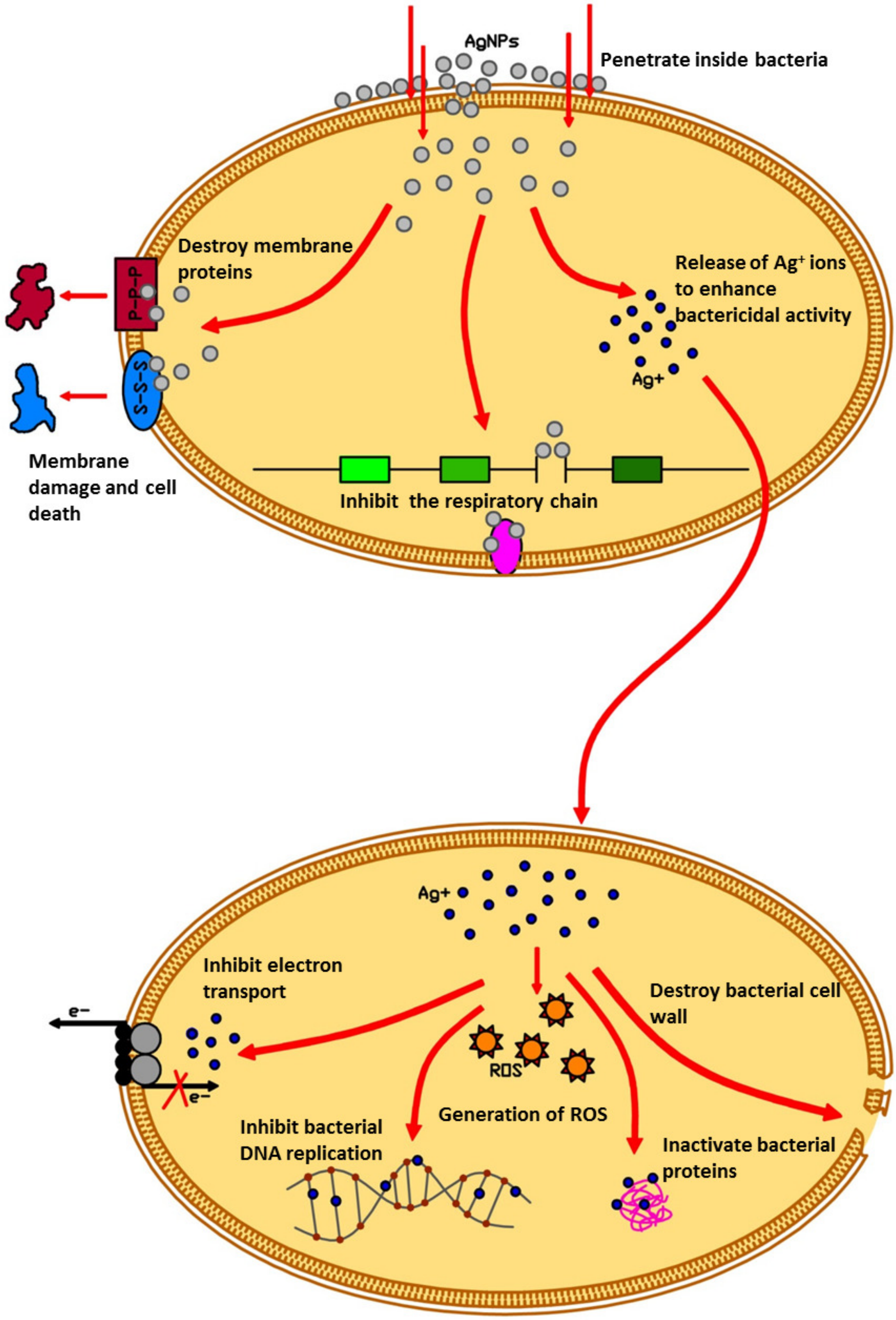

Figure 1.2 Schematic representations of known mechanisms of antibacterial action of silver nanoparticles and released ionic silver.

Despite the long history of silver as an antimicrobial, the mechanism of its microbicidal activity remains a matter of active research. The general explanation offered is that silver kills by at least one of the mechanisms explained above. It is certainly possible that all of these mechanisms contribute to the antimicrobial activity of silver, which would explain its broad effectiveness as well as the infrequent reports of silver–resistant bacterial strains.

1.3.5 Applications of silver and silver based materials

Presently 30 % of all registered products in nano–product databases claim to contain nanosilver and it has become one of the materials with highest degree of commercialization (Reidy *et al.* 2013). Silver is the most commonly used nanomaterial for microbial control in various consumer products such as nutritional supplements, food storage containers, kitchenware, refrigerators, textiles, laundry additives, washing machines, paints, sanitizers, contact lens solutions, catheters and wound dressings (Blaser *et al.* 2008; Chen and Schluesener 2008).

1.3.5.1 Food preservation and packaging

Antimicrobially active packaging based on metal nanocomposites which utilize the microbicidal property of metals is the new generation of nano food packaging (Chaudhry *et al.* 2008). Amongst metals and various other metal oxides, use of nanosilver as an antimicrobial is common in various products manufactured in food industry (Cushen *et al.* 2012). Based on the antimicrobial action of nanosilver, a number of ''active'' food contact materials that are claimed to preserve food longer by inhibiting the growth of microorganisms have been developed. These include storage containers, plastic storage bags, baby milk bottle, and inner surfaces of domestic refrigerators. Nanosilver coatings have also been used in antibacterial kitchenware, tableware and pet products (Chaudhry *et al.* 2008).

Food packaging films which incorporate silver nanoparticles are known to absorb and decompose ethylene by the process of oxidation (Hu and Fu 2003). This positive effect on the associated food may contribute to extending the shelf life of fruits and vegetables. In a study, the senescence of the Chinese fruit jujube was observed to retard by nanocomposite polyethylene film with silver nanoparticles (Li *et al.* 2009a). Silver nanomaterial coating was also reported to prolong the shelf life of asparagus samples by decreasing the microbial growth (An *et al.* 2008).

1.3.5.2 Implants and other medical devices

Nanosilver has also been revolutionary to the medical device industry due to its antimicrobial properties and the use of silver in wound dressings, dental hygiene, and treatment of eye conditions and other infections is well established (Reidy *et al.* 2013). There has been a proliferation of silver coated devices such as urinary catheters, cardiovascular implants, esophageal tubes, implants, wound plasters, salves, bandages, sutures and other instruments (Duncan 2011). Silver has been reported to delay or prevent the formation of biofilms in various medical devices where it exerts its effect by progressive elution from the devices. (Silvestry–Rodriguez *et al.* 2008)

In the hospital setting, nanosilver is extensively used for wound management, particularly for the treatment of burns, various ulcers, toxic epidermal necrolysis, for healing of donor sites and for meshed skin grafts (Wijnhoven *et al.* 2009). Silver–based wound dressings claim to offer improved infection management, in the form of the stimulation of healing in indolent wounds, prophylactic use for patients at risk of contracting a wound infection, and the management of critically colonized wounds (Chopra 2007; Senjen and Illuminato 2009).

Nanosilver could also prove very useful in the field of tissue engineering, as it is vital to keep the culture sterile and prevent microbial contamination during the cell multiplication process. A biocomposite composed of PLLA (poly–L–lactic acid) polymer and silver nanoparticles sized 30–100 nm showed antimicrobial activity against Gram–negative and Gram–positive bacteria as well as prevented the development of harmful microorganisms on the material surface (Chmielowiec–Korzeniowska *et al.* 2013; Li *et al.* 2009b). Nanosilver has also been used for development of novel chitin/nanosilver composite scaffolds for wound dressing due to its potent application as antimicrobial agent (Madhumathi *et al.* 2010)

1.3.5.3 Water purification and disinfection

Several silver–impregnated water filters have been registered by EPA since 1970s. These bacteriostatic water filters generally consist of activated carbon or ceramics that are impregnated with metallic/elemental silver of very small particle size (<100 nm).

Silver–impregnated water filters have been safely used for domestic water applications such as drinking water and swimming pool filters for decades without any reports of health or environmental effects (Nowack *et al.* 2011). The filter uses two mechanisms to disinfect the water. The first is removal of any harmful microorganisms or particles larger than 1 μm from the water by using the process of filtration. These would include most bacteria, and all protozoa and helminths. However, viruses and some bacteria will still pass through the filter. The second mechanism utilizes silver induced antimicrobial action to make the water completely germ free (Nagarajan and Jaiprakashnarain 2009).

Colloidal nanosilver algicides and disinfectants are based on elemental silver particles maintained in a stabilized solution with silver in very small particle size of less than 100 nm. Algicide applications have been used safely in high–exposure, direct water contact and down the drain applications such as swimming pool disinfection for decades without any known damaging impact on humans or the environment (Nowack *et al.* 2011).

1.3.5.4 Clothing and textiles

Antibacterial textiles containing nano–silver (and other forms of silver) make up the majority of commercially available nano–functionalized materials (Reidy *et al.* 2013). Textile products containing nanosilver include: socks, pants, T–shirts, shorts, swimwear, shoe pads/insoles, various business wear, sportswear, jackets, slippers, intimate wear, hats, gloves, bath towels and more. Silver nanoparticles are also embedded into textiles and fabrics for furniture, beddings and mattresses and for industrial material use (Senjen and Illuminato 2009). Silver used in textiles comes in a variety of forms including simple drenching of the cloth in silver salts and nanosilver impregnation of textiles (Senjen and Illuminato 2009). Silver (or other nanoparticles) may be embedded into the fibres or applied to the surface of the fibres. The preparation method will affect the durability of the functionalization and the potential for release of silver nanoparticle or ions into the environment (Reidy *et al.* 2013).

1.3.5.5 Cosmetics and personal care products

Cosmetics and personal care products containing nanosilver include: soap, toothpaste, shampoo, facial masks and creams, skin whiteners, hair dryers, hair straighteners, curling irons, hair brushes, and electric razors (Senjen and Illuminato 2009).

Silver in the form of nanoparticles seems to promote healing and achieve better cosmetic results. The proposed mechanism is that silver nanoparticles facilitate the proliferation and migration of keratinocytes, reduce the formation of collagen by fibroblasts and modulate the number of cytokines produced (Reidy *et al.* 2013).

1.3.6 Environmental toxicity

The toxicity of silver is dependent on (i) the form of silver, (ii) the concentration of silver in the environment and (iii) interaction with environmental components. When the silver is discharged in the wastewater, it is treated in the waste water treatment plant along with other domestic and industrial wastes. During the biological treatment of waste, a process where waste is treated with naturally occurring microorganisms, the silver complexes present are converted into silver sulfide and silver metal – both of which are nearly insoluble forms. These insoluble complexes are then separated from the water as part of the normal treatment process (Smith and Carson 1977). At this step, typically over 90 % of silver reaching the wastewater treatment plants is removed.

The silver that is separated from the water is then contained in the biological solids called sludge, which is disposed of through landfilling, land application or incineration. The silver contained in the sludge does not leach out to any significant extent in landfills or soil when used as a fertilizer owing to its very low water solubility. After this step a very small amount of silver is released from the treatment plants to the bodies of water in the form of tightly bound soluble silver complexes or nearly insoluble silver forms such as sulfide. These soluble silver complexes may react with a variety of naturally occurring substances such as chemical constituents of the water (e.g., chloride), organic constituents of the water (e.g., humic acids), reactive sulfides and solid particles suspended in the water. This renders any soluble silver nearly insoluble and removes it from the water. Silver sulphide and silver particulates then settle to the bottom through the process of sedimentation (Kodak 2003).

Toxicity is the measure of adverse chemical effects on an organism and is governed by several factors as mentioned above. Different forms of silver display different degrees of toxicity. Silver that is soluble in water and unattached to any other atoms while in solution is designated as free silver/ionic silver/hydrated silver (WHO 2002; Drake and Hazelwood 2005). Generally it is the free silver that is the most toxic form. The silver compounds which release ionic silver very slowly due to very low solubility (e.g., silver sulfide) or complexation of the silver (e.g., silver thiosulfate) are over 15,000 times less toxic than silver nitrate to organisms. Because of the tendency of silver to form nearly insoluble compounds in natural waters and sediments, the chance for organisms to be affected for long term is minimal (Kodak 2003).

In summary, the use of nanosilver is a matter of balancing risk and reward. There is a tremendous potential benefit to the use of some of the nanosilver products. Technologies need to be developed such that the benefits outweigh the risk (Seltenrich 2013). Also the use of silver recovery techniques that are efficient (more than 90% recovery) may be advantageous as there will be a small amount of silver discharged in the environment and the recovered silver could be recycled and reused.

1.4 Gaps in Existing Research

Antibiotic resistance of microorganisms is one of the major problems and hence currently a lot of research is focused on developing newer antimicrobials against antibiotic resistant microorganisms. Efforts need to be directed towards developing nanocomposite materials for enhanced antimicrobial activity by tuning its size, surface area, porosity and crystallinity. Likewise novel and simple low temperature based methods of synthesizing these nanoparticles using aqueous chemistry routes need to be developed. Although there has been a lot of literature reported on antimicrobial studies of silver incorporated TiO_2 nanoparticles, very few studies have reported the role of TiO_2 as a supporting and anti–aggregating agent wherein the antimicrobial activity is due to silver. By developing nanocomposites of silver and TiO_2, it is possible to attain the advantages of both materials wherein silver has superior antimicrobial activity and TiO_2 being a good supporting matrix facilitates long term bioactivity, thereby achieving control of silver ion release rate, better stability and novel properties due to their synergistic action.

However, in the natural world, more than 99 % of all bacteria exist as biofilms (Costerton *et al.* 1987). Biofilms can be as much as a thousand times more resistant than planktonic cells. The growth of biofilms is a major problem within the healthcare and food industries. Biofilms can form on many medical implants such as catheters, artificial hips and contact lenses. There are several approaches that are recognized in combating biofilms like physical and/or mechanical removal, chemical removal, and use of antimicrobials to kill planktonic cells, and prevention of biofilm formation. However, due to increasing tolerance of the biofilm community to antibiotics, biocides and mechanical stress, it has become just as difficult to completely eradicate mature biofilms as it is to completely avoid the presence of planktonic cells, the origin of the biofilm. Hence, novel methods of preventing the colonization of surfaces with biofilms are required. Thus, the potential of silver incorporated TiO_2 nanoparticles for antimicrobial activity and controlling biofilm formation is studied in the present work. Additionally, compounds that inhibit or interfere with quorum sensing have become significant as novel class of next generation antimicrobial and anti–biofilm agents. Conventional antibiotics prevent bacterial cell division (bacteriostatic) or kill the cell (bactericidal) and increase the selective pressure towards antibiotic resistance. Development of resistance to anti–quorum sensing compounds is minimal as these agents only target virulence mechanisms and do not impede growth. Hence, in the present work the anti–quorum sensing activity of the traditionally used bioactive agent silver incorporated within TiO_2 with potential in food preservation is studied.

A wide range of different materials have been tested for tissue engineering such as metals, natural and synthetic polymers, ceramics, polymer/inorganic composites. Among these, oxide ceramics (e.g. Al_2O_3, ZrO_2, and TiO_2) are bio–inert materials designed to be used as bone or dental implants (Rambo *et al.* 2006; Ahn *et al.* 2001). Although TiO_2 is known to be biocompatible and enhance the bone ingrowth capability, only few reports are available to demonstrate the use of titanium dioxide scaffolds as potential materials for implants. On the other hand, hydroxyapatite [(HAp), $Ca_{10}(PO_4)_6(OH)_2$], the main inorganic component of natural bone and all calcified tissues, has been widely used both as a structural material or as a coating onto metallic prosthesis to enhance their bioactivity. However, as it is intrinsically poor in mechanical properties, it would be advantageous to combine it with metals or ceramics like TiO_2 which have superior mechanical strength. Hence, in the present study attempts have been made to synthesize TiO_2–HAp nanocomposites scaffolds for bone tissue engineering and drug delivery applications. These nanocomposites would offer synergetic mechanisms to accomplish several functions simultaneously.

In view of the above perceived gaps in the literature, the following objectives have been proposed:

1. Synthesis and characterization of silver incorporated TiO_2 nanocomposite and studies on antimicrobial activity.
2. Studies on anti–biofilm efficacy of silver incorporated TiO_2 nanocomposite.
3. Synthesis and characterization of TiO_2–HAp nanocomposites and studies on their potential for tissue engineering and drug delivery applications.

CHAPTER 2

Chapter 2: Synthesis and Physico–chemical Characterization of Silver Incorporated Titanium dioxide Nanoparticles

2.1 Introduction

Titanium dioxide is a wide band gap and non–toxic semiconductor metal oxide and has attracted considerable attention due to its unique optical, electronic and catalytic properties (Fujishima *et al.* 2008). However, the antimicrobial activity of pure TiO_2 is only effective when it is irradiated with UV light. This drawback strongly restricts the practical application of TiO_2 as an antimicrobial material (Zhang *et al.* 2010). Doping with various metals has been shown to increase the photocatalytic efficiency of TiO_2 in UV range and/or shift its band gap energy to the visible region of the spectrum, and prevent recombination of electrons and holes (Zhou *et al.* 2006; Stathatos *et al.* 2001). Recent studies have focused on the antimicrobial activity of silver doped TiO_2 and Ag–TiO_2 nanocomposites in absence of photoactivation, wherein the antimicrobial activity is due to the silver, with TiO_2 acting as a support material facilitating uniform distribution and sustained release (Zhang and Chen 2009; Zhang *et al.* 2010).

Silver is well–known as an effective inorganic antimicrobial material since ancient time and is currently being used in different biomedical fields such as wound dressing materials, implants, tissue scaffolding and medical devices (Fer´nandez *et al.* 2008; Bosetti *et al.* 2002; B. Nowack *et al.* 2011). However, susceptibility to photoreduction, deactivation by protein anions and aggregation in suspensions are major drawbacks that affect the antimicrobial efficacy of silver. In addition, the high–cost and dark colour are notable obstacles for the applications of silver as large–area antimicrobial coatings (Silver Phung 1996; Sambhy *et al.* 2006; Lee *et al.* 2007). These limitations are being addressed by developing nanocomposites of silver with suitable supporting matrices (Babapour *et al.* 2011). Silver is being incorporated into various composite materials such as metal oxides (e.g., TiO_2, SiO_2, Fe_3O_4 and Al_2O_3), zeolites, polymers, carbon fibres, textile fabrics, clay etc. (Zhang and Chen 2009). This offers better chemical stability, in addition to providing improved control over the release rate of silver ions such that the antimicrobial activity is obtained for a prolonged duration. Therefore, it is desirable to combine the advantages of silver with TiO_2 to produce a kind of low–cost silver containing TiO_2 coating with all–weather antimicrobial property (Zhang *et al.* 2010). The importance of silver in medical applications and the antibacterial activity of

TiO_2 together led researchers to think about the manufacture of systems combining both titania and embedded silver compounds or silver nanoparticles, to expand the nanomaterial's antibacterial functions to a wide variety of working conditions (Yu *et al.* 2011).

TiO_2 nanoparticles are chemically stable, non–toxic, corrosion resistant, biocompatible and heat resistant and thus, hold good promise as support material because of their nanoparticulate and porous form which facilitates improved washing resistance with a slow dissolution rate of silver, yielding a long–term antimicrobial effect (Babapour *et al.* 2011). Moreover, TiO_2 nanoparticles serve as an anti–aggregating support material facilitating uniform dispersion of silver.

2.2 Sol–gel Technology

Sol–gel process was first discovered in the late 1800s and extensively studied since 1930s (Lev *et al.* 1995). Sol–gel processing is a soft–chemistry method which involves the transition of a system from a liquid (the colloidal sol) into a solid (the gel) phase for achieving functional materials which then connect with one another to create a three–dimensional (3D) solid network. It is a remarkably versatile approach for fabricating wide range of materials from the world's lightest materials to some of its toughest ceramics (Lev *et al.* 1997; Yamanaka *et al.* 1992; Bullen *et al.* 2004).

A typical sol–gel process (Figure 2.1) involves hydrolysis and polymerisation of a colloidal precursor solution (sol) into a loosely formed matrix, called gel. Titanium alkoxide and alcohol are mixed together in appropriate proportions and hydrolysis process begins upon addition of the hydration agent (water or acid). Alkoxide groups are exchanged for hydroxide with elimination of alcohol. This hydrated precursor then condenses with other precursor moieties, eliminating water after which network begins to grow and the colloidal sol is formed. Further these condensed titania species continue to polymerize together, forming a loosely held three dimensional network which densifies as it is allowed to age. At this stage the network contains the solvent eliminated during reaction. The aged sol/gel is then dried allowing solvent evaporation which leaves a mechanically weak and non–crystalline solid known as the xerogel (dried gel).

The xerogel has poor mechanical strength and is non–crystalline. In order to crystallize and densify the material, the xerogel is calcined at high temperature, usually around 500 °C to produce a dense and crystalline product. The above sol–gel process yields a solid powder. The sol–gel synthetic process for TiO_2 is mostly carried out with a titanium alkoxide as the titanium precursor solution (Page 2009).

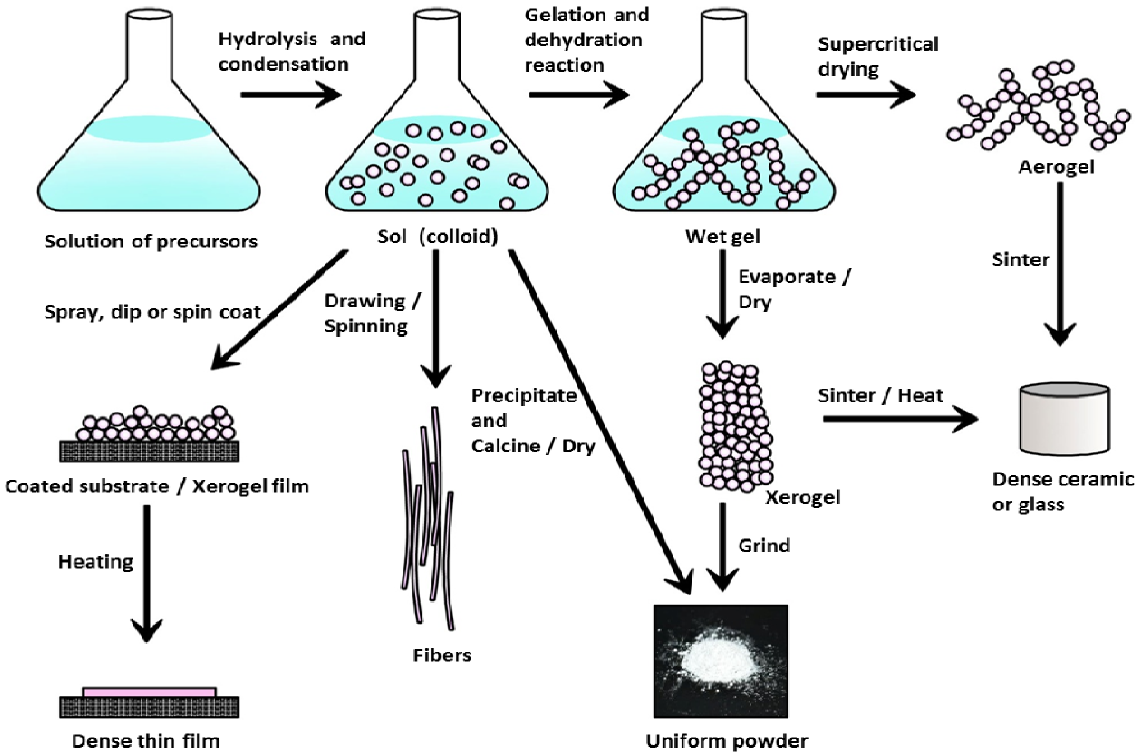

Figure 2.1 Schematic representation of the sol–gel process and various drying methods of the gel to develop materials with distinct properties.

Noble metal clusters can be introduced into a matrix through different conventional methods such as the traditional melt quenching, ion implantation, ion exchange, and sol–gel technique (Stepanov *et al.* 2000; Li *et al.* 2003b; Garrido *et al.* 1995). Synthesis of Ag/TiO_2 nanocomposites has been carried out through different synthetic techniques. In literature, solvothermal and sol–gel methods are commonly used, the sol–gel process being the most attractive method for practical applications (Yu *et al.* 2011). In this chapter, we report the synthesis of mesoporous $AgCl–TiO_2$ nanoparticles (ATNPs) using a simple, low temperature, sol–gel method and their physico–chemical characterization.

2.3 Materials and Methods

2.3.1 Chemicals and materials

Silver nitrate (99.8 %) was purchased from HiMedia. Titanium (IV) chloride (≥ 99 %) was obtained from Merck. Deionized water was used for all the experiments.

2.3.2 Synthesis of AgCl–TiO_2 nanoparticles

Stock solution of 100 mg/ml silver nitrate was prepared from which 140 µl was added to 50 ml of ice cold distilled water so that the final composition of silver was 1 weight % and magnetically stirred for 10 minutes. To this mixture, 1 ml of $TiCl_4$ was added dropwise and stirred for 2 h. The sol obtained was dialysed against deionized water until gel formation. The gel was dried at 100 °C for 24 h and milled using a mortar and pestle. The TiO_2 control was synthesized using the same protocol without addition of silver nitrate.

2.3.3 Characterization of samples

2.3.3.1 X–ray diffraction studies

X–ray powder diffraction is a non–destructive technique widely applied for the characterization of crystalline materials. This method has been traditionally used for phase identification, quantitative analysis and the determination of structure imperfections. In this technique, X–rays are passed through a crystalline material and the diffraction patterns produced give information of size and shape of the unit cell (David and Shankland 2008; Bish and Post 1989; Azaroff and Buerger 1975; Buerger 1942). X–ray diffraction studies were carried out by preparing a fine–grained sample by grinding it in a mortar and pestle. The sample was then put into the middle of the well and pressed flat with a glass slide to obtain a uniform smear, assuring a flat upper surface. Rigaku MiniFlex II X–ray diffractometer with monochromatic CuKα radiation (λ=1.5405 Å) was used. The scan range was from 2θ=20° to 80° and the crystallite size, D, was calculated using Scherrer formula: $D=k\lambda/\beta_{1/2}\cos\theta$, where λ=wavelength of X–ray applied (0.154 nm), k=numerical constant for which the obtained value is 0.9, $\beta_{1/2}$= full width (radians) at half maximum of the signal at (101) anatase peak and θ=Bragg angle for which 2θ is 25.28 (Scherrer 1918; Patterson 1939).

2.3.3.2 Surface area and porosity studies

Surface area and porosity studies were carried out using nitrogen sorption technique for the analysis of structure of porous materials. When a gas or vapour phase is brought into contact with a solid, part of it is taken up and remains on the outside attached to the surface and there is a weak Van der Waals attraction between the adsorbate and the solid surface. This is useful to characterise porous materials allowing for the determination of specific surface area, pore size distribution and pore volume. The Brunauer–Emmett–Teller (BET) gas adsorption is the standard method for determination of the surface area of finely–divided porous materials. N_2 adsorption–desorption isotherm and BET surface area of AgCl–TiO_2 nanoparticles was measured using surface area and porosimetry analyser (TriStar 3000, Micromeritics, USA).

2.3.3.3 High resolution transmission electron microscopy (HR TEM) analysis and selected area electron diffraction (SAED)

The transmission electron microscope operates on the same basic principles as the light microscope but uses electrons instead of light. A light microscope is limited by the wavelength of light, instead TEMs use electrons as "light source" and their much lower wavelength makes it possible to get a resolution a thousand times better than with a light microscope. The possibility for high magnifications has made the TEM a valuable tool in both medical, biological and materials research. SAED is a crystallographic experimental technique that can be performed using a transmission electron microscope. HR TEM analysis and SAED were carried out using a JEOL JEM–2100F operating at 200 kV. The AgCl–TiO_2 nanoparticle sample was prepared by ultrasonic dispersion (Microson TM Sonicator) in water for 15 minutes at 3 rps (revolutions per minute). Then, the colloidal solution thus obtained was dropped onto a carbon–coated copper grid and dried in air before TEM analysis.

2.3.3.4 EDX (Energy dispersive X–ray spectroscopy) analysis

EDX makes use of the X–ray spectrum emitted by a solid sample bombarded with a focused beam of electrons to obtain a localized elemental composition of the sample. EDX analysis was carried out using a SEM–EDX, JEOL JSM–6360 LV to determine the elemental composition of nanoparticles. The AgCl–TiO_2 powder was deposited on a carbon tape before mounting on a sample holder and gold coated for EDX.

2.3.3.5 Fourier transform infrared spectroscopy (FTIR)

Infrared spectroscopy, similar in principle to the UV–Visible spectroscopy is used to obtain absorption spectra of compounds that are a unique reflection of their molecular structure. Infrared spectroscopy measures transitions from one molecular vibrational energy level to another, and requires radiation from the infrared portion of the electromagnetic spectrum. Infrared absorption spectra were measured on a Shimadzu IRPrestige–21 spectrometer in the 248–4000 cm^{-1} frequency range, using spectroscopy grade KBr (Merck) as the reference. KBr (approximately 100 mg) was dried in oven at 100 °C for 6 h and ground into a fine powder in a clean mortar and pestle. Approximately 1 mg of the sample was added to it and ground again to form a homogenous mixture. Sample mix was then pressed into thin pellets at a pressure of 7 tonnes for 2 minutes using a KBr mini press. These pellets were then used for recording the spectra.

2.3.3.6 UV–visible diffuse reflection spectroscopy (DRS)

UV–visible diffuse reflectance spectroscopy (DRS) has been widely used to investigate the structures of various compounds. This technique is based on analysis of backscattered light that has propagated through a scattering and absorbing medium.The DRS were obtained for the samples using a UV–visible spectrophotometer (Shimadzu UV 2450), with $BaSO_4$ as the reflectance standard. The spectra were recorded at room temperature in air in the range of 800 to 200 nm.

2.3.3.7 Zeta potential analysis

The zeta potential is a measure of the electrokinetic potential in a colloidal system which gives an idea about the stability of the material (Wang *et al.* 2014). The zeta potential analysis of ATNPs and TiO_2 (control) was conducted using Delsa Nano C (Backman Coulter). 1mg/mL of nanoparticle suspensions in ultrapure deionized water were sonicated (Microson TM Sonicator) at 3 rps for 15 minutes.

2.4 Results and Discussion

In this work the AgCl–TiO_2 and TiO_2 nanoparticles were prepared using a simple one–pot sol–gel method and calcined at 100 °C. Sol–gel is an attractive method for obtaining nanoparticles with high surface area, porosity and monodispersity and requires low processing cost, is energy efficient with high production rate and rapid productivity of fine homogeneous powder (Liu *et al.* 2008; Azizi *et al.* 2012). Effective removal of adsorbed ions was achieved through frequent change (every 2 h) of the deionized water during dialysis. The simplicity of this method gives it an advantage over the conventional time consuming processes. Further, it requires very few chemicals, no harmful byproducts are generated and calcination is achieved at low temperature. Low temperature based methods as used in this work are beneficial as high temperature causes an increase in crystallinity, which leads to a reduction in silver release kinetics. In addition to this it also leads to aggregation of silver clusters to form bigger silver particles reducing their antimicrobial efficiency (Babapour *et al.* 2011).

Sol–gel has become one of the most useful and versatile methods of nanoparticle fabrication due to various advantages like (i) easy control of metal concentration and coating thickness during fabrication of a film, (ii) possibility to add reducing and oxidizing agents in small concentrations, (iii) morphology of the nanoparticles can be changed by changing the solvents, (iv) synthesis of materials with high purity and high degree of homogeneity, (v) synthesis of materials with low or high porosity by using appropriate heat treatment and firing times, (vi) capability of obtaining fully–dense amorphous solids at temperatures lower than those required for conventional compaction/densification or for melting and (vii) ability to obtain materials with novel distribution of phases (Li *et al.* 2003b; Naldoni 2009; Ramesh 2013).

The XRD analysis (Figure 2.2 (a) and (b)) showed that both samples exhibited diffraction peaks characteristic of anatase at 2θ=25.28°, 37.79°, 48.04°, 53.88°, 55.05°, and 62.68° corresponding to (101), (004), (200), (105), (211), and (204) crystal planes, respectively, conforming to anatase TiO_2 (JCPDS No. 21–1272). The ATNP sample exhibited additional diffraction peaks at 2θ=27.8, 32.2, 46.2, and 57.5° corresponding to (111), (200), (220) and (222) planes of AgCl crystals, (JCPDS file: 31–1238) indicating that AgCl is well compounded into TiO_2. The crystallite size was calculated for (101) anatase plane of TiO_2 using Scherrer formula and was found to be 3.7 nm.

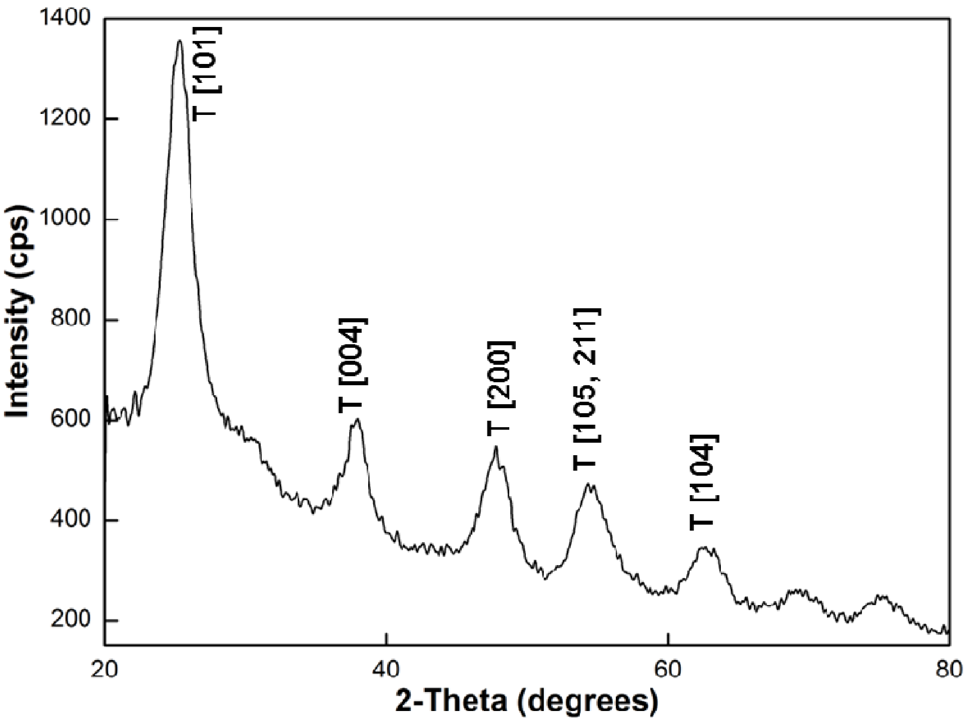

Figure 2.2 (a) XRD pattern of TiO_2 nanoparticles showing anatase as the predominant crystalline phase, where: T–anatase TiO_2.

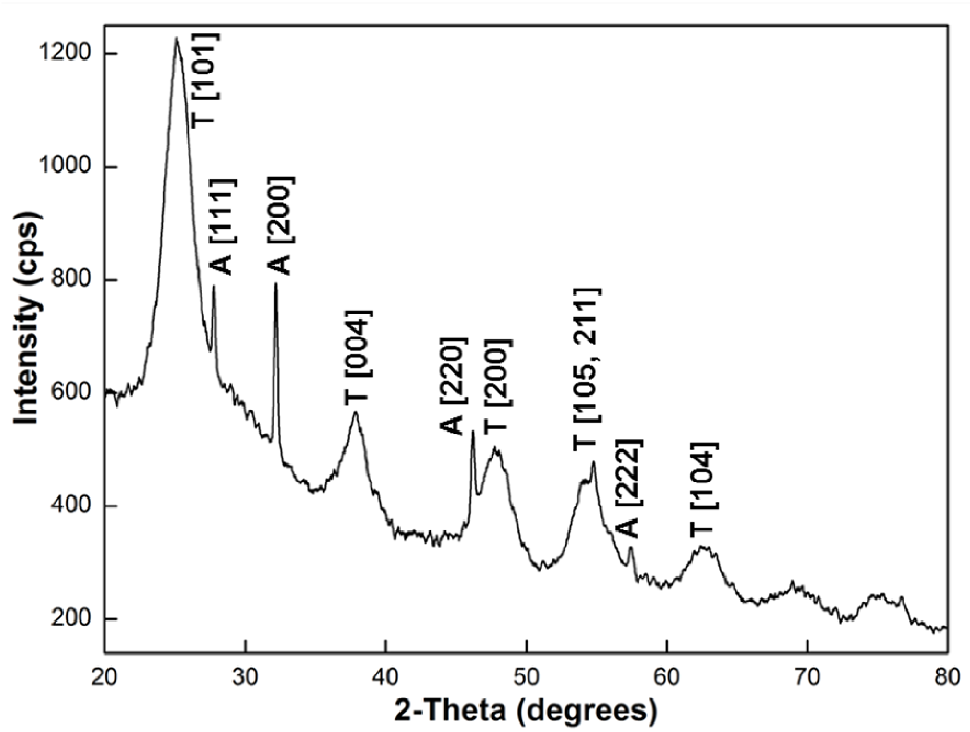

Figure 2.2 (b) XRD pattern of ATNPs showing peaks corresponding to crystal planes of AgCl in addition to TiO_2, where: T–anatase TiO_2 and A–AgCl.

Figure 2.3 shows the nitrogen adsorption–desorption isotherm (a) and pore size distribution curve (b) of ATNP. The material exhibits a type IV adsorption isotherm with an H2 hysteresis loop, characteristic of mesoporous structure (Sing *et al.* 1985). The pore size distribution was calculated from the desorption branch of the isotherm by Barret–Joyner–Halenda (BJH) method and was centred around 3.7 nm. The mesopores were of ~3 nm in size and BET surface area was found to be 266 m^2/g. Large surface area can be a major determining factor in enhancing the antimicrobial activity as it provides better contact between nanoparticles and microorganisms (Pal *et al.* 2007).

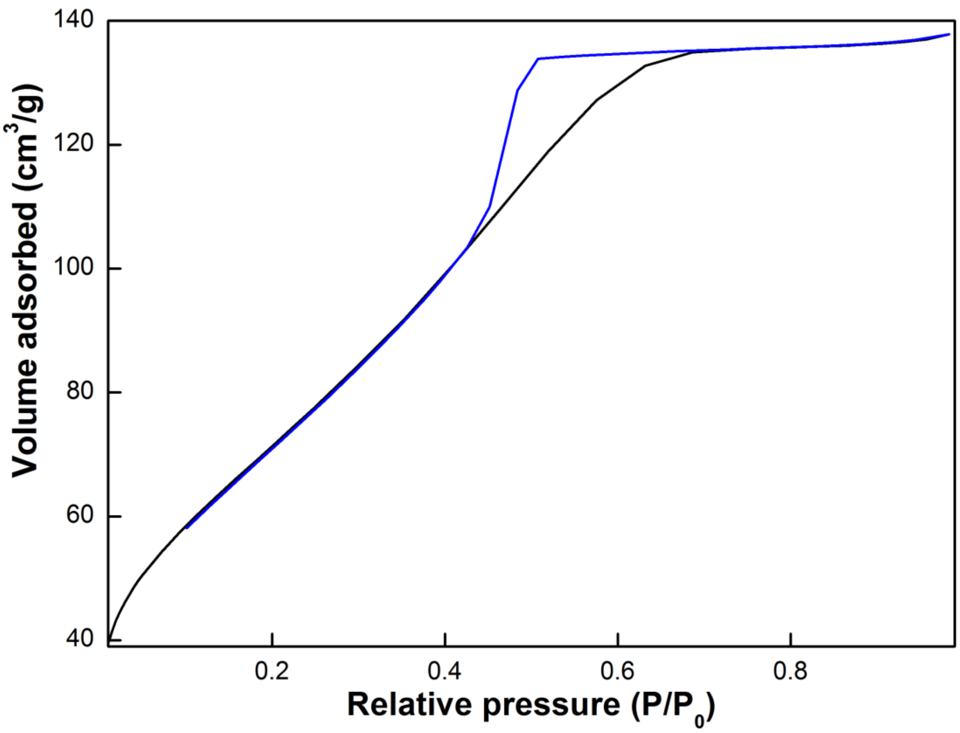

Figure 2.3 (a) N_2 adsorption–desorption isotherm of ATNPs showing type IV isotherm and H2 hysteresis loop.

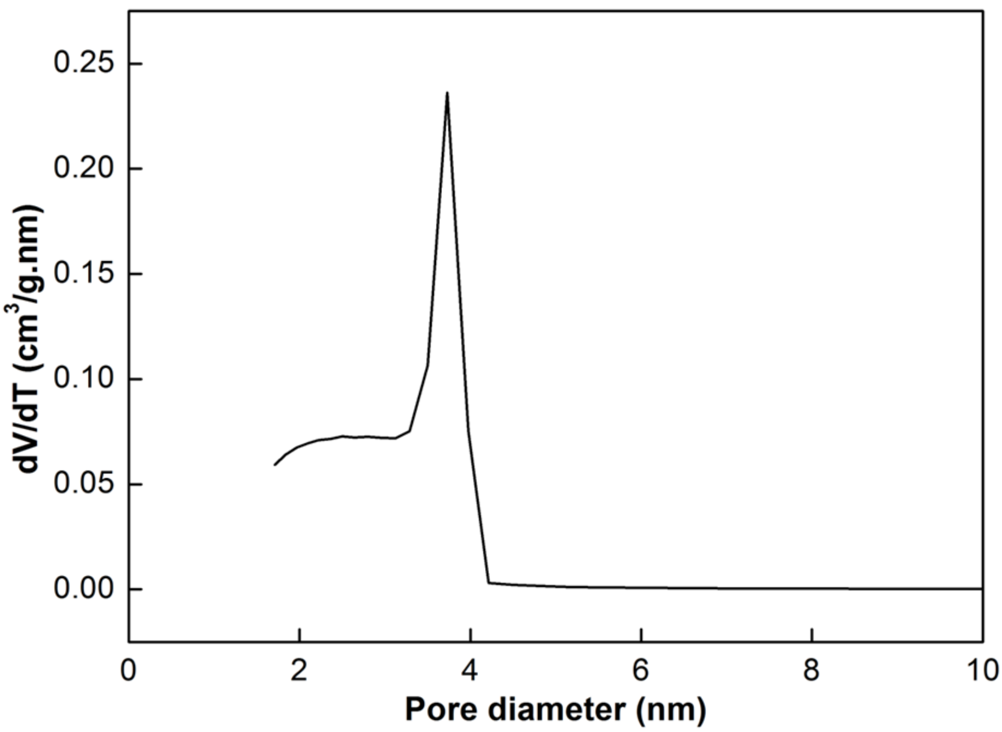

Figure 2.3 (b) Pore size distribution curve of ATNPs.

HR TEM data showed that the ATNPs were uniform with average particle size of 6 to 7 nm (Figure 2.4 (a) and (b)). SAED of ATNPs showed distinct and good diffraction rings (inset to Figure 2.4 (a)). The lattice fringes for a single particle (Figure 2.4(b)) were clearly seen with a lattice spacing of 0.35 nm, corresponding to the (101) anatase phase (Loganathan *et al.* 2011). Small particles have large portion of atoms on low–coordination and high energy sites like corners, edges, steps, kinks and adatoms, which make them more active than larger particles. Furthermore, they have increased surface area and high penetration efficiency (Zhang and Chen 2009; Pal *et al.* 2007). It has been reported that particles having a diameter of ~1–10 nm can directly interact with bacteria (Morones *et al.* 2005).

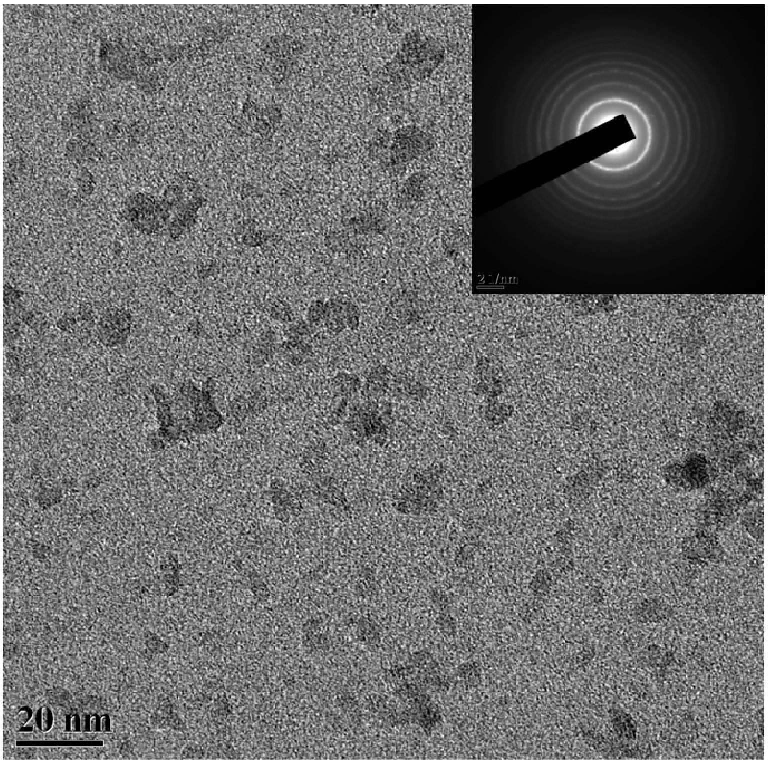

Figure 2.4 (a) HR TEM image of ATNPs; SAED is shown as an inset.

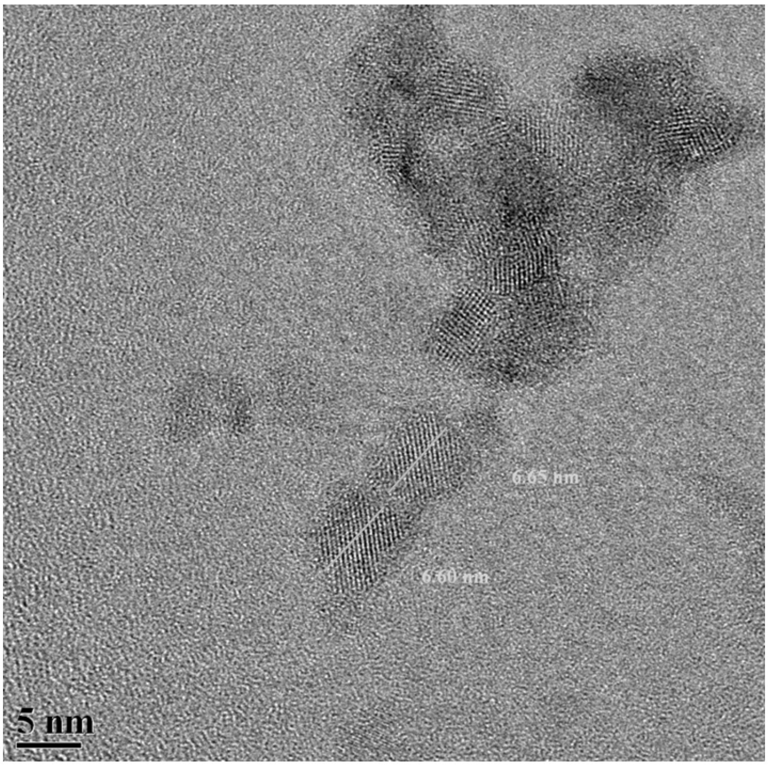

Figure 2.4 (b) Magnified HR TEM image of ATNPs with clear lattice fringes.

The EDX analysis showed a silver peak around ~2.7 keV, and stronger Ti peaks (Figure 2.5). No signals for organic impurities were found. The compound % and weight % of silver were 1.08 % and 1.01 % respectively.

FTIR spectroscopy (Figure 2.6) was used to determine the bonding characteristics in TiO_2. The absorption band in the region of 520–580 cm^{-1} corresponds to the Stretching vibration of Ti–O (Li *et al.* 2008; Liu *et al.* 2006). The absorption peaks at about 3420–3450 and 1630–1640 cm^{-1} are associated with the stretching vibrations of surface water molecules, including hydroxyl groups (OH^-) and molecular water on the samples. The surface hydroxyl groups (OH^-) play an important role in the microbicidal mechanism (Dong *et al.* 2009; Huang *et al.* 2008).

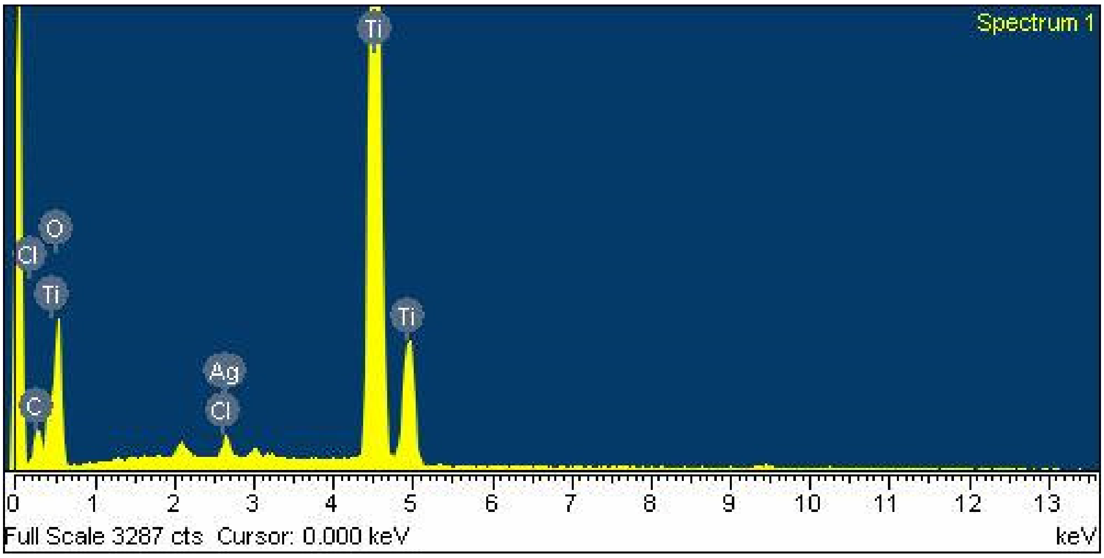

Figure 2.5 EDX spectrum of ATNPs.

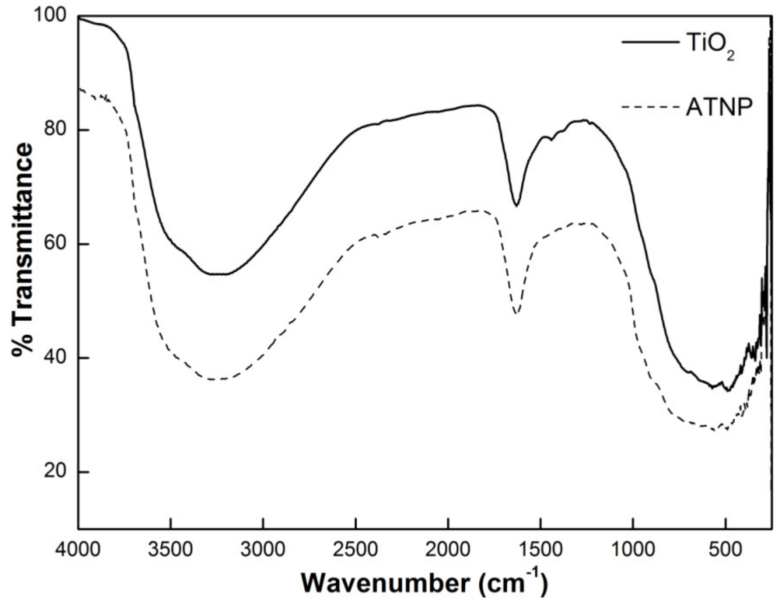

Figure 2.6 FTIR spectra of ATNP and TiO_2 (control) nanoparticles.

The UV–visible studies indicate that both TiO_2 and ATNPs have an absorbance onset at ~370 nm (Figure 2.7), showing that small loading of silver did not influence the absorbance pattern. A similar observation has been reported for Ag–TiO_2 synthesized by solution impregnation method with 4 weight % of Ag wherein no UV–visible spectral shift was observed (Kumar and Ghulam 2009).

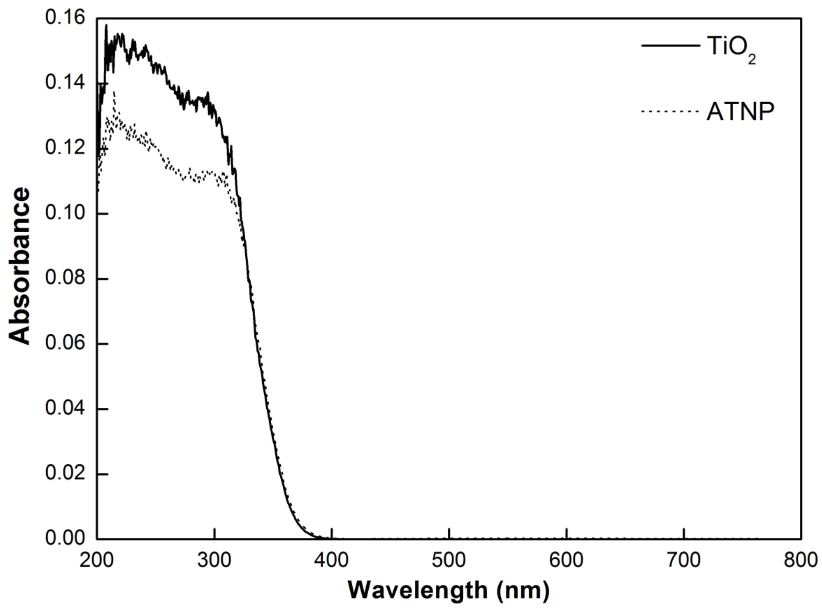

Figure 2.7 UV–visible absorption spectra of ATNP and TiO_2 (control) nanoparticles.

Zeta potential studies were conducted to assess the dispersibility of ATNPs. For investigations of the *in vivo* and *in vitro* effects of nanoparticles, they have to be well dispersed in solutions. If particles form coarse agglomerates in solution, it negatively affects the biological activity of the material (Murdock *et al.* 2008). As the zeta potential approaches 0 (from either the negative or the positive side) the solution becomes less stable (Wang *et al.* 2014). The zeta potential values were –18.18 mV and –16.8 mV for TiO_2 and ATNPs respectively, indicating that the nanoparticles were well dispersed in suspension.

2.5 Conclusion

Mesoporous ATNPs with TiO_2 homogenous anatase crystalline phase were synthesized using a one–pot sol–gel method. The sample was calcined at 100 °C and characterized by XRD, HR TEM, EDAX, IR spectroscopy, DRS, N_2 adsorption–desorption isotherm and Brunauer–Emmett–Teller (BET) analysis. The XRD analysis showed that the ATNPs exhibited diffraction peaks corresponding to anatase TiO_2 and AgCl. The crystallite size calculated using Scherrer formula was 3.76 nm. The material exhibited a characteristic mesoporous structure and the BET surface area of the sample was 266 m^2/g. HR TEM analysis showed that the ATNPs were uniform with average particle size of 6 to 7 nm. The elemental composition of ATNPs as determined by EDX analysis demonstrated silver and Ti peaks with 1 weight % of silver.

CHAPTER 3

Chapter 3: Antimicrobial Activity of $AgCl–TiO_2$ Nanoparticles and their Mechanism of Action

3.1 Introduction

The emergence of more resistant and virulent strains of microorganisms due to the indiscriminate use of antibiotics has led to the search for alternate sterilization technologies. Silver is well known for its antimicrobial effects since ancient times and was used in treatment of infections, ulcers etc., and to store water. However, after the introduction of penicillin in 1940s, antibiotics became the standard treatment for bacterial infections and the use of silver diminished (Fer´nandez *et al.* 2008). Lately, silver has regained its importance as an antimicrobial/biocide and is used to prevent the growth of bacteria on surfaces and within materials (Nowack *et al.* 2011; Bosetti *et al.* 2002). Silver nanoparticles (Fer´nandez *et al.* 2008; Jain *et al.* 2009; Eby *et al.* 2009; Kim *et al.* 2007) as well as various silver–based compounds containing ionic silver [Ag^+] and/or metallic silver [Ag^0] exhibiting antimicrobial activity are being actively synthesized (Panacek *et al.* 2006).

The inhibitory effect of silver is a result of the sum of distinct mechanisms of action. Whether supplied as a cation, in the elemental state, or as part of composite materials, silver destabilizes and increases the permeability of bacterial membranes, inactivates sulphur containing essential respiratory enzymes and proteins responsible for DNA replication, and disrupts ion transport processes, thereby killing microorganisms (Hatchett and White 1996; Feng *et al.* 2000). On account of this multi–targeted mechanism of action, silver has a far lower tendency to induce bacterial resistance than conventional antibiotics (Percival *et al.* 2005). Although silver indiscriminately forms complexes with several different amino acids and thereby inhibits protein function, it exhibits limited toxicity to mammalian cells (Berger *et al.* 1976).

In the present study, we report very high efficiency of antimicrobial activity of mesoporous ATNPs synthesized using a simple, low temperature, sol–gel method under ambient conditions. The increase in antimicrobial efficiency may be attributed to the mesoporous nature of the composite which endows on these nanoparticles an increase in surface area (Liu *et al.* 2008). This in turn would facilitate enhanced contact between the microorganisms and nanoparticles leading to the increase in activity. The increased efficiency of antimicrobial activity observed at lower concentrations of silver may also be attributed to the slow and sustained release of silver from the mesopores (Yu *et al.* 2011).

3.2 Materials and Methods

3.2.1 Chemicals and materials

Escherichia coli ATCC 10536, *Bacillus subtilis* ATCC 9524 were obtained from National Collection of Industrial Microorganisms (Pune, India). *Pseudomonas aeruginosa* ATCC 25668, *Staphylococcus aureus* ATCC 6538P and *Candida albicans* MTCC 3958 were obtained from MTCC (Chandigarh, India). *Candida albicans* 3958 was grown in Sabourauds Dextrose broth (pH 5.6) and Nutrient Broth (pH 7.4) was used for all the bacterial cultures. Muller Hinton (MH) broth and YES medium (0.5 % yeast extract and 1 % glucose, pH 5.6) were used for antimicrobial studies of the bacterial and fungal cultures, respectively. Deionized water was used for all the experiments. All experiments involving microorganisms were performed in triplicates on different days.

3.2.2 Antimicrobial assays

Microbial cells in the logarithmic growth phase were used for all studies. The cells (10^5 to 10^6 cells/mL) were suspended in 5 mL of aqueous ATNP suspensions and stirred using a magnetic stirrer. The concentrations of ATNP tested in water were 1–20 μg/mL. At intervals of 30 minutes, aliquots of the suspension were withdrawn and the cells were spread–plated on nutrient agar/sabourauds agar plates after appropriate dilutions with sterile saline. The plates were incubated at 37 ºC (30 ºC for *Candida albicans*) for 24 h. The number of viable organisms was determined by counting the number of colony forming units and multiplying it with the dilution factor. Control studies were carried out using pure TiO_2. Similar experiments were carried using Muller Hinton (MH) broth as the resuspension medium where the concentrations of ATNP tested were in the range of 100 to 1000 μg/mL.

3.2.3 Detection of silver ions

Detection of silver ions was carried out using a rhodamine–based fluorogenic and chromogenic probe (Chatterjee *et al.* 2009). 1 mg/mL (effective Ag concentration of 11.7 ppm) of ATNP was suspended in aqueous phase for 1 h and the amount of silver ions released was determined by centrifuging the sample at 12000 rpm for 15 minutes. Subsequently the sample was resuspended in fresh medium and silver ion release was further monitored. The probe was added to the supernatant and incubated for 1 h at 25 °C. The final concentration of the probe in the solution was 10 μM. The fluorescence spectra of the solutions were measured at 584 nm using a JASCO FP–6300 spectro–fluorometer. Known concentrations of $AgNO_3$ solutions were used to obtain the standard calibration curve to determine silver ion concentration. The detection limit of this probe is reported to be 14 ppb.

3.2.4 Detection of reactive oxygen species (ROS)

Intracellular ROS generation was determined using 2', 7'–dichlorofluorescin–diacetate (DCFH–DA) as an intracellular ROS–indicator (Su *et al.* 2009). The oxidation of non–fluorescent DCFH to highly fluorescent 2', 7'–dichlorofluorescein (DCF) provides a quantitative assay of ROS formation. *E. coli* cells were initially incubated with 10 μg/mL of ATNP for 30 minutes, 20 μM DCFH–DA was added and the mixture was further incubated for 30 minutes. *E. coli* cells without ATNP were used as a negative control. The fluorescence intensity of DCF was measured at 526 nm. Cells were exposed to the antioxidant and free radical scavenger N–acetylcysteine (NAC) to determine the effect of presence of antioxidant on ROS levels. H_2O_2 was used as a positive control. Change in ROS level as compared to the negative control was calculated using the formula, Relative ROS level (%) = Mean DCF FI[treated]/Mean DCF FI[control] × 100, where FI is the fluorescence intensity (Wang *et al.* 2011).

3.2.5 Antioxidant studies

NAC and glutathione (GSH) were used as the antioxidants. The effect of these agents on the antimicrobial activity was determined by carrying out the antimicrobial assays (as mentioned above) in presence of 10 mM NAC/GSH in MH medium (Kim *et al.* 2007; Su *et al.* 2009).

3.3 Results and Discussion

3.3.1 Antimicrobial activity of ATNPs

Antimicrobial activity with ATNP was obtained at a concentration as low as 1 µg/mL (effective Ag concentration of 11.7 ppb) for Gram–negative microorganisms and the fungal culture *Candida albicans* in aqueous phase. The kill curves obtained on exposure to ATNP at 1 µg/mL, 5 µg/mL, 10 µg/mL and 20 µg/mL for *Escherichia coli* ATCC 10536, *Pseudomonas aeruginosa* ATCC 25668, *Staphylococcus aureus* ATCC 6538P, *Bacillus subtilis* ATCC 9524 and *Candida albicans* MTCC 3958 are shown in Figures 3.1 (a), (b), (c), (d) and (e) respectively. Photographs showing decrease in number of microorganisms on exposure to ATNP with respect to time for these cultures are shown in Figure 3.2. At ATNP concentration of 1 µg/mL, and a starting cell number of ~10^5 cells/mL, complete reduction of *Escherichia coli* cells and 99.56 % reduction of *Pseudomonas aeruginosa* cells was obtained after 90 minutes and 120 minutes, respectively. Complete inhibition of *Pseudomonas aeruginosa* was obtained at a concentration of 5 µg/mL of ATNP (effective Ag concentration of 58.5 ppb) after 90 minutes. As seen from Figures 3.1 (a) to (e), the time required for complete killing decreased with increase in concentration of ATNP. The lowest reported bactericidal concentration against *E. coli* in aqueous phase is 1.6 µg/mL of silver in Ag/TiO_2 nanocomposites (Zhang and Chen 2009). Other studies on Ag–TiO_2 composites carried out in UV light have reported antimicrobial values in the range of 0.1 to 2 mg/mL of Ag–TiO_2 wherein the percentage of silver incorporated in TiO_2 differed from 1 weight % to 5 weight % (Kumar and Ghulam 2009; Reddy *et al.* 2007; Sokmen *et al.* 2001; Amin *et al.* 2009). The antimicrobial activity obtained during visible light photocatalysis is reported to be in the range of 0.5 to 2 mg/mL for Ag–TiO_2 (Medina–Ramirez *et al.* 2011).

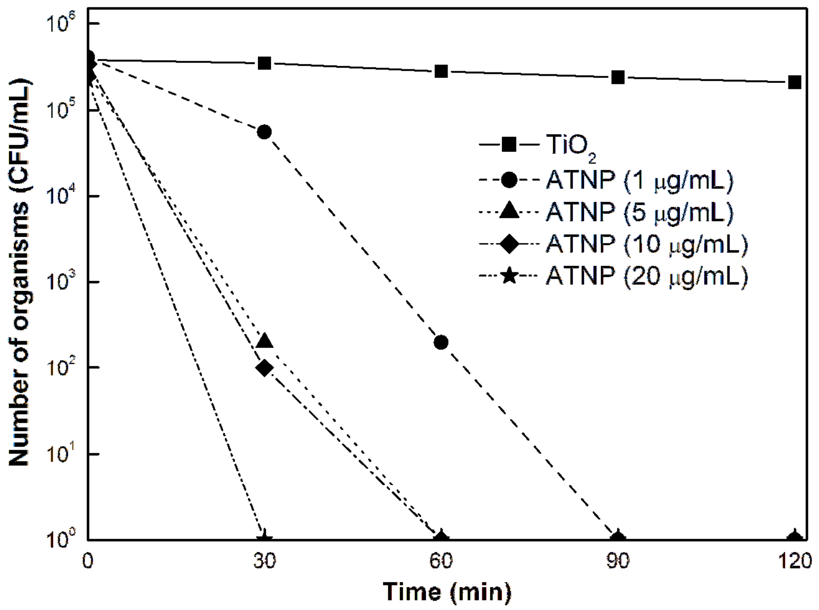

Figure 3.1 (a) Antibacterial activity of ATNP against *E. coli*.

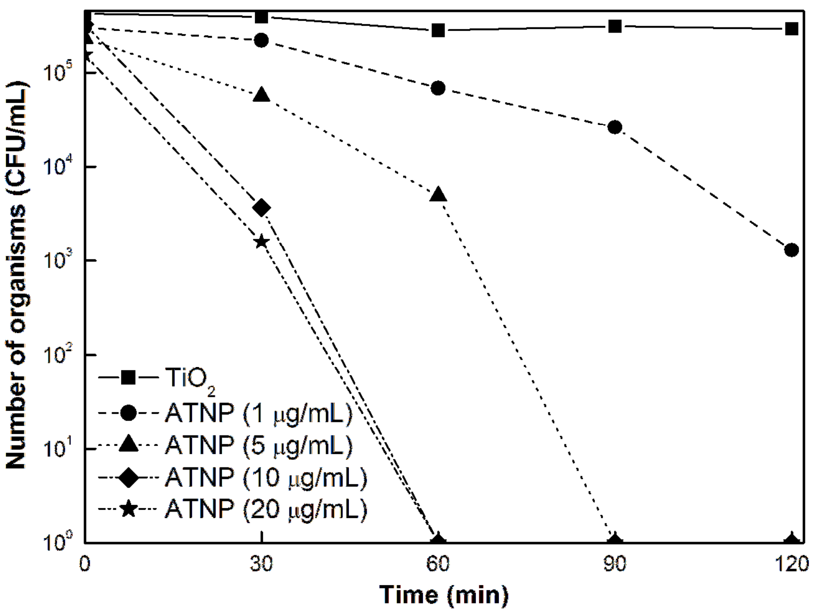

Figure 3.1 (b) Antibacterial activity of ATNP against *P. aeruginosa*.

In case of Gram–positive organisms, bactericidal activity of ATNP was obtained at 10 µg/mL (effective Ag concentration of 117 ppb), wherein complete killing of *Bacillus subtilis* and 99.9 % reduction in the number of *Staphylococcus aureus* cells occurred after 120 minutes. Complete killing of *Staphylococcus aureus* was obtained at a concentration of 20 µg/mL of ATNP (effective Ag concentration of 234 ppb) after 90 minutes. Bactericidal activity (99.99 % reduction) against *S. aureus* has been reported at 20 µg/mL for silver–supported TiO_2 core and carbon shell composite (TiO_2@C/Ag) with 1.52 weight % Ag after 6 hours of contact (Tan *et al.* 2009). Other reports on antimicrobial activity of Ag–TiO_2 against Gram–positive organisms reported killing of *Micrococcus lylae* at 0.1 mg/mL (Zhang *et al.* 2003) and *Streptomyces* at 10 µg/mL (2.5 µg/mL Ag) (Su *et al.* 2009b). It has been observed that antimicrobial activity of ATNP composite is more pronounced against Gram–negative microorganisms as compared to that against Gram–positive microorganisms. Similar observations have been reported for colloidal suspensions of silver–titania, TiO_2@C/Ag core–shell composites and electrically generated silver ions (Tan *et al.* 2009; Gavriliu *et al.* 2009; Jung *et al.* 2008). The difference in susceptibility has been attributed to compositions of bacterial cell wall. Gram–positive bacteria have thick multi–layered peptidoglycan in the cell wall whereas in Gram–negative bacteria, peptidoglycan is present as a thin layer surrounded by an outer membrane (Gavriliu *et al.* 2009). The outer membrane is negatively charged and serves as a selective permeability barrier, protecting bacteria against toxic agents. Therefore, cationic silver will have increased interaction with outer membrane, changing membrane permeability and facilitating transfer of silver across the outer membrane and thin layer of peptidoglycan (Jin *et al.* 2010). In case of Gram–positive bacteria, the thick peptidoglycan layer restricts the entry and thereby action of ATNP.

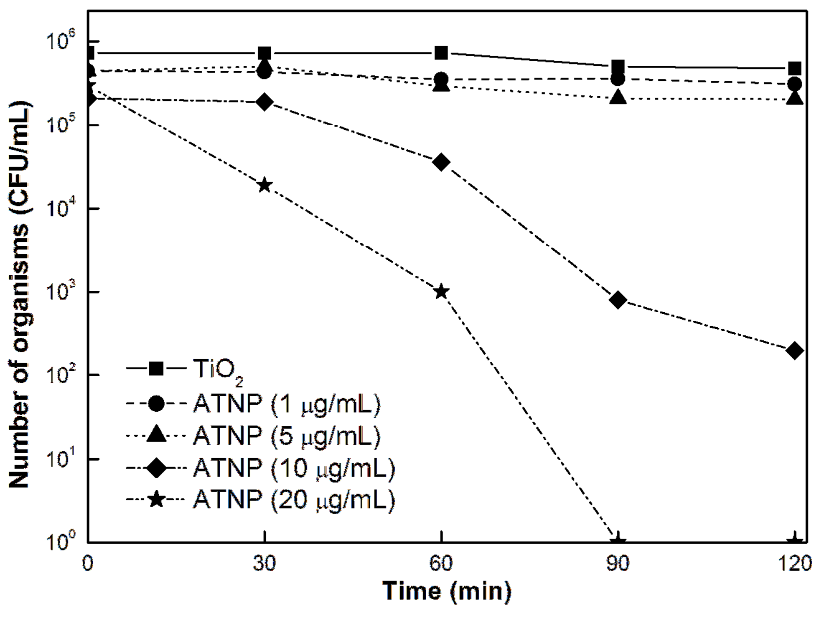

Figure 3.1 (c) Antibacterial activity of ATNP against *S. aureus*.

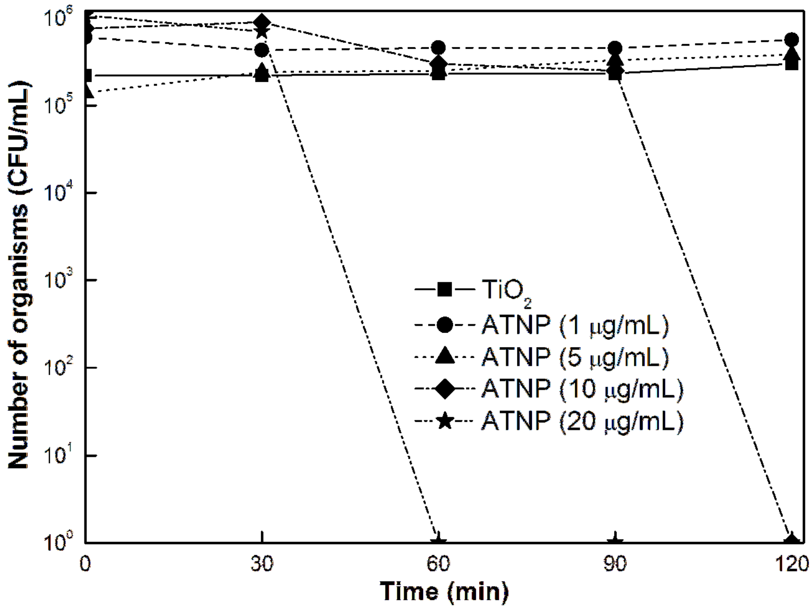

Figure 3.1 (d) Antibacterial activity of ATNP against *B. subtilis*.

For *Candida albicans*, 93 % reduction was obtained at 1 µg/mL of ATNP (effective Ag concentration of 11.7 ppb) after 120 minutes and complete killing was obtained at 10 µg/mL of ATNP (effective Ag concentration of 117 ppb) after 60 minutes (Figure 3.1 (e)). Although, numerous reports are available on antibacterial activity of silver plus TiO_2 based compounds, antifungal activity has not been extensively studied. Minimum inhibitory concentration (MIC) of 15.88 µg/mL of silver has been obtained for colloidal suspensions of silver–titania (Gavriliu *et al.* 2009). Silver nanoparticles have been reported to possess antifungal activity against *C. albicans*, however, the effective concentrations ranged from 2 to 25µg/mL (Jain *et al.* 2009; Eby *et al.* 2009; Kim *et al.* 2009). In our study, the MIC observed was as low as 1.75 ppm of silver (150 µg/mL of ATNP).

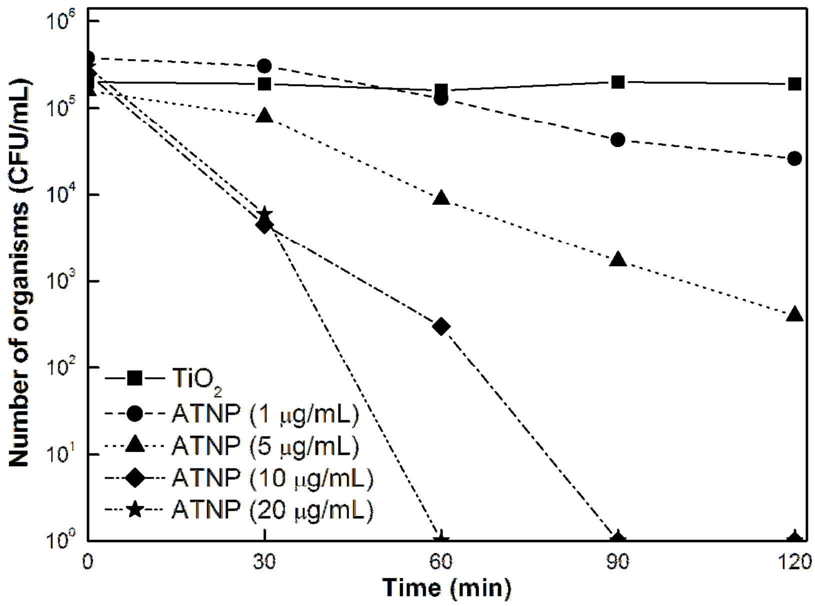

Figure 3.1 (e) Antibacterial activity of ATNP against *C. abicans*.

In order to determine the effect of composition of resuspension media on antimicrobial activity, we carried out antimicrobial studies in MH medium. The concentration of ATNP required for antimicrobial activity in MH media was higher as compared to that in aqueous phase. A 99.67 % reduction in the number of cells for *Pseudomonas aeroginosa* was obtained at 100 µg/mL ATNP (effective Ag concentration of 1.17 ppm) and 100 % reduction was obtained at 150 µg/mL (effective Ag concentration of 1.75 ppm) within 120 minutes. For *E coli*, 96 %, 99.89 % and 100 % reduction was obtained at 100 µg/mL, 150 µg/mL and 200 µg/mL of ATNP (effective Ag concentration of 1.17 ppm, 1.75 ppm and 2.34 ppm) respectively. Nanocomposites of Ag–TiO_2 have been reported to exhibit antimicrobial activity in growth medium in the range of 10–20 µg/mL of Ag for Gram–positive as well as Gram–negative cultures (Gavriliu *et al.* 2009; Chen *et al.* 2010). In the present study, among the Gram–positive cultures tested, *Bacillus subtilis* showed 99 % and 100 % inhibition at 300 µg/mL and 500 µg/mL of ATNP (effective Ag concentrations of 3.5 ppm and 5.85 ppm), respectively. The bactericidal concentration for *Staphylococcus aureus* could not be determined as ATNP was found to be bacteriostatic even at the highest concentration that was feasible for testing (1 mg/mL of ATNP; 11.7 ppm of Ag) and only a 26 % reduction in cell numbers was obtained at this concentration. The decrease of antimicrobial efficiency in medium could be attributed to the presence of dissolved organic matter, counter– and co– ions, which can mask the charge on silver ions and attenuate the effect of electrostatic double layer (EDL) repulsion between like–charged nanoparticles by neutralizing the particle surface charge, thereby leading to aggregation (Jin *et al.* 2010; Mukherjee and Weaver *et al.* 2010).

3.3.2 Detection of silver ions

Silver ion detection was carried out using rhodamine–based fluorogenic and chromogenic probe. The sensing mechanism of the probe is based on irreversible tandem ring opening and closing promoted by Ag^+ coordination to the iodide of the probe, accompanied by both colour change and turn–on type fluorescence (Chatterjee *et al.* 2009). Fluorescence peak of the Ag–iodide complex was obtained at 584 nm indicating the presence of silver ions. For these studies, sample was suspended in aqueous phase and the amount of silver ions released after 1 h was determined. The sample was resuspended in fresh medium and further release of silver ions was monitored. It was observed that after one hour, 15.67 % of silver was present as silver ions in suspension. On resuspending the sample in fresh solution, a further 18.44 % of silver ions were released. This was the maximum amount of silver ion detected and no further increase in the concentration was observed even on incubating for 24 h. Thus, the antimicrobial activity could be attributed to the silver ions released from within the TiO_2 matrix.

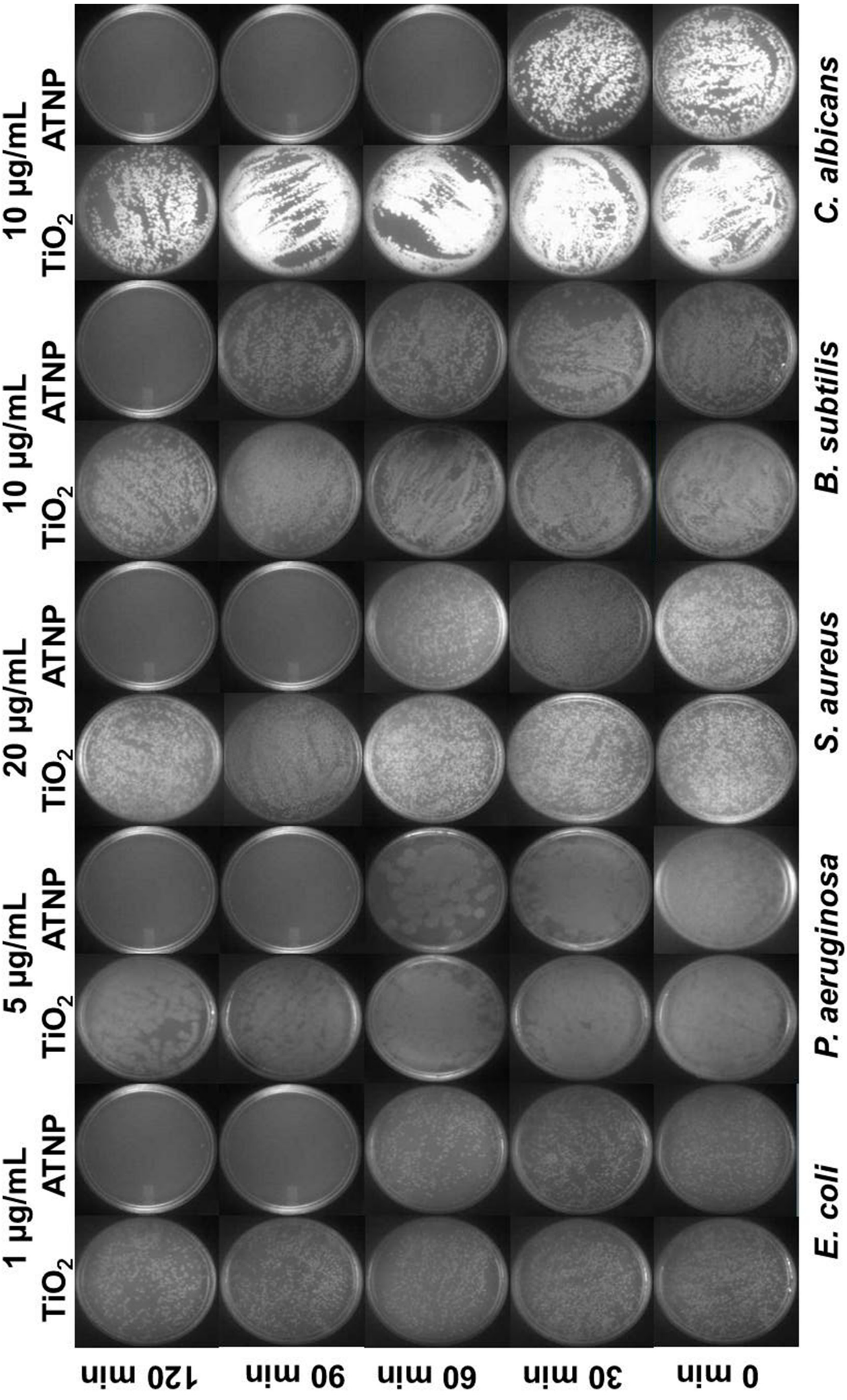

Figure 3.2 Photographs showing the decrease in the number of colony forming units of *E. coli*, *P. aeruginosa*, *S. aureus*, *B. subtilis* and *C. abicans* after exposure to TiO_2 control and ATNP for various time intervals.

3.3.3 ROS detection and antioxidant studies

When silver ions/AgNP come in contact with cells, they attach to the cell wall and disturb the normal physiological functioning of transmembrane proteins, such as channels, porins and/or receptors, consequently interfering with the proton pool in the inter–membrane space or the electron flow through the respiratory chains. Accumulated electrons, due to inhibition of thiol group containing respiratory enzyme(s) like NADH dehydrogenase II, could be transferred to oxygen to form reactive oxygen species (ROS) such as O_2^- and H_2O_2, which lead to oxidative and membrane damage in bacteria (Kim *et al.* 2007; Su *et al.* 2009a; Kumar *et al.* 2010). In addition, ROS can induce apoptotic pathways in bacteria which could ultimately lead to cell death (Kumar *et al.* 2010). In the present study, production of intracellular ROS in cells exposed to ATNP was determined using DCFH–DA which gets converted to DCF, a fluorescent molecule with emission at 526 nm, in the presence of ROS. It was observed that after 30 minutes of contact with ATNP, the levels of intracellular ROS increased 1.55 times as compared to the negative control without ATNP, indicating that ROS was generated and participated in the ATNP mediated cell death. The percentage of intracellular ROS decreased to levels similar to the negative control in the presence of the antioxidant, NAC. Similar observations were recorded by Su *et al.* (2009a) where 40.3 ± 10.2 % of the AgNP/Clay–treated bacteria became DCF+, indicating that ROS was generated.

ROS is neutralized by antioxidants such as NAC and GSH. It was observed that antimicrobial assays carried out in presence of these antioxidants, rendered the ATNP inactive against microorganisms (Figure 3.3 (a) and 3.3 (b)). NAC or GSH alone did not exhibit any antimicrobial activity nor did it enhance cell proliferation. These results suggest that the antimicrobial activity of ATNP nanoparticles is due to the combined effect of release of silver ions and ROS production resulting in membrane damage and/or apoptosis (Jung *et al.* 2008; Liau *et al.* 1997). The small size, large surface area and mesoporous nature of this material further contributes towards the antimicrobial activity. It is proposed that TiO_2 acts as a good supporting, stabilizing and antiaggregating agent facilitating uniform dispersion of silver.

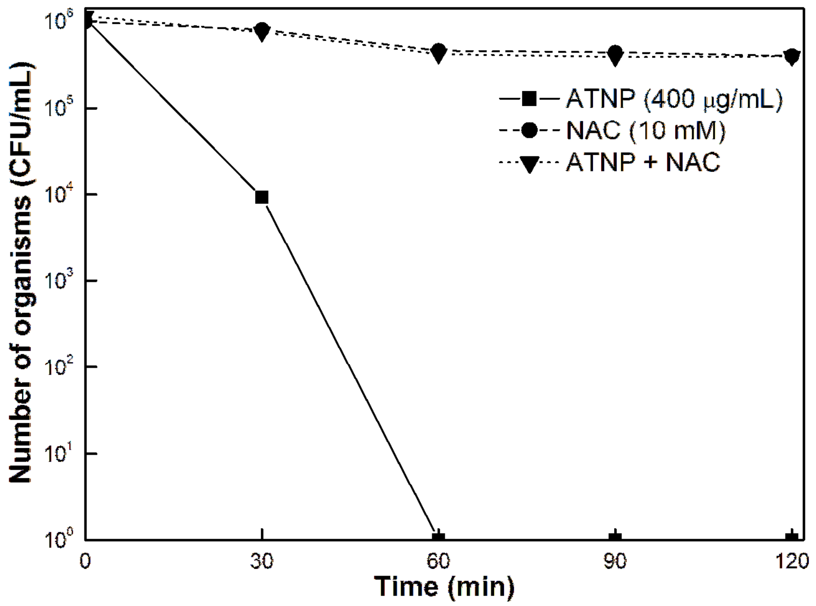

Figure 3.4 (a) Antioxidant study of ATNPs in growth inhibition with/without N acetyl cystein (NAC). Solution devoid of ATNP stands for the control.

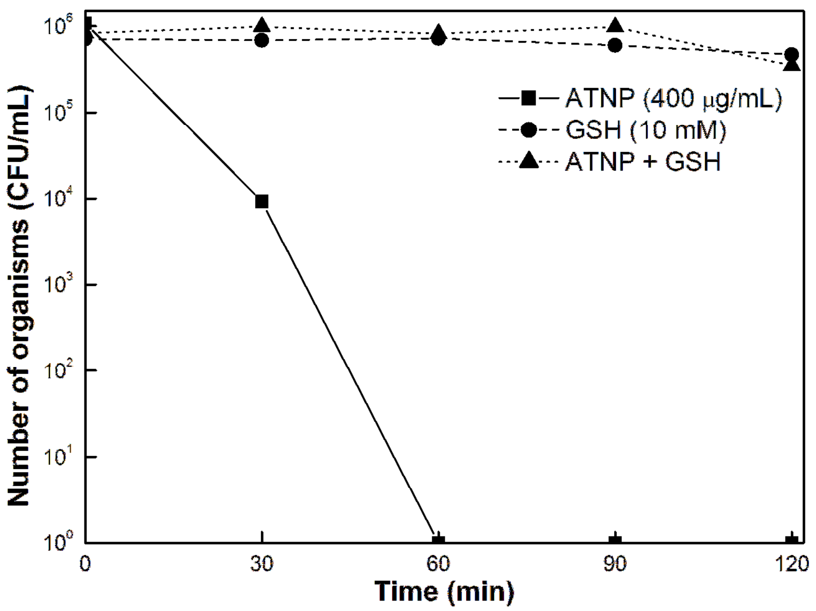

Figure 3.3 (b) Antioxidant study of ATNPs in growth inhibition with/without Glutathione (GSH). Solution devoid of ATNP stands for the control.

3.4 Conclusion

In conclusion, mesoporous ATNPs prepared by a simple sol–gel method have been shown to exhibit highly efficient antimicrobial activity. The antimicrobial activity was achieved at a remarkably low silver concentration in the range of 1–20 µg/mL of ATNP (effective Ag concentration of 11.7–234 ppb) in aqueous phase and 100–1000 µg/mL of ATNP (effective Ag concentration of 1.170–11.7 ppm) in growth medium within two hours of contact. The antimicrobial activity is attributed to the combined effect of release of silver ions and ROS production resulting in membrane damage and cell death. This material has a lot of potential for application as disinfectants/antiseptics in various biomedical and environmental areas.

This work was published as: **Naik, K.**, Chatterjee, A., Prakash, H. and Kowshik, M. Mesoporous TiO_2 nanoparticles containing Ag ion with excellent antimicrobial activity at remarkable low silver concentrations. J. Biomed. Nanotechnol. (2013) 9:664–673. **(Impact factor 7.578)**

CHAPTER 4

Chapter 4: Anti–biofilm Efficacy of Low Temperature Processed AgCl–TiO_2 Nanocomposite Coating

4.1 Introduction

In most natural, clinical and industrial settings, bacteria are predominantly found to be associated with biofilms, a community of microorganisms networked within an exopolysaccharide (EPS) matrix, rather than as planktonic forms (O'Toole and Kolter 1998). Biofilms can be described as the sessile (attached) mode of microbial growth that occurs in close association with surfaces (substrata). Biofilm development follows a sequence of events wherein microbial surface attachment is followed by cell proliferation and matrix production, which then leads to the formation of mature and complex structures. Finally, microbial detachment and dispersion occurs, at which point cells escape from the existing biofilms and colonize new niches (Valappil *et al.* 2007).

Biofilms impact our world in numerous ways. In the natural environment, they benefit us by contributing to nutrient cycling and plant growth by forming symbiotic relationships with plant roots in the rhizosphere. In the industrial environment, they are used in the treatment of water and wastewater, and the detoxification of hazardous waste and groundwater contaminated with petroleum products through bioremediation (Massol–Deya *et al.* 1995). Biofilms are associated with maintaining the health of other organisms through microbiome colonization by providing resistance and helping in gut nutrient sequestration (McBain 2010).

However, they are also detrimental in many ways. Biofilm formation is a matter of concern in areas such as medical settings, water distribution systems and food industries. Biofilm forming organisms are involved in diseases like cystic fibrosis, bacterial endocarditis, otitis media. They are also associated with dental caries, and infections at surgical sites and implants. Their interaction with industrial environment causes bio–fouling, bio–corrosion, and contamination (Chiang *et al.* 2009; McBain 2010).

Biofilms differ from their planktonic counterparts by exhibiting increased resistance to antimicrobial agents. They have been shown to be much more resistant to certain antibiotics as compared to planktonic cells (Smith 2005). This has been attributed to the various mechanisms of resistance exhibited by biofilms such as the failure of antimicrobials to penetrate the biofilm due to presence of EPS, deactivation of antimicrobials on interactions with EPS, slow growth and stress response, heterogeneity, induction of biofilm–specific phenotypes such as multidrug efflux pumps, alteration of membrane protein composition and the presence of persisters (Mah and O'Toole 2001; Lewis 2005). Presently, several approaches in combating biofilms are available. These include methods such as physical and/or mechanical removal, chemical removal, and the use of antimicrobials to kill planktonic cells. However, due to the increasing tolerance of the biofilm community to antibiotics, biocides and mechanical stress, it has become difficult to completely eradicate mature biofilms. Hence, novel and alternative methods of preventing the colonization of surfaces with biofilms are required.

Recently, there has been an interest in the use of silver–based antimicrobial coatings as anti–biofilm agents. Embedding silver into a supporting matrix facilitates a slow and sustained release of silver ions, resulting in a long–term antimicrobial effect (Furno *et al.* 2004). Various materials like silane (Babapour *et al.* 2011; Stobie *et al.* 2008) and palladium (Chiang *et al.* 2009) have been used as supporting matrices for coatings and films containing silver. TiO_2 nanoparticles, being porous and inorganic in nature, exhibit good potential as supporting matrices due to their excellent chemical stability, non–toxicity and biocompatibility. Moreover, nanoparticulate TiO_2 acts as an anti–aggregating agent to facilitate the uniform dispersion of silver (Naik *et al.* 2013; Desai *et al.* 2013; Desai and Kowshik 2013). It also provides stronger washing resistance, which aids in the slow and sustained release of silver ions thus leading to a long–term antimicrobial effect (Wang *et al.* 1998b). In this chapter, we describe the potential of $AgCl–TiO_2$ nanocomposite coating as an inhibitor of biofilm formation.

4.2 Materials and Methods

4.2.1 Synthesis of $AgCl–TiO_2$ nanocomposite coatings

Sol–gel titanium dioxide coatings containing 1 weight % nanosilver were prepared on glass slides. The ATNPs were prepared as described previously in section 2.3.2. The required amount of above powder was suspended in ethanol and sonicated (Microson™ Sonicator) for 15 minutes at 3 rps (revolutions per second) to obtain a uniformly dispersed solution which was then used for coating the slides. Coatings were obtained by suspending 25 µL of $AgCl–TiO_2$ and TiO_2 (control) suspension on a clean glass slide (2 cm × 2.5 cm) and drawing it with another clean slide to spread the solution on the surface producing uniform thin coatings. The films prepared were sterilized by autoclaving and showed no tendency towards delamination from the substrate.

4.2.2 Characterization of AgCl–TiO_2 nanocomposite coatings

X–ray diffraction studies for phase identification of the coatings were carried out using a Rigaku MiniFlex II X–ray diffractometer with monochromatic CuKα radiation (λ=1.5405 A°). The scan range was from 2θ=20° to 80° and the crystallite size, D, was calculated using Scherrer formula: $D=k\lambda/\beta_{1/2}\text{Cos }\theta$, where λ=wavelength of X–ray applied (0.154 nm), k=numerical constant for which the obtained value is 0.9, $\beta_{1/2}$=full width (radians) at half maximum of the anatase (101) peak and θ=Bragg angle for which 2θ is 25.28° (Scherrer 1918; Patterson 1939). Scanning electron microscope (SEM; Jeol JSM–5800LV scanning microscope) was used to study the surface morphology of the coating and estimate its thickness.

4.2.3 *In vitro* biofilm assay

Escherichia coli ATCC 10536 and *S. epidermidis* ATCC 12228 were obtained from National Collection of Industrial Microorganisms (NCIM, Pune, India) and *Pseudomonas aeruginosa* ATCC 25668 from Microbial Type Culture Collection (MTCC, Chandigarh, India). AgCl–TiO_2 coated glass slides and 5 mL of Tris minimal media (composition: 0.5 M Tris, 0.8 M Sodium chloride, 0.2 M Potassium chloride, 0.2 M Amonium chloride, 0.3 M Sodium sulphate, 0.01 M Magnesium chloride, 0.002 M Calcium chloride, 1% Sodium dihydrogen phosphate, 0.5 % Glucose and 0.1 % Tryptone) (Sambrook and Russell 2001) were added to wells of a sterile 6 well plate. Microbial cells in the late logarithmic growth phase were used for all studies. Cells (~ 10^6 cells/mL) of *E. coli, S. epidermidis* and *P. aeruginosa* were added to the wells and the plates were incubated for a period of 10 days at 37 °C under stationary conditions. Uncoated slide and silver–free TiO_2 slide were used as positive and negative controls, respectively. The slides in the wells were observed for the visible inhibition of biofilm formation. Subsequently, the slides were removed and washed with deionized water and tested for biofilm formation using the following protocols. One set of the glass slides were imprinted on nutrient agar plates. The second set was used for enumeration of microorganisms by scraping out the biofilm in sterile saline and determining the number of viable organisms by the plate count method after appropriate dilution. This was done once every 2 days for a period of 10 days. The third set was used to study the morphology of the biofilms using a scanning electron microscope (SEM). For SEM, glass slides were fixed in glutaraldehyde and dehydrated in ascending ethanol solutions ranging from 10 to 100 %. The slides were then sputter coated with gold using SPI 11430 sputter coater and imaged using a Jeol JSM–5800LV model with an accelerating voltage of 20 keV. All the experiments were conducted in triplicates.

4.2.4 Evaluation of silver ion release rates

Evaluation of silver ion release rates was performed to monitor the elution of silver from the coatings. The release of silver ions from the coatings was estimated by atomic absorption spectroscopy (AAS, Unicam, UK, Solar 929). Coated slides were immersed in deionised water and incubated at 37 °C initially for 1 h, followed by 2 h, 1 day, 2 days, 4 days, 6 days, 8 days and 10 days and estimated for amount of silver released by immersion in fresh test fluid respectively.

4.2.5 Cell culture

HaCaT cell lines (human epidermal keratinocyte) were purchased from NCCS, Pune, India and maintained in Dulbecco's Modified Eagle's medium (DMEM) with 10 % fetal bovine serum (FBS) at 37 °C in a humidified atmosphere with 5 % CO_2 and passaged at 70–90 % confluency. HaCaT homogenates were stored by freezing at −80 °C. For reviving the cells, thawing was carried out quickly by partially submerging the vial and shaking it in the 37 °C water bath followed by rinsing the outside of the vial with ethanol and wiping it dry.

4.2.6 Cell viability studies

Cell viability of TiO_2 nanoparticles and ATNPs was evaluated by using MTT (3–[4, 5–dimethylthiazol–2–yl]–2, 5–diphenyltetrazolium bromide) metabolic activity assay. MTT is reduced by metabolically active cells to insoluble purple formazan dye crystals. The rate of tetrazolium reduction is proportional to the rate of cell proliferation. HaCaT cells (2×10^4 cells/mL) were seeded in a 24 well plate at 37 °C for 24 h, and exposed to varying concentrations (20, 50, 75, 100, 125, 150 and 200 µg/mL) of ATNPs and TiO_2 nanoparticle solutions for 24, 48 and 72 h. Cells treated with medium only served as a negative control group. After removing the supernatant of each well and washing twice by PBS, medium with 0.5 mg/mL MTT dye was added and the plates were incubated at

37 °C for 4 h. After incubation, the medium was discarded and the resultant formazan crystals were dissolved in dimethyl sulfoxide (DMSO). The absorbance intensity was measured at 570 nm. All experiments were performed in triplicates, and the relative cell viability (%) was expressed as a percentage relative to the untreated control cells.

4.2.7 Cell adhesion assay

The biocompatibility of ATNP coated slides at concentrations (40, 50, 60, 75, 100, 125, 150 and 200 µg/cm^2), TiO_2 coated slide (control) at 200 µg/cm^2 and uncoated slide (negative control) was evaluated using well characterized HaCaT cell line. All coated slides were sterilized by autoclaving at 121 °C for 15 minutes, and placed in 6 well tissue culture plates. The plates were inoculated with 2×10^4cells/ml in 2 ml of complete medium (90 % DMEM and 10 % FBS) and allowed to grow in standard cell culture conditions for 24 h and 48 h. After the prescribed time, non–adherent cells were removed by rinsing two times with PBS, and adherent cells were observed under inverted microscope (Nikon Eclipse TS100).

4.3 Results and Discussion

4.3.1 Characterization of $AgCl–TiO_2$ nanocomposite coating The XRD analysis of $AgCl–TiO_2$ (Figure 4.1 (b)) and TiO_2 (Figure 4.1 (a)) control coated slides exhibited diffraction peaks at 2θ=25.28°, 37.79°, 48.04°, 53.88°, 55.05°, 62.68° corresponding to (101), (004), (200), (105), (211), (204) crystal planes, respectively, conforming to anatase TiO_2 (JCPDS No. 21–1272). The $AgCl–TiO_2$ coating exhibited additional diffraction peaks at 2θ=27.8, 32.2, 46.2, 57.5° corresponding to (111), (200), (220) and (222) planes of AgCl crystals, (JCPDS file: 31–1238) indicating that AgCl is well compounded into the films of TiO_2. The crystallite size was calculated for (101) plane of anatase TiO_2 using Scherrer formula and was found to be 3.7 nm.

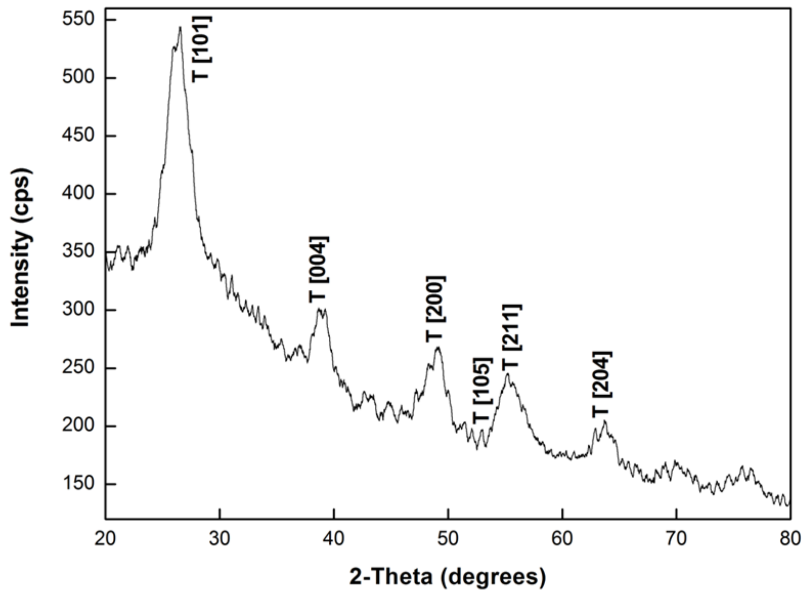

Figure 4.1 (a) XRD pattern of TiO$_2$ coating showing anatase as the predominant crystalline phase, where: T–anatase TiO$_2$.

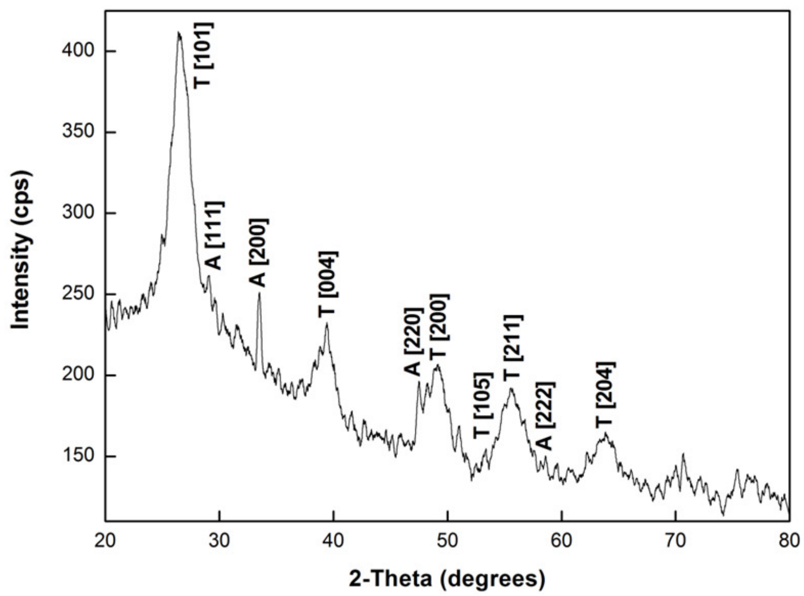

Figure 4.1 (b) XRD pattern of AgCl–TiO$_2$ coating showing peaks corresponding to crystal planes of AgCl in addition to TiO$_2$, where: T–anatase TiO$_2$ and A–AgCl.

The surface morphology and thickness of AgCl–TiO$_2$ nanocomposite coatings was examined by SEM. Figure 4.2 (a) shows the SEM image of the TiO$_2$ and Figure 4.2 (b) of AgCl–TiO$_2$ nanocomposite coating. In both the cases, the particles were of even size and were uniformly dispersed and the coating had a thickness of 30 µm (Figure 4.2 (c)). Similar surface morphology of films was observed for nanosilver embedded silane coating (Babapour *et al.* 2011) and Ag–TiO_2 nanoparticle co–doped SiO_2 films (Mukhopadhyay *et al.* 2010). Silver embedded inside similar films have been reported to exist close to the surface, as low temperature processing retains silver in the upper layers of the coating (Babapour *et al.* 2011; Stobie *et al.* 2008). As the radius of silver ions (ca. 126 pm) is much larger than that of Ti^{4+} (ca. 68 pm), the silver ions introduced by the sol–gel process do not enter the lattice of the TiO_2 anatase phase and have been reported to exist on the surface of the anatase grains by forming Ag–O–Ti bonds (Yu *et al.* 2011).

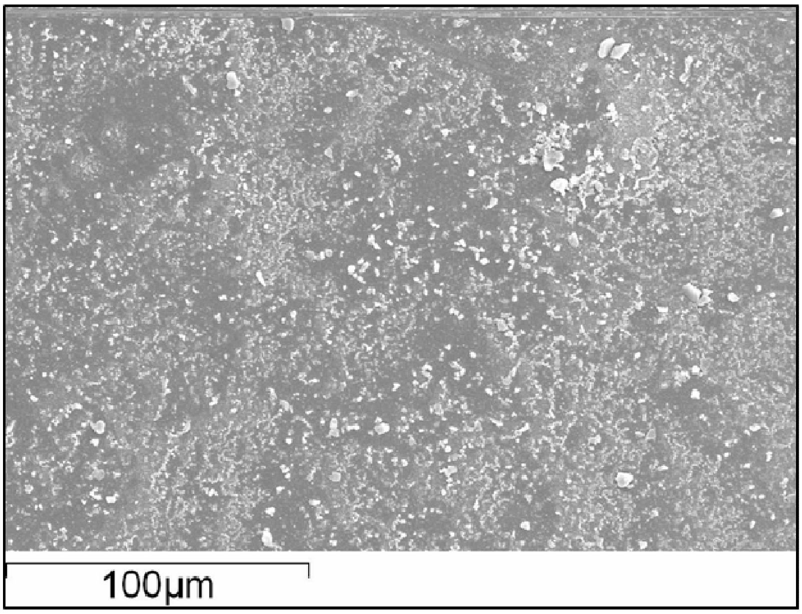

Figure 4.2 (a) SEM micrograph of TiO_2 coated glass slide**.**

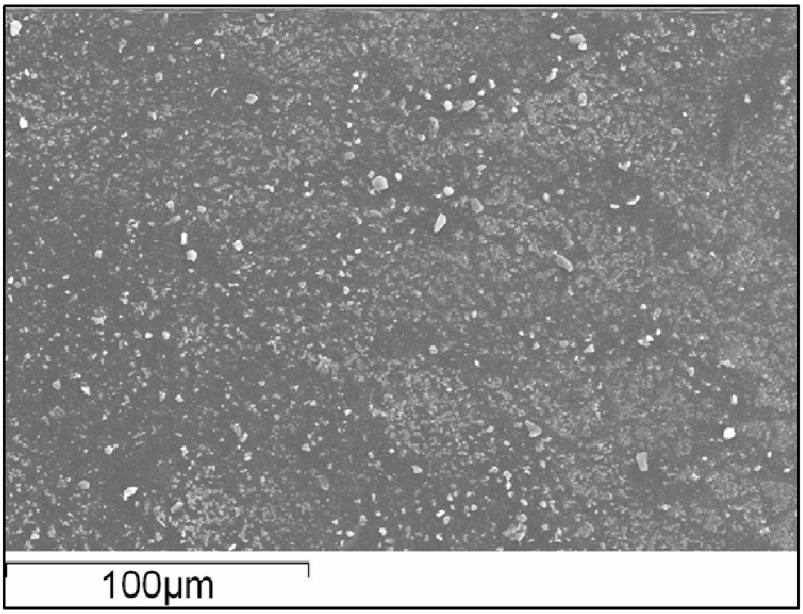

Figure 4.2 (b) SEM micrograph of AgCl–TiO_2 coated glass slide.

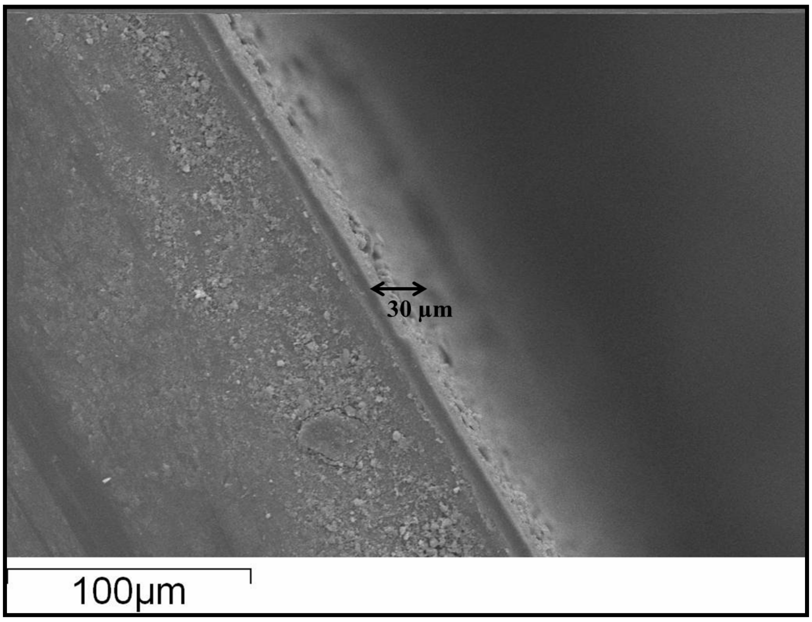

Figure 4.2 (c) SEM micrograph of the cross–sectional morphology of AgCl–TiO_2 coated glass slide.

4.3.2 *In vitro* biofilm assay

In vitro biofilm assay with *E. coli* (Figure 4.3 A and Figure 4.4 (a)) and *S. epidermidis* (Figure 4.3 B and Figure 4.4 (b)) showed that AgCl–TiO_2 nanocomposite coated surfaces inhibited the development of biofilm over a period of 10 days. At an AgCl–TiO_2 concentration of 100 µg/cm^2 (effective Ag concentration of 1.17 µg/cm^2) and incubation of 10 days, inhibition of biofilm was observed in the well and a few isolated colonies were obtained after imprinting the slides on nutrient agar plate. No growth on nutrient agar plates imprinted with slides was observed at an AgCl–TiO_2 concentration of 125 µg/cm^2 (effective Ag concentration of 1.46 µg/cm^2) indicating the complete inhibition of both, biofilm as well as isolated cells. However, in case of *P. aeruginosa* (Figure 4.3 C and Figure 4.4 (c)), at an AgCl–TiO_2 concentration of 125 µg/cm^2 (effective Ag concentration of 1.46 µg/cm^2) although there was no biofilm formation, the growth of a few isolated colonies after imprinting the slides was noted. The complete inhibition of biofilm formation and of isolated cells was obtained at 500 µg/cm^2 of AgCl–TiO_2 (effective Ag concentration of 5.85 µg/cm^2). Scanning electron micrographs of AgCl–TiO_2 coated slides showing the inhibition of biofilm formation at a concentration of 125 µg/cm^2 (effective Ag concentration of 1.46 µg/cm^2) for *E. coli* and *S. epidermidis* and 500 µg/cm^2 (effective Ag concentration of 5.85 µg/cm^2) for *P. aeruginosa* cells after 10 days of immersion in Tris minimal media are depicted in

Figure 4.5. It was observed that the biofilms of the bacteria were completely established on the surface of the coatings with no silver content (pure TiO_2 control), while the surface containing silver completely prevented the biofilm formation. Antimicrobial activity of AgCl–TiO_2 nanoparticles on planktonic microbial cells was achieved at a very low AgCl–TiO_2 concentration, in the range of 1.0 to 20 µg/mL (effective Ag concentrations were 11.7 to 234 ppb) in less than 2 h under ambient conditions (Naik *et al.* 2013).

The higher resistance of *Pseudomonas aeruginosa* towards AgCl–TiO_2 may be attributed to the production of catalase, which plays a protective role in case of oxidative damage (Elkins *et al.* 1999). Moreover, as compared to *E. coli* and *S. epidermidis,* it is known to form thicker biofilms due to the production of a thick extracellular matrix and its ability to display hyper–adhesive phenotypes (Sadovskaya *et al.* 2010). The high frequency appearance of antibiotic–resistant phenotypic variants with enhanced ability to form biofilms (Drenkard and Ausubel 2002) and the presence of extracellular DNA in the matrix have also been associated with the resistance of biofilms in this organism (Mulcahy *et al.* 2008). The extracellular DNA in the biofilm matrix is usually derived from lysed cells. However, some bacteria, including *P. aeruginosa*, produce substantial quantities of extracellular DNA through a mechanism that is thought to be independent of cellular lysis and appears to involve the release of small vesicles from the outer membrane. Extracellular DNA is required not only for the initiation of biofilm formation but also for the stabilization of biofilms (Whitchurch *et al.* 2002; Muto and Goto 1986; Kadurugamuwa and Beveridge 1995). This extracellular DNA might contribute towards the biofilm resistance by chelation of silver ions by the DNA.

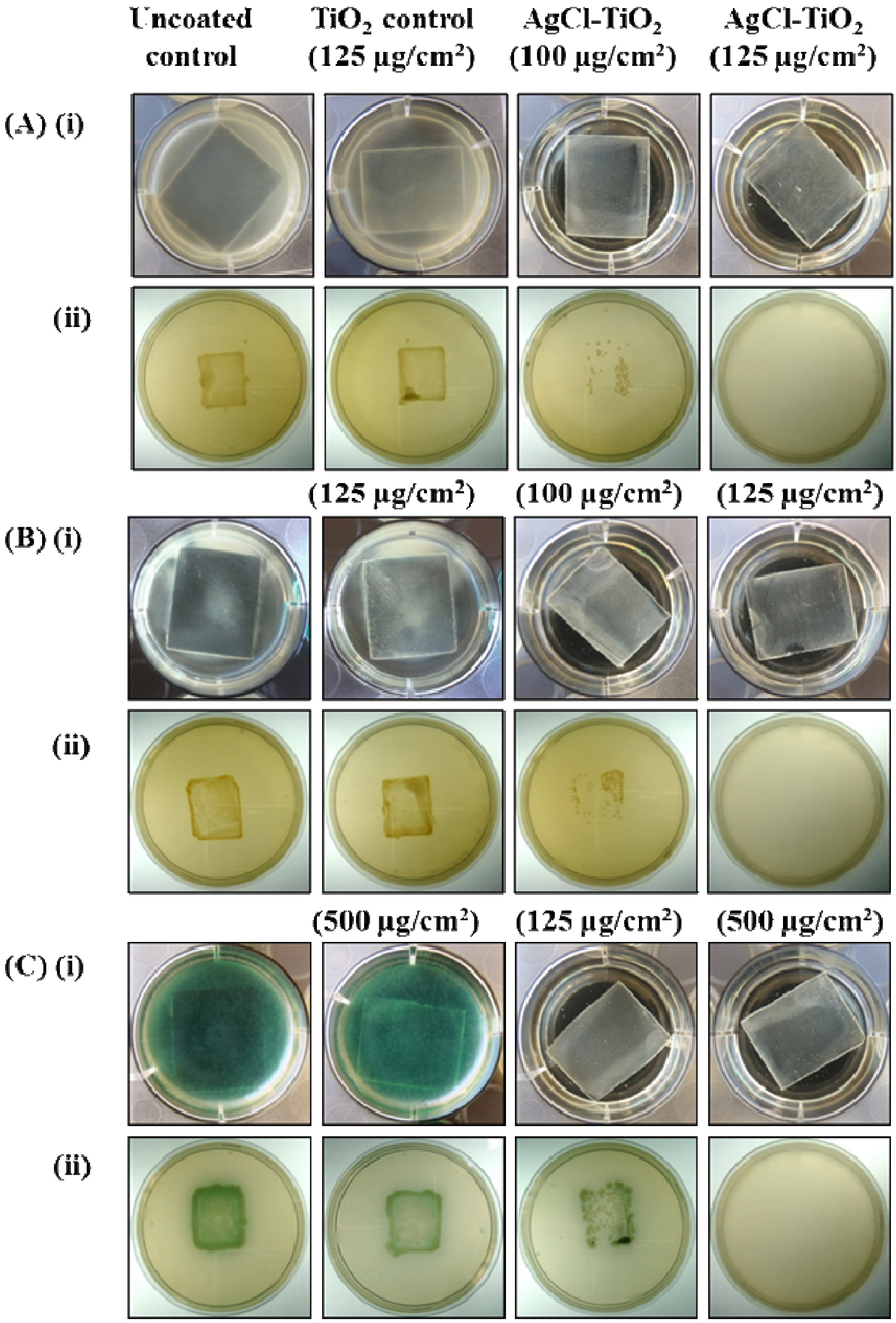

Figure 4.3 (i) Photographs showing inhibition of biofilm formation for (A) *E. coli*, (B) *S. epidermidis* and (C) *P. aeruginosa* after 10 days of incubation at 37 °C on glass slides coated with various concentrations of AgCl–TiO_2. (ii) Photographs of these glass slides imprinted on nutrient agar plates.

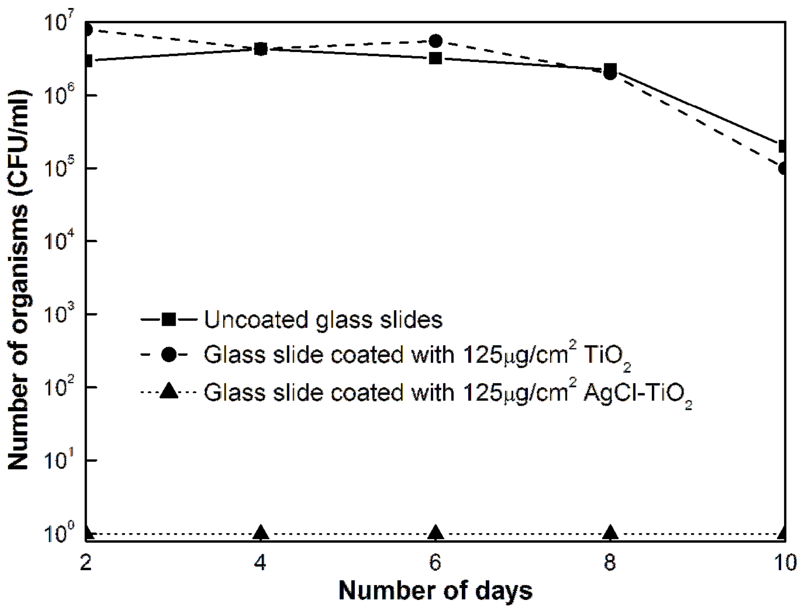

Figure 4.4 (a) Graph showing log number of *E. coli* cells with respect to time of incubation on AgCl–TiO_2 and TiO_2 (control) coated glass slides.

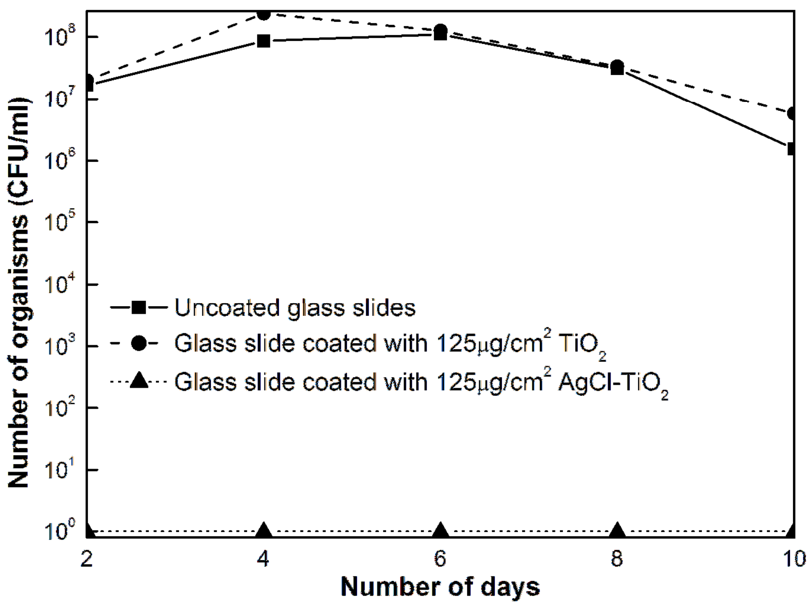

Figure 4.4 (b) Graph showing log number of *S. epidermidis* cells with respect to time of incubation on AgCl–TiO_2 and TiO_2 (control) coated glass slides.

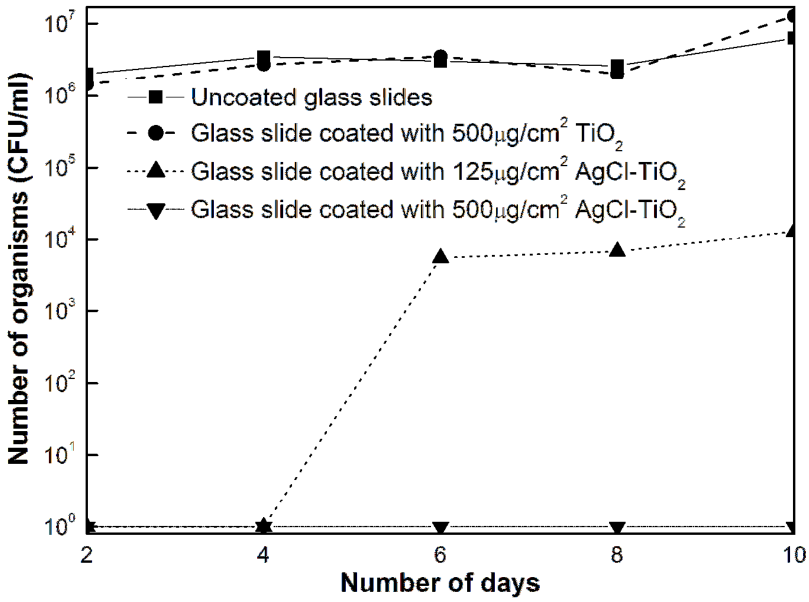

Figure 4.4 (c) Graph showing log number of *P. aeruginosa* cells with respect to time of incubation on AgCl–TiO_2 and TiO_2 (control) coated glass slides.

The anti–biofilm efficacy of the AgCl–TiO_2 coatings could be attributed to the release of silver ions, which prevent the initial bacterial adhesion required for biofilm formation. A study on the effect of silver ions on disruption of intermolecular forces within the *S. epidermidis* biofilm matrix using atomic force microscopy, has demonstrated that silver ions lead to destabilization of the biofilm structure by binding to electron donor groups of biological molecules and reducing the number of binding sites for hydrogen bonding and electrostatic and hydrophobic interactions (Chaw *et al.* 2005). This study investigating the use of silver ions for disruption of a biofilm structure is very significant in devising novel and efficient strategies to eliminate biofilms.

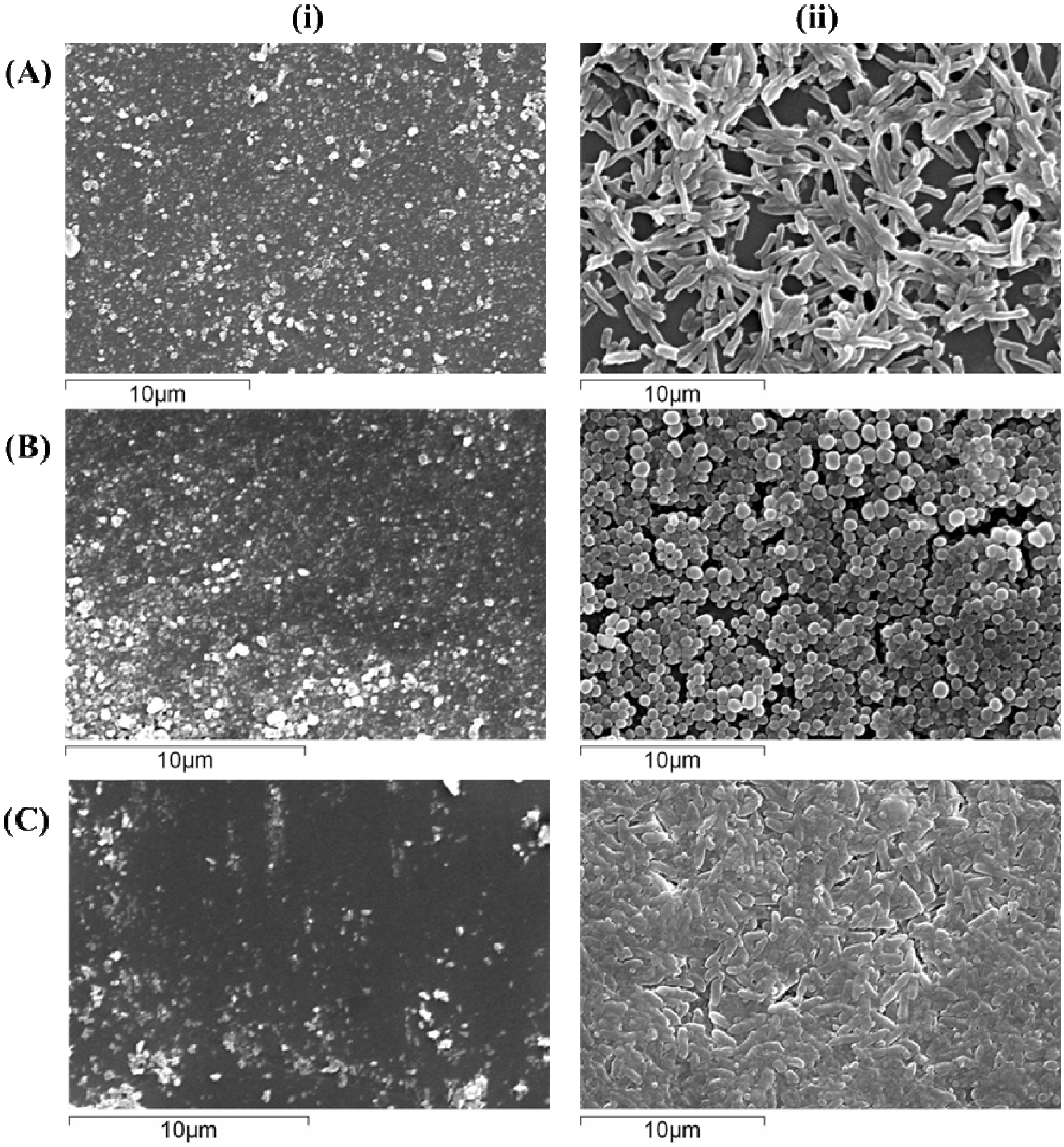

Figure 4.5 SEM micrographs showing (i) inhibition of biofilm formation on AgCl–TiO_2 coated glass slides for (A) *E. coli* (B) *S. epidermidis* and (C) *P. aeruginosa* cultures. TiO_2 controls with completely established biofilms of these cultures are shown in (ii).

Biologically synthesized silver nanoparticles (Kalishwaralal *et al.* 2010) and starch–stabilized silver nanoparticles (Mohanty *et al.* 2012) have been reported to demonstrate anti–biofilm activity for a period of 24 to 48 h. Several other anti–biofilm studies of biogenic silver nanoparticle coated medical devices (Namasivayam *et al.* 2013), silver nanoparticle incorporated PU (Polyurethane), PCLm (Polycaprolactam), PC (Polycarbonate) and PMMA (Polymethylmethaacrylate) nanocomposites (Sawant *et al.* 2013) and other silver nanoparticles (Martinez–Gutierrez *et al.* 2013; Gurunathan *et al.* 2014) have been recently reported. However, in order to obtain the long–term inhibition of biofilm formation, it has been suggested that silver be embedded in a support matrix, to facilitate a slow and sustained release of silver ions. Silane based nanocomposites have been investigated as hosts for silver containing anti–biofilm materials. Such nanocomposite films exhibit very high loading of silver nanoparticles near the surface of the film and desired silver release rate over prolonged periods of time can be achieved (Babapour *et al.* 2011; Stobie *et al.* 2008). Though silver containing TiO_2 nanoparticles have been extensively synthesized and studied for their antimicrobial activity, they have not been exploited for their anti–biofilm potential.

4.3.3 Evaluation of silver ion release rates

The concentration of silver ions released from the AgCl–TiO_2 nanocomposite coatings was estimated to study the silver release kinetics. Figure 4.6 shows the release rates of silver in deionized water with respect to time. The amount of silver ions released increased from 0.17 µg/mL in the first hour to 1.94 µg/mL in the second hour, beyond which there was a steady release of around 0.3 to 0.4 µg/mL. For an antimicrobial/anti–biofilm agent to be effective, initial high release of the agent is favourable for rapid killing of the bacterial cells so that they do not develop resistance (Brett 2006). Subsequently, a sustained and stable release of silver ions over longer periods of time helps in maintaining the long–term antimicrobial effect. Such a tendency of silver to release from nanocomposites is contrary to the bulk silver based materials, which exhibit initial minimum release followed by a rapid release (Kumar and Münstedt 2005).

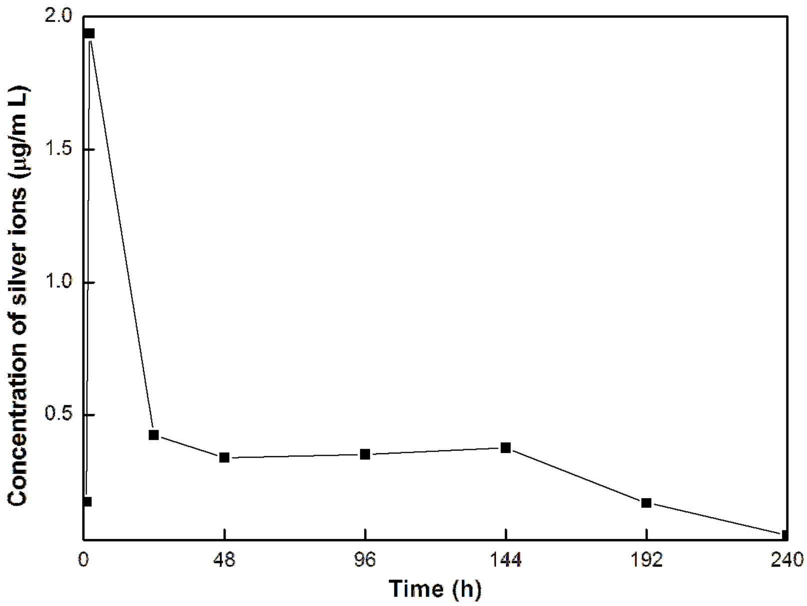

Figure 4.6 Release rates of silver ions from AgCl–TiO$_2$ coatings as determined by AAS.

Release behaviour of silver ions from the supporting matrix is controlled by the water diffusion characteristics on that matrix. The distinctive behaviour of silver ion release kinetics between the nanoparticulate and bulk composites occurs due to the differences in structures which influence water diffusion behaviour (Liu *et al.* 2008). In the initial stages the dissolution of silver particles at the surface dominates the release behaviour where no diffusion step is required. However with increasing immersion time, transport of silver ions from the interior to the surface becomes more important as the contribution of surface silver particles to the silver release decreases due to faster consumption as compared to the particles present in the bulk. Thus, the silver ion release becomes governed by diffusion because most of the silver ions to be released must move from the interior to the surface of the sample (Damm and Münstedt 2008; Hahn *et al.* 2011). In case of mesoporous composites, fast water diffusion on the outer surface induces significant increase in the initial amount of silver ions released, which is followed by a decrease in release rate due to slow diffusion of water in the pores of TiO$_2$ matrix (Liu *et al.* 2008). In addition, the silver release kinetics is also influenced by the concentration of silver on the surface and the crystallinity of the material, which in turn are dependent on the temperature of synthesis (Babapour *et al.* 2011).

The use of high temperature during processing of materials leads to an increase in crystallinity, causing reduction in silver release kinetics due to the retardation of water diffusion rate in the matrix and increased permeation barrier affecting the rate of migration of silver ions within the material (Kumar and Münstedt 2005). Moreover, at high temperatures, the majority of the silver ions migrate into the bulk of the matrix, i.e. away from the surface of films because silver particles get oxidized and eventually diffuse away from the surface (Li *et al.* 2003; Akhavan and Ghaderi 2009). In addition, high temperature also leads to aggregation of silver particles on the surface of the film, forming larger particles that are unable to permeate the cells (Babapour *et al.* 2011).

A reduction in available surface silver ions is undesirable, as an initial high release of antimicrobial agent is very important for preventing microbial attachment (Babapour *et al.* 2011; Stobie *et al.* 2008). In the present study, since the AgCl–TiO_2 nanocomposites have been synthesized using a low temperature based sol–gel method; most of the silver nanoparticles are expected to be localized on the surface.

4.3.4 Cell viability studies

The dose and time dependent cytotoxicity studies of TiO_2 nanoparticles and ATNPs with HaCaT cell lines were carried out using the MTT assay. All the samples were tested in the concentration range of 20–200 µg/mL for time intervals of 24, 48 and 72 hours (Figure 4.7 (a) and (b)). The viability of untreated cells was considered to be 100 %. There were no significant difference between the cell viability of ATNP samples and the TiO_2 controls at all the concentrations tested and they did not exhibit any cytotoxic effect on HaCaT cell lines up to 150 µg/mL of concentration.

4.3.5 Cell adhesion assay

Since the present work is also aimed at the development of ATNP coatings with anti–biofilm properties for biomedical applications, biocompatibility of this material is an important property that needs to be studied. In this study, HaCaT cells were cultured on the ATNP coated slides and their morphology was observed under an inverted microscope. Figure 4.8 shows the comparative study of cell morphology after 24 h and 48 h. HaCaT cell morphology on ATNP coatings was similar to the cell morphology on uncoated control. Cells were healthy and adhered with good spreading up to a concentration of 125 µg/cm^2. Similar observations of good cell adherence and spreading have been reported for silver coated materials such as silver coated stainless steel at non cytotoxic concentrations (Bosetti *et al.* 2002).

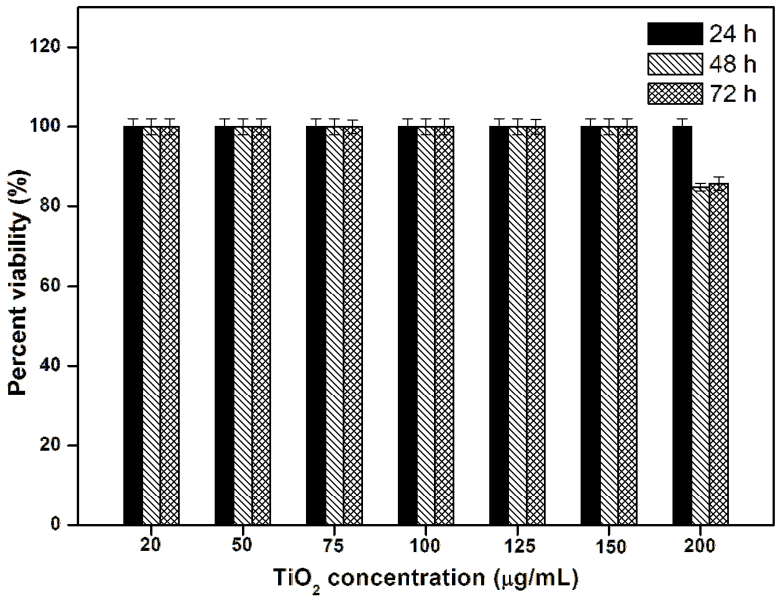

Figure 4.7 (a) Cell viability study of TiO_2 nanoparticles using HaCaT cells.

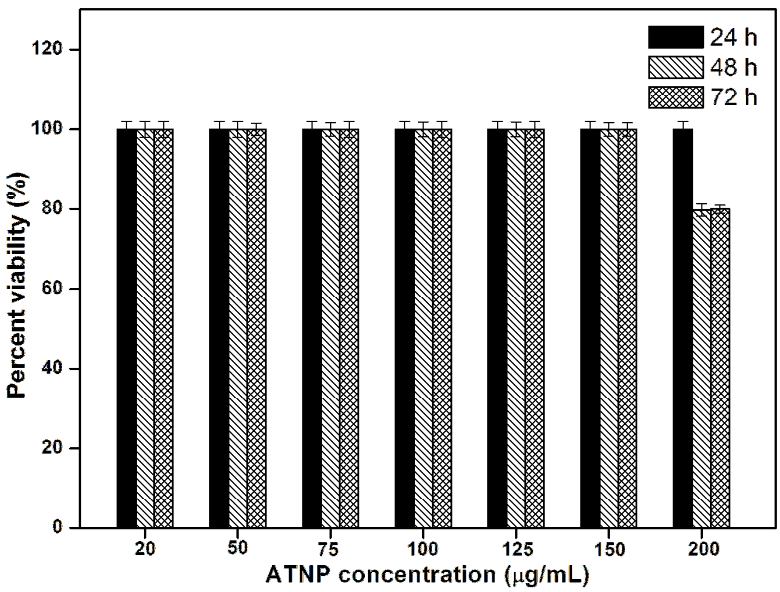

Figure 4.7 (b) Cell viability study of ATNPs using HaCaT cells.

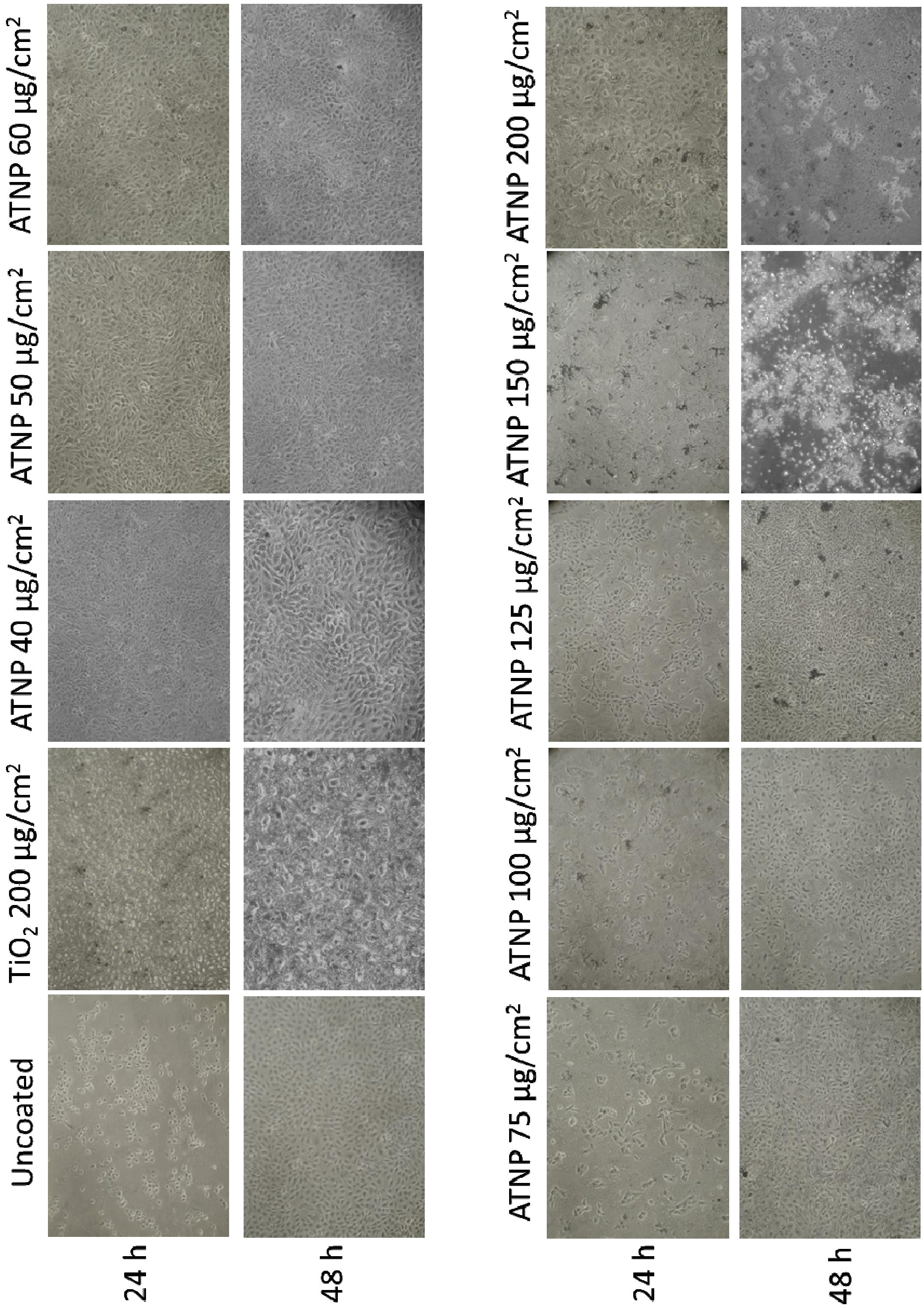

Figure 4.8 Images of HaCaT cell line incubated for 24 h and 48 h on ATNP coated glass slides.

4.4 Conclusion

Alternative methods of preventing the colonization of surfaces with biofilms are required due to the problems associated with conventional antimicrobial therapies to treat biofilms. In this work, the use of sol–gel based AgCl–TiO_2 coatings with bioactive silver has been proposed as a promising strategy for controlling biofilm formation. Low temperature processed AgCl–TiO_2 coatings synthesized using sol–gel method were found to be very effective in preventing biofilm formation by *E. coli*, *S. epidermidis* and *P. aeruginosa* over a period of 10 days. These coatings released an initial high amount of silver ions followed by a slow and gradual release facilitating sustained anti–biofilm activity. The initial high release of silver ions is beneficial for reducing bacterial adhesion, which is the first step in the development of a biofilm. To the best of our knowledge, silver containing TiO_2 nanocomposites have not been studied for their anti–biofilm efficiency. This is the first report of anti–biofilm activity of AgCl–TiO_2 nanocomposites where TiO_2 is used as a supporting matrix. As these coatings are very effective in controlling biofilm formation, they could find application in medical implants, medical equipment, water distribution systems, food production facilities or places where appropriate cleaning practices are required.

This work was published as: **Naik, K.** and Kowshik, M. Anti–biofilm efficacy of low temperature processed AgCl–TiO_2 nanocomposite coating. Mater. Sci. Eng. C (2014) 34:62–68. **(Impact factor 3.076)**

CHAPTER 5

Chapter 5: Anti–quorum Sensing Activity of AgCl–TiO_2 Nanoparticles with Potential Use as Active Food Packaging Material

5.1 Introduction

Food spoilage is a major problem and excessive amounts of food are lost due to microbial spoilage and/or contamination of food with human pathogens (Alvarez *et al.* 2012). The use of proper packaging technology can minimize food losses and provide safe and non–toxic food products. Lately, the potential of nanotechnology has influenced the food packaging industry to a great extent. It is being used for development of packaging with improved properties such as flexibility, gas barrier properties, temperature, and moisture stability. Further, incorporation of active antimicrobial or oxygen scavenging agents and intelligent nanosensors for monitoring the condition of food are expected to provide advanced packaging solutions (Emamifar 2011; Silvestre *et al.* 2011).

Bacterial spoilage of some food products is influenced by quorum sensing (QS) – a process through which bacteria communicate with each other. Understanding the role of QS in food microbial ecology could lead to the development of novel food preservatives that can specifically block quorum sensing systems and control food spoilage (Rasch *et al.* 2005; Skandamis and Nychas 2012). Quorum sensing was first reported in 1970s in a marine luminescent bacterium *Vibrio fischeri*, a facultative symbiont of marine animals like marine fishes and squids (Nealson *et al.* 1970). It was observed that these bacteria did not luminesce until they reached a high population density which led to the finding that bioluminescence in these organisms is regulated by AHL (N–acyl homoserine lactone) mediated population density dependent signalling which was later on termed as quorum sensing (Eberhard *et al.* 1981). Interruption of bacterial quorum sensing has broad application in biological control of disease causing organisms as many important animal and plant pathogens use quorum sensing to regulate virulence (Alvarez *et al.* 2012). Its importance in reduction or prevention of food spoilage reactions and in maintaining the product quality and safety is being actively investigated (Bruhn *et al.* 2004; Ammor *et al.* 2008; Alvarez *et al.* 2012; Skandamis and Nychas 2012).

Bacteria communicate and coordinate their behaviour by monitoring the environment using certain chemical signalling molecules called autoinducers so named as they function in part to stimulate their own synthesis. The concentration of these signalling molecules is directly proportional to the population density of bacteria. Once a critical threshold concentration has been reached, that is, when bacteria have a quorum, they switch on the transcription of quorum sensing dependent genes to change their behaviour. These signals are responsible for regulating various phenotypic and physiological characteristics including regulation of pectinase, protease, and cellulose activities and siderophore–mediated iron chelation, characteristics associated with food spoilage (Rasch *et al*. 2005). It is also associated with production of violacein pigment in *Chromobacterium violaceum*, virulence in *Pseudomonas aeruginosa*, flagellar motility in *Proteus mirabilis* and *Serratia marcescens*, bioluminescence in *Vibrio harveyi* and *Vibrio fischeri*, sporulation, cell differentiation and community organization which lead to the development of the mature biofilms (Sauer *et al*. 2002; Packiavathy *et al*. 2012). Quorum sensing occurs across both Gram–positive as well as Gram–negative bacteria in many species. Three major types of autoinducers have been recognized: acylated homoserine lactones (AHLs) in Gram–negative bacteria, autoinducing peptides (AIPs) in Gram–positive bacteria and autoinducer–2 (AI–2s) molecules in both Gram–positive and Gram–negative bacteria (Raffa *et al*. 2005).

Several studies have linked QS to biofilm formation in food related bacteria. Quorum sensing system appears to be involved in all phases of biofilm formation regulating the population density and the metabolic activity within the mature biofilm so as to fit the nutritional demands and resources available (Skandamis and Nychas 2012). Biofilms formed on stainless steel surfaces in food–processing environments need special attention because of their potential to act as chronic sources of microbial contamination, leading to food spoilage and transmission of diseases (Brooks and Flint 2008). Although bacteria are capable of existing in planktonic form, it is advantageous under certain circumstances for them to attain a biofilm phenotype. Biofilms provide protection to bacteria in a destructive environment and also help in holding nutrients for their inhabitants. Biofilms are much more resistant to antibiotics, biocides, heavy metals, antimicrobials and cleaning agents as compared to their planktonic counterparts. As a result, it has become extremely difficult to eradicate these biofilms from food processing equipment and environment (Rasmussen and Givskov 2006; Skandamis and Nychas 2012).

The study of quorum sensing inhibitors is emerging as one of the most attractive area of research in the field of anti–biofilm agents. Compounds that inhibit or interfere with quorum sensing have become significant as novel class of next generation antimicrobial and anti–biofilm agents, since they are key players in regulation of virulence and formation of tolerant biofilms (Persson *et al*. 2005). Additionally, unlike conventional antibiotics which prevent bacterial cell division (bacteriostatic) or kill the cell (bactericidal) and increase the selective pressure towards antibiotic resistance, the development of resistance to anti–QS compounds is minimum as they only target virulence mechanisms and do not impede growth (Hentzer and Givskov 2003; Njoroge and Sperandio 2009).

Silver nanoparticles are increasingly being used in food storage containers, wound dressings (Fong and Wood 2006), catheters (Samuel and Guggenbichler 2004), textiles, and various household and personal care consumer products due to their antimicrobial activity (Xiu *et al*. 2011). However, the anti–QS activity of this traditionally used bioactive agent with potential in food preservation has not yet been explored. In the present chapter the anti–QS activity of silver entrapped in a titanium dioxide (TiO_2) matrix has been evaluated. TiO_2 is non–toxic and has been approved by American Food and Drug Administration (FDA) for use in human food and food contact materials. Functionalization or entrapment of silver in a suitable matrix like TiO_2 facilitates controlled release of silver ions over a prolonged time period thereby achieving activity at a very low silver concentration.

In this study we investigated the anti–QS property of AgCl–TiO_2 nanoparticles (ATNPs) for potential use as active food packaging material; using *C. violaceum* strain as indicator of anti–QS activity. These ATNPs could find potential applications as active food packaging materials at much lower concentrations of silver, than required for antimicrobial activity.

5.2 Materials and Methods

5.2.1 Strain and culture conditions

Chrobacterium violaceum ATCC 12472 wild–type strain obtained from Microbial Type Culture Collection (MTCC, Chandigarh, India) was used to determine anti–QS activity of ATNPs. This strain is recommended for screening of anti–QS materials as it produces and responds to autoinducer molecule AHL. This bacteriological monitor system provides a phenotypic response by production of a violet coloured pigment known as violacein when induced by the presence of AHL in the extracellular environment (Alvarez *et al*. 2012). The bacteria were routinely grown aerobically in nutrient broth (NB) (Himedia) and incubated at 37 °C for 24 h. The Quorum sensing inhibition assay was performed in NB as well as modified Tris minimal media (composition: 0.5M Tris, 0.8M Sodium chloride, 0.2M Potassium chloride, 0.2M Amonium chloride, 0.3M Sodium sulphate, 0.01M Magnesium chloride, 0.002M Calcium chloride, 1% Sodium dihydrogen phosphate, 1 % Glucose and 0.5 % Tryptone) (Sambrook and Russell 2001) for testing the anti–biofilm potential. All the experiments were carried out in triplicates on different days.

5.2.2 Qualitative evaluation of anti–QS activity using disc diffusion assay

The ability of ATNPs to inhibit the violacein pigment production by *C. violaceum* was studied by qualitative screening using zone of inhibition test. The disc diffusion method given by Bauer *et al*. (1966) was used to test anti–QS activity of ATNPs. Sterile discs (6 mm diameter) were impregnated with different concentrations (100, 200, 300, 400 and 500 µg) of ATNPs. TiO_2 without silver (500 µg) was used as the control. These discs containing the test material were placed on nutrient agar plates which were uniformly spread plated with 10^6 CFU/mL (Set A) and 10^9 CFU/mL (Set B) of logarithmic phase cells. The plates were incubated at 37 °C for 24 h to check the inhibition of pigment production around the disc. The anti–QS activity at various concentrations was assessed by measuring the diameter of the halos formed due to inhibition of pigment production as per Ponce *et al*. (2003): "not sensitive" for diameter less than 8 mm, "sensitive" for diameter between 9 and 14 mm, "very sensitive" for diameter between 15 and 19 mm, and "extremely sensitive" for diameter larger than 20 mm (Ponce *et al*. 2003; Alvarez *et al*. 2012).

5.2.3 Quantitative QS inhibition assay to measure inhibition of violacein production

Quantification of anti–QS activity of ATNPs on violacein production by *C. violaceum* was carried out using the flask–incubation assay (Alvarez *et al*. 2012). Late logarithmic phase cells (10^6 cells/mL) were inoculated in Erlenmeyer flasks containing growth media supplemented with different concentrations of ATNPs. Two different growth media were used; (i) nutrient broth containing 0, 50, 75, 100, 200 and 300 µg/mL of ATNPs and (ii) modified Tris minimal medium containing 0, 10, 20, 25, 50 and 75 µg/mL of ATNPs. Media containing 0 µg/mL of ATNPs served as controls. The flasks were incubated on a shaker at 37 °C; 110 rpm for 24 h.

In order to confirm that the inhibition of pigment production was due to anti–QS activity and not a result of bacterial growth inhibition, the test medium after 24 h of growth was streaked on nutrient agar plates which were incubated at 37 °C for 24 h and observed for growth. The quantification of the violacein production was carried out as per the protocol described by Choo *et al*. (2006), where 2 mL of culture medium from each flask was centrifuged at 15,000 g for 10 minutes to precipitate the cells. The cell pellet was solubilized in 2 mL of DMSO (dimethyl sulfoxide), vortexed to extract the intracellular violacein, and centrifuged at 15,000 g for 10 minutes to separate the cells. Absorbance of the supernatant containing violacein was measured at a wavelength of 585 nm using an UV–Visible spectrophotometer (Shimadzu UV–2450). DMSO was used as the blank. The percent inhibition in violacein production was calculated by using the formula, Percent inhibition in violacein production = (control $OD_{585\ nm}$ – test $OD_{585\ nm}$ / control $OD_{585\ nm}$) × 100, where OD is the optical density (Packiavathy *et al.* 2012).

5.2.4 Extraction of AHL from culture supernatants

Chromobacterium violaceum was grown to maximum pigment production phase with 100 µg/mL of ATNPs. Culture grown in the absence of ATNPs served as positive control. Cell free supernatants were obtained by centrifugation at 15000 g for 10 minutes at 4 °C, followed by filtration through 0.2 µm filter. The AHL molecules were extracted from the filtrate by adding an equal volume of ethyl acetate containing 0.1 mL/L glacial acetic acid and shaking for 5 minutes. The extracts were evaporated to dryness using rotary evaporator at 40 °C. The residue was dissolved in minimum amounts of ethyl acetate and stored at –80 °C.

5.2.5 Chemical characterization of AHL

The ethyl acetate extracts (100 µL) of culture supernatant were evaporated in vacuo. The Infrared absorption spectra of the powder obtained after vacuum evaporation was measured using a FTIR Shimadzu IR Affinity–1 spectrometer in the 400–4000 cm^{-1} frequency range, using KBr as the reference. The results are presented as normalized Kubelka–Munk plots.

For HPLC analysis the vacuum evaporated extracts were redissolved in 500 µL methanol. 100 µL of methanol extract was injected into a 250 mm × 4.5 mm, 5 µm phenomenex C18 HPLC column operated at a flow rate of 0.5 mL/minute. Solvent A consisted of water (HPLC grade) and solvent B consisted of methanol (HPLC grade). A gradient elution method was used starting from 0 % solvent B for 10 minutes, which was gradually increased from 5 to 95 % of solvent B for 35 minutes, and maintained isocratic at 100 % solvent B for 15 minutes.

Mass spectrometric analysis of the methanol extracts were performed using ion trap mass spectrophotometer (Thermo LCQ Advantage LC–MS/MS system).

5.2.6 Antimicrobial activity

Antimicrobial activity of ATNPs against *C. violaceum* was evaluated. Microbial cells in the logarithmic growth phase were used for all the studies. The cells (10^6 cells/mL) were suspended in flasks containing 10 mL of nutrient broth with different concentrations of ATNPs (0, 100, 1000, 1500 and 2000 µg/mL) and incubated on a shaker at 37 ºC; 110 rpm. At intervals of 4, 8, 16, 24 and 32 h, aliquots of the suspension were withdrawn and the cells were spread–plated on nutrient agar plates after appropriate dilutions with sterile saline. The plates were incubated at 37 ºC for 24 h. The number of viable organisms was determined by counting the number of colony forming units and multiplying it by the dilution factor. Similar experiments were carried using modified Tris minimal media where the concentrations of ATNPs tested were 0, 25, 500, 1000 and 1500 µg/mL.

5.2.7 *In vitro* biofilm assay

C. violaceum cells in the late logarithmic growth phase were used for these studies. ATNP coated glass slides and 5 mL of modified Tris minimal media were added to wells of a sterile 6 well plate, followed by the addition of bacterial cells (~ 10^6 cells/mL). The plates were incubated for a period of 24 h at 37 °C under stationary conditions. Uncoated slide and silver–free TiO_2 slide were used as positive and negative controls, respectively. The slides in the wells were observed for the visible inhibition of biofilm formation. Subsequently, the slides were removed and washed with deionized water and tested for biofilm formation using the following protocols. One set of the glass slides were imprinted on nutrient agar plates. The second set was used to study the morphology of the biofilms using a scanning electron microscope (SEM). For SEM, glass slides were fixed in glutaraldehyde and dehydrated in ascending ethanol solutions ranging from 10 to 100 %. These slides were sputter coated with gold using SPI 11430 sputter coater and imaged using a Jeol JSM–5800LV model with an accelerating voltage of 20 keV. All the experiments were conducted in triplicates.

5.3 Results and Discussion

5.3.1 Qualitative anti–QS activity

C. violaceum has commonly been used as biosensor of quorum sensing activity. It is a Gram–negative water and soil bacterium which resides in the tropical and subtropical areas and produces the antibacterial purple pigment violacein as a result of quorum sensing using its autoinducer AHL, N–hexanoyl–L–homoserine lactone (HHL) (Lichstein and Van de Sand 1945; McClean *et al*. 1997). This has been the basis for the development of a simple protocol for screening of anti–QS compounds, based on the decrease in the production of violet coloured pigment of *C. violaceum* which acts as an indicator of QS inhibition (McLean *et al*. 2004).

Figure 1 shows the concentration dependent anti–QS activity of ATNPs against *C. violaceum*. Inhibition of quorum sensing in *C. violaceum* when exposed to ATNPs was found to increase with increasing concentrations of ATNPs (100–500 µg/mL), as exhibited by the diameter of halos showing pigment inhibition. The violacein production was classified as, sensitive at 100 and 200 µg/mL, and very sensitive at 300, 400 and 500 µg/mL of ATNPs, as per the measure of inhibition of halos (Ponce *et al*. 2003; Alvarez *et al*. 2012), when the plates were spread with 10^6 cells (set A). Growth of non–pigmented colonies of *C. violaceum* was observed inside the halos (Figure 1a). When 10^{12} cells were spread (set B), the zone of antibacterial activity, was clearly differentiated from the zone of pigment inhibition. In Figure 1b, the inner clearer zone of inhibition corresponds to the antibacterial activity and the larger outer zone represents, pigment inhibition. Zone of pigment inhibition was not observed for TiO_2 control at all the above concentrations.

Anti–QS activity was observed to increase with increasing concentration of ATNPs. Similar concentration dependent QS inhibition has been observed in studies of anti–QS activity of *Cuminum cyminum* (Packiavathy *et al*. 2012), natural agents like tea tree, rosemary essential oils (Alvarez *et al*. 2012) and silver nanowires (Wagh *et al*. 2013). Furthermore, the concentration at which ATNPs exhibited anti–QS activity was lower in minimal media as compared to nutrient broth. This difference can be attributed to the amount of organic matter, counter and co–ions present in the reaction medium, as they mask the charge on silver ions and neutralize the activity. Presence of high amounts of dissolved organic matter and ions in nutrient rich media (nutrient broth) as compared to modified Tris minimal media leads to an increase in concentration of ATNPs required for anti–QS activity (Naik *et al*. 2013).

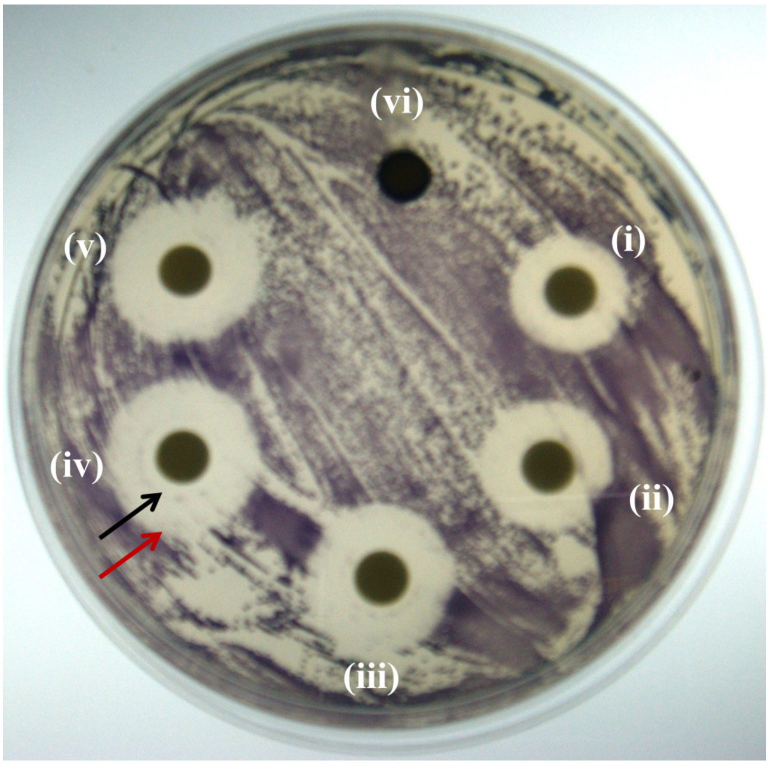

Figure 5.1 (a) Qualitative anti–QS activity of ATNPs at (i) 100 µg/mL, (ii) 200 µg/mL, (iii) 300 µg/mL, (iv) 400 µg/mL and (v) 500 µg/mL of ATNPs; (vi) TiO_2 control at 500 µg/mL against bioreporter strain *C. violaceum* using disk diffusion method when 10^6 CFU/mL were spread.

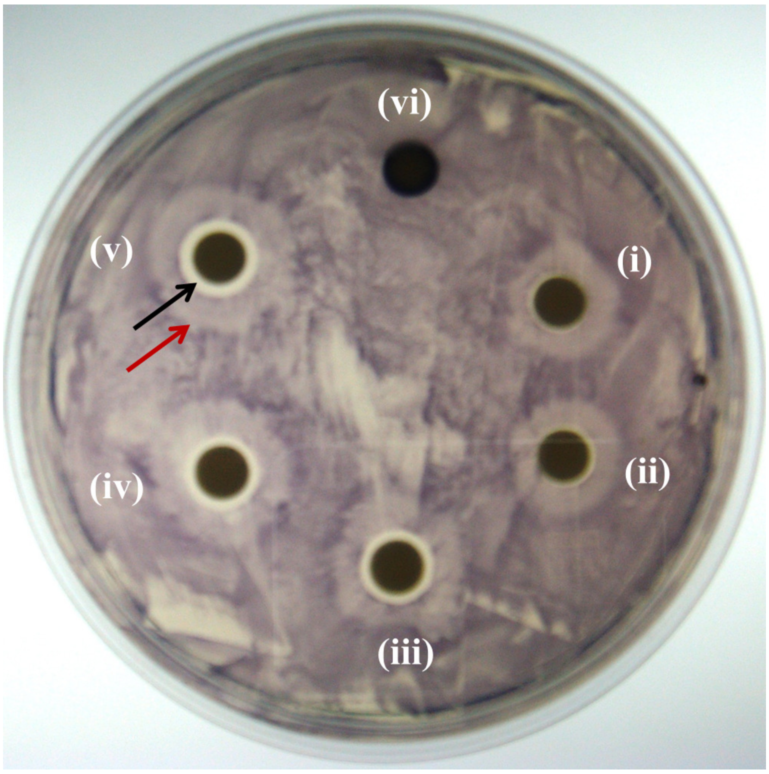

Figure 5.1 (b) Qualitative anti–QS activity of ATNPs at (i) 100 µg/mL, (ii) 200 µg/mL, (iii) 300 µg/mL, (iv) 400 µg/mL and (v) 500 µg/mL of ATNPs; (vi) TiO_2 control at 500 µg/mL against bioreporter strain *C. violaceum* using disk diffusion method when 10^9 CFU/mL were spread.

The zone of antibacterial activity is shown with a black arrow and the zone of pigment inhibition is shown with a red arrow.

5.3.2 Quantitative anti–QS activity

Figure 5.2 (A) shows the photographs of concentration dependent inhibition of violacein production by ATNPs, in nutrient broth and modified Tris minimal media, respectively. An inverse relationship was observed between the pigment production and the concentration of bioactive compound. A significant drop in violacein production was observed at 100, 200 and 300 µg/mL of ATNPs (effective silver concentration of 1.17, 2.34 and 3.52 µg/mL, respectively) using nutrient broth as the growth medium. The anti–QS concentration of ATNPs decreased to 25 µg/mL of ATNPs (effective silver concentration of 0.29 µg/mL) in modified Tris minimal media.

Violacein inhibiting substances are not expected to affect the cell growth (Alvarez *et al.* 2012). In order to verify whether the inhibition of violacein production by ATNPs was due to AHL inhibition and not microbial growth inhibition, the growth media from the flasks with no pigment production were streaked on nutrient agar plates. On incubation at 37 °C for 24 h, growth of *C. violaceum* was observed on the nutrient agar plates and was comparable to that of the control (Figure 5.2 (B)).

The percentage of violacein inhibition at different concentrations of ATNPs in nutrient broth (Figure 5.3 (a)) and modified Tris minimal media (Figure 5.3 (b)) is displayed respectively. Violacein production was reduced by 82 % at 100 µg/mL and by 100 % at 200 and 300 µg/mL of ATNPs with nutrient broth as the growth medium. During growth in modified Tris minimal medium, 86 %, 87 % and 99 % inhibition of violacein production was observed at ATNP concentrations of 25, 50 and 75 µg/mL, respectively.

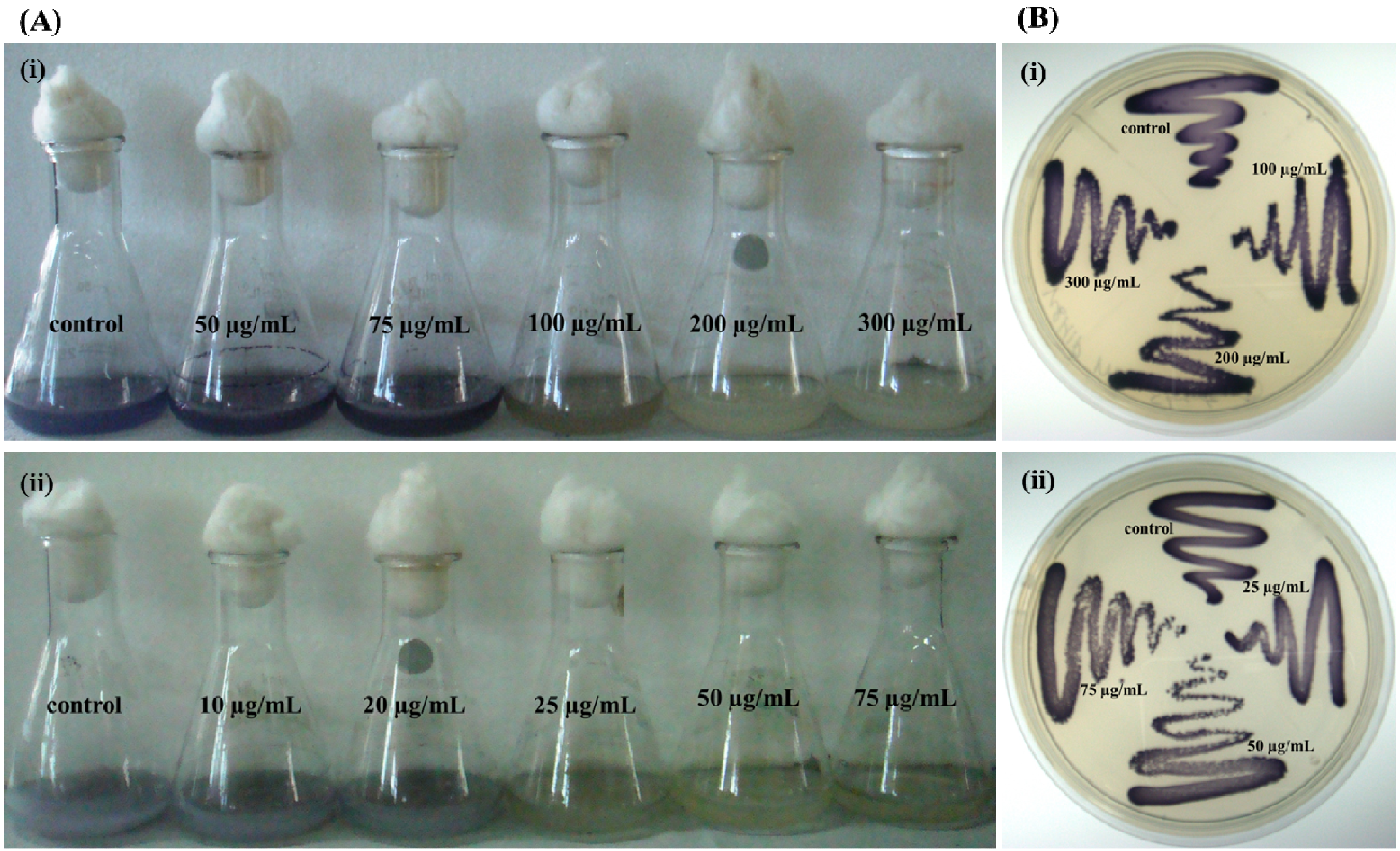

Figure 5.2 Inhibition of violacein production by ATNPs during flask incubation assay. (A) Photograph showing the decrease in production of violacein by *C. violaceum* with increase in concentration of ATNPs during growth in (i) nutrient broth and (ii) modified Tris minimal media. (B) Bacterial growth obtained after streaking the culture medium from the flasks showing no violacein production (i) nutrient broth and (ii) modified Tris minimal medium.

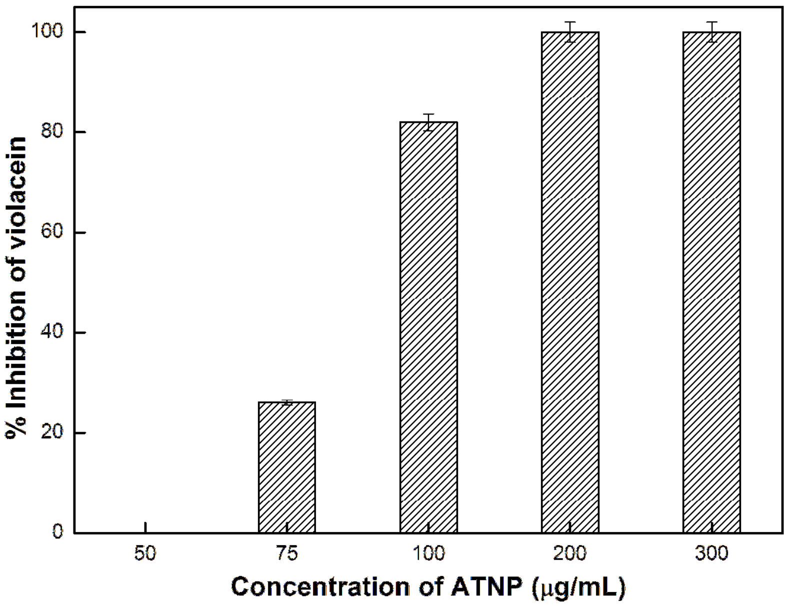

Figure 5.3 (a) Quantitative analysis of inhibition of violacein production by *C. violaceum* during growth in nutrient broth at increasing concentrations of ATNPs.

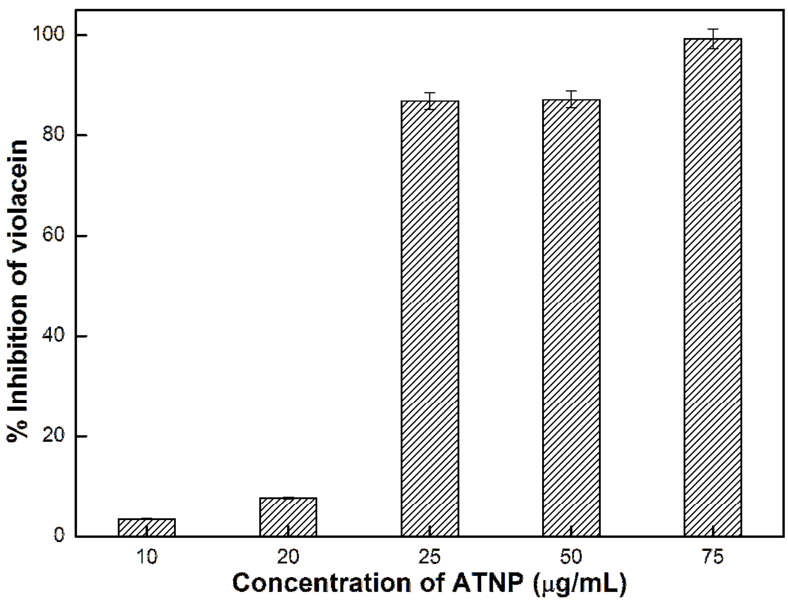

Figure 5.3 (b) Quantitative analysis of inhibition of violacein production by *C. violaceum* during growth in modified Tris minimal medium at increasing concentrations of ATNPs.

Evaluation of anti–quorum sensing activity of silver nanowires (SNW) has been reported earlier by Wagh *et al*. (2013). They obtained inhibition of violacein production at a concentration of 0.5 mg/mL of SNW with a 60 % reduction in violacein production which increased to 80 % at a SNW concentration of 4 mg/mL. The anti–QS activity of ATNPs in this study, has been achieved at a much lower concentration of silver (effective silver concentration of 1.17 µg/mL in nutrient broth and 0.29 µg/mL in modified Tris minimal media) suggesting that entrapment of silver in a suitable matrix or its functionalization leads to efficient anti–QS activity (Naik *et al*. 2013; Desai *et al*. 2013a; Desai and Kowshik 2013b).

5.3.3 Extraction and chemical characterization of AHL

AHLs produced by Gram–negative bacteria share a homoserine lactone ring and readily diffuse into the culture supernatant. Ethyl acetate was used for the extraction of AHL molecules due to their inherent lipophilicity and small amount of acetic acid was added to reduce the hydrolysis of lactone during workup and storage (Gould *et al*. 2006). The FTIR spectrum of the control sample showed the presence of bands in the range of 1780 to 1550 cm^{-1}. However these bands were absent in ATNP treated sample (Figure 5.4).

The infrared spectrum of the natural autoinducers are reported to give major bands at 1780, 1710, 1640 and 1550 cm^{-1} which are suggestive of the presence of a five–membered ring lactone and of a ketone and an amide group (Eberhard *et al*. 1981; Kim *et al*. 2011). Similar bands were obtained in the control when cells were grown in the absence of ATNPs, indicating the presence of functional groups within autoinducer. The bands associated with autoinducers were not present in the ATNP treated sample, indicating the absence of quorum sensing activity.

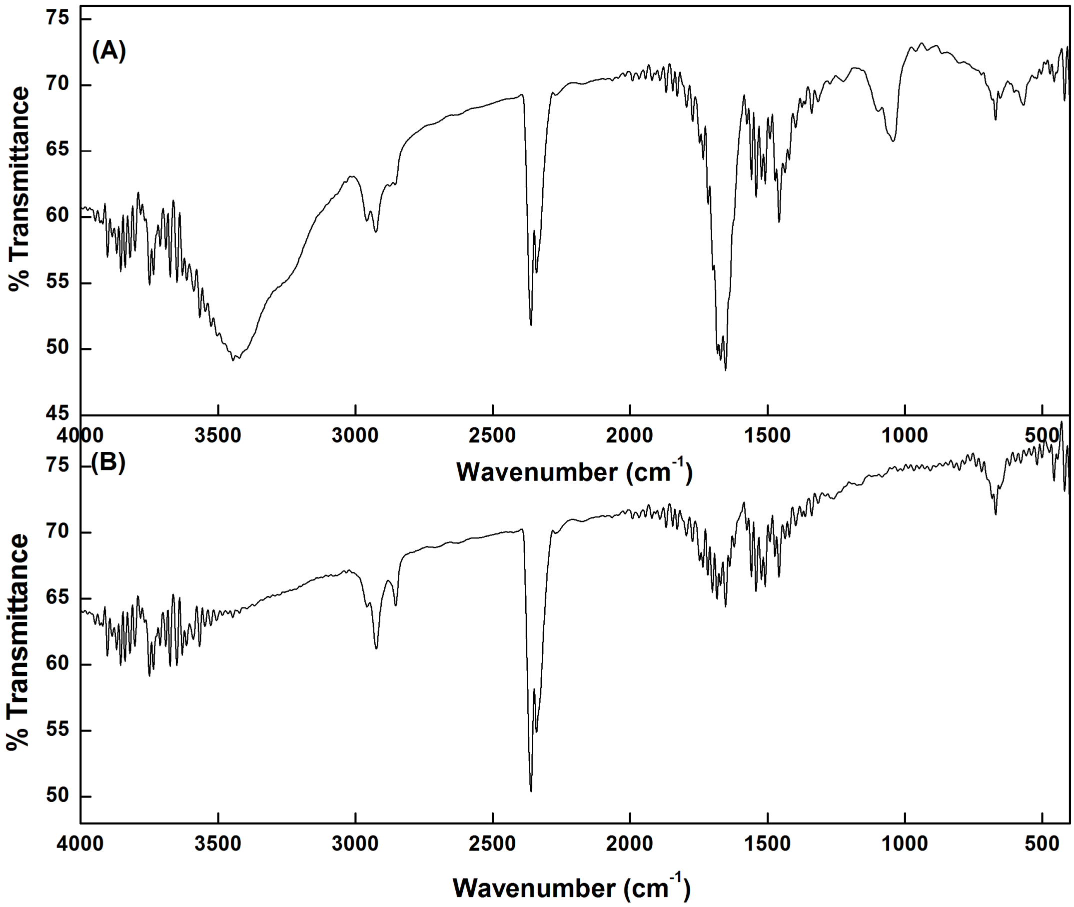

Figure 5.4 FTIR spectra of AHL extracts obtained from culture supernatants of cells grown in (A) absence of ATNPs [control] and (B) presence of 100 µg/mL ATNP.

HPLC chromatogram of AHL extract is shown in Figure 5.5 (a) and Figure 5.5 (b). A single sharp peak with retention time of 21 minutes was observed in the positive control, however no such peak was observed in case of the ethyl acetate extract of the culture supernatant of cells growing in presence of 100 µg/mL ATNP. In addition, two other peaks were observed around 6 and 8 minutes in the sample treated with ATNP (Figure 5.5 (b)). Mass spectrometry analysis of the peak obtained in control sample gave an m/z value of 242.

The major peak obtained in the control sample in HPLC analysis corresponded to 3–Oxo–C_8–HSL (3–Oxo–Octanoyl homoserine lactone) (Gould *et al*. 2006). No peak corresponding to 3–Oxo–C_8–HSL was obtained in the ATNP treated sample. However, the additional small peaks obtained may be attributed to the degradation products/precursors of the signalling molecule. The presence of 3–Oxo–C_8–HSL in the positive control was confirmed by mass spectrometry analysis wherein a peak was obtained at m/z value of 242 (Figure 5.5 (c)) (Bruhn *et al*. 2004; Gould *et al*. 2006).

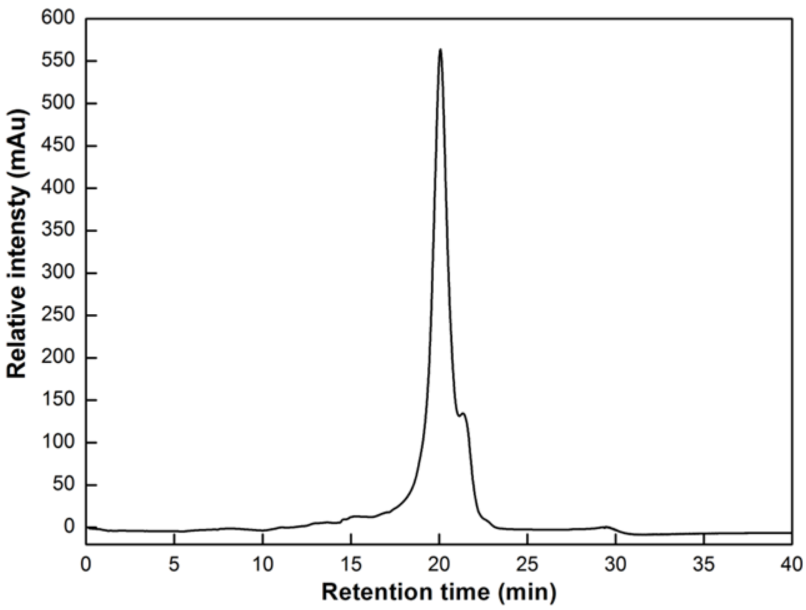

Figure 5.5 (a) HPLC analysis of AHL extract from culture supernatants of cells grown in the absence of ATNPs (control).

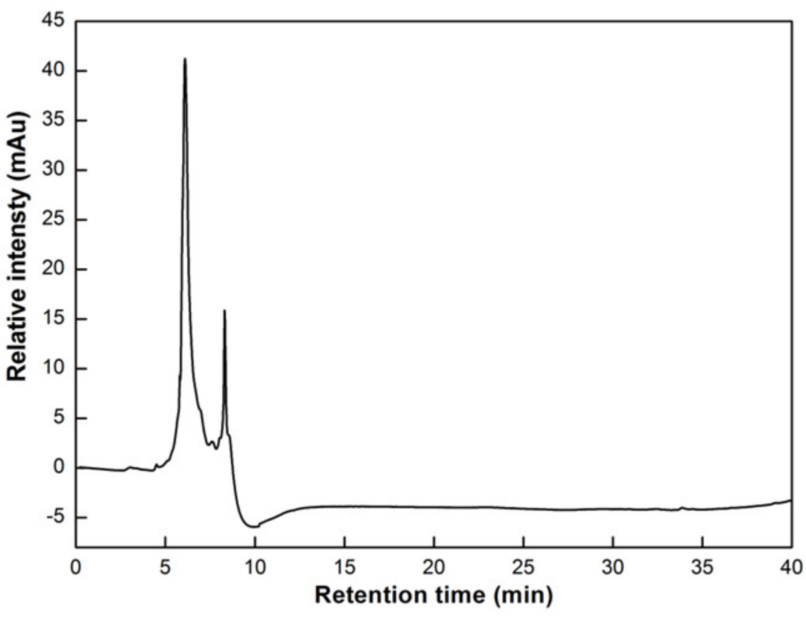

Figure 5.5 (b) HPLC analysis of AHL extracts from culture supernatants of cells grown in the presence of 100 µg/mL ATNP.

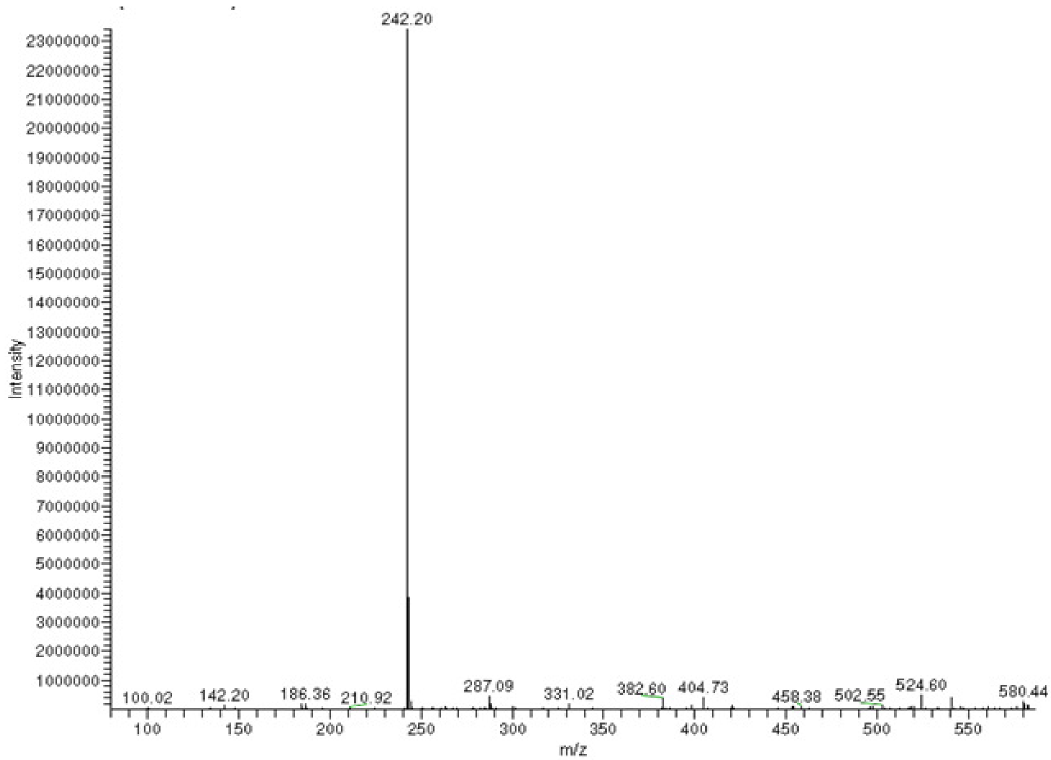

Figure 5.5 (c) Mass spectrometry analysis of AHL detected in HPLC analysis of the control.

5.3.4 Antimicrobial activity

The anti–QS concentration of 100 µg/mL ATNPs (effective silver concentration of 1.17 µg/mL) exhibited bacteriostatic activity towards *C. violaceum* in nutrient broth (Figure 5.6 (a)). Similar bacteriostatic activity with minimal reduction in cell numbers was observed up to a concentration of 1500 µg/mL ATNPs. Bactericidal activity, with complete inhibition of *C. violaceum* was obtained at an ATNP concentration of 2000 µg/mL (effective Ag concentration of 23.4 µg/mL). Similar results were obtained with modified Tris minimal media, wherein, no bactericidal activity was observed at anti–QS concentration of 25 µg/mL, and complete inhibition was obtained at 500 µg/mL ATNPs (effective Ag concentration of 5.85 µg/mL) (Figure 5.6 (b)). These studies further confirmed that the inhibition of violacein production was due to AHL inhibition and not microbial growth reduction.

Interestingly, in both the growth media, it was observed that the anti–QS concentration was 20 times lower than the concentration at which bactericidal activity was obtained

(Figure 5.6 (a) and (b)). These studies are in congruence with the anti–QS studies of natural agents which report the requirement of higher concentrations of bioactive compound to produce a significant inhibition in the growth of *C. violaceum* (Alvarez *et al*. 2012).

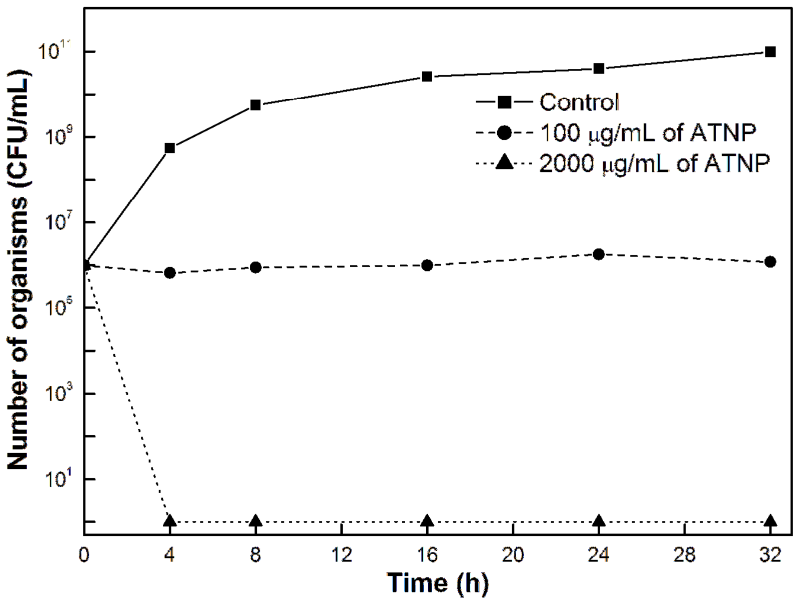

Figure 5.6 (a) Antimicrobial activity of ATNPs towards *C. violaceum* in nutrient broth.

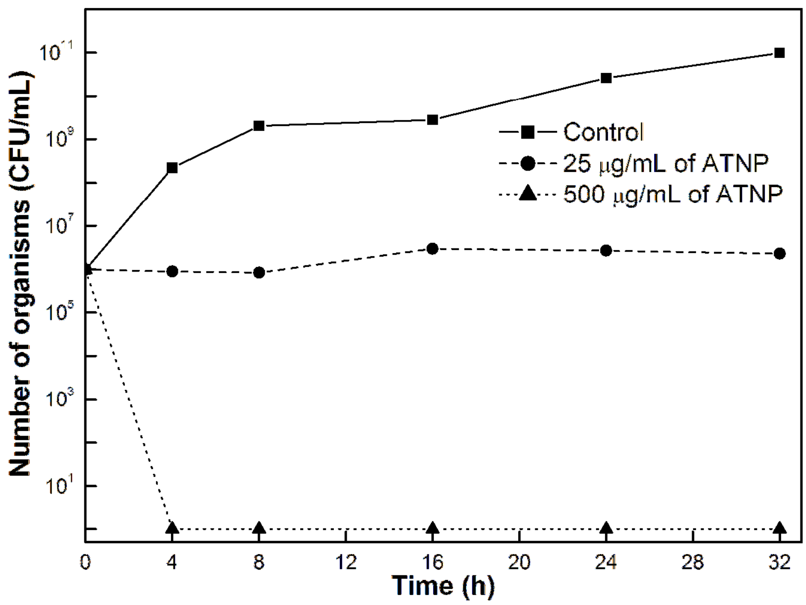

Figure 5.6 (b) Antimicrobial activity of ATNPs towards *C. violaceum* in modified Tris minimal media.

5.3.5 *In vitro* biofilm assay

In vitro biofilm assay with *C. violaceum* (Figure 5.7) showed that ATNP coated surfaces inhibited the development of biofilm when exposed to 10^6 cells in modified Tris minimal media. At an ATNP concentration of 20 µg/mL (effective Ag concentration of 234 ng/mL) and incubation of 24 h, inhibition of biofilm was observed in the well and a few isolated colonies were obtained after imprinting the coated slides on nutrient agar plate. Complete inhibition of both, biofilm as well as isolated cells was noted at an ATNP concentration of 100 µg/mL (effective Ag concentration of 1.17 µg/mL) (Figure 5.7).

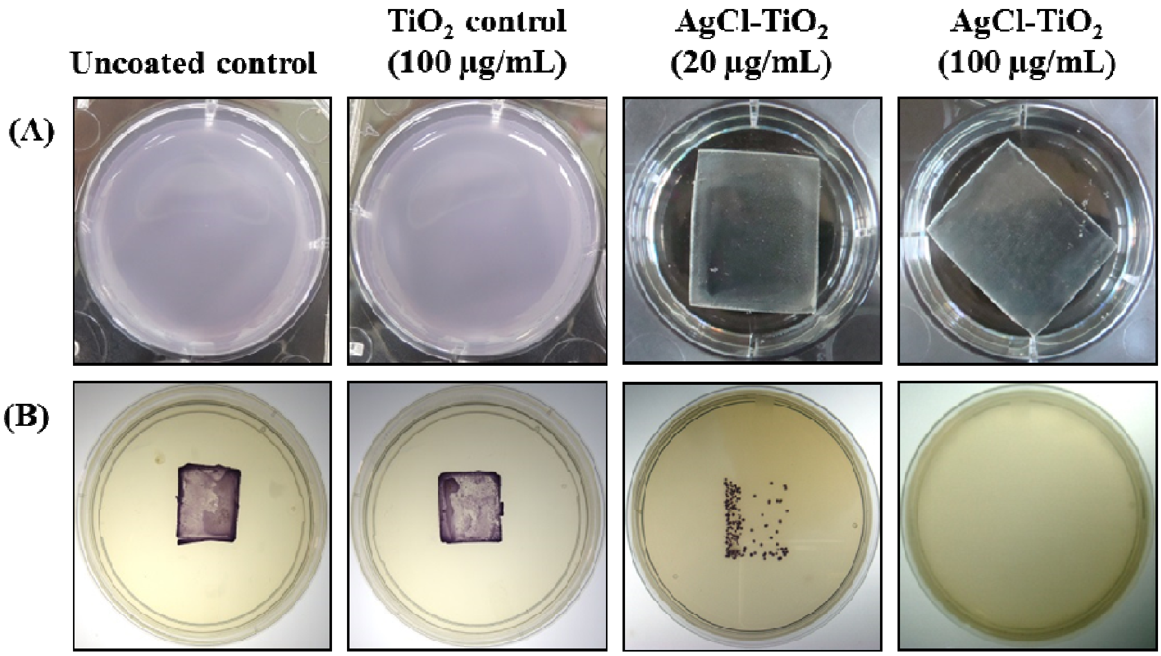

Figure 5.7 Anti–biofilm activity of ATNPs towards *C. violaceum*. Photographs showing (A) anti–QS activity and inhibition of biofilm formation after 24 h of incubation on glass slides coated with various concentrations of ATNPs for *C. violaceum*. (B) glass slides imprinted on nutrient agar plates and incubated for 24 h confirming inhibition of biofilm.

Figure 5.8 (a) shows the scanning electron micrographs of ATNP coated slides exhibiting inhibition of biofilm formation at a concentration of 100 µg/mL (effective Ag concentration of 1.17 µg/mL) for *C. violaceum* cells after 10 days of immersion in modified Tris minimal media. It was observed that the biofilms of the bacteria were completely established on the surface of the coatings with no silver content (Figure 5.8 (b)), while the surface containing silver completely inhibited biofilm formation.

In the present study biofilm inhibition was obtained at anti–QS concentration without affecting the viability of cells. Complete killing was observed at a much higher concentration than required for anti–QS activity. A similar observation has been reported in the study of anti–QS activity of SNW, wherein, biofilm formation was significantly arrested at a concentration of 4 mg/mL, without affecting viability of microbial cells and inhibition of growth was observed above 4 mg/mL of SNW (Wagh *et al*. 2013).

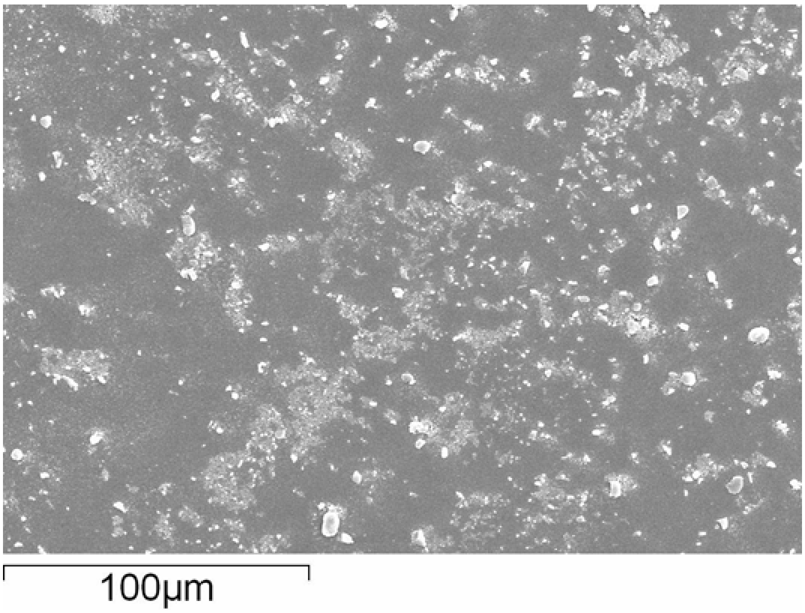

Figure 5.8 (a) SEM micrograph showing inhibition of biofilm formation on ATNP coated glass slides for *C. violaceum*.

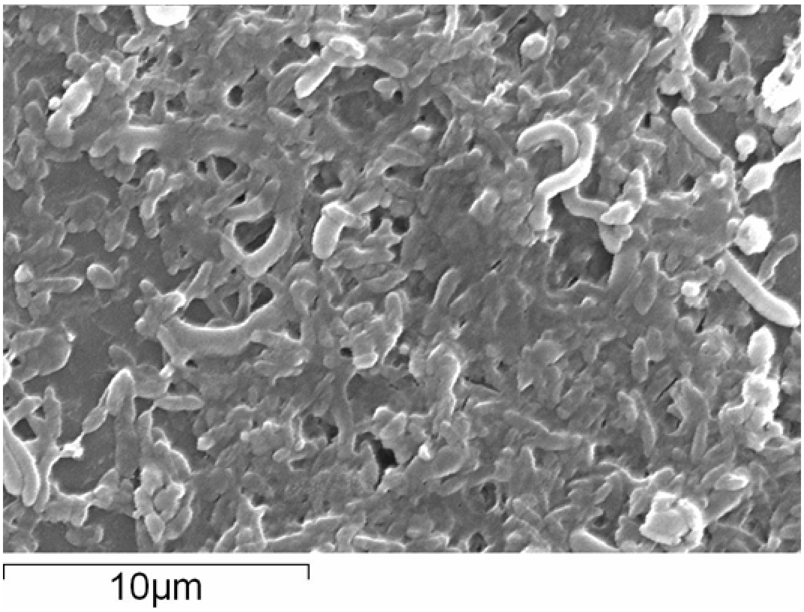

Figure 5.8 (b) SEM micrograph showing completely established biofilms on TiO_2 (control) coated glass slides for *C. violaceum*.

While a previous work by Wagh *et al*. (2013) has shown that silver nanowires act as anti–QS agents, the present work proceeded to test the anti–QS activity of silver which is entrapped in TiO_2 matrix. Compared to the anti–QS studies of SNW where 80 % of pigment inhibition was obtained at a concentration of 4 mg/mL, in the present study 82 % of pigment inhibition was obtained at a concentration 100 µg/mL of ATNPs (effective silver concentration of 1.17 µg/mL). Although, silver is traditionally believed to be relatively non–toxic to mammalian cells, care must be taken in the use of silver in applications like food packaging so that the burden of silver exposure does not exceed sub–toxic levels. Entrapping silver in a suitable matrix such as TiO_2 is one such attempt in the effective use of silver.

Although, natural agents and spices exhibit good anti–QS activity with potential food packaging applications, (Choo *et al*. 2006; Packiavathy *et al*. 2012; Alvarez *et al*. 2012), direct addition of these agents in the food is of concern due to loss of activity as a result of leaching into the food matrix, and cross–reaction with other food components such as lipids or proteins. Organic bioactive materials like natural agents and spices are often less stable particularly at high temperatures and/or pressures compared to inorganic materials and hence are required in large amounts, resulting in loss of flavour. Hence, inorganic materials such as metal and metal oxides are being actively studied over the past decade due to their ability to withstand harsh process conditions (Zhang *et al*. 2007; Emamifar 2011). Further, the efficiency of these active agents can be enhanced by incorporating or coating them in polymers/plastics. Such compounds when entrapped in a suitable matrix would result in a slow and sustained release into the foods resulting in initial inhibition of undesirable microorganisms and residual activity over time (Emamifar 2011).

5.4 Conclusion

The results demonstrate the anti–QS potential of ATNPs against the QS dependent phenotypic expressions in *C. violaceum* ATCC 12472. Specifically, this study aimed to determine the dynamics of QS inhibition by ATNPs in relation to its concentration for potential application as active food packaging material. In summary, the silver ions released by ATNPs inhibited QS by interfering with the AHL activity and thus inhibited the production of violacein pigment which was further confirmed using FTIR, HPLC and mass spectrometry analysis. TiO_2 acted as a good supporting matrix facilitating effective use of silver by reducing its concentration required for bioactivity. The findings of the present work strengthens the previous report that proposed silver to be a potential QS inhibitor and can be further studied and developed for its use as an bacteriostatic but non–toxic bioactive material. Though, silver is well known for its bioactive potential of antibacterial, antifungal, anti–inflammatory, antiviral, and anti–platelet properties (Wong and Liu 2010) the present study adds further note on its anti–QS activity and its potential use in food packaging industry.

This work was published as: **Naik, K.** and Kowshik, M. Anti–quorum sensing activity of AgCl–TiO_2 nanoparticles with potential use as active food packaging material. Journal of Applied Microbiology (2014) 117: 972–983. **(Impact factor 2.386)**

CHAPTER 6

Chapter 6: Bone Tissue Engineering and Drug Delivery Applications of Biocompatible Nano TiO_2−Hap−Alginate Composite Scaffolds

6.1 Introduction

Bone is an organ that plays key roles in critical functions such as protection, movement and support of other critical organs, blood production, etc. When the bone does not function properly it leads to various diseases such as osteoarthritis, osteomyelitis, and osteoporosis. These diseases along with traumatic injury, orthopaedic surgeries and primary tumour resection induce bone defects or voids. Even though osseous tissue has the unique internal repair capacity to heal and remodel without scarring, there are several conditions, both congenital and acquired, where bone replacement is needed (Buckwalter *et al.* 1996a; Buckwalter *et al.* 1996b). However, the clinical and economic impact of treatments of bone defects (Porter *et al.* 2009) and success in therapy has not been overwhelming. The key issues for this failure include inability to maximize drug access to bone and maintain optimum drug concentration for prolonged periods of time.

The current treatments for bone disorders and defects are based on autologous/autogenous bone grafts or metals/ceramics implants. Even though autologous bone grafts present relatively good percentages of success, the spectrum of cases in which it can be used is restricted mainly due to the donor site morbidity and limited amount of autografts that can be obtained (Yaszemski *et al.* 1994; Spitzer *et al.* 2002; Simon *et al.* 2002; Rose and Oreffo 2002; Petite *et al.* 2000).

In allografts where bone is taken from somebody else's body the rate of graft incorporation is lower as compared to the autograft. However, allograft bone introduces the possibilities of immune rejection and pathogen transmission from donor to host resulting in infections (Yaszemski *et al.* 1994; Spitzer *et al.* 2002; Simon *et al.* 2002; Rose and Oreffo 2002; Petite *et al.* 2000; Williams 1999). Although metals provide immediate mechanical support at the site of the defect, they exhibit poor overall integration with the tissue at the implantation site and can fail because of infection or fatigue loading (Yaszemski *et al.* 1994). On the other hand, ceramics have very low tensile strength and are brittle and thus, cannot be used in locations of significant torsion, bending, or shear stress (Yaszemski *et al.* 1994). To overcome these problems, tissue engineering approaches are emerging as convenient alternatives to promote the regenerative ability of the host body (Mourino and Boccaccini 2010; Goessler *et al.* 2007; Lee and Shin 2007; Bran *et al.* 2008; Kanczler and Oreffo 2008).

Since bone has a three–dimensional (3D) configuration and cells do not grow in a 3D fashion *in vitro*, tissue engineering approaches using 3D scaffolds which mimic bone structure are being developed. Such synthetic scaffolds must be capable of presenting a physiochemical biomimetic environment; while at the same time should biodegrade as native tissue integrates. (Kretlow and Mikos 2007; Langer and Vacanti 1993; Albrektsson and Johansson 2001; Mistry and Mikos 2005; Porter *et al.* 2009). Design and processing of a porous, biodegradable three–dimensional structure called as "scaffold", exhibiting high porosity and pore interconnectivity and uniform pore distribution is one of the most vital steps of bone tissue engineering (Hutmacher 2000). These scaffolds act as a temporary extracellular matrix inducing the natural processes of tissue regeneration and development, providing structural support for cells and new tissue formation (Chen *et al.* 2001; Lee and Shin 2007). Hence, improvement in the bioactivity and performance of bone–substitute materials and scaffolds is one of the main concerns in bone regeneration (Le Bolay *et al.* 2009). Advantages of utilizing synthetic bone scaffolds include elimination of disease transmission risk, fewer surgical procedures, reduced risk of infection or immunogenicity, and the abundant availability of synthetic scaffold materials (Porter *et al.* 2009).

In this context, ceramic TiO_2 has been studied as a material for bone tissue engineering applications (Fostad *et al.* 2009; Nygren *et al.* 1997; Rincon *et al.* 2005; Sabetrasekh *et al.* 2010; Tiainen *et al.* 2010). TiO_2 has gained much interest as an implant material and as bioactive coating for metallic implants. Highly porous and well–interconnected TiO_2 scaffolds with superior mechanical strength have been recently developed (Tiainen *et al.* 2010; Gomez–Florit *et al.* 2012; Haugen *et al.* 2013; M. Rubert *et al.*, 2012). Composites of TiO_2 with materials such as HAp are being developed to improve its biocompatibility and osteoconductive properties. HAp is widely used as an implant material and coating in clinical applications owing to its chemical and biological similarity to human bone, which in turn promotes osseointegration (Kim *et al.* 2005b). The combination of TiO_2 and HAp is expected to give better strength and corrosion resistance and superior biocompatibility. Moreover, incorporation of polymers such as PMMA [Polymethylmethacrylate], PCL [Polycaprolactone], PHBV [Polyhydroxybutyrate–co–hydroxyvalerate], PLGA [Polylactide–co–glycolide]), carbohydrates (chitosan, alginate), and proteins (collagen, gelatin) (Soundrapandian *et al.* 2009) in such composites provides desired mechanical stability because of the inherent higher stiffness and strength of the inorganic material, improved tissue integration, and controlled drug release. In addition, most natural materials are composites made up of both inorganic and organic components organized in complex structures like in case of bone which is a composite matrix of collagen (organic) strengthened with HAp (inorganic) (Soundrapandian *et al.* 2009).

Moreover, addition of inorganic materials to bioresorbable polymers can change the polymer degradation behaviour by buffering the pH of the nearby solution, thus preventing the autocatalytic effect of the acidic end groups resulting from hydrolysis of polymer chains, e.g. in polylactic acid. It is well known that incorporation of bioactive inorganic phases in biodegradable polymers can enhance water ingress owing to the internal interfaces formed between the polymer and the more hydrophilic bioactive inclusions, hence enabling control of the degradation kinetics of scaffolds (Boccaccini and Maquet 2003; Mourino and Boccaccini 2010). In this work, Alginate (Alg) was chosen as the polymer of interest for fabricating the TiO_2–HAp scaffolds, and the morphological features, dynamic mechanical properties, and biocompatibility and drug loading and release potential of TiO_2–HAp–Alginate scaffolds were investigated.

6.2 Materials and Methods

6.2.1 Preparation of nanostructured TiO_2–HAp composites

TiO_2 sol was prepared by adding 1 ml of $TiCl_4$ (Merck) dropwise to 50 ml of ice cold distilled water and magnetically stirred for 10 minutes. Fully crystalline and pure HAp nanorods were synthesized using a modified sol gel method (Jadalannagari *et al.* 2011). Calcium chloride (S D Fine Chemicals), Orthophosphoric acid (S D Fine Chemicals), Triethylamine (Merck) and Ammonium hydroxide (Merck) were used. A solution 14.7 g of 2M $CaCl_2 \cdot 2H_2O$ in 50 mL of water and 2.8 mL of 1M H_3PO_4 in 47.2 mL of triethylamine were prepared. Both solutions were taken in amounts that maintained a Ca/P molar ratio of 1.67. Orthophosphoric acid solution was slowly added to calcium chloride solution dropwise under continuous stirring using a magnetic stirrer. A translucent sol was obtained after 15 minutes, which turned into white color indicating formation of HAp. The pH of this sol was adjusted to 10 by using ammonium hydroxide solution under continuous stirring. Subsequently the sol was dialyzed against deionized water for 12 h, changing the water every 2 h. TiO_2–HAp composites with variable ratios (30:70, 50:50 and 70:30 weight percentages) were prepared by mixing the as prepared HAp and TiO_2 sols under continuous stirring on a magnetic stirrer for 2 h to obtain a uniform sol.

6.2.2 Characterization of nanostructured TiO_2–HAp composites

TiO_2–HAp nanocomposites were characterized using XRD and FTIR analysis. TEM analysis was carried out using a Phillips CM 200 microscope.

6.2.3 Maintenance of cell culture

MG–63 cell lines (human osteosarcoma cells) were purchased from NCCS, Pune, India and maintained in Dulbecco's Modified Eagle's medium (DMEM) with 10 % fetal bovine serum (FBS) at 37 °C in a humidified atmosphere with 5 % CO_2 and passaged at 70–90 % confluency. MG–63 homogenates were prepared by freezing at −80 °C and thawing the cells. Though these osteosarcoma cells possess abnormal growth characteristics, they initially represent clonal populations derived from specific stages of the osteoblast lineage. MG–63 cells are considered to show a number of features typical of an undifferentiated osteoblast phenotype. This includes the synthesis of collagen types I and III, expression of alkaline phosphatase and production of osteocalcin. Due to these advantages offered by the MG–63 cells, they have been chosen to evaluate their role in alveolar bone regeneration, a periodontal tissue (Clover and Gowen 1994; Price *et al.* 1997; Srinivasan *et al.* 2012).

6.2.4 Biocompatibility studies of nanostructured TiO_2–HAp composites using cell adhesion assay

The biocompatibility of nanostructured TiO_2–HAp composites, TiO_2 and HAp coated slides (controls) at 1, 2 and 4 % concentrations was evaluated using well characterized MG–63 cell line. All coated slides were sterilized by autoclaving at 121 °C for 15 minutes, and placed in 6 well tissue culture plates. The plates were inoculated with 2×10^4cells/ml in 2 ml of complete medium (90 % DMEM and 10 % FBS) and allowed to grow in standard cell culture conditions for 24 h and 48 h. After the prescribed time, non–adherent cells were removed by rinsing two times with PBS, and adherent cells were observed under inverted microscope (Nikon Eclipse TS100).

6.2.5 Fabrication of nano TiO_2–HAp–Alginate composite scaffolds

Freeze drying method was used to fabricate TiO_2–HAp–Alginate nanocomposite scaffolds (Figure 6.1). Sodium alginate (S D Fine Chemicals) was used without further purification. 2 % (w/v) of sodium alginate powder was dissolved in distilled water by stirring at room temperature to obtain a homogenous alginate solution. To the above prepared alginate gel, required amount of, 1, 2 and 4 % of TiO_2–HAp composites, TiO_2 and HAp (control) were added and stirred well until completely mixed into the solution. The resultant mixture was then transferred to a 96 well plate and pre–freezed at –20 °C for 12 h followed by lyophilization at –80 °C for 12 h using a lyophilizer (Christ, Alpha 1–2 LD plus). These scaffolds were then immersed in 2 % $CaCl_2$ solution for 1 h and again freeze dried for 12 h to obtain TiO_2–HAp–Alginate composite scaffolds of cylindrical shape and 5 mm x 5 mm size and stored for further use. For carrying out the dynamic mechanical analysis (DMA), the scaffolds were made in the form of 2 mm thick sheets by using petri plates for freeze drying the scaffold slurry mix. These sheets were then cut into rectangular pieces of required dimensions for the DMA analysis.

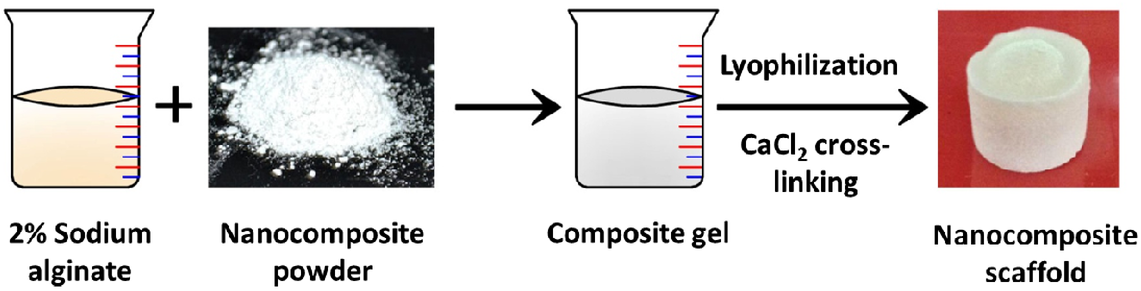

Figure 6.1 Fabrication of nano TiO_2–HAp–Alginate composite scaffolds.

6.2.6 Cell viability studies of scaffolds

The viability of cells seeded on the scaffolds was evaluated using a tetrazolium salt, MTT (3–[4,5–dimethylthiazol–2–yl]–2,5–diphenyltetrazolium bromide) (HiMedia), which measures the ability of mitochondrial dehydrogenase enzymes of metabolically active cells to convert the soluble yellow MTT salt into insoluble purple formazan salt. The rate of tetrazolium reduction is proportional to the rate of cell proliferation. The viability studies of scaffolds were conducted using MG–63 cells cultured in non–coated

48 well tissue culture plates containing DMEM supplemented with 10 % FBS. Prior to cell seeding, scaffolds were sterilized by autoclaving and incubated with culture medium for 2 h at 37 °C in a humidified incubator with 5 % CO_2 and 85 % humidity. After the incubation period, the culture medium was removed completely from the scaffolds. Cells were seeded drop wise onto the top of the scaffolds (2×10^4 cells/mL), which fully absorbed the media, allowing the cells to distribute through–out the scaffolds. After 4 h, the scaffolds were fed with additional culture medium and the cell–seeded scaffolds were incubated at 37 °C in a humidified incubator for 24, 48 and 72 h to allow the cells to attach and proliferate throughout the scaffolds. After incubation, medium in each well was removed and the scaffolds were washed twice using PBS. Next, medium containing 0.5 mg/mL MTT dye was added and the plates were incubated for 4 h. The medium was discarded and the resultant formazan crystals were dissolved in 10 % SDS solution in 0.01N HCl by squeezing the scaffolds. The absorbance intensity was measured at 570 nm. All the experiments were performed in triplicates.

6.2.7 Cell adhesion assay of scaffolds

The cell adhesion studies of scaffolds were conducted using MG–63 cells cultured in non–coated 48 well tissue culture plates containing DMEM supplemented with 10 % FBS. Prior to cell seeding, sterile scaffolds were incubated with culture medium for 2 h at 37 °C in a humidified incubator with 5 % CO_2 and 85 % humidity. After the incubation period, the culture medium was removed completely from the scaffolds. Cells were seeded drop wise onto the top of the scaffolds (2×10^4 cells/mL), which fully absorbed the media, allowing the cells to distribute through–out the scaffolds. After 4 h, the scaffolds were fed with additional culture medium. Consequently, the cell–seeded scaffolds were kept at 37 °C in a humidified incubator for 24, 48 and 72 h to allow the cells to attach and proliferate throughout the scaffolds. After incubation, medium in each well was removed and non–adherent cells were removed by rinsing two times with PBS. The morphology of the adherent cells proliferating on the scaffolds was examined using SEM. For SEM analysis, cell seeded scaffolds were fixed with 2.5 % glutaraldehyde for 6 h following which the scaffolds were thoroughly washed with PBS and sequentially dehydrated in a graded ethanol series from 10 to 100 % at 15 minutes interval. Ethanol was removed and the cells were left at room temperature to air dry and evaporate the remaining ethanol. The scaffolds were then sputter coated with gold using SPI 11430 sputter coater and imaged using a Jeol JSM – 5800LV model with an accelerating voltage of 20 keV.

6.2.8 Dynamic mechanical analysis

Dynamic−mechanical analysis (DMA) was carried out using a Q800 model from TA Instruments. The samples dimensions were 38 mm length, 14 mm width and thickness of 2 mm. Two kinds of experiments were performed:

(i) Strain sweep test. These experiments were carried out at 37 °C and 1 Hz frequency, where the dynamic stress was varied between 0.0100 MPa and 1.5000 MPa. These experiments were performed to evaluate the range in which the materials present viscoelastic behaviour. The storage modulus (E′) was obtained as the slope of the stress strain curve.

(ii) Temperature scans. The temperature scans were obtained to study the variation of storage modulus (E′) with temperature. The experiments were performed in the temperature range between 25 and 80 °C with a heating rate of 3 °C/minute and 1 Hz frequency. Amplitude was chosen from 1 to 1500 μm.

6.2.9 Characterization of nano TiO_2−HAp−Alginate composite scaffolds

The nanocomposite scaffolds were characterized using XRD and FTIR. FTIR was performed in the attenuated total reflection (ATR) mode by using a system equipped with an ATR cell with a diamond reflection element. Scaffolds were applied directly onto the surface of ATR crystal. SEM was used to study the structural morphology of the scaffolds.

6.2.10 Swelling studies

The swelling ability of the scaffolds was studied using phosphate buffered saline (PBS) (pH 7.4) at 37 °C (Liuyun *et al.* 2009). The dry weight of the scaffolds was noted as W_d and they were immersed in PBS solution for a period of 7 days. After the predetermined time, the scaffolds were removed and the absorbed water on the surface was gently blotted onto a filter paper and wet weight was recorded as W_w. The ratio of swelling was determined using the equation, swelling ratio = $W_w - W_d / W_d$. The experiments were carried out in triplicates and the swelling ratio was expressed as mean.

6.2.11 Porosity estimation

Liquid displacement method was used to determine the porosity of the scaffolds (Liuyun *et al.* 2009). Scaffolds were immersed in distilled water for 48 h until they got fully saturated and the porosity was determined using the equation, $P = W_2 - W_1 / \rho V_1$ where W_1 and W_2 represent the weight of the scaffolds before and after immersing in distilled water, V_1 is the volume of scaffold before immersing and ρ is a constant of the density of water. The experiments were carried out in triplicates and the porosity was expressed as mean.

6.2.12 *In vitro* degradation studies

The degradation of the scaffolds was studied in PBS (pH 7.4) containing lysozyme at 37 °C (Peter *et al.* 2010). The scaffolds were immersed in lysozyme (10,000 U/ml) containing PBS and incubated at 37 °C for 7 days. Initial weight of the scaffolds was noted as W_i. After soaking for 7 days, the scaffolds were removed from the solution and rinsed with deionised water to remove the adsorbed ions on the surface and freeze dried. The dry weight after lyophilisation was noted as W_t. The degradation of scaffold was calculated using the equation, degradation (rate of weight loss %) = $W_i - W_t / W_i \times 100$. The experiments were carried out in triplicates and the degradation rate was expressed as mean.

6.2.13 *In vitro* biomineralization studies

Scaffolds of equal weight and shape were immersed in 5X simulated body fluid (SBF) (Jayasuriya 2008) prepared by adding NaCl (40.62 g), KCl (1.86 g), $CaCl_2{\cdot}2H_2O$ (1.84 g), $MgCl_2{\cdot}6H_2O$ (1.52 g), NaH_2PO_4 (0.60 g), $NaHCO_3$ (1.76 g) and Na_2SO_4 (0.36 g) to 1 L of distilled water. The pH of the solution was adjusted to 6.8 with the help of 1M NaOH and 1M HCl. The samples immersed in SBF were kept for incubation at 37 °C in closed falcon tubes for 3 h. After the time duration, the scaffolds were removed, washed with deionised water to remove the adsorbed minerals, lyophilized and viewed using SEM (Jeol JSM – 5800LV scanning microscope).

6.2.14 Preparation of methotrexate incorporated TiO_2–HAp–Alginate nanocomposite scaffolds

The drug methotrexate (Sigma Aldrich) was incorporated into 50:50 TiO_2–HAp–Alginate (0.5:1) nanocomposite scaffold, TiO_2–Alginate and HAp–Alginate nanocomposite scaffolds (controls) using two methods.

(i) The drug, methotrexate, was loaded by immersing precisely weighed amount of scaffolds (11 mg x 6n) in 2 % (of the weight of the scaffolds) of drug solution in 5 mL of PBS for 48 h at room temperature. After 48 h, the scaffolds were removed and freeze dried. To calculate the total amount of drug incorporated in the scaffolds, they were dissolved in solution of 1 mL of acetonitrile and 0.1 mol/L hydrochloric acid (1:9 ratio). The amount of the drug was determined by recording the absorbance at 305 nm and estimating the concentration from the calibration curve.

(ii) The second method involved the incorporation of methotrexate during scaffold fabrication. Methotrexate solution of 200 µg/mL concentration was prepared in distilled water. To this, 2 % (w/v) of sodium alginate powder was added and dissolved by stirring at room temperature to obtain a homogenous gel. To this methotrexate–alginate gel, 1 % of 50:50 TiO_2–HAp composite, TiO_2 and HAp (controls) powders were added and stirred well until completely mixed into the solution. The resultant mixture was transferred to a 96 well plate and pre–freezed at −20 °C for 12 h followed by lyophilization at −80 °C for 12 h. These scaffolds were then immersed in 2 % $CaCl_2$ solution for 1 h and again freeze dried for 12 h to obtain TiO_2–HAp–Alginate–MTX composite scaffolds of cylindrical shape and 5 mm x 5 mm size and stored for further use. To calculate the total amount of drug incorporated in the scaffolds, the scaffold was dissolved in solution of 1 mL of acetonitrile and 0.1 mol/L hydrochloric acid (1:9 ratio) and the amount of methotrexate was estimated as given above.

The percentage of drug incorporated in the scaffold was calculated using the formula, Incorporation efficiency (%) = amount of drug in the scaffold / total amount of drug × 100.

6.2.15 Drug release from the methotrexate incorporated TiO_2–HAp–Alginate nanocomposite scaffolds

Drug incorporated scaffolds were suspended in 2 mL of phosphate buffered solution at pH 7.4. This dissolution medium was stirred at 100 rpm in a laboratory shaker maintained at 37 °C. Samples (1 mL) were periodically removed for testing and transferred back after the absorbance was recorded. The amount of released methotrexate was analysed by recording the absorbance at 303 nm. Release profiles were calculated in terms of the cumulative release percentage of MTX with incubation time. The drug release studies were performed in triplicate for each of the samples.

6.3 Results and Discussion

6.3.1 Characterization of nanostructured TiO_2–HAp composites

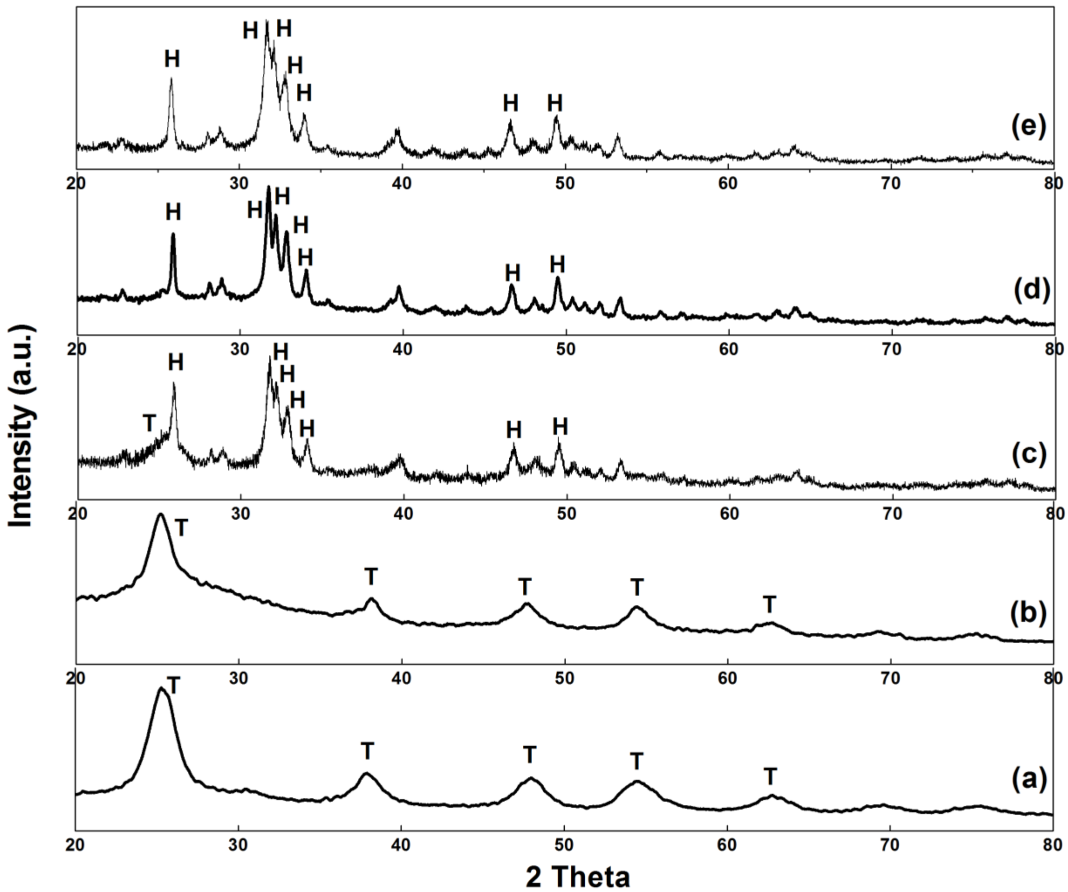

Figure 6.2 XRD pattern of (a) TiO_2 (control), (b) 70:30 TiO_2–HAp, (c) 50:50 TiO_2–HAp, (d) 30:70 TiO_2–HAp and (e) HAp (control) nanoparticles, where: T–anatase TiO_2 and H–HAp.

The XRD patterns for the TiO_2–HAp nanocomposites prepared with variable ratios of TiO_2 and HAp are shown in Figure 6.2. The XRD pattern for pristine TiO_2 is shown as curve (a) wherein all the peaks for anatase TiO_2 (JCPDS No. 21–1272) are seen. Addition of 30 % HAp to TiO_2 (b) shows almost similar diffraction pattern in which all the anatase TiO_2 peaks (2θ=25.28°, 37.79°, 48.04°, 53.88°, 55.05°, and 62.68° corresponding to (101), (004), (200), (105), (211), and (204) crystal planes are observed. For the 50:50 TiO_2–HAp (c), all the peaks corresponding to HAp and the 100 intensity peak of TiO_2 corresponding to (1 0 1) was observed. In the 30:70 TiO_2–HAp (d) nanocomposite, all the HAp peaks were observed. In all the three samples, no peaks other than HAp/TiO_2 were noted indicating that no impurities were present and that there was no decomposition of the samples. Curve (e) shows the XRD pattern of the pure HAp corresponding to JCPDS card No. 09–0432 with peaks at 25.940°, 31.800°, 32.240°, 32.940°, 34.120°, 46.68° and 48.08° corresponding to (002), (211), (112), (300), (202), (222) and (213) crystal planes of HAp, respectively. There was a decrease in the XRD peak intensity in the HAp with the addition of 30 % and 50 % TiO_2. Similar observation was noted in hydroxyapatite/titania nanocomposite thin films (Nathanael *et al.* 2010).

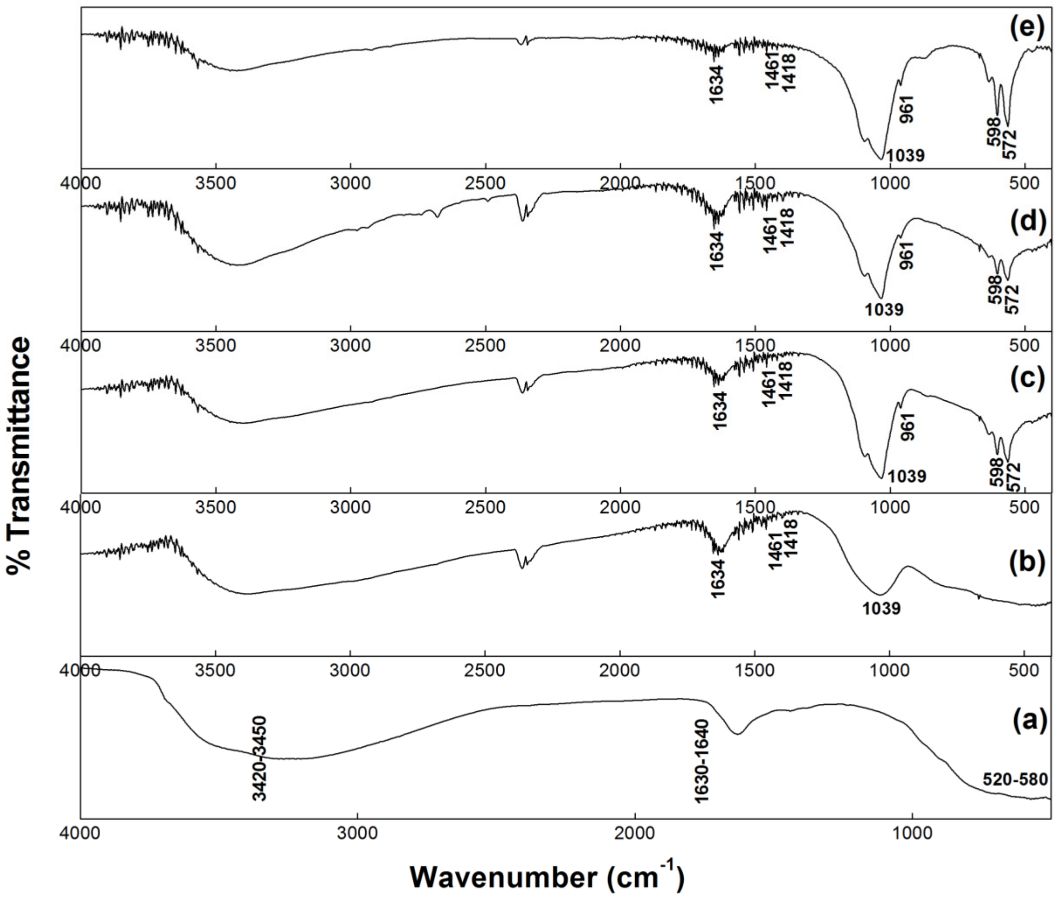

Figure 6.3 FTIR spectra of (a) TiO_2 (control), (b) 70:30 TiO_2–HAp, (c) 50:50 TiO_2–HAp, (d) 30:70 TiO_2–HAp and (e) HAp (control) nanoparticles.

FTIR spectroscopy (Figure 6.3) was used to determine the bonding characteristics in TiO_2–HAp nanocomposites. In case of TiO_2 (a), the absorption band in the region of 520–580 cm^{-1} corresponds to the stretching vibration of Ti–O (Li *et al.* 2003a; S. Liu, 2006). The vibration bands corresponding to 572–605, 961 and 1039 of PO_4^{3-} and corresponding to 1418–1478 of CO_3^{2-} are observed in 50:50 TiO_2–HAp (c), 30:70 TiO_2–HAp (d) and HAp (e) curves. In case of 70:30 TiO_2–HAp (b), vibrational band corresponding to 1039 of $PO_4^{3-}$and corresponding to 1418–1478 of $CO_3^{2-}$are observed along with the bands corresponding to TiO_2 (Pushpakanth *et al.* 2008). The absorption peaks at about 3420–3450 and 1630–1640 cm^{-1} in all the samples are associated with the stretching vibrations of surface water molecules, including hydroxyl groups (OH^-) and molecular water. Presence of these OH absorption bands in spectra of TiO_2–HAp indicates that no dehydroxylation has occurred during the formation of TiO_2–HAp nanocomposites, which is quite difficult to achieve during synthesis by plasma spraying (Zhao *et al.* 2005).

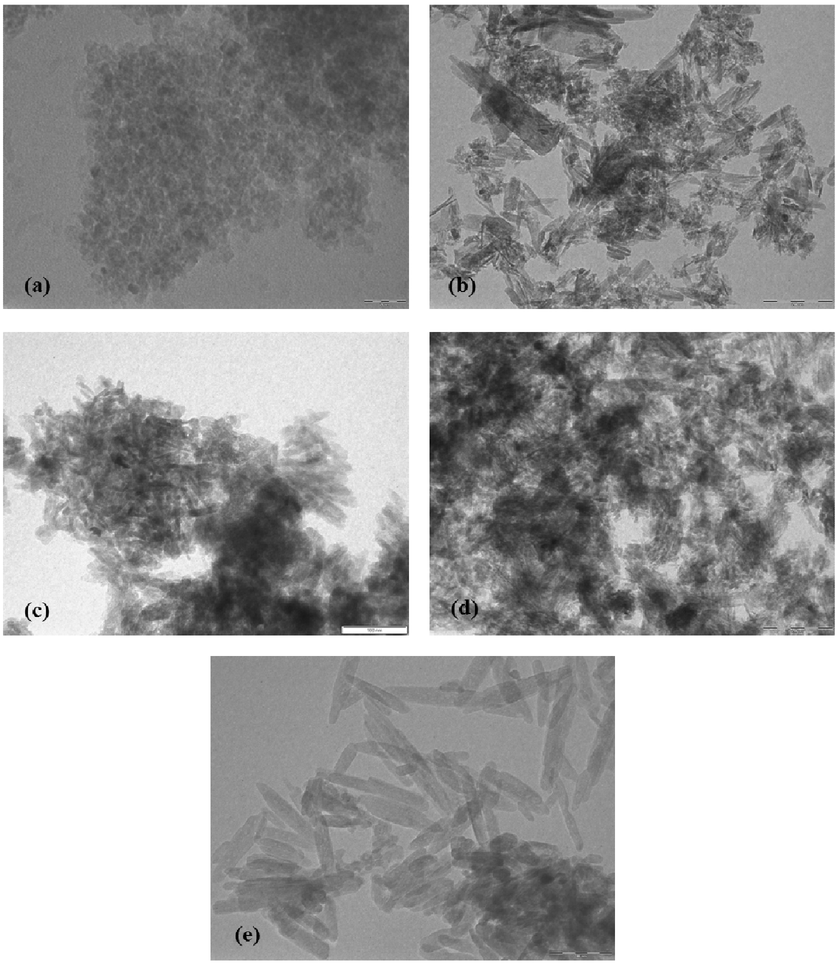

Figure 6.4 TEM micrographs of (a) TiO_2 (control), (b) 30:70 TiO_2–HAp, (c) 50:50 TiO_2–HAp, (d) 70:30 TiO_2–HAp and (e) HAp (control) nanoparticles.

TEM data (Figure 6.4) showed that the TiO_2 nanoparticles (a) were spherical and loosely agglomerated with average particle size of 3 to 4 nm. The TEM micrograph of pristine HAp (e), showed discrete rod–like HAp crystals of uniform size and morphology, having diameter between 20 and 25 nm and length between 110 and 115 nm. In case of TiO_2–HAp nanocomposites (b), (c) and (d), presence of both, the circular as well as rod shaped nanoparticles were observed indicating the presence of both TiO_2 and HAp in the nanocomposites.

6.3.2 Biocompatibility studies of nanostructured TiO_2–HAp composites using cell adhesion assay

The principal issue with regard to tissue engineering is the choice of suitable material. The desirable characteristics of these materials are biocompatibility and biodegradability. A biocompatible material does not induce any unwanted tissue response, provides the right surface chemistry to promote cell attachment and function and is degraded into nontoxic products (Yang *et al.* 2001b). In this study, MG–63 cells were cultured on the TiO_2–HAp nanocomposite coated slides and their morphology was observed under an inverted microscope. Figure 6.5, 6.6 and 6.7 shows the comparative study of cell morphology at 1, 2 and 4 % concentration respectively, after 24 h and 48 h. Cells were healthy and adhered with good spreading on HAp coated slides at all concentrations as compared to TiO_2 coated slides. In case of TiO_2–HAp nanocomposites, 50:50 TiO_2–HAp coated slides showed superior biocompatibility in the form of healthy cells with good spreading as compared to 30:70 TiO_2–HAp and 70:30 TiO_2–HAp nanocomposites.

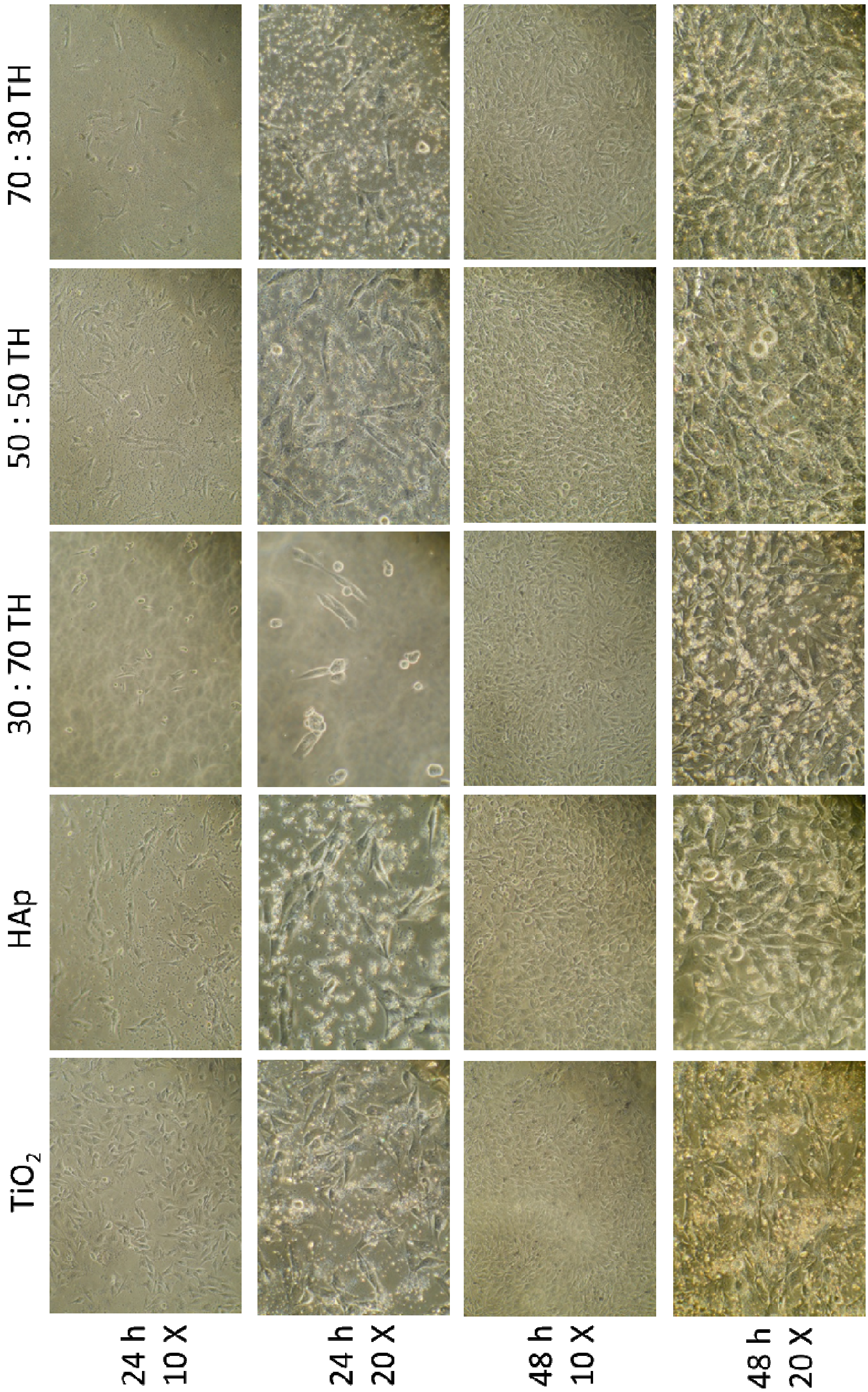

Figure 6.5 Images of MG-63 cell line incubated for 24 h and 48 h on 1 % TiO_2-HAp composite powders, TiO_2 and HAp coated glass slides.

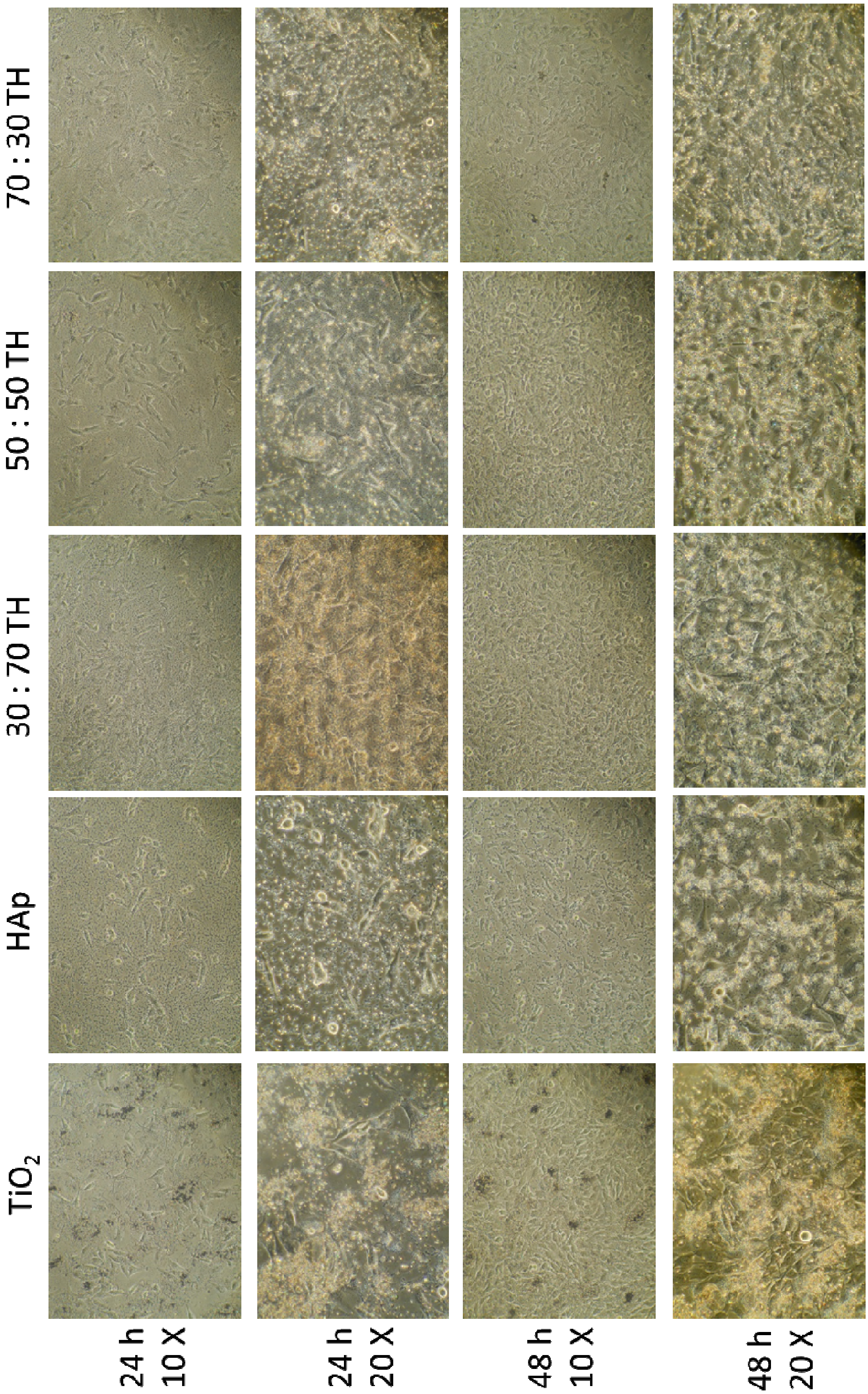

Figure 6.6 Images of MG-63 cell line incubated for 24 h and 48 h on 2 % TiO_2-HAp composite powders, TiO_2 and HAp coated glass slides.

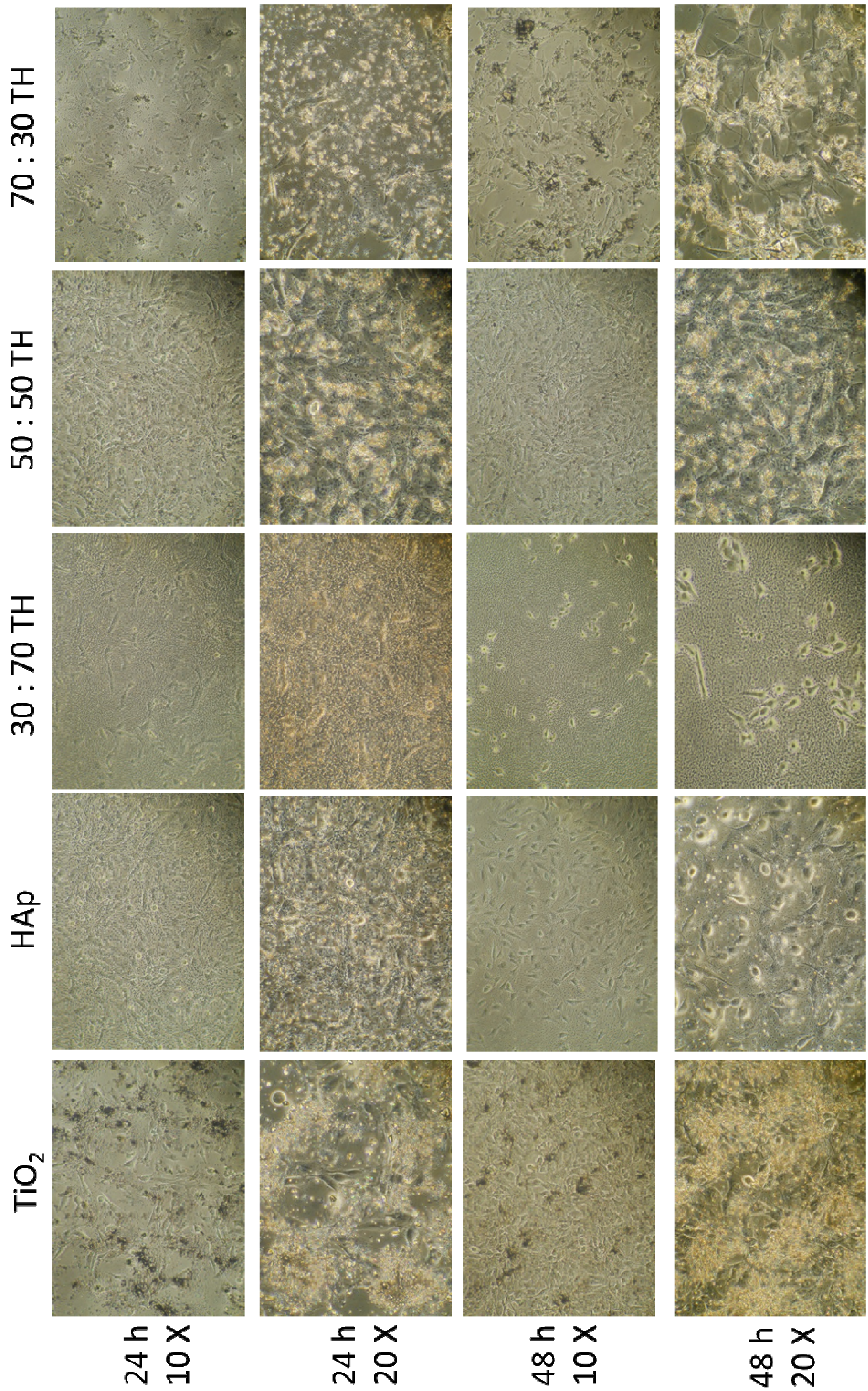

Figure 6.7 Images of MG-63 cell line incubated for 24 h and 48 h on 4 % TiO_2-HAp composite powders, TiO_2 and HAp coated glass slides.

6.3.3 Fabrication of nano TiO_2−HAp−Alginate composite scaffolds

Freeze drying method was used to fabricate the nanocomposites scaffolds which resulted in formation of porous scaffolds with well interconnected pores due to water removal. Alginate (Alg), a natural polysaccharide extracted from brown seaweeds was selected as the polymer of choice. It is highly hydrophilic, biocompatible, relatively economical and widely utilized in the food and pharmaceutical industry (Srinivasan *et al.* 2012). Chemically, alginate is a linear polymeric acid composed of 1,4−linked β−D−mannuronic acid (M) and α−L−guluronic acid (G) residues. In the presence of certain divalent cations like Ca^{2+}, Sr^{2+} and Ba^{2+} at low concentrations, alginate has the ability to form stable hydrogels through ionic interaction between the cation and the carboxyl functional group of G units located on the polymer chain (Wang *et al.* 1993). Due to their highly hydrophilic nature, seeding of cells onto the scaffolds is simple and rapid (Wang *et al.* 2003). Cross linking makes alginate insoluble in aqueous solution and culture medium. This enables it to remain as supporting structure for the seeded cells when it is used as a scaffold both *in vitro* and *in vivo*. When used *in vivo*, ionically cross−linked alginate degrades when the calcium ions are exchanged with other ions in the body, such as Na^+ (Bonino *et al.* 2011; Mohan and Nair 2005).

6.3.4 Cell viability studies of scaffolds

Since the present work is aimed at the development of scaffolds for biomedical applications, biocompatibility of the aforementioned material which is an important property needs to be studied. The dose and time dependent cytotoxicity studies of nanocomposites scaffolds with MG−63 cell lines were carried out using the MTT assay. All the samples were tested for time intervals of 24, 48 and 72 hours. As seen in Figure 6.8, the 50:50 TiO_2−HAp−Alginate scaffold with ceramic : polymer ratio of 0.5:1 showed superior viability up to 72 h as compared to the other nanocomposite scaffolds.

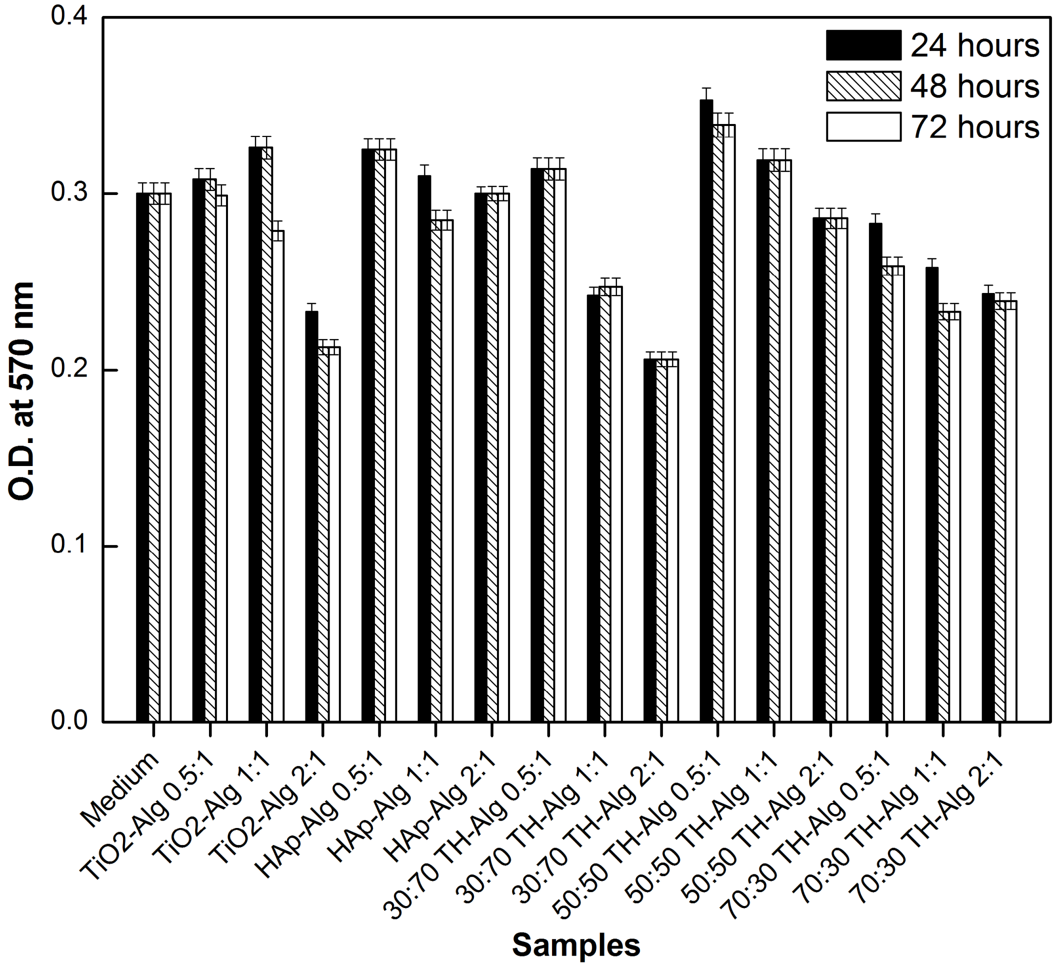

Figure 6.8 Cell viability of composite scaffolds for MG–63 cells using MTT assay.

6.3.5 Dynamic mechanical analysis

(i) Stress–amplitude scans.

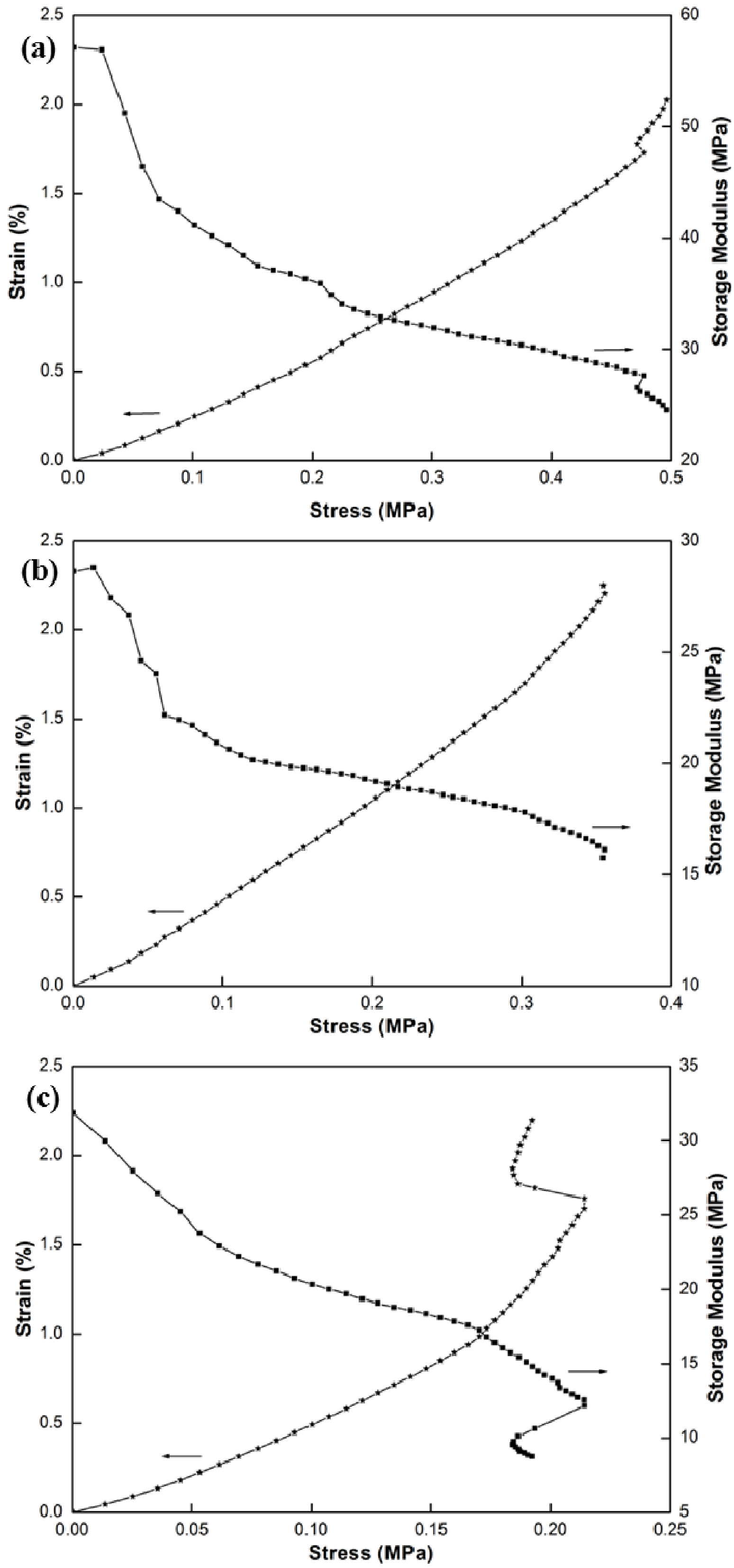

Figure 6.9 Dynamic mechanical behaviour of HAp–Alginate scaffolds with ceramic : polymer ratio as (a) 0.5:1, (b) 1:1 and (c) 2:1 at 37 °C.

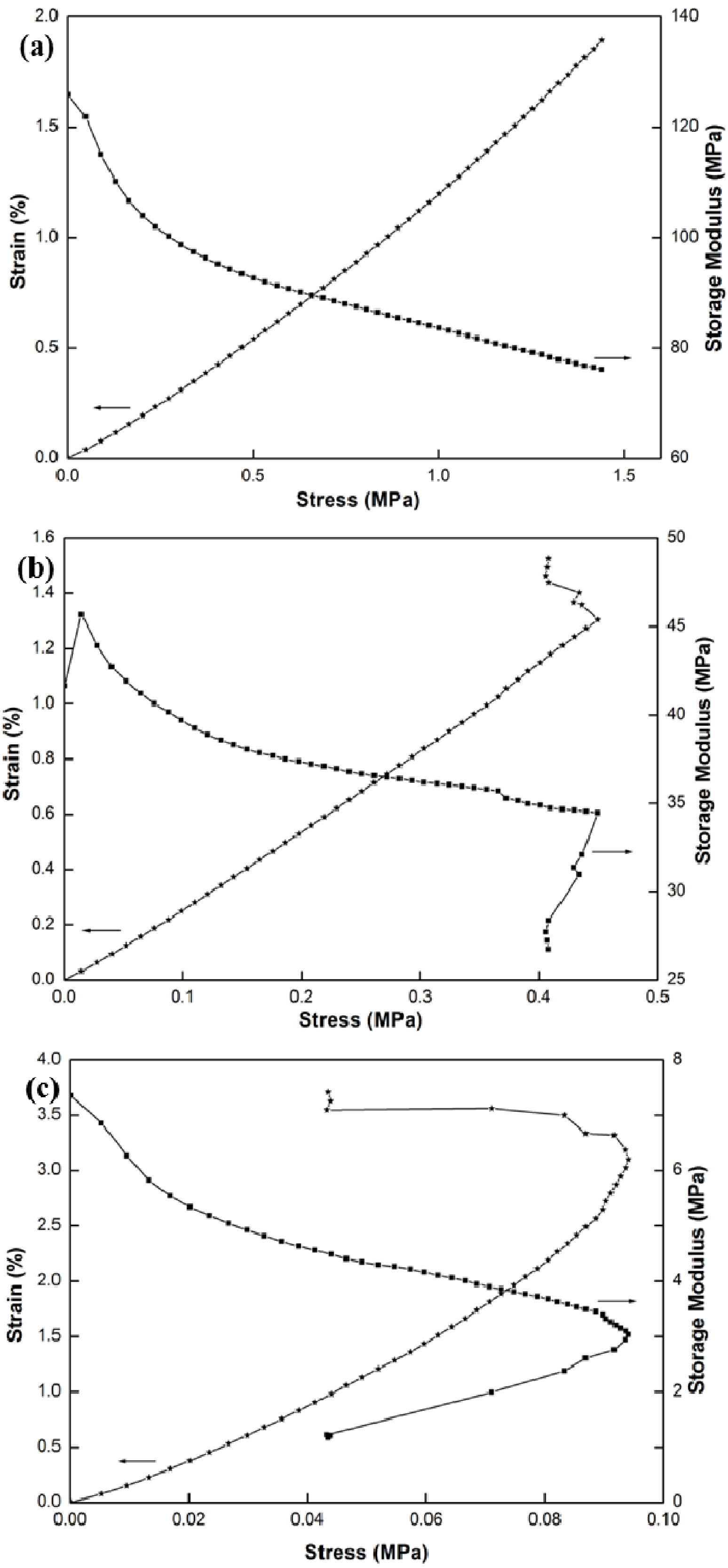

Figure 6.10 Dynamic mechanical behaviour of 30:70 TiO_2–HAp–Alginate scaffolds with ceramic : polymer ratio as (a) 0.5:1, (b) 1:1 and (c) 2:1 at 37 °C.

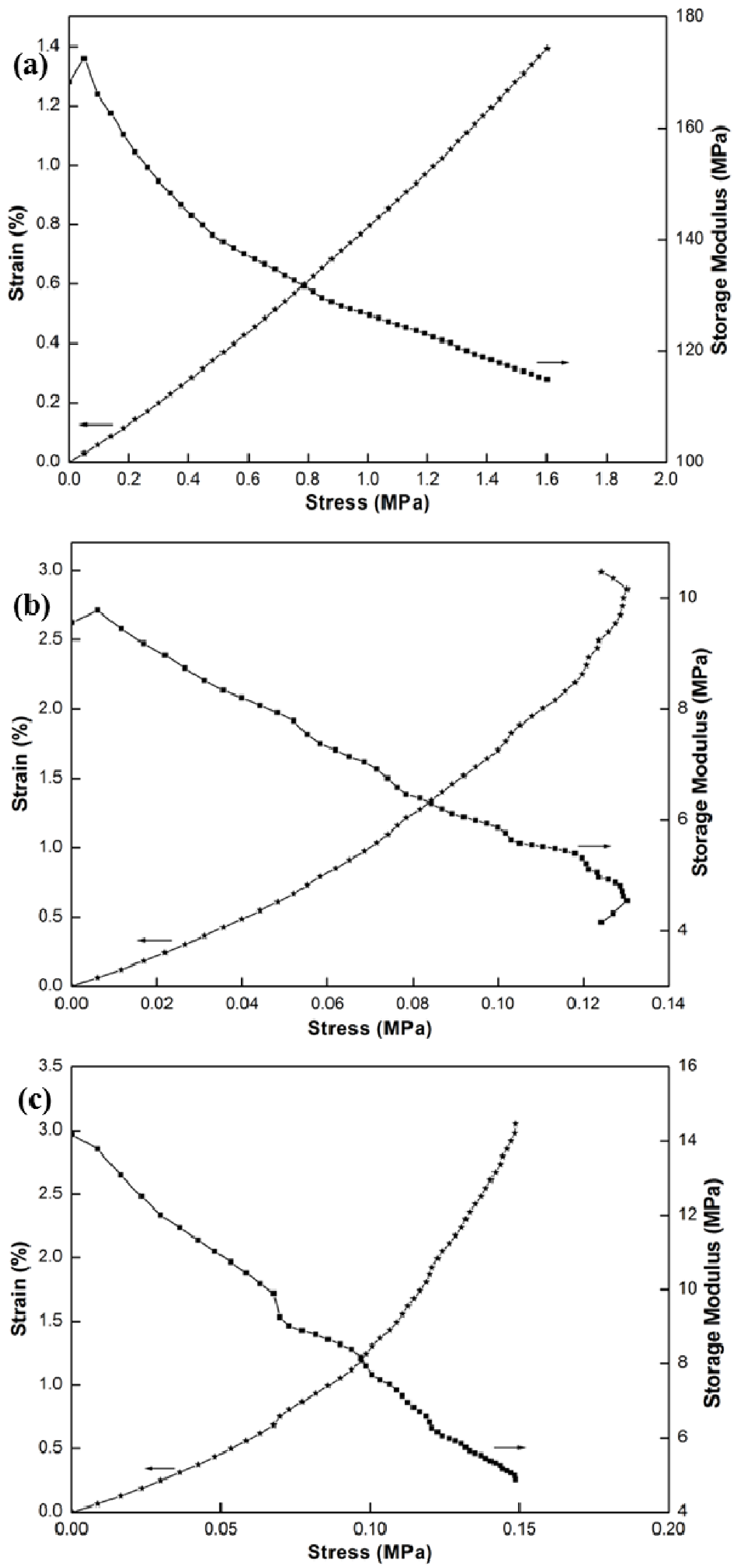

Figure 6.11 Dynamic mechanical behaviour of 50:50 TiO_2−HAp−Alginate scaffolds with ceramic : polymer ratio as (a) 0.5:1, (b) 1:1 and (c) 2:1 at 37 °C.

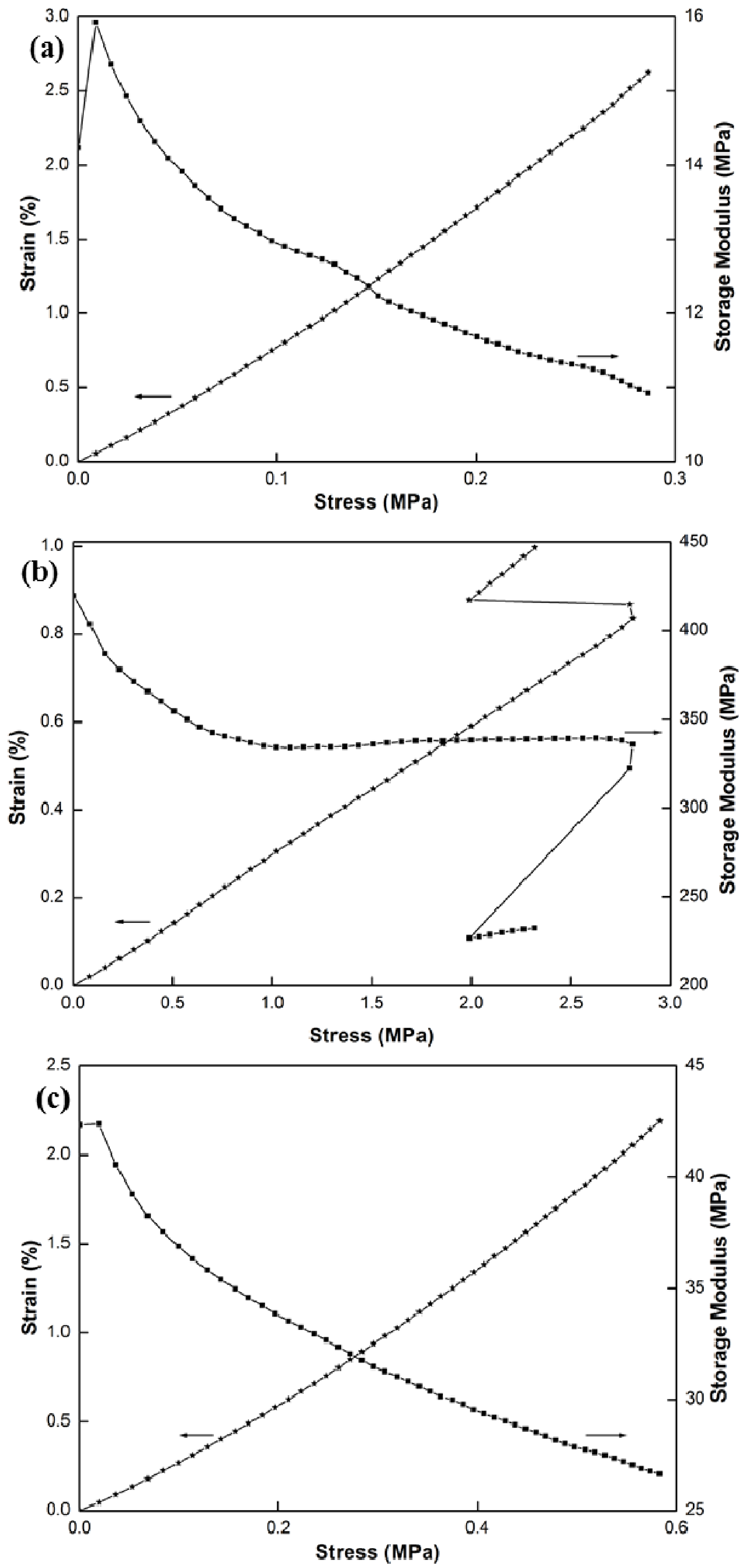

Figure 6.12 Dynamic mechanical behaviour of 70:30 TiO_2–HAp–Alginate scaffolds with ceramic : polymer ratio as (a) 0.5:1, (b) 1:1 and (c) 2:1 at 37 °C.

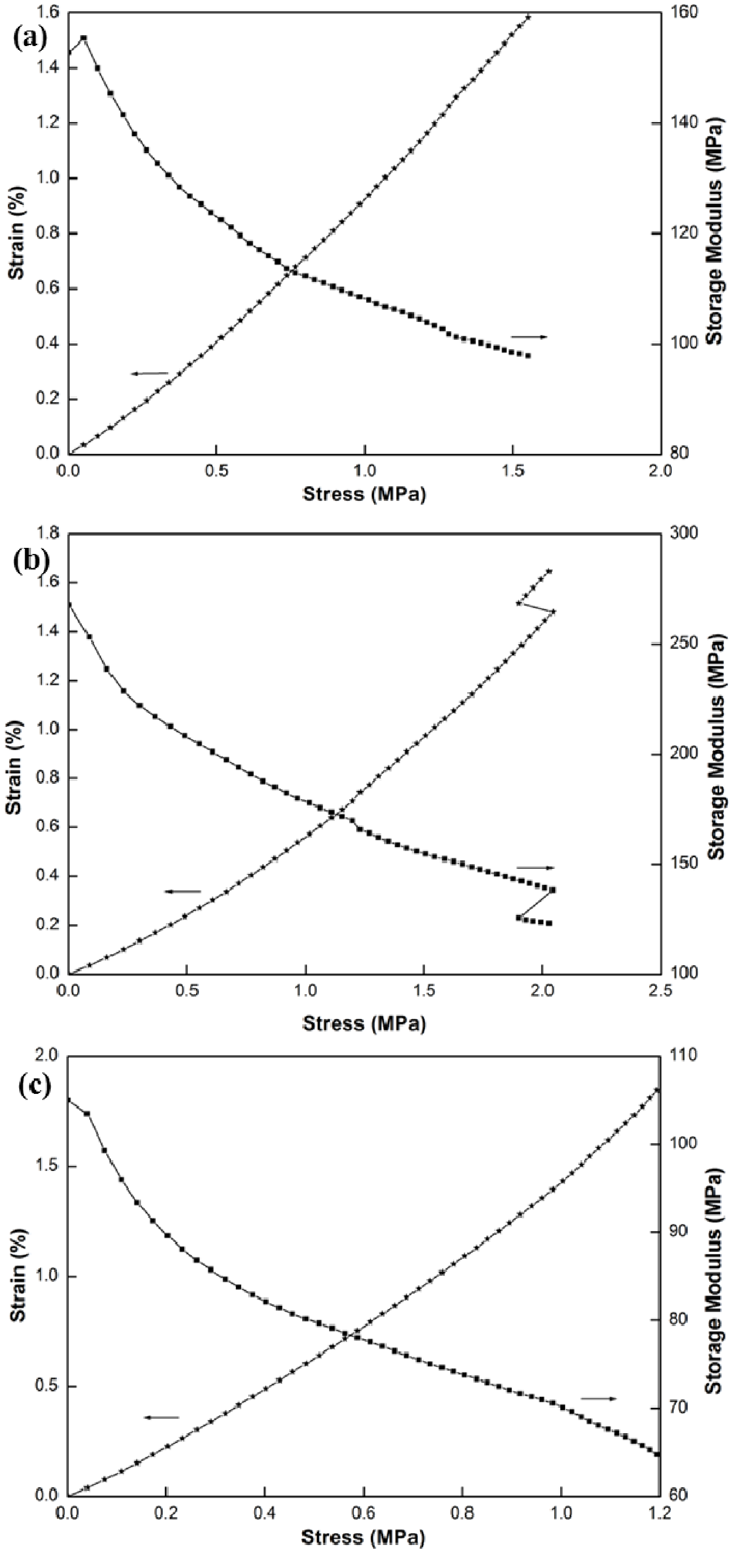

Figure 6.13 Dynamic mechanical behaviour of TiO_2−Alginate scaffolds with ceramic : polymer ratio as (a) 0.5:1, (b) 1:1 and (c) 2:1 at 37 °C.

Since the main aim of this work was to produce scaffolds with adequate mechanical properties, the viscoelastic properties of the hybrid scaffolds were analysed using dynamic mechanical analysis (DMA). This technique measures the deformation response of the material under a cyclic load excitation, as a function of frequency or temperature, being adequate to probe the viscoelastic properties of polymeric systems (Ferry 1980; Mano *et al.* 2002). In addition to being biocompatible both in bulk and degraded form, these scaffolds should possess appropriate mechanical properties to provide the correct stress environment for the new tissues, particularly in the reconstruction of hard, load–bearing tissues, such as bones and cartilages.

The stress–strain curves were plotted for all the composite scaffold samples (Figures 6.9 to 6.13) and the stress at 1 % of strain was examined. The storage modulus was also determined for all the composite scaffolds. The storage modulus is often times associated with "stiffness" of a material and is related to the Young's modulus (Wang *et al.* 1998a). A viscoelastic material is characterised by a storage modulus, E', and a loss modulus, E''. The storage modulus represents the elastic part of the response (where energy is stored and used for elastic recoil of the specimen when a stress is removed) and the loss modulus represents the viscous response (where energy is dissipated and the material flows) (Fulcher *et al.* 2009). Mechanical properties of nanocomposite scaffolds as determined from DMA (Figures 6.9 to 6.13) are summarised in Table 6.1. In case of 50:50 TiO_2–HAp–Alginate scaffold with ceramic : polymer ratio as 0.5:1, a larger dynamic stress of 1.224 MPa was required to create 1 % starin superior as compared to other scaffolds. This stress was comparable to the TiO_2–Alginate scaffolds which showed a dynamic stress in the range of 0.7 to 1.5 MPa. Moreover, 50:50 TiO_2–HAp–Alginate scaffold with ceramic : polymer ratio as 0.5:1 showed a higher storage modulus of 172.4 MPa. This can be attributed to the presence of TiO_2 in the sample which has superior mechanical properties. Bone exhibits extraordinary mechanical properties displaying both elastic and semi–brittle behaviour and is reported to have an elasticity modulus in the range of 20 to 500 MPa (Yang *et al.* 2001b). Although 70:30 TiO_2–HAp–Alginate scaffold with ceramic : polymer ratio as 1:1 showed the highest storage modulus of 419.6 and required larger dynamic stress of 2.317 MPa to create 1 % strain as compared to 50:50 TiO_2–HAp–Alginate scaffold with ceramic : polymer ratio as 0.5:1, it had a poor biocompatibility. Hence, as 50:50 TiO_2–HAp–Alginate scaffold with ceramic : polymer ratio as 0.5:1 demonstrated a superior biocompatibility and mechanical strength, it was selected for further characterization and analysis.

Table 6.1 Mechanical properties of nanocomposite scaffolds.

Sr. No.	Sample	Maximum Storage modulus (MPa)	Stress required for 1 % strain (MPa)
1	HAp–Alginate (0.5:1)	56.91	0.3155
2	HAp–Alginate (1:1)	28.76	0.1934
3	HAp-Alginate (2:1)	31.86	0.1712
4	30:70 TiO_2–HAp–Alginate (0.5:1)	125.9	0.8600
5	30:70 TiO_2–HAp–Alginate (1:1)	45.66	0.3577
6	30:70 TiO_2–HAp–Alginate (2:1)	7.350	0.04463
7	50:50 TiO_2–HAp–Alginate (0.5:1)	172.4	1.224
8	50:50 TiO_2–HAp–Alginate (1:1)	9.770	0.06988
9	50:50 TiO_2–HAp–Alginate (2:1)	14.18	0.08632
10	70:30 TiO_2–HAp–Alginate (0.5:1)	15.93	0.1268
11	70:30 TiO_2–HAp–Alginate (1:1)	419.6	2.317
12	70:30 TiO_2–HAp–Alginate (2:1)	42.38	0.3118
13	TiO_2–Alginate (0.5:1)	155.3	1.067
14	TiO_2–Alginate (1:1)	267.6	1.536
15	TiO_2–Alginate (2:1)	104.9	0.7480

(ii) Temperature scans.

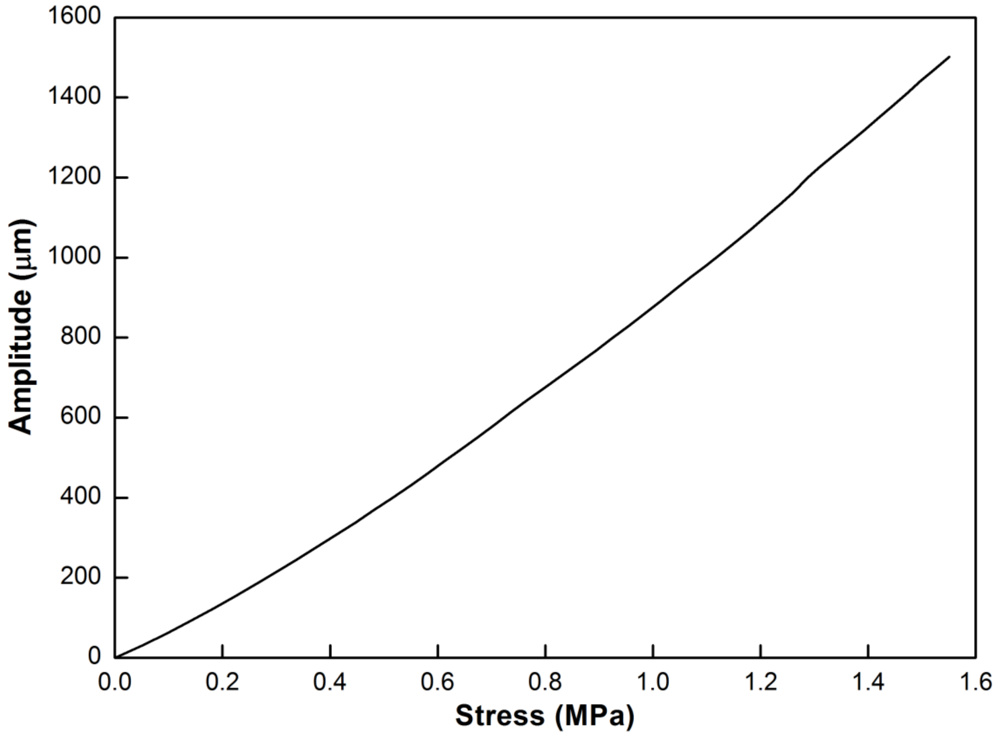

Figure 6.14 Stress versus amplitude scan of TiO_2−Alginate scaffold at 1 Hz and 37 °C.

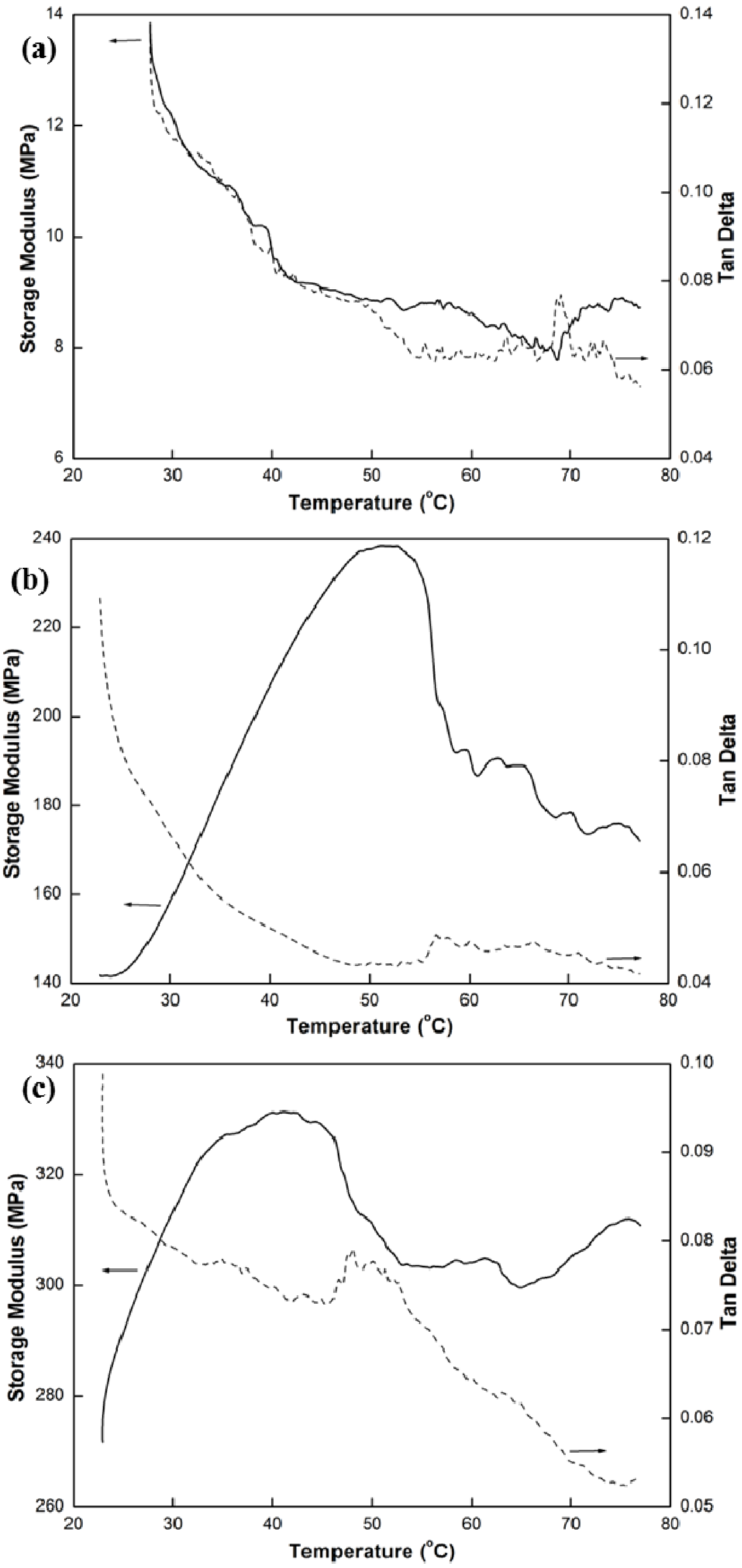

Figure 6.15 Dynamic mechanical behaviour of (a) HAp–Alginate (control), (b) TiO_2–HAp–Alginate scaffolds and (c) TiO_2–Alginate (control) at 1 Hz, obtained during temperature scans.

A direct comparison between the mechanical performance of TiO_2−HAp−Alginate scaffold and TiO_2−Alginate and HAp−Alginate scaffolds (controls) was obtained from temperature scans (Figure 6.15), at a fixed frequency of 1 Hz. Amplitude of 1 to 1500 μm was selected for the temperature scans as observed from Figure 6.14. The maximum storage modulus of TiO_2−HAp−Alginate scaffold was 238.3 MPa which was comparable to TiO_2-Alginate scaffold with maximum storage modulus of 331.3 MPa. Additionally the storage modulus of TiO_2−HAp−Alginate scaffold was much higher as compared to HAp−Alginate scaffold. Hence it can be concluded that the mechanical property of scaffolds was drastically improved due to the presence of TiO_2 without compromising the biocompatibility.

6.3.6 Cell adhesion assay of scaffolds

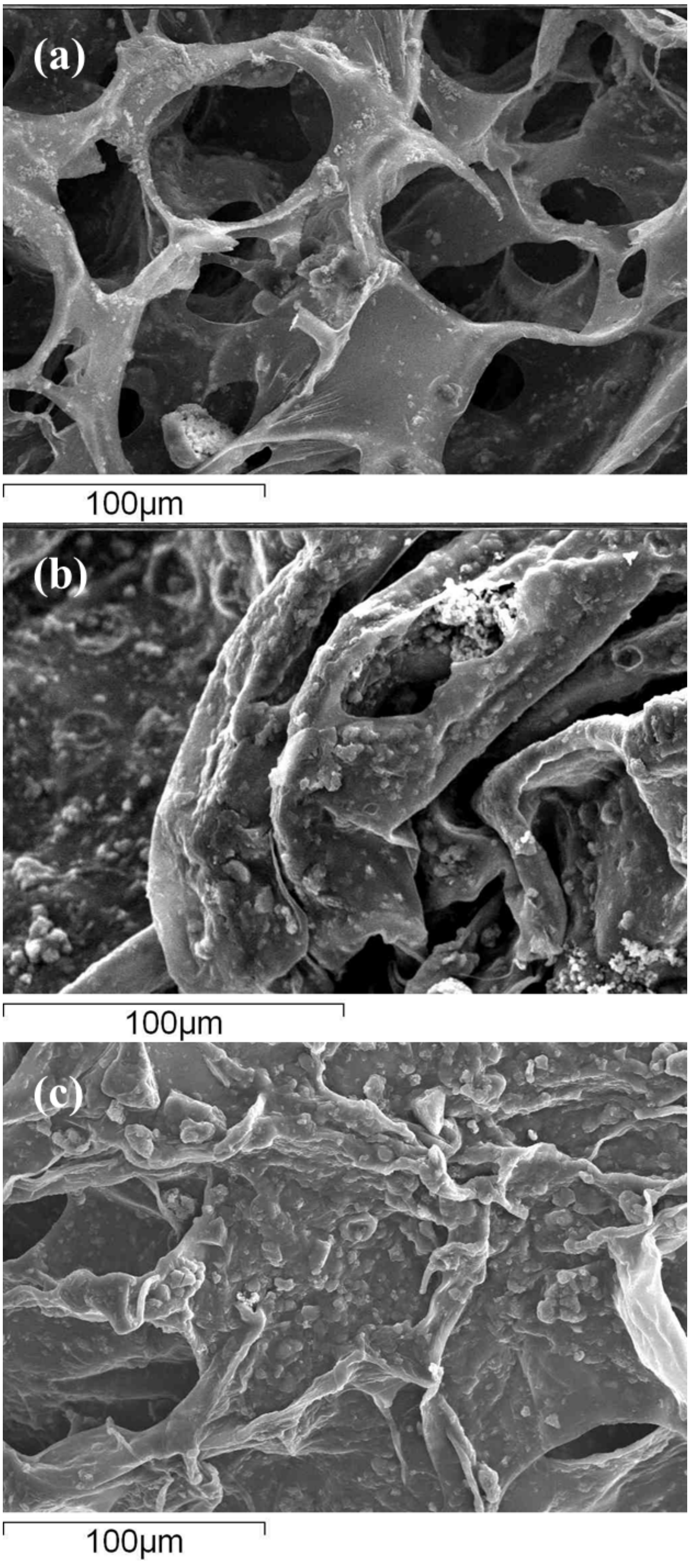

Figure 6.16 SEM images of cell attachment after 48 h of MG–63 cells on (a) TiO_2–Alginate scaffold (control), (b) HAp–Alginate scaffold (control) and (c) TiO_2–HAp–Alginate nanocomposite scaffold.

The cell attachment and proliferation of MG–63 cells on nanocomposite scaffolds was studied using the SEM. SEM micrographs (Figure 6.16) revealed that cells adhered to the surface and proliferated well on the composite scaffolds and retained their characteristic morphology after incubation. The number of cells growing on HAp–Alginate and TiO_2–HAp–Alginate scaffolds was higher than TiO_2–Alginate scaffolds. The enhanced attachment and proliferation may be attributed to the biocompatibility of the scaffold due to the presence of HAp and increased surface area and surface roughness due to the well–formed pores on the scaffold. The data clearly showed the ability of the scaffold to attract cells towards it and attach and proliferate on the scaffolds.

6.3.7 Characterization of nano TiO_2–HAp–Alginate composite scaffolds

Figure 6.17 shows the XRD spectra of the prepared nanocomposite scaffolds. The XRD spectra of TiO_2-Alginate scaffold exhibited the characteristic diffraction peaks of anatase TiO_2 (JCPDS No. 21–1272) at 2θ=25.28°, 37.79°, 48.04°, 53.88°, 55.05°, and 62.68° corresponding to (101), (004), (200), (105), (211), and (204) crystal planes. The XRD spectrum of HAp-Alginate scaffold showed the characteristic diffraction peaks of HAp (JCPDS No. 09-0432). The highly crystalline apatite peaks at 2θ=25.940°, 31.800°, 32.240°, 32.940°, 34.120°, 46.68° and 48.08° corresponded to (002), (211), (112), (300), (202), (222) and (213) crystal planes of HAp, respectively. Whereas in case of TiO_2–HAp–Alginate scaffold, the spectrum exhibited all the HAp peaks and the (101) anatase TiO_2 peak. All the three spectra exhibited a broad peak of alginate between 20° and 50° (2θ) (Srinivasan *et al.* 2011).

Figure 6.18 shows the FTIR spectra of the nanocomposite scaffolds. All the three spectra exhibited an intense peak around 3420 cm^{-1} indicating the absorption of O–H group. A peak around 1400–1444 cm^{-1} was due to the presence of carboxyl group of alginate. Peaks at 1630 and 1000–1240 cm^{-1} were ascertained to the presence of carbonyl groups in alginate. In particular the peaks at 1000–1125 and 1240 cm^{-1} region confirmed the presence of guluronic acid, mannuronic acid and o–acetyl ester, the building blocks of alginic acid (Kazy *et al.* 2002). For HAp–Alginate scaffold, FTIR spectra showed the combined peaks of alginate and HAp which confirmed the incorporation of HAp into the alginate scaffold. The peaks in the region of 872–884

cm^{-1} corresponded to CO_3^{2-} groups and 572–605 cm^{-1} corresponded to PO_4^{3-} groups contained in HAp.

The regeneration of specific tissues aided by synthetic materials is dependent on the porosity and pore size of the supporting three–dimensional matrix (Cima *et al.* 1991). Pores are essential for the migration and proliferation of the cells, nutrient supply and vascularisation (Peter *et al.* 2010; Srinivasan *et al.* 2012). A large surface area favors cell attachment and growth, whereas a large pore volume is required to accommodate and subsequently deliver a cell mass sufficient for tissue repair. The surface area/volume ratio of porous materials depends on the density and average diameter of the pores (Yang *et al.* 2001b). Depending on the envisioned applications, pore size must be carefully controlled. The optimum pore size of 100–350 μm was found to be suitable for the regeneration of bone (Klawitter and Hulbert 1971). Figure 6.19 shows the SEM images of naocomposite scaffolds, indicating their porous nature. The size of the pores was larger in the TiO_2–HAp–alginate nanocomposite scaffold as compared to the controls viz. TiO_2–Alginate and HAp–Alginate scaffolds. The pore size was 70, 90 and 120 μm for TiO_2–Alginate, HAp–Alginate and TiO_2–HAp–Alginate, respectively. The pore size of 120 μm is suitable for bone tissue engineering applications (Klawitter and Hulbert 1971; Karageorgiou and Kaplan, 2005). Another important consideration is the continuity of the pores within a synthetic matrix. Material transport and cell migration are inhibited if the pores are not interconnected (Mooney *et al.* 1996). As observed from the SEM micrographs, the pores were well interconnected in all scaffold samples.

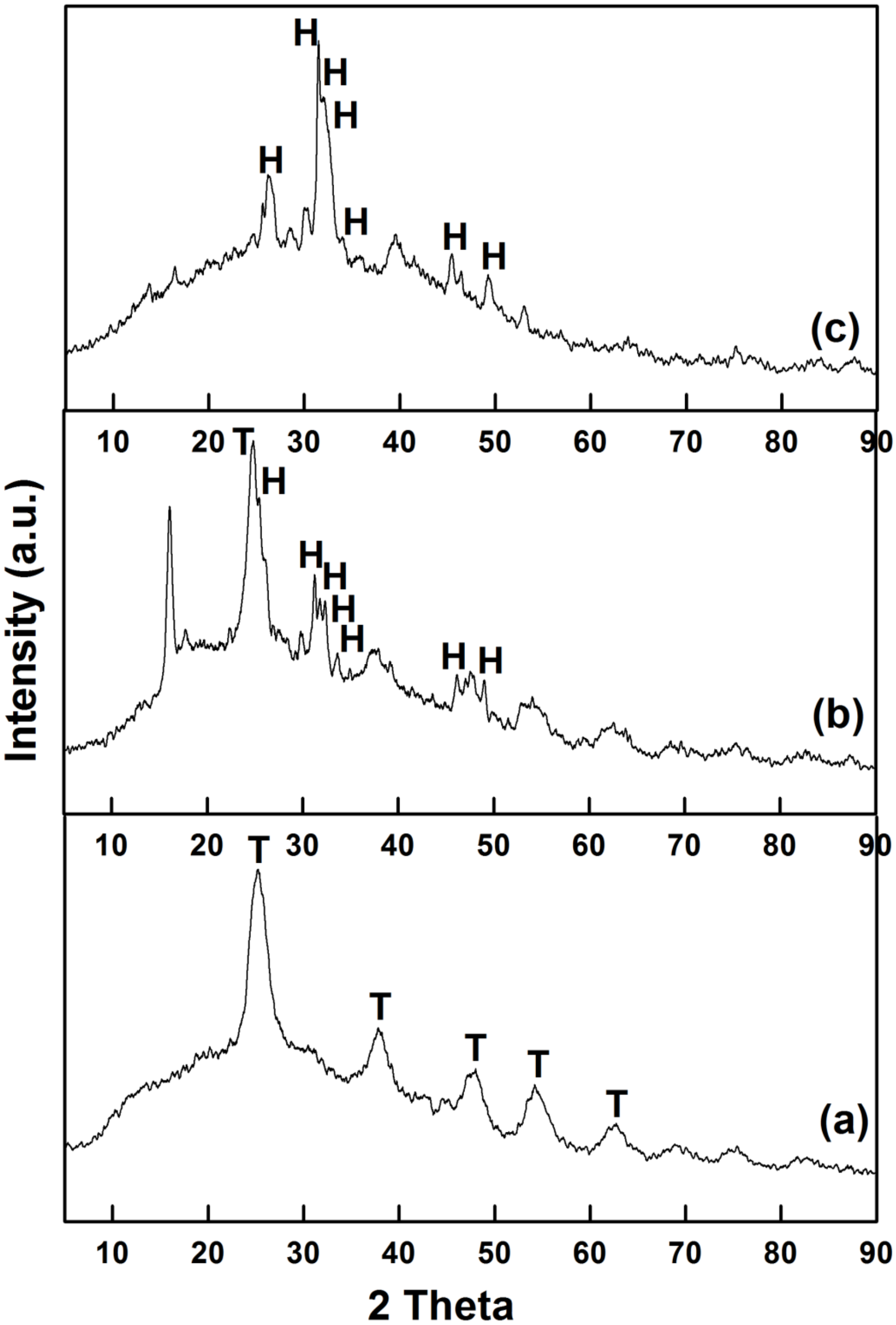

Figure 6.17 XRD spectra of (a) TiO$_2$–Alginate scaffold (control), (b) TiO$_2$–HAp–Alginate nanocomposite scaffold and (c) HAp–Alginate scaffold (control), where: T–anatase TiO$_2$ and H–HAp.

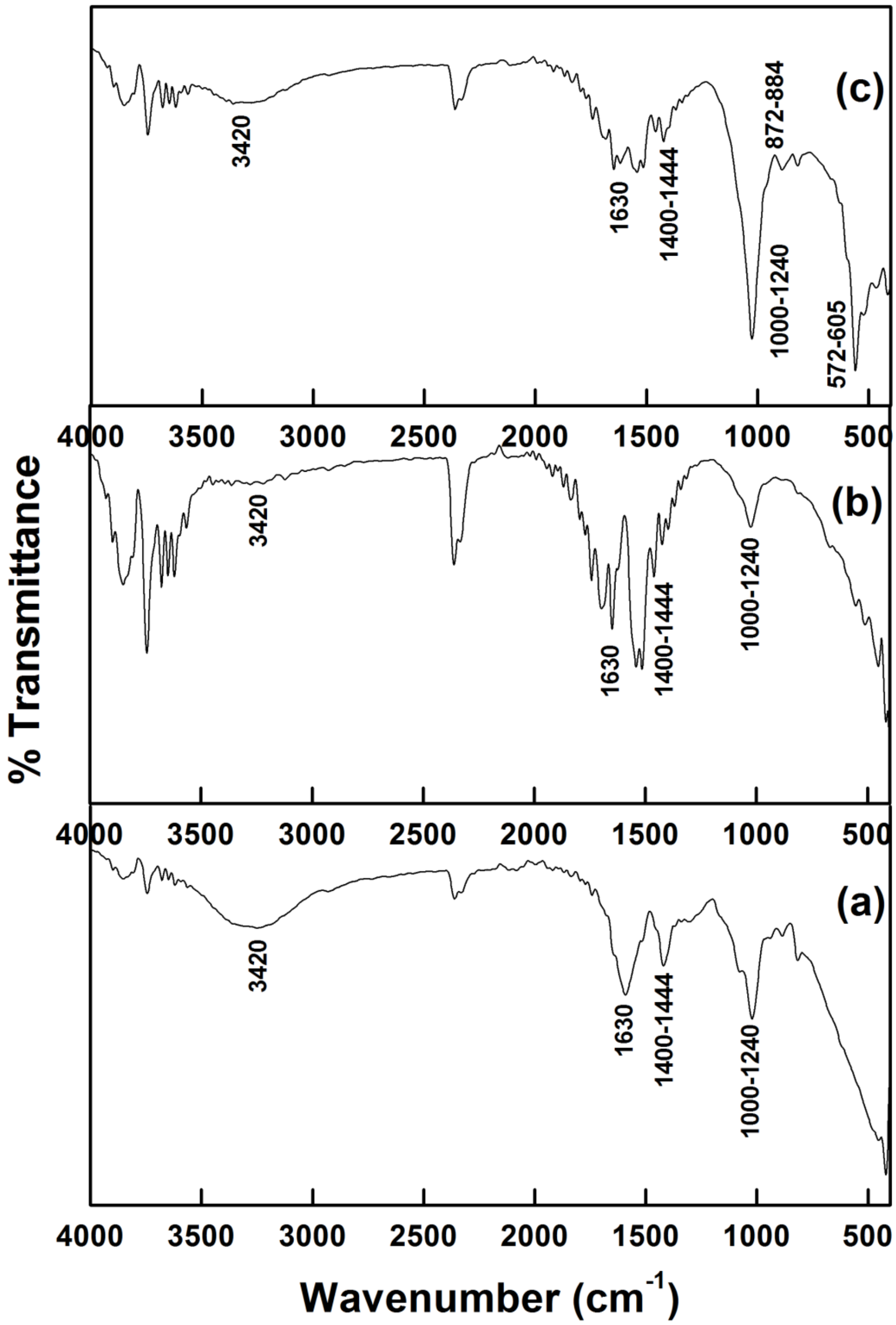

Figure 6.18 FTIR spectra of (a) TiO_2–Alginate scaffold (control), (b) TiO_2–HAp–Alginate nanocomposite scaffold and (c) HAp–Alginate scaffold (control).

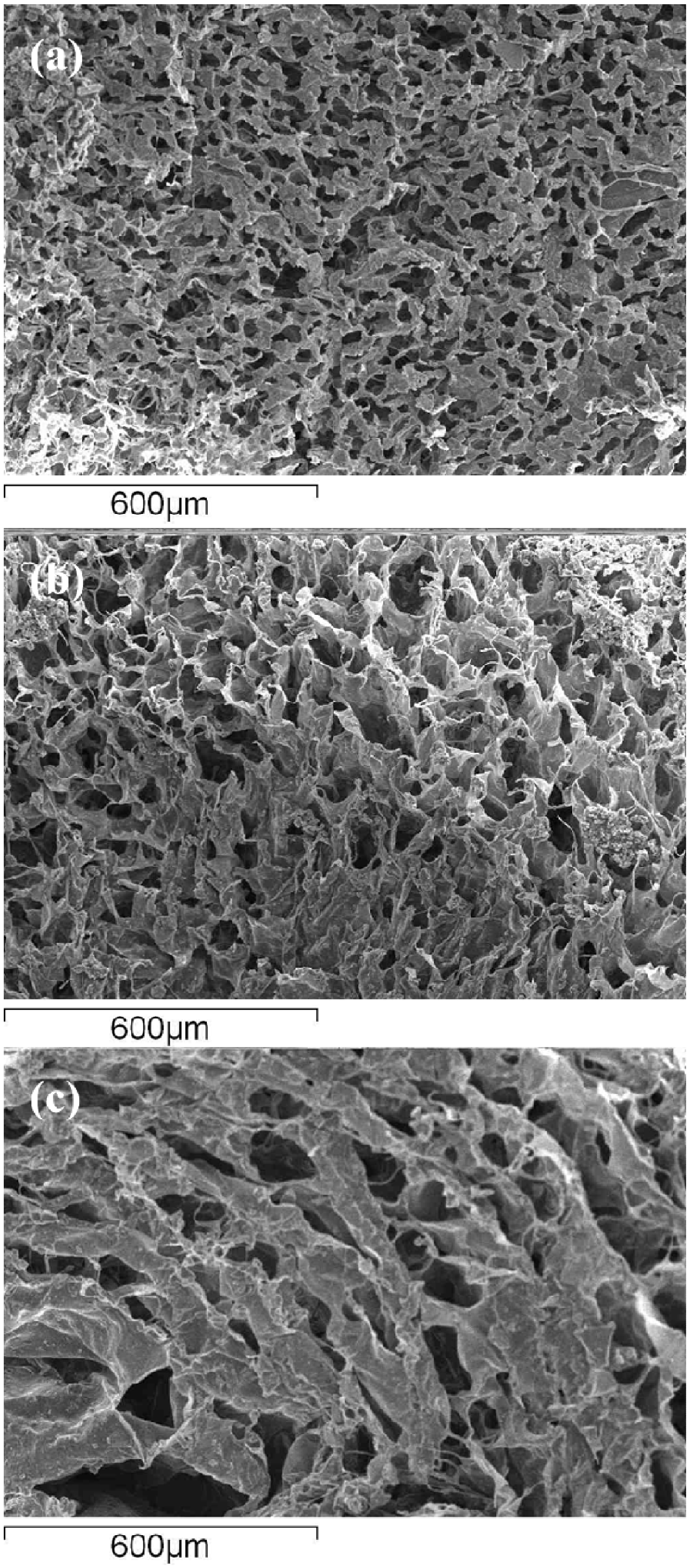

Figure 6.19 SEM images showing macroporous structure of (a) TiO_2−Alginate scaffold (control), (b) HAp−Alginate scaffold (control) and (c) TiO_2−HAp−Alginate nanocomposite scaffold.

6.3.8 Swelling studies

The swelling behaviour of the scaffolds is shown in Figure 6.20. The swelling ratio of the TiO_2–HAp–Alginate nanocomposite scaffold was 14.9. Similar observation was reported for pectin–chitin/nano $CaCO_3$ composite scaffolds which was proposed for bone tissue engineering applications (Kumar *et al.* 2013). When TiO_2 was incorporated in HAp to make composite scaffolds with alginate, the swelling ratio decreased as compared to the HAp–Alginate scaffolds which had a swelling ratio of 17. This may be due to the strong interaction between TiO_2 and HAp. The nanocomposite scaffolds seem to have controlled swelling ratio. This may be attributed to the highly uniform porous structure of the scaffolds. Swelling and porosity aid in the supply of nutrients to the interior of the composite scaffolds and also increase the surface area for the cells to adhere, essential factors for tissue engineering applications. But increased swelling affects the mechanical property of the material, thus, controlled swelling is favoured (Peter *et al.* 2009; Peter *et al.* 2010).

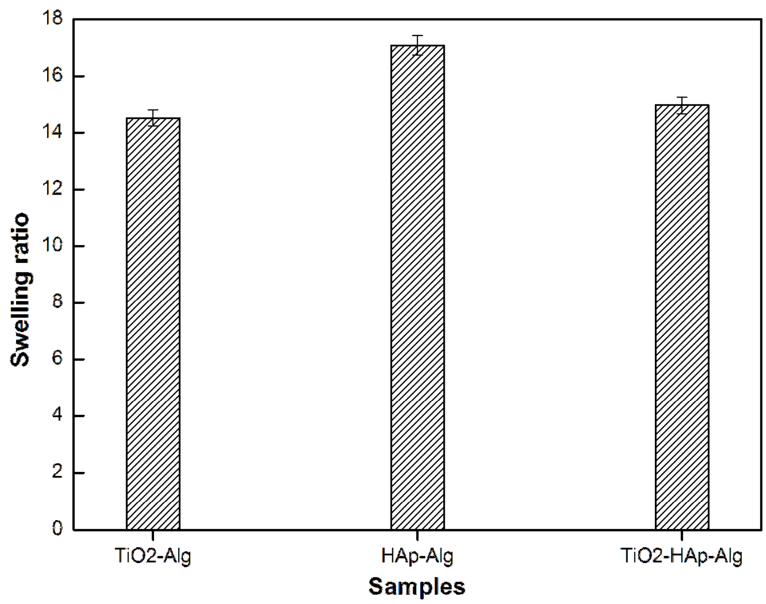

Figure 6.20 Swelling studies of composite scaffolds in PBS.

6.3.9 Porosity estimation

The porosity of the nanocomposite scaffolds as estimated by liquid displacement method is shown in Figure 6.21. The scaffolds exhibited a network structure with good porosity. This was attributed to the use of freeze drying method for the removal of water from the scaffold (Kumar *et al.* 2013). There are several advantages of the freeze–drying method such as regulation of pore diameter and porosity in the scaffolds by the freeze–drying pressure and use of water and ice crystals instead of an organic solvent in the scaffold fabrication process which is more suitable for biomedical applications (Lu *et al.* 2013) TiO_2–HAp–Alginate scaffold showed a higher percentage of porosity of 98 % as compared to HAp-Alginate (96 %) and TiO_2–Alginate (79 %) scaffolds. Porosity is essential for the transport of oxygen and nutrients to the interior of the scaffolds. Porosity offered by the composite scaffold enhances the bone bonding ability due to the following reasons: (i) high surface area to volume ratio offered by HAp has the tendency to bioresorb and induce bioactivity, (ii) interconnected pores can provide a framework for bone growth into the matrix of the implant, and thus anchor them with the surrounding bone, preventing micro–motion that in turn increases further bone growth, (iii) interconnected porosity is also a source of nutrient supply, vascularization and waste removal (Srinivasan *et al.* 2012; Nandi *et al.* 2009).

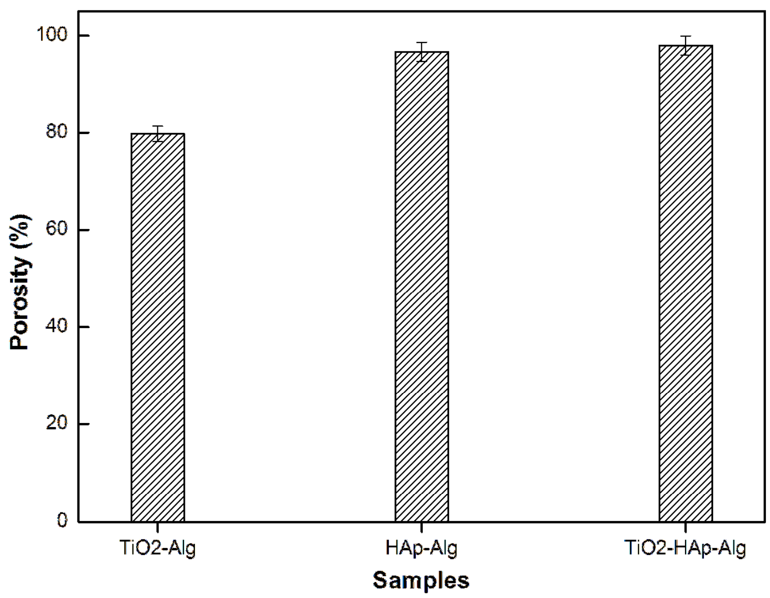

Figure 6.21 Porosity studies of composite scaffolds.

6.3.10 *In vitro* degradation studies

The *in vitro* degradation profile of nanocomposite scaffolds is shown in Figure 6.22. TiO_2–HAp–Alginate scaffold showed only 8.94 % of degradation in 7 days as compared to 21.94 % and 27.16 % degradation of TiO_2–Alginate and HAp–Alginate scaffolds respectively. The 1–4 glycosidic linkages of alginate are susceptible to degradation by lysozyme due to the ionic interaction of the negatively charged alginate with lysozyme. This results in the formation of simple glucose type residues (Hunt *et al.* 2010). The degradation rate of alginate is drastically reduced due to the presence of HAp and TiO_2 and ionic cross–linking with calcium ions. The divalent calcium ions dissipate as a result of exposure to monovalent cations such as sodium, potassium and phosphate ions present in the media containing lysozyme (Mohan and Nair 2005). An ideal tissue engineering scaffold should be biodegradable and the rate of degradation should match the rate of tissue regeneration (Srinivasan *et al.* 2012; Roman *et al.* 2003). The results show that the TiO_2–HAp–Alginate nanocomposite scaffold is biodegradable thus, satisfying the ideal requirements for tissue engineering applications. Further the controlled degradation would be helpful to deliver drugs, growth factors, etc. (Kumar *et al.* 2013).

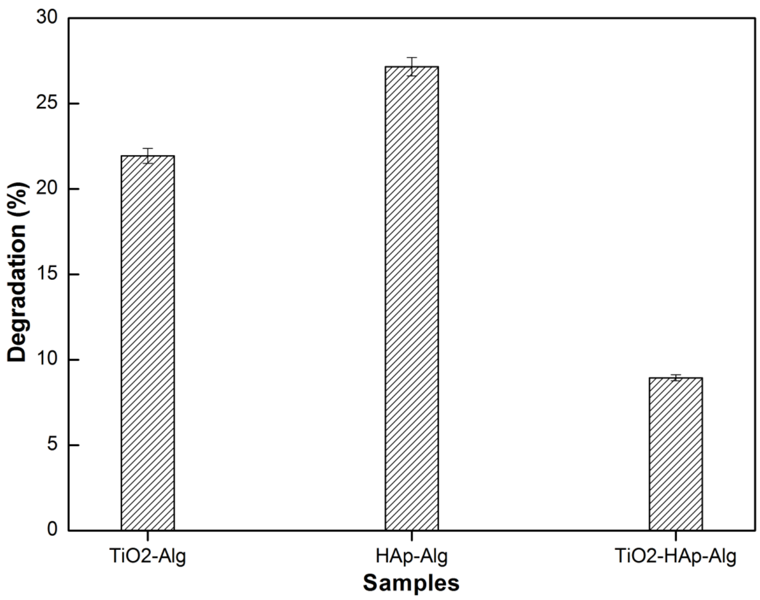

Figure 6.22 *In vitro* degradation profile of composite scaffolds in PBS containing lysozyme.

6.3.11 *In vitro* biomineralization studies

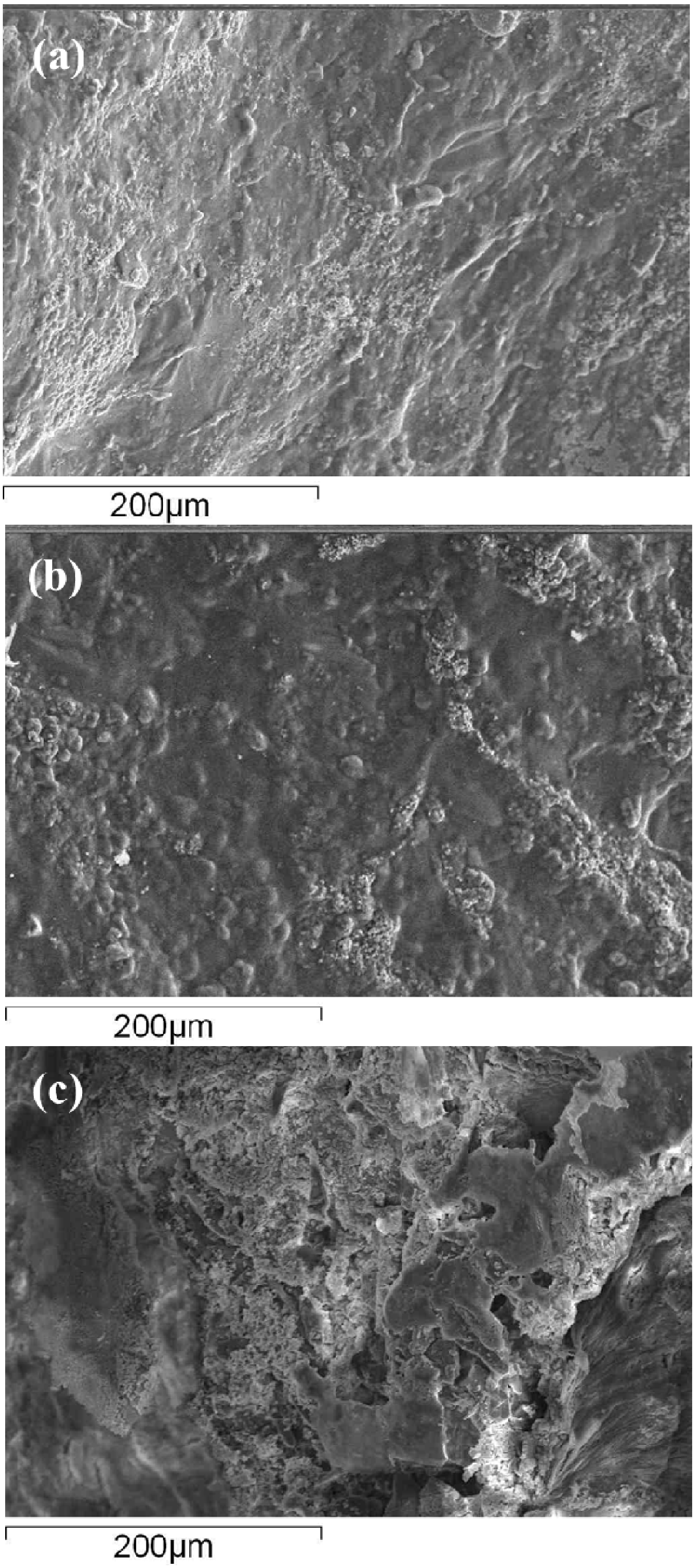

Figure 6.23 SEM images of *in vitro* biomineralization of (a) TiO_2−Alginate scaffold, (b) HAp−Alginate scaffold and (c) TiO_2−HAp−Alginate nanocomposite scaffold in 5X SBF after 3 h.

The essential requirement for an artificial material to bond to living bone is the formation of bonelike apatite on its surface when implanted in the living body. This *in vivo* apatite formation can be reproduced in SBF which has ion concentrations nearly equal to those of human blood plasma (Kokubo 1991). The *in vivo* bone bioactivity of a material can be predicted from the apatite formation on its surface in SBF. However, a long period is often necessary in the biomimetic process. The classical biomimetic process usually involves immersion of samples in SBF, with the fluid being refreshed every other day for about 1 to 4 weeks. Factors, such as temperature and ion concentration influence the growth rate of the apatite layer (Kokubo and Takadama 2006). Recently, several studies have made efforts to shorten this process by using higher ion concentration in SBF. Formation of apatite on metal substrate within a period of 24 h has been reported by using supersaturated SBF (5X SBF) (Barrere *et al.* 2002a; Barrere *et al.* 2002b; Chou *et al.* 2004). Shortening the immersion period can be particularly significant to degradable biopolymers because some polymers degrade significantly during the long incubation period.

Figure 6.23 shows the SEM images of *in vitro* biomineralization studies of the TiO_2–HAp–Alginate nanocomposite scaffolds, TiO_2–Alginate and HAp–Alginate scaffolds (controls) after 3 h of incubation in 5X SBF. Deposition of an apatite rich layer on the surface of the scaffolds was observed indicating the bioactive nature of the scaffolds. This property is essential for cell and extracellular matrix deposition of bone composed of inorganic apatite in dental and orthopaedic applications for direct bonding of the scaffold with the bone defect. Presence of calcium serves as a nucleation site for the mineralization (Srinivasan *et al.* 2012, Kumar *et al.* 2013).

6.3.12 Preparation of methotrexate incorporated TiO_2–HAp–Alginate nanocomposite scaffolds

In this work, methotrexate (MTX), an antifolate drug which is nearly insoluble in water and has comprehensive pharmacological effects against cancer and autoimmune diseases, was selected as a drug model and loaded on the TiO_2–HAp–Alginate nanocomposite scaffolds, TiO_2–Alginate and HAp–Alginate scaffolds (controls). The chemical structure of Methotrexate (4–amino–10–methylfolic acid or 4–amino–4–deoxy–10–methylpteroyl–L–glutamic acid) is shown in Figure 6.24. Methotrexate, is an antineoplastic drug which inhibits dihydrofolateredutase (DHFR), an enzyme essential in the biosynthesis of thymidylate (Sartori *et al.* 2008; Hitchings and Smith 1980). It is widely used in the treatment of malignancies including childhood acute lymphocytic leukemia, osteosarcoma, non-Hodgkin's lymphoma, Hodgkin's disease, head and neck cancer, lung cancer, breast cancer, psoriasis, choriocarcinoma and related trophoblastic tumors (Calabresi 1975; Seo 2009).

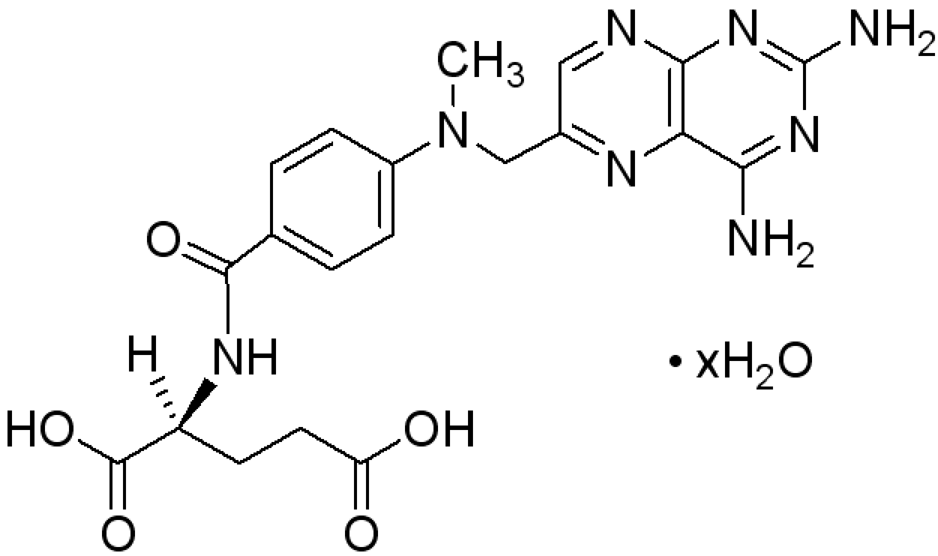

Figure 6.24 Chemical structure of methotrexate.

Various strategies for incorporating drugs within scaffolds have been proposed. Most commonly used strategies include (i) adsorbing drugs onto the pore surface of the scaffolds wherein the drug release is by diffusion, (ii) entrapping drugs within the scaffold structure wherein the drug is released in a controlled manner during degradation of the scaffold (Mourino and Boccaccini 2010). The incorporation efficiency when MTX was adsorbed on the scaffold by immersing the scaffold in the MTX solution was 83.50 % whereas it was 100 % when MTX was added to the scaffold slurry during synthesis.

6.3.13 Drug release from the methotrexate incorporated TiO_2–HAp–Alginate nanocomposite scaffolds

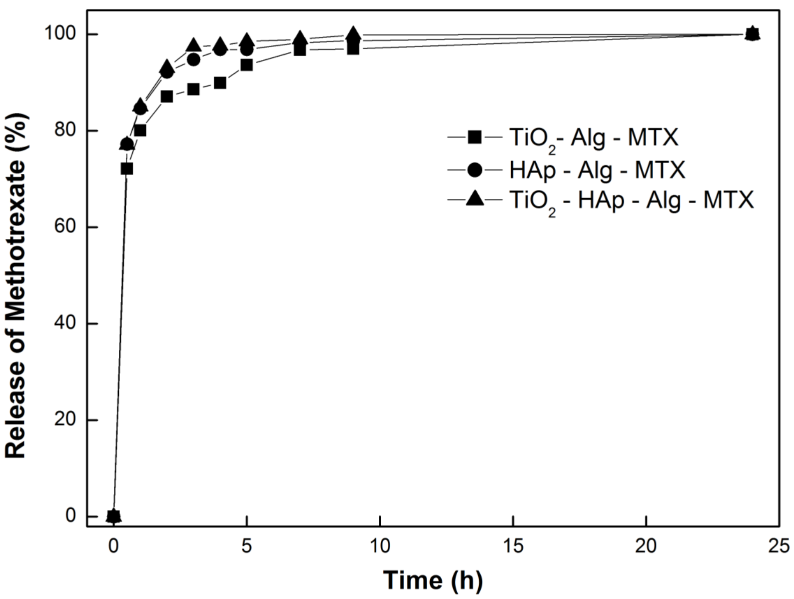

Figure 6.25 Cumulative drug release curve of MTX incorporated composite scaffolds in which MTX was adsorbed on the scaffold by immersing the scaffold in the MTX solution.

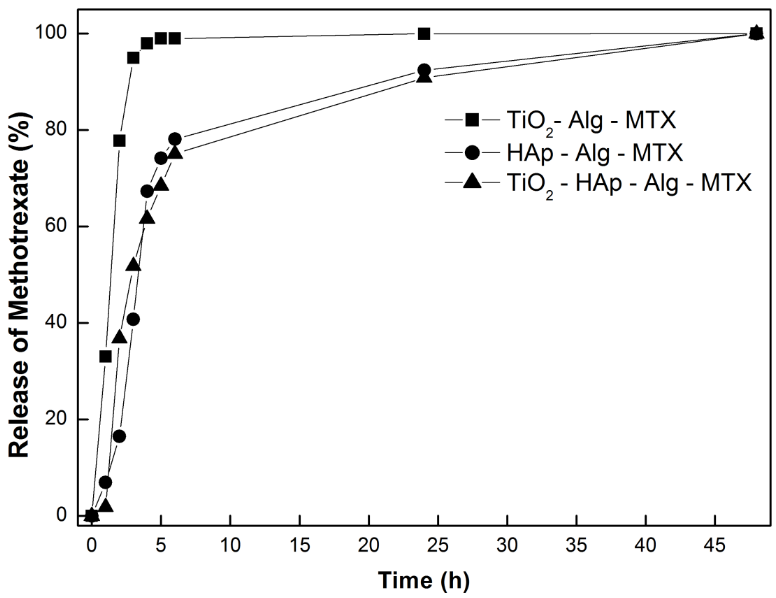

Figure 6.26 Cumulative drug release curve of MTX incorporated composite scaffolds in which MTX was added to the scaffold slurry during synthesis.

In recent years, there has been an increasing interest to fabricate scaffolds that can deliver drugs such as antibiotics, anticancer agents, and growth factors (Rai *et al.* 2005; Kim *et al.* 2004a; Kim *et al.* 2004b; Murphy *et al.* 2000) and hence there is an increasing interest in incorporating a drug delivery function in tissue engineering applications (Gomes and Reis 2004; Duarte *et al.* 2009a; Duarte *et al.* 2009b). The increasing amount of work dealing with this approach is leading to the establishment of an emerging field which has been termed tissue engineering therapeutics (Baroli 2009). *In vitro* MTX release studies were performed in PBS (pH 7.4; 37 °C). Figure 6.25 shows the *in vitro* MTX release profile of nanocomposites scaffolds when the MTX was incorporated in the scaffold by adsorption. As shown in Figure 6.25, more than 80 % of the MTX was released from all the three scaffold samples within 2 h. Generally, two potential therapy hazards could be caused by this kind of release profile. First, complete release within a short period could lead to a high drug concentration, which stimulates and enhances the metabolic drug clearance of the body ultimately reducing the drug bioavailability (Huang and Brazel 2001; Duncan *et al.* 2005). Second, such uncontrolled burst release, especially of the chemotherapeutic drugs, could result in a local drug concentration that is too high, which not only hampers the drug's targeted delivery, but also severely jeopardizes local tissues (Chen *et al.* 2013; Wolinsky *et al.* 2012).

The drug release profile of MTX in scaffolds where the drug was incorporated during scaffold fabrication was biphasic (Figure 6.26), with an initial burst release followed by a much slower release period. For the TiO_2–HAp–Alginate scaffold, the accumulative drug release was 1.86 % within the first 60 min, 75 % after 6 h and 90 % after 24 h, which remained steady for the next 24 h. Accumulative MTX release curves of TiO_2-HAp–Alginate and HAp–Alginate scaffolds almost overlapped, the former showing slightly higher percentage of release. In contrast, the drug retention efficiency of the TiO_2–Alginate scaffold was much lower and the drug was released more rapidly. About 33 % of the drug was released within the first 60 minutes, which reached 77.81 % in 2 h and 95 % after 3 h, and remained steady thereafter. The initial burst release of MTX incorporated porous TiO_2–HAp–Alginate scaffolds can be due to MTX absorbed onto or loosely bound with the matrix surface which is released as soon as the drug–loaded porous scaffolds comes in contact with the release medium.

The drug release is generally dominated by three factors: (1) type of association between the drug and the matrix, (2) the solubility of the drug in the release medium, and (3) the degree and speed of infiltration of the release medium in the scaffolds, which can be comprehensively affected by the type of material of the matrix, the physical and chemical properties of the release medium, the volume of the porous scaffolds, and the diameter of the pores (Siepmann *et al.* 2008; Borgquist *et al.* 2006). The later slow and sustained release of methotrexate was due to entrapment of the drug inside the network of the scaffold matrix and good drug adsorption capacity of HAp. All of the above results demonstrate that drug incorporated porous scaffolds prepared by freeze drying method exhibit controlled drug release, which offers great potential for drug delivery and therapy for bone diseases and defects (Chen *et al.* 2013).

6.4 Conclusion

Nanocomposite scaffolds were successfully fabricated using freeze drying technique and characterized. The 50:50 TiO_2–HAp–Alginate scaffolds with ceramic : polymer ratio as 0.5:1, were found to have physico–chemical and biological properties essential to facilitate bone regeneration. The nanocomposite scaffold had a pore size of about 120 µm, exhibited controlled porosity and swelling ability, limited degradation and enhanced biomineralization. MG–63 cells exhibited good viability, cell attachment and cell proliferation on the scaffolds. These hybrid scaffolds exhibit much higher stiffness, indicating that TiO_2–based structures are good candidates in tissue engineering applications requiring mechanical features. The methotrexate incorporated scaffold demonstrated ideal drug release characteristics indicating their potential for application as bioactive matrix for bone tissue regeneration and drug delivery.

Summary of Results and Conclusion

Sol–gel method of synthesis was used to prepare mesoporous AgCl–TiO_2 nanoparticles (ATNPs) with TiO_2 as homogenous anatase crystalline phase. The crystallite size as calculated using Scherrer formula was 3.76 nm and the BET surface area was 266 m^2/g. In this method, effective removal of adsorbed ions was achieved through frequent change of the deionized water during dialysis. The simplicity of this method gives it an advantage over the conventional time consuming processes. Further, it requires very few chemicals, no harmful by–products are generated and calcination is achieved at low temperature. Sol–gel is an attractive method for obtaining nanoparticles with high surface area, porosity and monodispersity.

The antimicrobial activity of these ATNPs was studied and they were found to be highly efficient antimicrobial agents. The antimicrobial activity was achieved at a remarkably low silver concentration in the range of 1–20 µg/mL of ATNP (effective Ag concentration of 11.7–234 ppb) in aqueous phase and 100–1000 µg/mL of ATNP (effective Ag concentration of 1.170–11.7 ppm) in growth medium within two hours of contact. The antimicrobial activity is attributed to the combined effect of release of silver ions and ROS production resulting in membrane damage and cell death. Therefore, this material has a lot of potential for application as disinfectants/antiseptics to render surfaces germ free, in filters to disinfect water, in textile industries to manufacture self–cleaning textiles, as coatings of implants to avoid bacterial infections and in food packaging industry.

AgCl–TiO_2 coatings were studied for their anti–biofilm activity and were found to be very effective in preventing biofilm formation by *E. coli*, *S. epidermidis* and *P. aeruginosa* over a period of 10 days. These low temperature processed coatings released an initial high amount of silver ions followed by a slow and gradual release facilitating sustained anti–biofilm activity. The initial high release of silver ions is beneficial for reducing bacterial adhesion, which is the first step in the development of a biofilm. As these coatings are very effective in controlling biofilm formation, they could find application in medical implants, medical equipment, water distribution systems, food production facilities or places where appropriate cleaning practices are required.

Furthermore, the anti–quorum sensing potential of ATNPs was studied using *C. violaceum* ATCC 12472. Specifically, this study aimed to determine the dynamics of quorum sensing inhibition by ATNPs in relation to its concentration for potential application as active food packaging material. The silver present in ATNPs inhibited quorum sensing by interfering with the AHL activity and thus inhibited the production of violacein pigment which was further confirmed using Fourier transform infrared spectroscopy, High–performance liquid chromatography and Mass spectrometry analysis. TiO_2 acted as a good supporting matrix facilitating effective use of silver by reducing its concentration required for bioactivity. The findings of the work present silver as a potential quorum sensing inhibitor which can be developed for its use as an anti–pathogenic but non–toxic bioactive material.

The potential of nano TiO_2 was also explored for bone tissue engineering applications. Nanocomposite scaffolds containing TiO_2, HAp and Alginate were successfully fabricated using freeze–drying technique and characterized. The 50:50 TiO_2–HAp–Alginate scaffold with ceramic : polymer ratio as 0.5:1 was found to have ideal physico–chemical and biological properties essential to facilitate bone regeneration. The nanocomposite scaffold had a pore size of about 120 µm, exhibited controlled porosity and swelling ability, limited degradation and enhanced biomineralization. MG–63 cells exhibited good viability, cell attachment and cell proliferation on the scaffolds. These hybrid scaffolds exhibit much higher stiffness, indicating that TiO_2–based structures are good candidates in tissue engineering applications requiring mechanical features. The methotrexate incorporated scaffold demonstrated ideal drug release characteristics indicating their potential for application as bioactive matrix for bone tissue regeneration and drug delivery.

Thus some of the important contributions emerging from the present thesis are as follows:

1) In this study, a new silver based nanocomposite has been synthesized using a novel sol–gel method of synthesis. These nanoparticles exhibited excellent antimicrobial activity at very low silver concentrations.

2) This is the first report of anti–biofilm activity of AgCl–TiO_2 where the nanoparticles were immobilized by coating them on glass slides. These coatings exhibited anti–

biofilm activity tested over a period of ten days, which is attributed to the controlled release of silver ions from the coatings.

3) In the present work, anti–quorum sensing activity of silver entrapped in TiO_2 was demonstrated for the first time.

4) Novel TiO_2–HAp–Alginate scaffolds with superior mechanical and biocompatible properties were fabricated using the freeze–drying method. Drug delivery potential of these scaffolds using chemotherapeutic drug methotrexate was studied and these scaffolds were proposed as ideal candidates for bone tissue engineering and drug delivery applications.

Future Scope of Work

1) The AgCl–TiO_2 nanoparticles exhibited excellent antimicrobial and anti–biofilm activity. This material has a lot of potential for application as disinfectants/antiseptics to render surfaces germ free where appropriate cleaning practices are required, in filters and water distribution systems to disinfect water, in textile industries to manufacture self–cleaning textiles, in medical implants and equipment and as coatings on implants to avoid bacterial infections. Further studies of this material can be conducted to evaluate their *in vivo* potential to prevent biofilm related implant based infections using animal models.

2) Additionally, AgCl–TiO_2 nanoparticles also demonstrated efficient anti–quorum sensing activity. Unlike conventional antibiotics which prevent bacterial cell division (bacteriostatic) or kill the cell (bactericidal) and increase the selective pressure towards antibiotic resistance, the development of resistance to anti–quorum sensing compounds is minimal as they only target virulence mechanisms and do not impede growth. Hence, these nanoparticles could find potential applications in various fields such as food and beverage industry, household uses and treatment of burns where bacteriostatic effect of silver is required. Silver in active food packaging material can prevent the growth of microorganisms at much lower concentrations, than required for antimicrobial activity. The potential of these nanoparticles for such applications needs to be further investigated.

3) The methotrexate incorporated TiO_2–HAp–Alginate nanocomposite scaffolds exhibited ideal mechanical properties, biocompatibility and drug release characteristics indicating their potential for application as bioactive matrix for bone tissue regeneration and drug delivery. These materials can be investigated for fabrication of hybrid scaffolds using animal models for potential applications in the field of bone tissue engineering.

References

Adams, N. W. H. and Kramer, J. R. (1999) Silver speciation in wastewater effluent, surface waters, and pore waters. *Environmental Toxicology and Chemistry* **18**, 2667–2673.

Agency for Toxic Substances and Disease Registry (ATSDR) (1990) Toxicological profile for silver. In: US Department of Health and Human Services, Public Health Service and Agency for Toxic Substances and Disease Registry (Eds), Atlanta, GA.

Ahn, E. S., Gleason, N. J., Nakahira, A. and Ying, J. Y. (2001) Nanostructure processing of hydroxyapatite–based bioceramics. *Nano Letters* **1**, 149–153.

Akhavan, O. and Ghaderi, E. (2009) Bactericidal effects of Ag nanoparticles immobilized on surface of SiO_2 thin film with high concentration. *Current Applied Physics* **9**, 1567–1739.

Albrektsson, T. and Johansson, C. (2001) Osteoinduction, osteoconduction and osseointegration. *Eur Spine J* **10**, S96–S101.

Allhoff, F., Lin, P. and Moore, Daniel. (2010) What is nanotechnology and why does it matter?: From science to ethics. Wiley–Blackwell, John Wiley & Sons Ltd, United Kingdom.

Alvarez, M. V., Moreira, M. R. and Ponce, A. (2012) Antiquorum sensing and antimicrobial activity of natural agents with potential use in food. *J Food Saf* **32**, 379–387.

Amin, S. A., Pazouki, M. and Hosseinnia, A. (2009) Synthesis of TiO_2–Ag nanocomposite with sol–gel method and investigation of its antibacterial activity against *E. coli*. *Powder Technol* **196**, 241–245.

Ammor, M. S., Michaelidis, C. and Nychas, G. J. E. (2008) Insights into the role of quorum sensing in food spoilage. *J Food Prot* **71**, 1510–1525.

An, J., Zhang, M., Wang, S., and Tang, J. (2008) Physical, chemical and microbiological changes in stored green asparagus spears as affected by coating of silver nanoparticles–PVP. *LWT–Food Science and Technology* **41**, 1100–1107.

Andreescu, S., Ornatska, M., Erlichman, J. S., Estevez, A. and Leiter, J. C. (2012) Biomedical Applications of Metal Oxide Nanoparticles. In: Fine Particles in Medicine and Pharmacy, Springer, United States.

Andrievski, R. A. and Glezer, A. M. (2001) Size effects in properties of nanomaterials. *Scripta mater* **44**, 1621–1624.

Ayon, A. A., Cantu, M., Chava, K., Agrawal, C. M., Feldman, M. D., Johnson, D., Patel, D., Marton, D. and Shi, E. (2006) Drug loading of nanoporous TiO_2 films. Biomed Mater **1**, L11–15.

Azaroff, L. V. and Buerger, M. J. (1975) The Powder Method in X–ray Crystallography, McGraw Hill Book Company, Inc.

Azizi, R., Rasouli, S., Ahmadi, N. P., Kolaei, A. J. J. and Azizi, M. (2012) A systematic investigation of experimental conditions on the particle size and structure of TiO_2 nanoparticles synthesized by a sol–gel method. *Journal of Ceramic Processing Research* **13**, 164–169.

Babapour, A., Yang, B., Bahang, S. and Cao, W. (2011) Low–temperature Sol–gel–derived nanosilver–embedded silane coating as biofilm inhibitor. *Nanotechnology* **22**, 155602.

Banerjee, S., Judy, G., Muraleedharan, P., Tyagi, A. K. and Baldev, R. (2006) Physics and chemistry of photocatalytic titanium dioxide: visualization of bactericidal activity using atomic force microscopy. *Current Science* **90**, 1378–1383.

Baroli, B. (2009) From natural bone graft to tissue engineering therapeutics: brainstorming on pharmaceutical formulative requirements and challenges. *J Pharm Sci* **98**, 1317–1375.

Barrere, F., Blitterswijk, C. A., Groot, K. and Layrolle, P. (2002a) Influence of ionic strength and carbonate on the Ca–P coating formation from SBF×5 solution. *Biomaterials* **23**, 1921–1930.

Barrere, F., Blitterswijk, C. A., Groot, K. and Layrolle, P. (2002b) Nucleation of biomimetic Ca–P coatings on Ti6Al4V from a SBF×5 solution: influence of magnesium. *Biomaterials* **23**, 2211–2220.

Bauer, A. W., Kirby, W. M., Sherris, J. C. and Turck, M. (1966) Antibiotic susceptibility testing by a standardized single disk method. *Am J Clin Pathol* **45**, 493–496.

Baumer, M. and Freund, H. J. (1999) Metal deposits on well–ordered oxide films. *Progress in Surface Science* **61**, 127–198.

Berger, T. J., Spadaro, J. A., Chapin, S. E. and Becker, R. O. (1976) Electrically Generated Silver Ions: Quantitative Effects on Bacterial and Mammalian Cells. *Antimicrob Agents Chemother* **9**, 357–358.

Bersani, D., Lottici, P. P. and Ding, X. Z. (1998) Phonon confinement effects in the Raman scattering by TiO_2 nanocrystals. *Applied Physics Letters* **72**, 73–75.

Bessekhouad, Y., Robert, D. and Weber, J. V. (2003) Synthesis of photocatalytic TiO_2 nanoparticles: optimization of the preparation conditions. *Journal of Photochemistry and Photobiology A: Chemistry* **157**, 47–53.

Bhat, M. H., Chakravarthy, B. P., Ramakrishnan, P. A., Levasseur, A. and Rao, K. J. (2000) Microwave synthesis of electrode materials for lithium batteries. *Bull Mater Sci* **23**, 461–466.

Bish, D. L. and Post, J. E. (1989) Modern Powder Diffraction, The Mineralogical Society of America, Washington.

Blake, D. M., Maness, P., Huang, Z., Wolfrum, E. J. and Huang, J. (1999) Application of the photocatalytic chemistry of titanium dioxide to disinfection and the killing of cancer cells. *Sep Purif Methods* **28**, 1–50.

Blaser, S. A., Scheringer, M., MacLeod, M. and Hungerbühler, K. (2008) Estimation of cumulative aquatic exposure and risk due to silver: Contribution of nano–functionalized plastics and textiles. *Science of The Total Environment* **390**, 396–409.

Blesic, M. D., Saponjic, Z. V., Nedeljkovic, J. M. and Uskokovic, D. P. (2002) TiO_2 films prepared by ultrasonic spray pyrolysis of nanosize precursor. *Mater Lett* **54**, 298–302.

Boccaccini, A. R. and Maquet, V. (2003) Bioresorbable and bioactive polymer/bioglass® composites with tailored pore structure for tissue engineering applications. *Comp Sci Technol* **63**, 2417–2429.

Bonino, C. A., Krebs, M. D., Saquing, C. D., Jeong, S. I., Shearer, K. L., Alsberg, E. and Khan, S. A. (2011). Electrospinning alginate–based nanofibers: from blends to crosslinked low molecular weight alginate–only systems. *Carbohydrate Polymers* **85**, 111–119.

Borgquist, P., Korner, A., Piculell, L., Larsson, A. and Axelsson, A. (2006) A model for the drug release from a polymer matrix tablet–effects of swelling and dissolution. *J Control Release* **113**, 216–225.

Bosetti, M., Masse, A., Tobin, E. and Cannas, M. (2002) Silver coated materials for external fixation devices: *in vitro* biocompatibility and genotoxicity. *Biomaterials* **23**, 887–892.

Brandt, O., Mildner, M., Egger, A. E., Groessl, M., Rix, U., Posch, M., Keppler, B. K., Strupp, C., Mueller, B. and Stingl, G. (2012) Nanoscalic silver possesses broad–spectrum antimicrobial activities and exhibits fewer toxicological side effects than silver sulfadiazine. *Nanomedicine* **8**, 478–488.

Brett, D. W. (2006) A discussion of silver as an antimicrobial agent: alleviating the confusion. *Ostomy Wound Manage* **52**, 34–41.

Brooks, J. D. and Flint, S. H. (2008) Biofilms in the food industry: problems and potential solutions. *Int J Food Sci Tech* **43**, 2163–2176.

Bruhn, J. B., Christensen, A. B., Flodgaard, L. R., Nielsen, K. F., Larsen, T. O., Givskov, M. and Gram, L. (2004) Presence of acylated homoserine lactones (AHLs) and AHL–producing bacteria in meat and potential role of AHL in spoilage of meat. *Appl Environ Microb* **70**, 4293–4302.

Buckwalter, J. A., Glimcher, M. J., Cooper, R. R. and Recker, R. (1996a) Bone biology. I. Structure, blood supply, cells, matrix, and mineralization. *Instr Course Lect* **45**, 371–386.

Buckwalter, J. A., Glimcher, M. J., Cooper, R. R. and Recker, R. (1996b) Bone biology. II. Formation, form, modeling, remodeling, and regulation of cell function. *Instr Course Lect* **45**, 387–399.

Buerger, M. J. (1942) X–ray Crystallography, J Wiley, New York.

Bullen, C., Mulvaney, P., Sada, C., Ferrari, M., Chiasera, A. and Martucci, A. (2004) Incorporation of a highly luminescent semiconductor quantum dot in ZrO_2–SiO_2 hybrid sol–gel glass film. *J Mater Chem* **14**, 1112–1116.

Calabresi. P. (1975) The Pharmacological Basis of Therapeutics, Macmillan, New York.

Cao, H. and Liu, X. (2010) Silver nanoparticles–modified films versus biomedical device–associated infections. *Wiley Interdiscip Rev Nanomed Nanobiotechnol* **2**, 670–684.

Cao, H., Liu, X., Meng, F. and Chu, P. K. (2011) Biological actions of silver nanoparticles embedded in titanium controlled by micro–galvanic effects. *Biomaterials* **32**, 693–705.

Chang, B. Y., Huang, N. M., An'amt, M. N., Marlinda, A. R., Norazriena, Y., Muhamad, M. R., Harrison, I., Lim, H. N. and Chia, C. H. (2012) Facile hydrothermal preparation of titanium dioxide decorated reduced graphene oxide nanocomposite. *Int J Nanomedicine* **7**, 3379–3387.

Chatterjee, A., Santra, M., Won, N., Kim, S., Kim, J. K., Kim, S. B. and Ahn, K. H. (2009) Selective Fluorogenic and Chromogenic Probe for Detection of Silver Ions and Silver Nanoparticles in Aqueous Media. *J Am Chem Soc* **131**, 2040–2041.

Chaturvedi, S., Dave, P. N. and Shah, N.K. (2012) Applications of nano–catalyst in new era. *Journal of Saudi Chemical Society* **16**, 307–325.

Chaudhry, Q., Scotter, M., Blackburn, J., Ross, B., Boxall, A., Castle, L., Aitken, R. and Watkins, R. (2008) Applications and implications of nanotechnologies for the food sector. *Food Addit Contam Part A Chem Anal Control Expo Risk Assess* **25**, 241–258.

Chaw, K. C., Manimaran, M. and Tay, F. E. (2005) Role of silver ions in destabilization of intermolecular adhesion forces measured by atomic force microscopy in *Staphylococcus epidermidis* biofilms. *Antimicrob Agents Chemother* **49**, 4853–4859.

Chawengkijwanich, C. and Hayata, Y. (2008) Development of TiO_2 powder–coated food packaging film and its ability to inactivate *Escherichia coli in vitro* and in actual tests. *Int J Food Microbiol* **123**, 288–292.

Chen, A. Z., Yang, Y. M., Wang, S. B., Wang, G. Y., Liu, Y. G. and Sun, Q. Q. (2013) Preparation of methotrexate–loaded, large, highly–porous PLLA microspheres by a high–voltage electrostatic antisolvent process. *J Mater Sci Mater Med* **24**, 1917–1925.

Chen, G. P., Ushida, T. and Tateishi, T. (2001) Preparation of poly (L–lactic acid) and poly (DL–lactic–co–glycolic acid) foams by use of ice microparticulates. Biomaterials **18**, 2563–2567.

Chen, S., Li, J., Qian, K., Xu, W., Lu, Y., Huang, W. and Yu, S. (2010) Large scale photochemical synthesis of M@TiO_2 nanocomposites (M = Ag, Pd, Au, Pt) and their optical properties, CO oxidation performance, and antibacterial effect. *Nano Res* **3**, 244–255.

Chen, X. and Mao, S. S. (2007) Titanium Dioxide Nanomaterials: Synthesis, Properties, Modifications, and Applications. *Chem Rev* **107**, 2891–2959.

Chen, X. and Schluesener, H. J. (2008) Nanosilver: A nanoproduct in medical application. *Toxicology Letters* **176**, 1–12.

Chen, Y., Wan, Y., Wang, Y., Zhang, H. and Jiao, Z. (2011) Anticancer efficacy enhancement and attenuation of side effects of doxorubicin with titanium dioxide nanoparticles. *International Journal of Nanomedicine* **6**, 2321–2326.

Chiang, W.C., Schroll, C., Hilbert, L. R., Møller, P., Tolker–Nielsen, T. (2009) Silver–palladium surfaces inhibit biofilm formation. *Appl Environ Microbiol* **75**, 1674–1678.

Chmielowiec–Korzeniowska, A., Krzosek, Ł., Tymczyna, L., Pyrz, M. and Drabik, A. (2013) Bactericidal, fungicidal and virucidal properties of nanosilver. Mode of action and potential application. A review. *Annales Universitatis Mariae Curie–Skłodowska Lublin–Polonia* **31**.

Choi, O. and Hu, Z. (2008) Size dependent and reactive oxygen species related nanosilver toxicity to nitrifying bacteria. *Environ Sci Technol* **42**, 4583–4588.

Choo, J. H., Rukayadi, Y. and Hwang, J. K. (2006) Inhibition of bacterial quorum sensing by vanilla extract. *Lett Appl Microbiol* **42**, 637–41.

Chopra, I. (2007) The increasing use of silver–based products as antimicrobial agents: a useful development or a cause for concern? *Journal of Antimicrobial Chemotherapy* **59**, 587–590.

Chou, Y. F., Chiou, W. A., Xu, Y. H., Dunn, J. C. Y. and Wu, B. M. (2004) The effect of pH on the structural evolution of accelerated biomimetic apatite. *Biomaterials* **25**, 5323–5331.

Cima, L. G., Vacanti, J. P., Vacanti, C., Ingber, D., Mooney, D. and Langer, R. (1991) Tissue engineering by cell transplantation using degradable polymer substrates. *J Biomech Eng* **113**, 143–151.

Clover, J. and Gowen, M. (1994) Are MG–63 and HOS TE85 human osteosarcoma cell lines representative models of the osteoblastic phenotype? *Bone* **15**, 585–591.

Corradi, A. B., Bondioli, F., Focher, B., Ferrari, A. M., Grippo, C., Mariani, E. and Villa, C. (2005) Conventional and Microwave–Hydrothermal Synthesis of TiO_2 Nanopowders. *J Am Ceram Soc* **88**, 2639–2641.

Costerton, J. W., Cheng, K. J., Geesey, G. G., Ladd, T. I., Nickel, J. C., Dasgupta, M. and Marrie, T. J. (1987) Bacterial biofilms in nature and disease. *Annu Rev Microbiol* **41**, 435–464.

Cushen, M., Kerry, J., Morris, M., Cruz–Romero, M. and Cummins, E. (2012) Nanotechnologies in the food industry–Recent developments, risks and regulation. *Trends in Food Science & Technology* **24**, 30–46.

Damm, C. and Münstedt, H. (2008) Kinetic aspects of the silver ion release from antimicrobial polyamide/silver nanocomposites. *Applied Physics A* **91**, 479–486.

David, W. I. F. and Shankland, K. (2008) Structure determination from powder diffraction data. *Acta Cryst* **A64**, 52–64.

Desai, V. and Kowshik, M. (2013) Synthesis and characterization of fumaric acid functionalized AgCl/titania nanocomposite with enhanced antibacterial activity. *J Nanosci Nanotechnol* **4**, 2826–2834.

Desai, V., Naik, B., Ghosh, N. N. and Kowshik, M. (2013) Functionalization of AgCl/titania nanocomposite with folic acid – a promising strategy for enhancement of antimicrobial activity. *Science of Advanced Materials* **5**, 431–439.

Dong, F., Wang, H., and Wu, Z. (2009) One–step "Green" synthetic approach for mesoporous C–doped titanium dioxide with efficient visible light photocatalytic activity. *J Phys Chem C* **113**, 16717–16723.

Drake, P. L. and Hazelwood, K. J. (2005) Exposure–related health effects of silver and silver compounds: A review. *Ann Occup Hyg* **49**, 575–585.

Drenkard, E. and Ausubel, F. M. (2002) *Pseudomonas* biofilm formation and antibiotic resistance are linked to phenotypic variation. *Nature* **18**, 740–743.

Drexler, K. E. (1986) Engines of creation: the coming era of nanotechnology. Anchor Press, New York.

Drexler, K. E., Peterson, C. and Pergamit, G. (1991) Unbounding the future: the nanotechnology revolution. William Morrow, New York.

Duarte, A. R., Mano, J. F. and Reis, R. L. (2009a) Dexamethasone–loaded scaffolds prepared by supercritical–assisted phase inversion. *Acta Biomater* **5**, 2054–2062.

Duarte, A. R., Mano, J. F. and Reis, R. L. (2009b) Preparation of chitosan scaffolds loaded with dexamethasone for tissue engineering applications using supercritical fluid technology. *Eur Polym J* **45**, 141–148.

Ducheyne, P. and Qiu Q. (1999) Bioactive ceramics: the effect of surface reactivity on bone formation and bone cell function. *Biomaterials* **20**, 2287–2303.

Duncan, G., Jess, T. J., Mohamed, F., Price, N. C., Kelly, S. M. and van der Walle, C. F. (2005) The influence of protein solubilisation, conformation and size on the burst release from poly (lactide–co–glycolide) microspheres. *J Control Release* **110**, 34–48.

Duncan, R. (2004) Nanomedicines in action. *Pharm. J.* **273**, 485–488.

Duncan, T. V. (2011) Applications of nanotechnology in food packaging and food safety: barrier materials, antimicrobials and sensors. *J Colloid Interface Sci* **363**, 1–24.

Eberhard, A., Burlingame, A. L., Eberhard, C., Kenyon, G. L., Nealson, K. H. and Oppenheimer, N. J. (1981) Structural identification of autoinducer of *Photobacterium fischeri* luciferase. *Biochemistry* **20**, 2444–2449.

Eby, D. M., Schaeublin, N. M., Farrington, K. E., Hussain, S. M. and Johnson, G. R. (2009) Lysozyme Catalyzes the Formation of Antimicrobial Silver Nanoparticles. *ACS Nano* **3**, 984–999.

Elechiguerra, J. L., Burt, J. L., Morones, J. R., Camacho–Bragado, A., Gao, X., Lara, H. H. and Yacaman, M. J. (2005) Interaction of silver nanoparticles with HIV–1. *J Nanobiotechnology* **3**, 6.

Elkins, J. G., Hassett, D. J., Stewart, P. S., Schweizer, H. P. and McDermott, T. R. (1999) Protective role of catalase in *Pseudomonas aeruginosa* biofilm resistance to hydrogen peroxide. *Appl Environ Microbiol* **65**, 4594–4600.

Emamifar, A. (2011) Applications of Antimicrobial Polymer Nanocomposites in Food Packaging. In Advances in Nanocomposite Technology, InTech. Ed. Hashim, A. 299–318.

Emerich, D. F. and Thanos, C. G. (2003) Nanotechnology and medicine. *Expert Opin Biol Ther* **3**, 655–663.

Endres, P. J., Paunesku, T., Vogt, S., Meade, T. J. and Woloschak, G. E. (2007) DNA–TiO_2 nanoconjugates labeled with magnetic resonance contrast agents. *J Am Chem Soc* **129**, 15760–15761.

Feng, Q. L., Wu, J., Chen, G. Q., Cui, F. Z., Kim, T. N. and Kim, J. O. (2000) A mechanistic study of the antibacterial effect of silver ions on *Escherichia coli* and *Staphylococcus aureus*. *J Biomed Mater Res* **52**, 662–668.

Fer´nandez, E. J., Gar´cıa–Barrasa, J., Laguna, A., L'opezde–Luzuriagal, J. M., Monge, M. and Torres, C. (2008) The preparation of highly active antimicrobial silver nanoparticles by an organometallic approach. *Nanotechnology* **19**, 185602.

Ferry, J. D. (1980) Viscoelastic Properties of Polymers, Wiley, New York.

Feynman, R. P. (1960) There's plenty of room at the bottom. *Eng Sci (CalTech)* **23**, 22–36.

Fong, J. and Wood, F. (2006) Nanocrystalline silver dressings in wound management: a review. *Int J Nanomedicine* **1**, 441–449.

Forsgren, J., Svahn, F., Jarmar, T. and Engqvist, H. (2007) Formation and adhesion of biomimetic hydroxyapatite deposited on titanium substrates. *Acta Biomater* **3**, 980–984.

Fostad, G., Hafell, B., Førde, A., Dittmann, R., Sabetrasekh, R., Will, J., Ellingsen, J. E., Lyngstadaas, S. P. and Haugen, H. J. (2009) Loadable TiO_2 scaffolds–A correlation study between processing parameters, micro CT analysis and mechanical strength. *J Eur Ceram Soc* **29**, 2773–2781.

Freitas, R. A. Jr. (1999) Basic capabilities. In: Nanomedicine. Landes Bioscience, Georgetown, TX.

Freitas, R. A. Jr. (2003) Biocompatibility. In: Nanomedicine. Landes Bioscience, Georgetown, TX.

Freitas, R. A. Jr. (2005) What is nanomedicine? *Nanomedicine: Nanotechnology, Biology, and Medicine* **1**, 2–9.

Fujishima, A. and Honda, K. (1972) Electrochemical Photolysis of Water at a Semiconductor Electrode. *Nature* **238**, 37–38.

Fujishima, A., Rao, T. N. and Tryk, D. A. (2000) Titanium dioxide photocatalysis. *Journal of Photochemistry and Photobiology C: Photochemistry Reviews* **1**, 1–21.

Fujishima, A., Zhang, X. T. and Tryk, D. A. (2008) TiO_2 photocatalysis and the related surface phenomena. *Surf Sci Rep* **63**, 515–582.

Fulcher, G. R., Hukins, D. W. L. and Shepherd, D. E. T. (2009) Viscoelastic properties of bovine articular cartilage attached to subchondral bone at high frequencies. *BMC Musculoskeletal Disorders* **10**, 61.

Furno, F., Morley, K. S., Wong, B., Sharp, B. L., Arnold, P. L., Howdle, S. M., Bayston, R., Brown, P. D., Winship, P. D. and Reid, H. J. (2004) Silver nanoparticles and polymeric medical devices: a new approach to prevention of infection? *J Antimicrob Chemother* **54**, 1019–1024.

Garrido, F., Caccavale, F., Gonella, F. and Quaranta, A. (1995) Silver colloidal waveguides for non–linear optics: a new methodology *Pure Appl Opt* **4,** 771.

Gavriliu, S., Lungu, M., L. Gavriliu, C., Grigore, F. and Groza, C. (2009) Antimicrobial Colloidal Suspensions of Silver–Titania. *The Open Chemical and Biomedical Methods Journal* **2**, 77–85.

Gayaa, U. I. and Abdullaha, A. H. (2008) Heterogeneous photocatalytic degradation of organic contaminants over titanium dioxide: a review of fundamentals, progress and problems. *Journal of Photochemistry and Photobiology C: Photochemistry Reviews* **9**, 1–12.

Gleiter, H. (1995) Nanostructured materials: state of the art and perspectives *Nanostructured Materials* **6**, 3–14.

Gogoi, S. K., Gopinath, P., Paul, A., Ramesh, A., Ghosh, S. S. and Chattopadhyay, A. (2006) Green Fluorescent Protein–Expressing *Escherichia coli* as a Model System for Investigating the Antimicrobial Activities of Silver Nanoparticles. *Langmuir* **22**, 9322–9328.

Gomes, M. E. and Reis, R. L. (2004) Biodegradable polymers and composites in biomedical applications from catgut to tissue engineering. Part II. Systems for temporary replacement and advanced tissue regeneration. *Int Mater Rev* **49**, 274–285.

Gomez–Florit, M., Rubert, M., Ramis, J. M., Tianinen, H., Haugen, H. J., Lyngstadaas, S. P. and Monjo, M. (2012) TiO_2 scaffolds sustain differentiation of MC3T3–E1 cells. *J Biomater Tissue Eng* **2**, 336–344.

Gould, T. A., Herman, J., Krank, J., Murphy, R. C. and Churchill, M. E. A. (2006) Specificity of Acyl–Homoserine Lactone Synthases Examined by Mass Spectrometry. *J Bacteriol* **188**, 773–783.

Gressel–Michel, E., Chaumont, D. and Stuerga, D. (2005) From a microwave flash–synthesized TiO_2 colloidal suspension to TiO_2 thin films. *J Colloid Interface Sci* **285**, 674–679.

Grujic–Brojcin, M., Scepanovic, M. J., Dohcevic–Mitrovic, Z. D., Hinic, I., Matovic, B., Stanisic, G. and Popovic, Z. V. (2005) Infrared Study of Laser Synthesized Anatase TiO_2 Nanopowders. *J Phys D* **38**, 1415–1420.

Guo, W., Lin, Z., Wang, X. and Song, G. (2003) Sonochemical synthesis of nanocrystalline TiO_2 by hydrolysis of titanium alkoxides. *Microelectron Eng* **66,** 95–101.

Gurav, A., Kodas, T., Pluym, T. and Xiong, Y. (1993) Aerosol processing of materials. *Aerosol Sci Technol* **19**, 411–452.

Gurunathan, S., Han, J. W., Kwon, D. N. and Kim, J. H. (2014) Enhanced antibacterial and anti–biofilm activities of silver nanoparticles against Gram–negative and Gram–positive bacteria. *Nanoscale Res Lett* **9**, 373.

Hahn, A., Brandes, G., Wagener, P. and Barcikowski, S. (2011) Metal ion release kinetics from nanoparticle silicone composites. *J Control Release* **154**, 164–170.

Hashimoto, K., Irie, H. and Fujishima, A. (2005) TiO_2 Photocatalysis: A Historical Overview and Future Prospects. *J Appl Phys* **44**, 8269–8285.

Hatchett, D. W. and White, H. S. (1996) Electrochemistry of Sulfur Adlayers on the Low–Index Faces of Silver. *The Journal of Physical Chemistry* **100**, 9854–9859.

Haugen, H. J., Monjo, M., Rubert, M., Verket, A., Lyngstadaas, S. P., Ellingsen, J. E., Ronold, H. J. and Wohlfahrt, J. C. (2013) Porous ceramic titanium dioxide scaffolds promote bone formation in rabbit peri–implant cortical defect model. *Acta Biomater* **9**, 5390–5399.

Haugen, H., Will, J., Kohler, A., Hopfner, U., Aigner, J. and Wintermantel, E. (2004) Ceramic TiO_2–foams: characterisation of a potential scaffold. *J Eur Ceram Soc* **24**, 661–668.

Henrich, V. E. and Cox, P. A. (1994) The Surface Chemistry of Metal Oxides. Cambridge University Press, Cambridge, United Kingdom.

Hentzer, M. and Givskov, M. (2003) Pharmacological inhibition of quorum sensing for the treatment of chronic bacterial infections. *J Clin Invest* **112**, 1300–1307.

Hippocrates and Adams, F. (Trans.) (400 B.C.E.) On Ulcers.
http://www.classics.mit.edu/Hippocrates/ulcers.html

Hitchings, G. H. and Smith, S. L. (1980) Dihydrofolate reductases as targets for inhibitors. *Advances in Enzyme Regulation* **18**, 349–371.

Holt, K. B. and Bard, A. J. (2005) Interaction of silver (I) ions with the respiratory chain of *Escherichia coli*: an electrochemical and scanning electrochemical microscopy study of the antimicrobial mechanism of micromolar Ag^+. *Biochemistry* **44**, 13214–13223.

Hong, S. S., Lee, M. S., Park, S. S. and Lee, G. D. (2003) Synthesis of nano–sized TiO_2/SiO_2 particles in the microemulsion and their photo–catalytic activity on the decomposition of *p*–nitrophenol. *Catal Today* **87**, 99–105.

Hu, A.W., and Fu, Z. H. (2003) Nanotechnology and its applications in packaging and packaging machinery. *Packaging Engineering* **24**, 22–24.

Huang, W., Tang, X., Wang, Y., Koltypin, Y. and Gedanken, A. (2000) Selective synthesis of anatase and rutile *via* ultrasound irradiation. *Chem Commun* **15**, 1415–1416.

Huang, X. and Brazel, C. S. (2001) On the importance and mechanisms of burst release in matrix–controlled drug delivery systems. *J Control Release* **73**, 121–136.

Huang, Y., Ho, W., Lee, S., Zhang, L., Li, G. and Yu, J. C. (2008) Effect of carbon doping on the mesoporous structure of nanocrystalline titanium dioxide and its solar–light–driven photocatalytic degradation of NOx. *Langmuir* **24**, 3510–3516.

Hunt, N. C., Smith, A. M., Gbureck, U., Shelton, R. M. and Grover, L. M. (2010) Encapsulation of fibroblasts causes accelerated alginate hydrogel degradation. *Acta Biomaterialia* **6**, 3649–3656.

Hutmacher, D.W. (2000) Polymeric scaffolds in tissue engineering bone and cartilage. *Biomaterials* **21**, 2529–2543.

Hwang, E. T., Lee, J. H., Chae, Y. J., Kim, Y. S., Kim, B. C., Sang, B. I. and Gu, M. B. (2008) Analysis of the toxic mode of action of silver nanoparticles using stress–specific bioluminescent bacteria. *Small* **4**, 746–750.

Jadalannagari, S., More, S., Kowshik, M. and Ramanan, S. R. (2011) Low temperature synthesis of hydroxyapatite nano–rods by a modified sol–gel technique. *Materials Science and Engineering: C* **31**, 1534–1538.

Jain, J., Arora, S., Rajwade, J. M., Omray, P., Khandelwal, S. and Paknikar, K. M. (2009) Silver Nanoparticles in Therapeutics: Development of an Antimicrobial Gel Formulation for Topical Use. *Mol Pharmaceut* **6**, 1388–1401.

Jang, H. D. and Kim, S. K. (2001) Controlled synthesis of titanium dioxide nanoparticles in a modified diffusion flame reactor. *Mater Res Bull* **36**, 627–637.

Jayasuriya, A. C. (2008) Acceleration of biomimetic mineralization to apply in bone regeneration *Biomed Mater* **3**, 015003.

Jin, X., Li, M., Wang, J., Marambio–Jones, C., Peng, F., Huang, X., Damoiseaux, R. and Hoek, E. (2010) High–Throughput Screening of Silver Nanoparticle Stability and Bacterial Inactivation in Aquatic Media: Influence of Specific Ions. *Environ Sci Technol* **44**, 7321–7328.

Jokanovic, V., Spasic, A. M. and Uskokovic, D. (2004) Designing of nanostructured hollow TiO_2 spheres obtained by ultrasonic spray pyrolysis. *J Colloid Interface Sci* **278**, 342–352.

Jonásová, L., Müller, F. A., Helebrant, A., Strnad, J. and Greil, P. (2004) Biomimetic apatite formation on chemically treated titanium. *Biomaterials* **25**, 1187–1194.

Jung, W. K., Koo, H. C., Kim, K. W., Shin, S., Kim, S. H. and Park, Y. H. (2008) Antibacterial Activity and Mechanism of Action of the Silver Ion in *Staphylococcus aureus* and *Escherichia coli*. *Appl Environ Microbiol* **74**, 2171–2178.

Kadurugamuwa, J. L. and Beveridge, T. J. (1995) Virulence factors are released from *Pseudomonas aeruginosa* in association with membrane vesicles during normal growth and exposure to gentamicin: a novel mechanism of enzyme secretion. *J Bacteriol* **177**, 3998–4008.

Kalishwaralal, K., ManiKanth, S. B., Pandian, S. R. K., Deepak, V. and Gurunathan, S. (2010) Silver nanoparticles impede the biofilm formation by *Pseudomonas aeruginosa* and *Staphylococcus epidermidis*. *Colloids Surfaces B: Biointerfaces* **79**, 340–344.

Kangarlou, H. and Rafizadeh, S. (2012) Influence of Thickness on Structural and Optical Properties of Titanium Oxide Thin Layers. In: Scanning Probe Microscopy–Physical Property Characterization at Nanoscale. InTech, Europe.

Kazy, S. K., Sar, P., Singh, S. P., Sen, A. K. and D'Souza, S. F. (2002) Extracellular polysac–charides of a copper–sensitive and a copper–resistant Pseudomonas aeruginosa strain: synthesis, chemical nature and copper binding. *World Journal of Microbiology & Biotechnology* **18**, 583–588.

Kim, C. S., Moon, B. K., Park, J. H., Choi, B. C. and Seo, H. J. (2003a) Solvothermal synthesis of nanocrystalline TiO_2 in toluene with surfactant, Journal of Crystal Growth. *J Cryst Growth* **257**, 309–315.

Kim, C. S., Moon, B. K., Park, J. H., Chung, S. T. and Son, S. M. (2003b) Synthesis of nanocrystalline TiO_2 in toluene by a solvothermal route. *J Cryst Growth* **254**, 405–410.

Kim, H. W., Kim, H. E., Salih, V. and Knowles, J. C. (2005b) Hydroxyapatite and titania sol–gel composite coatings on titanium for hard tissue implants; mechanical and *in vitro* biological performance. *J Biomed Mater Res B Appl Biomater* **72**, 1–8.

Kim, H. W., Knowles, J. C. and Kim, E. (2004b) Hydroxyapatite and gelatine composite foams processed via novel freeze–drying and crosslinking for use as temporary hard tissue scaffolds. *J Biomed Mater Res A* **72**, 136–145.

Kim, H. W., Knowles, J. C. and Kim, H. E. (2004a) Development of hydroxyapatite bone scaffold for controlled drug release via poly (e–caprolactone) and hydroxyapatite hybrid coatings. *J Biomed Mater Res Part B: Appl Biomater* **70**, 240–249.

Kim, J. S., Kuk, E., Yu, K. N., Kim, J. H., Park, S. J., Lee, H. J., Kim, S. H., Park, Y. K., Park, Y. H., Hwang, C. Y., Kim, Y. K., Lee, Y. S., Jeong, D. H. and Cho, M. H. (2007) Antimicrobial effects of silver nanoparticles. *Nanomed–Nanotechnol* **3**, 95–101.

Kim, J., Kim, S. K., Grégoire, G., Manil, B. and Schermann, J. P. (2011) Infrared study of the bacterial autoinducer N–hexanoyl–homoserine lactone (C6–HSL) in the gas–phase, water, and octanol solutions. *J Phys Chem A* **115**, 9199–9206.

Kim, K. D., Kim, S. H. and Kim, H. T. (2005a) Applying the Taguchi method to the optimization for the synthesis of TiO_2 nanoparticles by hydrolysis of TEOT in micelles. *Colloid Surfaces Physicochem and Eng Aspects* **254**, 99–105.

Kim, K. J., Sung, W. S., Moon, S. K., Choi, J. S., Kim, J. G. and Lee, D. G. (2008) Antifungal effect of silver nanoparticles on dermatophytes. *Journal of Microbiology and Biotechnology* **18**, 1482–1484.

Kim, K. J., Sung, W. S., Suh, B. K., Moon, S. K., Choi, J. S., Kim, J. G. and Lee, D. G. (2009) Antifungal activity and mode of action of silver nano–particles on *Candida albicans*. *Biometals* **22**, 235–242.

Kim, Y. S., Song, M. Y., Park, J. D., Song, K. S., Ryu, H. R., Chung, Y. H., Chang, H. K., Lee, J. H. and Oh, K. H., Kelman, B. J., Hwang, I. K. and Yu, I. J. (2010) Subchronic oral toxicity of silver nanoparticles. *Part Fibre Toxicol* **7**, 20.

Klabunde, K. J., Stark, J., Koper, O., Mohs, C., Park, D. G., Decker, S., Jiang, Y., Lagadic, I. and and Zhang, D. (1996) Nanocrystals as Stoichiometric Reagents with Unique Surface Chemistry. *The Journal of Physical Chemistry* **100**, 12142–12153.

Klasen, H. J. (2000) Historical review of the use of silver in the treatment of burns. I. Early uses. *Burns* **26**, 117–130.

Klawitter, J. J. and Hulbert, S. F. (1971) Application of porous ceramics for the attachment of load–bearing internal orthopaedic applications. *J Biomed Mater Res Symp* **5**, 161–229.

Kneser, U., Schaefer, D. J., Munder, B., Klemt, C., Andree, C. and Stark, G. B. (2002) Tissue engineering of bone. *Min Invas Sur & Allied Technol* **3**, 107–116.

Kodak Publication No. J–216 (ENG) (2003) The Fate and Effects of Silver in the Environment, Eastman Kodak Company, Rochester, NY.

Kokubo, T. (1991) Bioactive glass ceramics: properties and applications. *Biomaterials* **12**, 155–163.

Kokubo, T. and Takadama, H. (2006) How useful is SBF in predicting *in vivo* bone activity? *Biomaterials* **27**, 2907–2915.

Kongkanand, A., Tvrdy, K., Takechi, K., Kuno, M. and Kamat, P. V. (2008) Quantum Dot Solar Cells. Tuning Photoresponse through Size and Shape Control of CdSe–TiO_2 Architecture. *J Am Chem Soc* **130**, 4007–4015.

Kretlow, J. D. and Mikos, A. G. (2007) Review: mineralization of synthetic polymer scaffolds for bone tissue engineering. *Tissue Eng* **13**, 927–938.

Kudo, A. and Miseki, Y. (2009) Heterogeneous photocatalyst materials for water splitting. *Chem Soc Rev* **38**, 253–278.

Kulinowski, K. M. (2008) Environmental Impacts of Nanosilver. ICON Backgrounder, http://cohesion.rice.edu/centersandinst/icon/resources.

Kumar, P. T., Ramya, C., Jayakumar, R., Nair, S. K. and Lakshmanan, V. K. (2013) Drug delivery and tissue engineering applications of biocompatible pectin–chitin/nano $CaCO_3$ composite scaffolds. *Colloids Surf B Biointerfaces* **106**, 109–116.

Kumar, P., Venkataraman, D., Kalimuthu, K., Pushpa, V. and Sangiliyandi, G. (2010) Mechanism of bactericidal activity of Silver Nitrate – a concentration dependent bi–functional molecule. *Braz J Microbiol* **41**, 805–809.

Kumar, R. and Ghulam, R. (2009) Photocatalytic disinfection of water with Ag–TiO_2 nanocrystalline composite. *Ionics* **5**, 579–587.

Kumar, R. and Münstedt, H. (2005) Silver ion release from antimicrobial polyamide/silver composites. *Biomaterials* **26**, 2081–2088.

Kuznetsova, I. N., Blaskov, V., Stambolova, I., Znaidi, L. and Kanaev, A. (2005) TiO_2 pure phase brookite with preferred orientation, synthesized as a spin–coated film. *Mater Lett* **59**, 3820–3823.

Lancelle–Beltran, E., Prené, P., Boscher, C., Belleville, P., Buvat, P. and Sanchez, C. (2006) All–Solid–State Dye–Sensitized Nanoporous TiO_2 Hybrid Solar Cells with High Energy–Conversion Efficiency. *Adv Mater* **18**, 2579–2582.

Langer, R. and Vacanti J. P. (1993) Tissue engineering. *Science* **260**, 920–926.

Lara, H. H., Garza–Treviño, E. N., Ixtepan–Turrent, L. and Singh, D. K. (2011) Silver nanoparticles are broad–spectrum bactericidal and virucidal compounds. *J Nanobiotechnology* **3**, 9–30.

Le Bolay, N., Santran, V., Dechambre, G., Combes, C., Drouet, C., Lamure, A. and Rey, C. (2009) Production, by co–grinding in a media mill, of porous biodegradable polylactic acid–apatite composite materials for bone tissue engineering. *Powder Technol* **190**, 89–94.

Lea, M. C. (1889) On allotropic forms of silver. *Am J Sci* **38**, 47–49.

Lee, H. Y., Park, H. K., Lee, Y. M., Kim, K. and Park, S. B. (2007) A practical procedure for producing silver nanocoated fabric and its antibacterial evaluation for biomedical applications. *Chem Commun* **28**, 2959–2961.

Lee, J. H. and Yang, Y. S. (2005) Effect of hydrolysis conditions on morphology and phase content in the crystalline TiO_2 nanoparticles synthesized from aqueous $TiCl_4$ solution by precipitation. *Mater Chem Phys*, **93**, 237–242.

Lee, S. H. and Shin, H. (2007) Matrices and scaffolds for delivery of bioactive molecules in bone and cartilage tissue engineering. *Adv Drug Deliv Rev* **59**, 339–359.

Lei, Y., Zhang, L. D. and Fan, J. C. (2001) Fabrication, characterization and Raman study of TiO_2 nanowire arrays prepared by anodic oxidative hydrolysis of $TiCl_3$. *Chem Phys Lett* **338**, 231–236.

Lev, O., Tsionsky, M., Rabinovich, L., Glezer, V., Sampath, S., Pankratov, I. and Gun, J. (1995) Organically Modified Sol–Gel Sensors. *Analytical Chemistry* **67**, 22A–30A.

Lev, O., Wu, Z., Bharathi, S., Glezer, V., Modestov, A., Gun, J., Rabinovich, L. and Sampath, S. (1997) Sol–Gel Materials in Electrochemistry. *Chemistry of Materials* **9**, 2354–2375.

Lewis, K. (2005) Persister cells and the riddle of biofilm survival. *Biochemistry (Mosc)* **70**, 267–274.

Li, H., Khor, K. A. and Cheang, P. (2003a) Impact formation and microstructure characterization of thermal sprayed hydroxyapatite/titania composite coatings. *Biomaterials* **24**, 949–957.

Li, H., Li, F., Wang, L., Sheng, J., Xin, Z., Zhao, L., Xiao, H., Zheng, Y., Hu, Q. (2009a) Effect of nano–packing on preservation quality of Chinese jujube (*Ziziphus jujuba Mill. var. inermis (Bunge) Rehd*). *Food Chemistry* **114**, 547–552.

Li, L., Li, Y., Li, J., Yao, L., Mak, A. E. T., Ko, F. and Qin, L. (2009b) Antibacterial properties of nanosilver PLLA fibrous membranes. *J Nanomater* 1–5.

Li, W., Seal, S., Megan, E., Ramsdell, J., Scammon, K., Lelong, G., Lachal, L., and Richardson, K. A. (2003b) Physical and optical properties of sol–gel nano–silver doped silica film on glass substrate as a function of heat–treatment temperature. *Journal of Applied Physics* **93**, 9553–9561.

Li, X. L., Peng, Q., Yi, J. X., Wang, X. and Li, Y. D. (2006) Near Monodisperse TiO_2 Nanoparticles and Nanorods. *Chemistry–A European Journal* **12**, 2383–2391.

Li, Y., Lee, N. H., Hwang, D. S., Song, J. S., Lee, E. G. and Kim, S. J. (2004) Synthesis and characterization of nano titania powder with high photoactivity for gas–phase photo–oxidation of benzene from TiOCl(2) aqueous solution at low temperatures. *Langmuir* **20**, 10838–10844.

Li, Y., Xie, C., Peng, S., Lu, G. and Li, S. (2008) Eosin Y–sensitized nitrogen doped TiO_2 for efficient visible light photocatalytic hydrogen evolution. *J Mol Catal A: Chem* **282**, 117–123.

Liau, S., Read, D., Pugh, W., Furr, J. and Russell, A. (1997) Interaction of silver nitrate with readily identifiable groups: relationship to the antibacterial action of silver ions. *Lett Appl Microbiol* **25**, 279–283.

Lichstein, H. C. and Van de Sand, V. F. (1945) Violacein, an antibiotic pigment produced by *Chromobacterium violaceum*. *J Infect Dis* **76**, 47–51.

Lim, K. T., Hwang, H. S., Hong, S. S., Park, C., Ryoo, W. and Johnston, K. P. (2004b) Synthesis of Ultrafine TiO_2 Particles from Hydrolysis of $Ti(O^iPr)_4$ with PEO–*b*–PFOMA Reverse Micelles in CO_2. *Stud Surf Sci Catal* **153**, 569–572.

Lim, K. T., Hwang, H. S., Ryoo, W. and Johnston, K. P. (2004a) Synthesis of TiO_2 nanoparticles utilizing hydrated reverse micelles in CO_2. *Langmuir* **20**, 2466–2471.

Liu, J., Sonshine, D. A., Shervani, S. and Hurt, R. H. (2010) Controlled Release of Biologically Active Silver from Nanosilver Surfaces. *ACS Nano* **4**, 6903–6913.

Liu, S. and Huang, K. (2005) Straight forward fabrication of highly ordered TiO_2 nanowire arrays in AAM on aluminum substrate. *Sol Energy Mater Sol Cells* **85**, 125–131.

Liu, S., Chen, X. and Chen, X. (2006) Preparation of N–doped visible–light response nanosize TiO_2 photocatalyst using the acid–catalyzed hydrolysis method. *Chinese J Catal* **27**, 697–702.

Liu, Y., Wang, X., Yang, F. and Yang, X. (2008) Excellent antimicrobial properties of mesoporous anatase TiO_2 and Ag/TiO_2 composite films. *Microporous and Mesoporous Materials* **114**, 431–439.

Liuyun, J., Yubao, L. and Chengdong, L. (2009) A novel composite membrane of chitosan–carboxymethyl cellulose polyelectrolyte complex membrane filled with nano–hydroxyapatite I. Preparation and properties. *Journal of Materials Science: Materials in Medicine* **20**, 1645–1652.

Loganathan, K., Bommusamy, P., Muthaiahpillai, P. and Velayutham, M. (2011) The syntheses, characterizations, and photocatalytic activities of silver, platinum, and gold doped TiO_2 nanoparticles. *Environ Eng Res* **16**, 81–90.

Lok, C. N., Ho, C. M., Chen, R., He, Q. Y., Yu, W. Y., Sun, H., Tam, P. K., Chiu, J. F. and Che, C. M. (2006) Proteomic analysis of the mode of antibacterial action of silver nanoparticles. *J Proteome Res* **5**, 916–924.

López, T., Manjarrez, J., Rembao, D., Vinogradova, E., Moreno, A. and González, R. D. (2006) An implantable sol–gel derived titania–silica carrier system for the controlled release of anticonvulsants. *Mater Lett* **60**, 2903–2908.

López, T., Ortiz, E., Quintana, P. and González, R. D. (2007) A nanostructured titania bioceramic implantable device capable of drug delivery to the temporal lobe of the brain. *Colloids and Surfaces A: Physicochem Eng Aspects* **300**, 3–10.

Lu, L., Sun, R. W., Chen, R., Hui, C. K., Ho, C. M., Luk, J. M., Lau, G. K. and Che, C. M. (2008) Silver nanoparticles inhibit hepatitis B virus replication. *Antivir Ther* **13**, 253–262.

Lu, T., Li, Y. and Chen, T. (2013) Techniques for fabrication and construction of three–dimensional scaffolds for tissue engineering. *International Journal of Nanomedicine* **8**, 337–350.

Lubick, N. (2008) Nanosilver toxicity: ions, nanoparticles–or both? *Environmental Science & Technology* **42**, 8617–8617.

Ma, G., Zhao, X. and Zhu, J. (2005) Microwave hydrothermal synthesis of rutile TiO_2 nanorods. *Int J Mod Phys B* **19**, 2763–2768.

Madhumathi, K., Kumar, P. T., Abhilash, S., Sreeja, V., Tamura, H., Manzoor, K., Nair, S. V. and Jayakumar, R. (2010) Development of novel chitin/nanosilver composite scaffolds for wound dressing applications. *J Mater Sci Mater Med* **21**, 807–813.

Mah, T. F. and O'Toole, G. A. (2001) Mechanisms of biofilm resistance to antimicrobial agents. *Trends Microbiol* **9**, 34–39.

Mano, J. F., Reis, R. L. and Cunha, A. M. (2002) Dynamic mechanical analysis in polymers for medical applications. In: Polymer Based Systems on Tissue Engineering, Replacement and Regeneration. *NATO Science Series* **86**, 139–164.

Martinez–Gutierrez, F., Boegli, L., Agostinho, A., Sánchez, E. M., Bach, H., Ruiz, F. and James, G. (2013) Anti–biofilm activity of silver nanoparticles against different microorganisms. *Biofouling* **29**, 651–660.

Massol–Deya, A. A., Whallon, J., Hickey, R. F. and Tiedje, J. M. (1995) Channel structure in aerobic biofilms of fixed film reactors treating contaminated groundwater. *Appl Environ Microbiol* **61**, 769–777.

Matsuda, A., Kotani, Y., Kogure, T., Tatsumisago, M. and Minami, T. (2000) Transparent Anatase Nanocomposite Films by the Sol–Gel Process at Low Temperatures. *J Am Ceram Soc* **83**, 229–231.

Matsunaga, T., Tomodam, R., Nakajima, T. and Wake, H. (1985) Photochemical sterilization of microbial cells by semiconductor powders. *FEMS Microbiol Lett* **29**, 211–214.

McBain, A. J. (2010) Biofilms: an introduction to their significance and recalcitrance. *Microbiologist* **11**, 28–32.

McClean, K. H., Winson, M. K., Fish, L., Taylor, A., Chhabra, S. R., Camara, M., Daykin, M., Lamb, J. H., Swift, S., Bycroft, B. W., Stewart, G. S. and Williams, P. (1997) Quorum sensing and *Chromobacterium violaceum*: exploitation of violacein production and inhibition for the detection of N–acyl homoserine lactones. *Microbiology* **143**, 3703–3711.

McLean, R. J., Pierson, L. S. and Fuqua, C. (2004) A simple screening protocol for the identification of quorum signal antagonists. *J Microbiol Meth* **58**, 351–360.

Medina–Ramirez, I., Luo, Z., Bashir, S., Mernaugh, R. and Liu, J. L. (2011) Facile design and nanostructural evaluation of silver–modified titania used as disinfectant. *Dalton Trans* **40**, 1047–1054.

Mehrbod, P., Motamed, N., Tabatabaian, M., Soleimani, E. R., Amini, E., Shahidi, M. and Kheiri, M. (2009) *In Vitro* Antiviral Effect of "Nanosilver" on Influenza Virus. *DARU Journal of Pharmaceutical Sciences* **17**, 88–93.

Mistry, A. S. and Mikos, A. G. (2005) Tissue engineering strategies for bone regeneration. *Adv Biochem Eng Biotechnol* **94**, 1–22.

Mohan, N. and Nair, P. D. (2005) Novel porous, polysaccharide scaffolds for tissue engineering applications. *Trends in Biomaterials and Artificial Organs* **18**, 219–224.

Mohanty, S., Mishra, S., Jena, P., Jacob, B., Sarkar, B. and Sonawane, A. (2012) An investigation on the antibacterial, cytotoxic, and antibiofilm efficacy of starch–stabilized silver nanoparticles. *Nanomedicine* **8**, 916–924.

Mooney, D. J., Baldwin, D. F., Suh, N. P., Vacanti, J. P. and Langer, R. (1996) Novel approach to fabricate porous sponges of poly (D,L–lactic–co–glycolic acid) without the use of organic solvents. *Biomaterials* **17**, 1417–1422.

Mor, G. K., Shankar, K., Paulose, M., Varghese, O. K. and Grimes, C. A. (2006) Use of highly–ordered TiO(2) nanotube arrays in dye–sensitized solar cells. *Nano Lett* **6**, 215–218.

Morones, J. R, Elechiguerra, J. L., Camacho, A., Holt, K., Kouri, J. B., Ramírez, J. T. and Yacaman, M. J. (2005) The bactericidal effect of silver nanoparticles. *Nanotechnology* **16**, 2346–2353.

Mourino, V. and Boccaccini, A. R. (2010) Bone tissue engineering therapeutics: controlled drug delivery in three–dimensional scaffolds. *J R Soc Interface* **7**, 209–227.

Moyer, C. A. (1965) A treatment of burns. *Trans Stud Coll Physicians Phila* **33**, 53–103.

Mukherjee, B. and Weaver, J. W. (2010) Aggregation and Charge Behavior of Metallic and Nonmetallic Nanoparticles in the Presence of Competing Similarly–Charged Inorganic Ions. *Environ Sci Technol* **44**, 3332–3338.

Mukhopadhyay, A., Basak, S., Das, J. K., Medda, S. K., Chattopadhyay, K. and De, G. (2010) Ag–TiO_2 Nanoparticle Codoped SiO_2 Films on ZrO_2 Barrier–Coated Glass Substrates with Antibacterial Activity in Ambient Condition. *Applied Materials & Interfaces* **2**, 2540–2546.

Mulcahy, H., Charron–Mazenod, L. and Lewenza, S. (2008) Extracellular DNA Chelates Cations and Induces Antibiotic Resistance in *Pseudomonas aeruginosa* Biofilms. *PLoS Pathog* **4**, e1000213.

Murdock, R. C., Braydich–Stolle L., Schrand A. M., Schlager J. J. and Hussain S. M. (2008) Characterization of nanomaterial dispersion in solution prior to *in vitro* exposure using dynamic light scattering technique. *Toxicological Sciences* **101**, 239–253.

Murphy, W. L., Peters, M. C., Kohn, D. H. and Mooney, D. J. (2000) Sustained release of vascular endothelial growth factor from mineralized poly (lactide–co–glycolide) scaffolds for tissue engineering. *Biomaterials* **21**, 2521–2527.

Muto, Y. and Goto, S. (1986) Transformation by Extracellular DNA Produced by *Pseudomonas aeruginosa*. *Microbiology and Immunology* **30**, 621–628.

Nagarajan, B. and Jaiprakashnarain, G. B. (2009) Design and Application of Nano Silver Based Pou Appliances for Disinfection of Drinking Water. *Indian Journal of Science and Technology* **2**, 5–8.

Naik, K. and Kowshik, M. (2014) Anti–biofilm efficacy of low temperature processed AgCl–TiO_2 nanocomposite coating. *Mater Sci Eng C Mater Biol Appl* **34**, 62–68.

Naik, K., Chatterjee, A., Prakash, H. and Kowshik, M. (2013) Mesoporous TiO_2 Nanoparticles Containing Ag Ion with Excellent Antimicrobial Activity at Remarkable Low Silver Concentrations. *J Biomed Nanotechnol* **9**, 664–673.

Naldoni, A. (2009) Nanostructured TiO_2 as a Multifunctional Material: From Photocatalysis To Biomedical Applications, Università Degli Studi Di Milano.

Naldoni, A., Minguzzi, A., Vertova, A., Dal Santo, V., Borgese, L. and Bianchi, C. L. (2011) Electrochemically–assisted Deposition on TiO_2 Scaffold for Tissue Engineering: an Apatite Bio–Inspired Crystallization Pathway. *J Mater Chem* **21**, 400–407.

Namasivayam, S. K. R., Christo, B. B., Arasu, S. M. K., Kumar, K. A. M. and Deepak, K. (2013) Anti Biofilm Effect of Biogenic Silver Nanoparticles Coated Medical Devices against Biofilm of Clinical Isolate of *Staphylococcus aureus*. *Global Journal of Medical research Pharma, Drug Discovery, Toxicology and Medicine* **13**, 24–30.

Nandi, S. K., Kundu, B., Datta, S., De, D. K. and Basu, D. (2009) The repair of segmental bone defects with porous bioglass: an experimental study in goat. *Research in Veterinary Science* **86**, 162–173.

Nathanael, A. J., Mangalaraj, D. and Ponpandian, N. (2010) Controlled growth and investigations on the morphology and mechanical properties of hydroxyapatite/titania nanocomposite thin films. *Compos Sci Technol* **70**, 1645–1651.

National Nanotechnology Initiative: What it is and how it works. (2011) Available at: http://www.nano.gov/.

Navarro, E., Piccapietra, F., Wagner, B., Marconi, F., Kaegi, R., Odzak, N., Sigg, L. and Behra, R. (2008) Toxicity of silver nanoparticles to *Chlamydomonas reinhardtii*. *Environ Sci Technol* **42**, 8959–8664.

Nealson, K. H., Platt, T. and Hastings, J. W. (1970) Cellular control of the synthesis and activity of the bacterial luminescent system. *J Bacteriol* **104**, 313–322.

Nedeljkovic, J. M., Saponjic, Z. V., Rakocevic, Z., Jokanovic, V. and Uskokovic, D. P. (1997) Ultrasonic Spray Pyrolysis of TiO_2 Nanoparticles. *Nanostruct Mater* **9**, 125–128.

Niederberger, M. (2007) Nonaqueous Sol–Gel Routes to Metal Oxide Nanoparticles. *Acc Chem Res* **40**, 793–800.

Niederberger, M., Bartl, M. H. ad Stucky, G. D. (2002) Benzyl Alcohol and Titanium Tetrachloride A Versatile Reaction System for the Nonaqueous and Low–Temperature Preparation of Crystalline and Luminescent Titania Nanoparticles. *Chem Mater* **14**, 4364–4370.

Njoroge, J. and Sperandio, V. (2009) Jamming bacterial communication: New approaches for the treatment of infectious diseases. *EMBO Mol Med* **1**, 201–210.

Noguera, C. (1996) Physics and Chemistry at Oxide Surfaces. Cambridge University Press, Cambridge, United Kingdom.

Noorbakhsh, F. (2011) Antifungal Effects of Silver Nanoparticle alone and with Combination of Antifungal Drug on Dermatophyte Pathogen Trichophyton Rubrum. *International Conference on Bioscience, Biochemistry and Bioinformatics* **5**, 364–367.

Nowack, B., Krug, H. F. and Height, M. (2011) 120 years of nanosilver history: implications for policy makers. *Environ Sci Technol* **45**, 1177–1183.

Nygren, H., Tengvall, P. and Lundstrom, I. (1997) The initial reactions of TiO_2 with blood. *J Biomed Mater Res* **34**, 487–492.

O'Regan, B. and Graetzel, M. (1991) A low–cost, high–efficiency solar cell based on dye–sensitized colloidal TiO_2 films. *Nature* **353**, 737–740.

Oh, S. M., Li, J. G. and Ishigaki, T. (2005a) Nanocrystalline TiO_2 Powders Synthesized by In–Flight Oxidation of TiN in Thermal Plasma: Mechanisms of Phase Selection and Particle Morphology Evolution. *J Mater Res* **20**, 529–537.

Osterloh, F. E. (2008) Inorganic Materials as Catalysts for Photochemical Splitting of Water. *Chem Mater* **20**, 35–54.

O'Toole, G. A. and Kolter, R. (1998) Initiation of biofilm formation in *Pseudomonas fluorescens* WCS365 proceeds via multiple, convergent signalling pathways: a genetic analysis. *Mol Microbiol* **28**, 449–461.

Packiavathy, I. A. S. V., Agilandeswari, P., Musthafa, K. S., Pandian, S. K. and Ravi, A. V. (2012) Antibiofilm and quorum sensing inhibitory potential of *Cuminum cyminum* and its secondary metabolite methyl eugenol against Gram negative bacterial pathogens. *Food Res Int* **45**, 85–92.

Page, K. (2009) Photocatalytic thin films their characterisation and antimicrobial properties. Doctoral thesis, University College London.

Pal, S., Tak, Y. K. and Song, J. M. (2007) Does the antibacterial activity of silver nanoparticles depend on the shape of the nanoparticle? A study of the Gram–negative bacterium *Escherichia coli*. *Appl Environ Microbiol* **73**, 1712–1720.

Panacek, A., Kvítek, L., Prucek, R., Kolar, M., Vecerova, R., Pizúrova, N., Sharma, V. K., Nevecna, T. and Zboril, R. (2006) Silver colloid nanoparticles: synthesis, characterization, and their antibacterial activity. *J Phys Chem B* **110**, 16248–16253.

Parala, H., Devi, A., Bhakta, R. and Fischer, R. A. (2002) Synthesis of nano–scale TiO_2 particles by a nonhydrolytic approach. *J Mater Chem* **12**, 1625–1627.

Park, D. G. and Burlitch, J. M. (1992) Nanoparticles of anatase by electrostatic spraying of an alkoxide solution. *Chem Mater* **4**, 500–502.

Patterson, A. L. (1939) The Scherrer Formula for X–Ray Particle Size Determination. *Phys Rev* **56**, 978–982.

Paulose, M., Varghese, O. K., Mor, G. K., Grimes, C. A. and Ong, K. G. (2006) Unprecedented ultra–high hydrogen gas sensitivity in undoped titania nanotubes. *Nanotechnology* **17**, 398–402.

Paunesku, T., Rajh, T., Maser, J., Vogt, S., Stojicevic, N., Protic, M., Lai, B., Oryhon, J., Thurnauer, M. and Woloschak, G. E. (2003) Biology of TiO_2–oligonucleotide nanocomposites. *Nat Mater* **2**, 343–346.

Paunesku, T., Vogt, S., Maser, J., Stojicevic, N., Thurn, K. T., Osipo, C., Liu, H., Legnini, D., Wang, Z., Lee, C. and Woloschak, G. E. (2007) Intracellular distribution of TiO_2–DNA oligonucleotide nanoconjugates directed to nucleolus and mitochondria indicates sequence specificity. *Nano letters* **7**, 596–601.

Percival, S. L., Bowler, P. G. and Russell, D. (2005) Bacterial resistance to silver in wound care. *Journal of Hospital Infection* **60**, 1–7.

Persson, T., Givskov, M. and Nielsen, J. (2005) Quorum sensing inhibition: targeting chemical communication in gram–negative bacteria. *Curr Med Chem* **12**, 3103–3115.

Peter, M., Binulal, N. S., Nair, S. V., Selvamurugan, N., Tamura, H. and Jayakumar, R. (2010) Novel biodegradable chitosan–gelatin/nano–bioactive glass ceramic composite scaffolds for alveolar bone tissue engineering. *Chemical Engineering Journal* **158**, 353–361.

Peter, M., Kumar, S. P. T., Binulal, N. S., Nair, S. V., Tamura, H. and Jayakumar, R. (2009) Development of novel α–chitin/nanobioactive glass ceramic composite scaffolds for tissue engineering applications. *Carbohydrate Polymers* **78**, 926–931.

Peterson, A., López, T., Islas, E. O. and González, R. D. (2007) Pore structures in an implantable sol–gel titania ceramic device used in controlled drug release applications: A modeling study. *Appl Surf Sci* **253**, 5767–5771.

Petite, H., Viateau, V. Bensaid, W., Meunier, A., de Pollak, C., Bourguignon, M., Oudina, K., Sedel, L. and Guillemin, G. (2000) Tissue–engineered bone regeneration. *Nat Biotechnol* **18**, 959–963.

Pingali, K. C., Rockstraw, D. A. and Deng, S. (2005) Silver Nanoparticles from Ultrasonic Spray Pyrolysis of Aqueous Silver Nitrate. *Aerosol Science and Technology* **39**, 1010–1014.

Ponce, A. G., Fritz, R., Del Valle, C. E. and Roura, S. I. (2003) Antimicrobial activity of essential oils on the native microflora of organic Swiss chard. *Lebensm Wiss Technol* **36**, 679–684.

Porter, J. R., Ruckh, T. T. and Popat, K. C. (2009) Bone Tissue Engineering: A Review in Bone Biomimetics and Drug Delivery Strategies. *Biotechnol Prog* **25**, 1539–1560.

Price, N., Bendall, S. P., Frondoza, C., Jinnah, R. H. and Hungerford, D. S. (1997) Human osteoblast–like cells (MG63) proliferate on a bioactive glass surface. *Journal of Biomedical Materials Research* **37**, 394–400.

Pushpakanth, S., Srinivasan, B., Sreedhar, B. and Sastry, T. P. (2008) An in situ approach to prepare nanorods of titania–hydroxyapatite (TiO_2–HAp) nanocomposite by microwave hydrothermal technique. *Materials Chemistry and Physics* **107**, 492–498.

Raffa, R. B., Lannuzo, J. R., Levine, D. R., Saeid, K. K., Schwartz, R. C., Sucic, N. T., Terleckyj, O. D. and Young, J. M. (2005) Bacterial communication ("Quorum sensing") via ligands and receptors: a novel pharmacological target for the design of antibiotic drugs. *J Pharmacol Exp Ther* **312**, 417–423.

Rai, B., Teoh, S. H., Hutmacher, D. W., Cao, T. and Ho, K. H. (2005) Novel PCL–based honeycomb scaffolds as drug delivery systems for rhBMP–2. *Biomaterials* **26**, 3739–3748.

Rambo, C. R., Junkes, J., Sieber, H. and Hotza, D. (2006) Biomorphic Ceramics as Porous Supports for Zeolite Coating. *Advances in Science and Technology* **45**, 819–828.

Ramesh, S. (2013) Sol–gel Synthesis, Structural and Characterization of $Ag_{3(2+x)}Gd_xTi_{4-x}O_{11+\delta}$ Nanocomposites. *Journal of Chemical Science and Technology* **2**, 1–4.

Rao, K. J., Vaidhyanathan, B., Ganguli, M. and Ramakrishnan, P. A. (1999) Synthesis of Inorganic Solids Using Microwaves. *Chem Mater* **11**, 882–895.

Rasch, M., Andersen, J. B., Nielsen, K. F., Flodgaard, L. R., Christensen, H., Givskov, M. and Gram, L. (2005) Involvement of bacterial quorum–sensing signals in spoilage of bean sprouts. *Appl Environ Microb* **71**, 3321–3330.

Rasmussen, T. B. and Givskov, M. (2006) Quorum sensing inhibitors: a bargain of effects. *Microbiology* **152**, 895–904.

Reddy, M. P., Venugopal, A. and Subrahmanyam, M. (2007) Hydroxyapatite–supported Ag–TiO_2 as *Escherichia coli* disinfection photocatalyst. *Water Res* **41**, 379–386.

Reidy, B., Haase, A., Luch, A., Dawson, K. A. and Lynch, I. (2013) Mechanisms of Silver Nanoparticle Release, Transformation and Toxicity: A Critical Review of Current Knowledge and Recommendations for Future Studies and Applications. *Materials* **6**, 2295–2350.

Rincon, J. C., Xiao, Y., Young, W. G. and Bartold, P. M. (2005) Enhanced proliferation, attachment and osteopontin expression by porcine periodontal cells exposed to Emdogain. *Arch Oral Biol* **50**, 1047–5104.

Rodriguez, J. A., Liu, G., Jirsak, T., Hrbek, J., Chang, Z., Dvorak, J. and Maiti, A. (2002) Activation of gold on titania: adsorption and reaction of SO(2) on Au/TiO(2)(110). *J Am Chem Soc* **124**, 5242–5250.

Roman, J., Padilla, S., and Vallet–Regí, M. (2003) Sol–Gel Glasses as Precursors of Bioactive Glass Ceramics. *Chemistry of Materials* **15**, 798–806.

Rose, F. R. and Oreffo, R. O. (2002) Bone tissue engineering: hope vs hype. *Biochem Biophys Res Commun* **292**, 1–7.

Ruan, C., Paulose, M., Varghese, O. K., Mor, G. K. and Grimes, C. A. (2005) Fabrication of highly ordered TiO_2 nanotube arrays using an organic electrolyt. *J Phys Chem B* **109**, 15754–15759.

Sabetrasekh, R., Tiainen, H., Lyngstadaas, S. P., Reseland, J. and Haugen, H. (2011) A novel ultraporous titanium dioxide ceramic with excellent biocompatibility. *J Biomater Appl* **25**, 559–580.

Sabetrasekh, R., Tiainen, H., Reseland, J. E., Will, J., Ellingsen, J. E., Lyngstadaas, S. P. and Haugen, H. J. (2010) Impact of trace elements on biocompatibility of titanium scaffolds. *Biomed Mater* **5**, 15003.

Sadovskaya, I., Vinogradov, E., Li, J., Hachani, A., Kowalska, K. and Filloux, A. (2010) High–level antibiotic resistance in *Pseudomonas aeruginosa* biofilm: the ndvB gene is involved in the production of highly glycerol–phosphorylated beta–(1–>3)–glucans, which bind aminoglycosides. *Glycobiology* **20**, 895–904.

Sambhy, V., MacBride, M. M., Peterson, B. R. and Sen, A. (2006) Silverbromide nanoparticle/polymer composites: Dual action tunable antimicrobial materials. *J Am Chem Soc* **128**, 9798–9808.

Sambrook, J. and Russell, D. (2001) Molecular cloning: A laboratory manual, Cold Spring Harbor Laboratory Press, Cold Spring Harbor, New York.

Samuel, U. and Guggenbichler, J. P. (2004) Prevention of Catheter– Related Infections: The Potential of a New Nano–Silver Impregnated Catheter. *Int J Antimicrob Ag* **23**, S75–S78.

Sartori, T., Murakami, F. S, Cruz, A. P. and Campos, A. M. (2008) Development and Validation of a Fast RP–HPLC Method for Determination of Methotrexate Entrapment Efficiency in Polymeric Nanocapsules. *J Chromatogr Sci* **46**, 505–509.

Sauer, K., Camper, A. K., Ehrlich, G. D., Costerton, J. W. and Davies, D. G. (2002) *Pseudomonas aeruginosa* displays multiple phenotypes during development as a Biofilm. *J Bacteriol* **184**, 1140–1154.

Sauvage, F., Di Fonzo, F., Li Bassi, A., Casari, C. S., Russo, V., Divitini, G., Ducati, C., Bottani, C. E., Comte, P. and Graetzel, M. (2010) Hierarchical TiO_2 Photoanode for Dye–Sensitized Solar Cells. *Nano Letters* **10**, 2562–2567.

Sawant, S. N., Selvaraj, V., Prabhawathi, V. and Doble, M. (2013) Antibiofilm Properties of Silver and Gold Incorporated PU, PCLm, PC and PMMA Nanocomposites under Two Shear Conditions. *PLoS ONE* **8**, e63311.

Scepanovic, M., Dohcevic–Mitrovic, Z. D., Hinic, I., Grujic–Brojcin, M., Stanisic, G. and Popovic, Z. V. (2005) Photoluminescence of Laser–Synthesized Anatase Titanium Dioxide Nanopowders. *Mater Sci Forum* **494**, 265–270.

Scherrer, P. (1918) Bestimmung der Grösse und der Inneren Struktur von Kolloidteilchen Mittels Röntgenstrahlen, Nachrichten von der Gesellschaft der Wissenschaften, Göttingen. *Mathematisch–Physikalische Klasse* **2**, 98–100.

Seltenrich, N. (2013) Nanosilver: weighing the risks and benefits. *Environ Health Perspect* **121**, A220–A225.

Senjen, R. and Illuminato, I. (2009) Nano and biocidal silver: extreme germ killers present a growing threat to public health. Friends of the Earth, Australia.

Seo, D. H. (2009) Methotrexate–incorporated polymeric nanoparticles of methoxypoly (ethyleneglycol) – grafted chitosan. *Colloids Surf B* **69**, 157–163.

Shahverdi, A. R., Fakhimi, A., Shahverdi, H. R. and Minaian, S. (2007) Synthesis and effect of silver nanoparticles on the antibacterial activity of different antibiotics against *Staphylococcus aureus* and *Escherichia coli*. *Nanomedicine* **3**, 168–171.

Shankar, K., Paulose, M., Mor, G. K., Varghese, O. K. and Grimes, C. A. (2005) A study on the spectral photoresponse and photoelectrochemical properties of flame–annealed titania nanotube–arrays. *J Phys D* **38**, 3543–3549.

Shrivastava, S., Bera, T., Roy, A., Singh, G., Ramachandrarao, P. and Dash, D. (2007) Characterization of enhanced antibacterial effects of novel silver nanoparticles. *Nanotechnology* **18**, 225103.

Siepmann, F., Siepmann, J., Walther, M., MacRae, R. J. and Bodmeier, R. (2008) Polymer blends for controlled elease coatings. *J Control Release* **125**, 1–15.

Silver, S. and Phung, L. T. (1996) Bacterial heavy metal resistance: New surprises. *Annu Rev Microbiol* **50**, 753–789.

Silvestre, C., Duraccio, D. and Cimmino, S. (2011) Food packaging based on polymer nanomaterials. *Prog Polym Sci* **36**, 1766–1782.

Silvestry–Rodriguez, N., Bright, K. R., Slack, D. C., Uhlmann, D. R. and Gerba, C. P. (2008) Silver as a Residual Disinfectant to Prevent Biofilm Formation in Water Distribution Systems. *Appl Environ Microbiol* **74**, 1639–1641.

Simon, G. C., Khatri, C. A., Wight, S. A. and Wang, F. W. (2002) Preliminary report on the biocompatibility of a moldable, resorbable, composite bone graft consisting of calcium phosphate cement and poly (lactide–co–glycolide) microspheres. *J Orthop Res* **20**, 473–482.

Sing, K. S. W., Everett, D. H., Haul, R. A. W., Moscou, L., Pierotti, R. A., Rouquerol. J. and Siemieniewska, T. (1985) Reporting physisorption data for gas/solid systems with special reference to the determination of surface area and porosity. *Pure Appl Chem* **57**, 603–619.

Skandamis, P. N. and Nychas, G. J. (2012) Quorum sensing in the context of food microbiology. *Appl Environ Microb* **78**, 5473–5482.

Skrabalak, S. E. and Suslick, K. S. (2005) Porous MoS2 Synthesized by Ultrasonic Spray Pyrolysis. *Journal of the American Chemical Society* **127**, 9990–9991.

Smith, A. W. (2005) Biofilms and antibiotic therapy: is there a role for combating bacterial resistance by the use of novel drug delivery systems? *Adv Drug Deliv Rev* **57**, 1539–1550.

Smith, I. and Carson, B. (1977) Silver. In: Trace metals in the environment, Ann Arbor Science Publishers, Michigan.

Sokmen, M., Candan, F. and Sumer, Z. (2001) Disinfection of *E. coli* by the Ag–TiO_2/UV system: lipidperoxidation. *J Photochem Photobiol A* **143**, 241–244.

Sondi, I. and Salopek–Sondi, B. (2004) Silver nanoparticles as antimicrobial agent: a case study on *E. coli* as a model for Gram–negative bacteria. *J Colloid Interface Sci* **275**, 177–182.

Song, H. Y., Ko, K. K., Oh, L. H. and Lee, B. T. (2006) Fabrication of Silver Nanoparticles and Their Antimicrobial Mechanisms. *European Cell and Materials journal* **11**, 58.

Sotiriou, G. A. and Sotiris, E. Pratsinis **(**2010) Antibacterial Activity of Nanosilver Ions and Particles. *Environmental Science & Technology* **44**, 5649–5654.

Soundrapandian, C., Sa, B. and Datta, S. (2009) Organic–Inorganic Composites for Bone Drug Delivery. *AAPS PharmSciTech* **10**, 1158–1171.

Speshock, J. L., Murdock, R. C., Braydich–Stolle, L. K., Schrand, A. M. and Hussain, S. M. (2010) Interaction of silver nanoparticles with Tacaribe virus. *Journal of Nanobiotechnology* **8**, 19.

Spitzer, R., Perka, C., Lindenhayn, K. and Zippel, H. (2002) Matrix engineering for osteogenic differentiation of rabbit periosteal cells using alpha–tricalcium phosphate particles in a three–dimensional fibrin culture. *J Biomed Mater Res* **59**, 690–696.

Srinivasan, S., Jayasree, R., Chennazhi, K. P., Nair, S. V. and Jayakumar, R. (2012) Biocompatible alginate/nano bioactive glass ceramic composite scaffolds for periodontal tissue regeneration. *Carbohydrate Polymers* **87**, 274–283.

Stathatos, E., Petrova, T. and Lianos, P. (2001) Study of the efficiency of visible–light photocatalytic degradation of basic blue adsorbed on pure and doped mesoporous titania films. *Langmuir* **17**, 5025–5030.

Stepanov, A. L., Hole, D. E. and Townsend, P. D. (2000) Excimer laser annealing of glasses containing implanted metal nanoparticles. *Nuclear Instruments and Methods in Physics Research B* **167**, 882–886.

Stobie, N., Duffy, B., McCormack, D. E., Colreavy, J., Hidalgo, M., McHale, P. and Hinder, S. J. (2008) Prevention of *Staphylococcus epidermidis* biofilm formation using a low–temperature processed silver–doped phenyltriethoxysilane sol–gel coating. *Biomaterials* **29**, 963–969.

Su, H. L., Chou, C. C., Hung, D. J., Lin, S. H., Pao, I. C., Lin, J. H., Huang, F. L., Dong, R. X. and Lin, J. J. (2009a) The disruption of bacterial membrane integrity through ROS generation induced by nanohybrids of silver and clay. *Biomaterials* **30**, 5979–5987.

Su, W., Wei, S. S., Hu, S. Q. and Tang, J. X. (2009b) Preparation of TiO_2/Ag colloids with ultraviolet resistance and antibacterial property using short chain polyethylene glycol. *J Hazard Mater* **172**, 716–720.

Subramanian, V., Chen, C.L., Chou, H.S. and Fey, G.T.K. (2001) Microwave–assisted solid state synthesis of $LiCoO_2$ and its electrochemical properties as a cathode material for lithium batteries. *J Mater Chem* **11**, 3348–3353.

Sugimoto, T., Zhou, X. and Muramatsu, A. (2003) Synthesis of uniform anatase TiO_2 nanoparticles by gel–sol method: 3. Formation process and size control. *J Colloid Interface Sci* **259**, 43–52.

Sun, R. W., Chen, R., Chung, N. P., Ho, C. M., Lin, C. L. and Che, C. M. (2005) Silver nanoparticles fabricated in Hepes buffer exhibit cytoprotective activities toward HIV–1 infected cells. *Chem Commun (Camb)* **28**, 5059–5061.

Szabo, D. V., Vollath, D. and Arnold, W. (2001) Microwave Plasma Synthesis of Nanoparticles–Application of Microwaves to produce New Materials. *Ceram Trans* **111**, 217–224.

Tan, S. X., Tan, S. Z., Chen, J. X., Liu, Y. L. and Yuan, D. S. (2009) Preparation and properties of antibacterial TiO_2@C/Ag core–shell composite. *Sci Technol Adv Mater* **10**, 045002.

Tang, J., Durrant, J. R. and Klug, D. R. (2008) Mechanism of Photocatalytic Water Splitting in TiO_2. Reaction of Water with Photoholes, Importance of Charge Carrier Dynamics, and Evidence for Four–Hole Chemistry. *Journal of the American Chemical Society* **130**, 13885–13891.

Tang, J., Redl, F., Zhu, Y., Siegrist, T., Brus, L. E. and Steigerwald, M. L. (2005) An organometallic synthesis of TiO_2 nanoparticles. *Nano Lett* **5**, 543–548.

Thannickal, V. J. and Fanburg, B. L. (2000) Reactive oxygen species in cell signaling. *Am J Physiol Lung Cell Mol Physiol* **279**, L1005–L1028.

Tiainen, H., Lyngstadaas, S. P., Ellingsen, J. E. and Haugen, H. J. (2010) Ultra–porous titanium oxide scaffold with high compressive strength. J Mater Sci Mater Med **21**, 2783–2792.

Tiainen, H., Wohlfahrt, J. C., Verket, A., Lyngstadaas, S. P. and Haugen, H. J. (2012) Bone formation in TiO_2 bone scaffolds in extraction sockets of minipigs. *Acta Biomater* **8**, 2384–2391.

Trentler, T. J., Denler, T. E., Bertone, J. F., Agrawal, A., and Colvin, V. L. (1999) Synthesis of TiO_2 Nanocrystals by Nonhydrolytic Solution–Based Reactions. *Journal of the American Chemical Society* **121**, 1613–1614.

Trudeau, M. L. and Ying, J. Y. (1996) Nanocrystalline materials in catalysis and electrocatalysis: Structure tailoring and surface reactivity. *Nanostructured Materials* **7**, 245–258.

Tsukimura, N., Kojima, N., Kubo, K., Att, W., Takeuchi, K., Kameyama, Y. (2008) The effect of superficial chemistry of titanium on osteoblastic function. *J Biomed Mater Res Part A* **84**, 108–116.

Uchida, M., Kim, H. M., Kokubo, T., Fujibayashi, S. and Nakamura, T. (2003) Structural dependence of apatite formation on titania gels in a simulated body fluid. *J Biomed Mater Res Part A* **64**, 164–170.

Uchida, S., Tomiha, M., Masaki, N., Miyazawa, A. and Takizawa, H. (2004) Preparation of TiO_2 nanocrystalline electrode for dye–sensitized solar cells by 28 GHz microwave irradiation. *Sol Energy Mater Sol Cells* **81**, 135–139.

Uhlmann, D. R. and Gerba, C. P. (2008) Silver as a Residual Disinfectant to Prevent Biofilm Formation in Water Distribution Systems. *Applied and Environmental Microbiology* **74**, 1639–1641.

Uskokovic, V. (2007) Nanotechnologies: What we do not know. *Technology in Society* **29**, 43–61.

Vaidyanathan, R., Kalishwaralal, K., Gopalram, S. and Gurunathan, S. (2009) Nanosilver–the burgeoning therapeutic molecule and its green synthesis. *Biotechnol Adv* **27**, 924–937.

Valappil, S. P., Pickup, D. M., Carroll, D. L., Hope, C. K., Pratten, J., Newport, R. J., Smith, M. E., Wilson, M. and Knowles, J. C. (2007) Effect of silver content on the structure and antibacterial activity of silver–doped phosphate–based glasses. *Antimicrob Agents Chemother* **51**, 4453–4461.

Valden, M., Lai, X. and Goodman, D. W. (1998) Onset of catalytic activity of gold clusters on titania with the appearance of nonmetallic properties. *Science* **281**, 1647–50.

Varghese, O. K., Paulose, M., Shankar, K., Mor, G. K. and Grimes, C. A. (2008) Water–photolysis properties of micron–length highly–ordered titania nanotube–arrays. *J Nanosci Nanotechnol* **5**, 1158–1165.

Vioux, A. (1997) Nonhydrolytic Sol–Gel Routes to Oxides. *Chemistry of Materials* **9**, 2292–2299.

Wagh (nee Jagtap), M. S., Patil, R. H., Thombre, D. K., Kulkarni, M. V., Gade, W. N. and Kale, B. B. (2013) Evaluation of anti–quorum sensing activity of silver nanowires. *Appl Microbiol Biotechnol* **97**, 3593–601.

Wagner, V., Dullaart, A., Bock, A. K. and Zweck, A. (2006) The emerging nanomedicine landscape. *Nature Biotechnology* **24**, 1211–1217.

Wang, H., Burgess, R. M., Cantwell, M. G., Portis, L. M., Perron, M. M., Wu, F. and Ho, K. T. (2014) Stability and aggregation of silver and titanium dioxide nanoparticles in seawater: role of salinity and dissolved organic carbon. *Environ Toxicol Chem* **33**, 1023–1029.

Wang, L., Shelton, R. M., Cooper, P. R., Lawson, M., Triffitt, J. T. and Barralet, J. E. (2003) Evaluation of sodium alginate for bone marrow cell tissue engineering. *Biomaterials* **24**, 3475–3481.

Wang, M., Joseph, R. and Bonfield, W. (1998a) Hydroxyapatite–polyethylene composites for bone substitution: effects of ceramic particle size and morphology. *Biomaterials* **19**, 2357–2366.

Wang, X. H., Li, J. G., Kamiyama, H., Katada, M., Ohashi, N., Moriyoshi, Y. and Ishigaki, T. (2005a) Pyrogenic iron (III)–doped TiO_2 nanopowders synthesized in RF thermal plasma: phase formation, defect structure, band gap, and magnetic properties. *J Am Chem Soc* **127**, 10982–10990.

Wang, X., Zhuang, J., Peng, Q. and Li, Y. D. (2005b) A general strategy for nanocrystal synthesis. *Nature* **437**, 121–124.

Wang, Y. L., Wan, Y. Z., Dong, X. H., Cheng, G. X., Tao, H. M. and Wen, T. Y. (1998b) Preparation and characterization of antibacterial viscose–based activated carbon fiber supporting silver. *Carbon* **36**, 1567–1571.

Wang, Z. Y., Zhang, Q. Z., Konno, M. and Saito, S. (1993) Sol–gel transition of algi–nate solution by the addition of various divalent cations: 13C–NMR spectroscopic study. *Biopolymers* **33**, 703–711.

Wang, Z., Li, J., Zhao, J. and Xing, B. (2011) Toxicity and Internalization of CuO Nanoparticles to Prokaryotic Alga Microcystis aeruginosa as Affected by Dissolved Organic Matter. *Environ Sci Technol* **45**, 6032–6040.

Wen, B., Liu, C. and Liu, Y. (2005a) Solvothermal synthesis of ultralong single–crystalline TiO_2 nanowires. *New J Chem* **29**, 969–971.

Wen, B., Liu, C. and Liu, Y. (2005b) Depositional Characteristics of Metal Coating on Single–Crystal TiO_2 Nanowires. *J Phys Chem B* **109**, 12372–12375.

Whitchurch, C. B., Tolker–Nielsen, T., Ragas, P. C. and Mattick, J. S. (2002) Extracellular DNA required for bacterial biofilm formation. *Science* **295**, 1487.

Wijnhoven, S. W. P., Peijnenburg, W. J. G. M., Herberts, C. A., Hagens, W. I., Oomen, A. G., Heugens, E. H. W., Roszek, B., Bisschops, J., Gosens, I., Van De Meent, D., Dekkers, S., De Jong, W. H., van Zijverden, M., Sips, A. J. A. M. and Geertsma, R. E. (2009) Nano–silver – A review of available data and knowledge gaps in human and environmental risk assessment. *Nanotoxicology* **3**, 109–138.

Williams, D. F. (1999) Bone Engineering Em squared, Toronto.

Wolinsky, J. B., Colson, Y. L. and Grinstaff, M. W. (2012) Local drug delivery strategies for cancer treatment: gels, nanoparticles, polymeric films, rods, and wafers. *J Control Release* **159**, 14–26.

Wong, K. K. Y. and Liu, X. (2010) Silver nanoparticles–the real ''silver bullet'' in clinical medicine? *Med Chem Commun* **1**, 125–131.

World Health Organization (WHO). (2002) Silver and silver compounds: Environmental aspects. *Concise international chemical assessment document* **44**.

Wright, J. B., Lam, K., Hansen, D. and Burrell, R. E. (1999) Efficacy of topical silver against fungal burn wound pathogens. *Am J Infect Control* **27**, 344–350.

Wu, J. M. and Zhang, T. W. (2004) Photodegradation of rhodamine B in water assisted by titania films prepared through a novel procedure. *J Photochem Photobiol A* **162**, 171–177.

Wu, J. M., Hayakawa, S., Tsuru, K. and Osaka, A. (2002) Nanocrystalline Titania Made from Interactions of Ti with Hydrogen Peroxide Solutions Containing Tantalum Chloride. *Cryst Growth Des* **2**, 147–149.

Wu, J. M., Shih, H. C. and Wu, W. T. (2005b) Electron field emission from single crystalline TiO_2 nanowires prepared by thermal evaporation. *Chem Phys Lett* **413**, 490–494.

Wu, J. M., Shih, H. C., Wu, W. T., Tseng, Y. K. and Chen, I. C. (2005c) Thermal evaporation growth and the luminescence property of TiO_2 nanowires. *J Cryst Growth* **281**, 384–390.

Wu, J. M., Zhang, T. W., Zeng, Y. W., Hayakawa, S., Tsuru, K. and Osaka, A. (2005a) Large–scale preparation of ordered titania nanorods with enhanced photocatalytic activity. *Langmuir* **21**, 6995–7002.

Wu, K. C. W., Yamauchi, Y., Hong, C. Y., Yang, Y. H., Liang, Y. H., Funatsud, T. and Tsunodad, M. (2011) Biocompatible, surface functionalized mesoporous titania nanoparticles for intracellular imaging and anticancer drug delivery. *Chem Commun* **47**, 5232–5234.

Wzorek, Z. and Konopka, M. (2007) Nanosilver–a new bactericidal agent. *Czasopismo Techniczne Chemia* **104**, 175–181.

Xiang, B., Zhang, Y., Wang, Z., Luo, X. H., Zhu, Y. W., Zhang, H. Z. and Yu, D. P. (2005) Field–emission properties of TiO_2 nanowire arrays. *J Phys D* **38**, 1152–1155.

Xiu, Z. M., Ma, J. and Alvarez, P. J. J. (2011) Differential Effect of Common Ligands and Molecular Oxygen on Antimicrobial Activity of Silver Nanoparticles versus Silver Ions. *Environ Sci Technol* **45**, 9003–9008.

Xu, J., Ge, J. P. and Li, Y. D. (2006) Solvothermal synthesis of monodisperse PbSe nanocrystals. *J Phys Chem B* **110**, 2497–2501.

Yamanaka, S. A., Nishida, F., Ellerby, L. M., Nishida, C. R., Dunn, B., Valentine, J. S. and Zink, J. I. (1992) Enzymatic activity of glucose oxidase encapsulated in transparent glass by the sol–gel method. *Chemistry of Materials* **4**, 495–497.

Yang, J., Mei, S. and Ferreira, J. M. F. (2000) Hydrothermal Synthesis of Nanosized Titania Powders: Influence of Peptization and Peptizing Agents on the Crystalline Phases and Phase Transitions. *J Am Ceram Soc* **83**, 1361–1368.

Yang, J., Mei, S. and Ferreira, J. M. F. (2001a) Hydrothermal Synthesis of Nanosized Titania Powders: Influence of Tetraalkyl Ammonium Hydroxides on Particle Characteristics. *J Am Ceram Soc* **84**, 1696–1702.

Yang, J., Mei, S. and Ferreira, J. M. F. (2002) Hydrothermal synthesis of well–dispersed TiO_2 nano–crystals. *J Mater Res* **17**, 2197–2200

Yang, J., Mei, S. and Ferreira, J. M. F. (2004a) Hydrothermal processing of nanocrystalline anatase films from tetraethylammonium hydroxide peptized titania sols. *J Eur Ceram Soc* **24**, 335–339

Yang, J., Mei, S. and Ferreira, J. M. F. (2004b) Hydrothermal Fabrication of Rod–like Rutile Nano–Particles. *Mater Sci Forum* **455–456**, 556–559.

Yang, S. W. and Gao, L. (2006) Fabrication and shape–evolution of nanostructured TiO_2 via a sol–solvothermal process based on benzene–water interfaces *Mater Chem Phys* **99**, 437–440.

Yang, S., Leong, K. F., Du, Z. and Chua, C. K. (2001b) The design of scaffolds for use in tissue engineering. Part I. Traditional factors. *Tissue Eng* **7**, 679–689.

Yaszemski, M. J., Oldham, J. B., Lu, L. and Currier, B. L. (1994) Bone Engineering Em squared, Toronto.

Yu, B., Leung, K. M., Guo, Q., Lau, W. M. and Yang, J. (2011) Synthesis of Ag–TiO_2 composite nano thin film for antimicrobial application. *Nanotechnology* **22**, 115603.

Zaban, A., Aruna, S. T., Tirosh, S., Gregg, B. A. and Mastai, Y. (2000) The effect of the preparation condition of TiO_2 colloids on their surface structures. *J Phys Chem B* **104**, 4130–4133.

Zettili, N. (2009) Quantum Mechanics Concepts and Applications. Wiley–Blackwell, John Wiley & Sons Ltd, United Kingdom.

Zhang Q., Sun, C., Zhao, Y., Zhou, S., Hu, X. and Chen, P. (2010) Low Ag–Doped Titanium Dioxide Nanosheet Films with Outstanding Antimicrobial Property. *Environmental Science & Technology* **44**, 8270–8275.

Zhang, H. and Banfield, J. F. (2005) Size–dependence of the kinetic rate constant for phase transformation in TiO_2 nanoparticles. *Chem Mater* **17**, 3421–3425.

Zhang, H. and Chen, G. (2009) Potent antibacterial activities of Ag/TiO_2 nanocomposite powders synthesized by a one–pot sol–gel method. *Environ Sci Technol* **43**, 2905–2910.

Zhang, H., Wang, C., Chen, B. and Wang, X. (2012) Daunorubicin–TiO_2 nanocomposites as a “smart” pH–responsive drug delivery system. *International Journal of Nanomedicine* **7**, 235–242.

Zhang, L., Jiang, Y., Ding, Y., Povey, M. and York, D. (2007) Investigation into the antibacterial behaviour of suspensions of ZnO nanoparticles (ZnO nanofluids). *J Nanopart Res* **9**, 479–489.

Zhang, L., Yu, J. C., Yip, H. Y., Li, Q., Kwong, K. W., Xu, A. W. and Wong, P. K. (2003) Ambient Light Reduction Strategy to Synthesize Silver Nanoparticles and Silver–Coated TiO_2 with Enhanced Photocatalytic and Bactericidal Activities. *Langmuir* **19**, 10372–10380.

Zhang, Q. and Gao, L. (2003) Preparation of Oxide Nanocrystals with Tunable Morphologies by the Moderate Hydrothermal Method: Insights from Rutile TiO_2. *Langmuir* **19**, 967–971.

Zhao, X., Liu, X. and Ding, C. (2005) Acid–induced bioactive titania surface. *J Biomed Mater Res A* **75**, 888–894.

Zhou, J., Zhang, Y., Zhao, X. S. and Ray, A. K. (2006) Photodegradation of benzoic acid over metal–doped TiO_2. *Ind Eng Chem Res* **45**, 3503–3511.

Appendix I

1) Calibration curve for silver ion detection using a rhodamine–based fluorogenic and chromogenic probe

Calibration curve for silver ion detection was prepared using known concentrations of $AgNO_3$ (Chatterjee *et al.* 2009). The correlation coefficient for calibration curve was 0.9709.

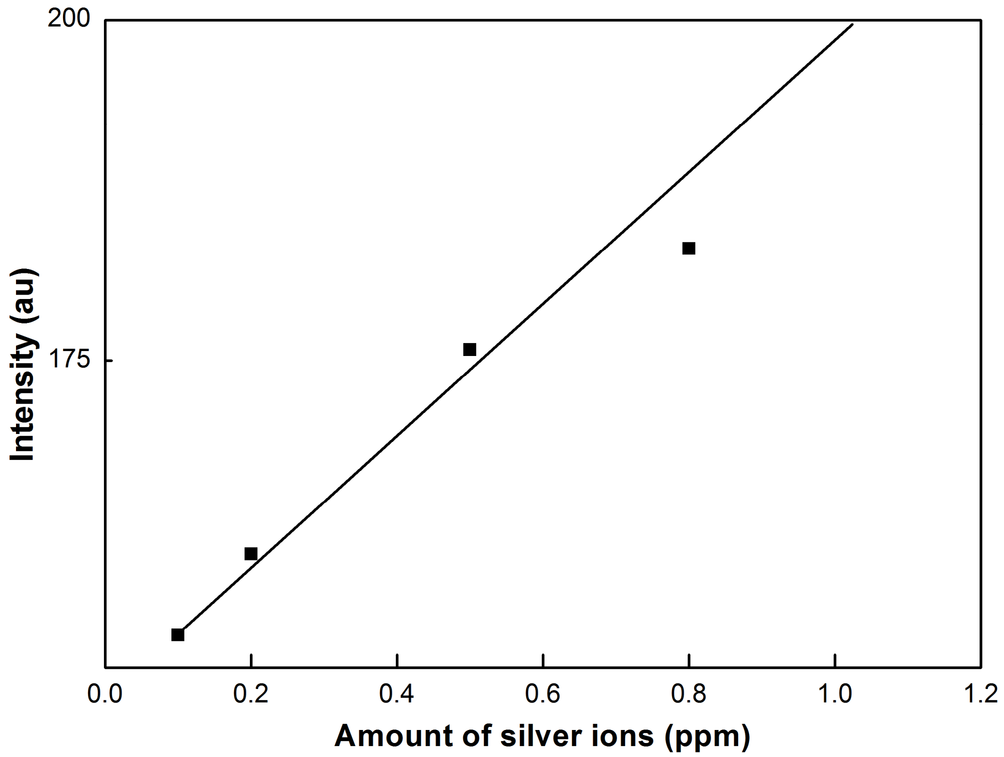

Figure A1. Calibration curve for silver ion detection using a rhodamine–based fluorogenic and chromogenic probe.

2) Calibration curve of methotrexate for total drug determination

The standard solutions were made in 0.1 mol/L hydrochloric acid and absorbance was recorded at 305 nm (Jaroslaw Ciekot *et al.* 2012; Cristina Magalhaes Santos *et al.* 2013). The correlation coefficient for calibration curve of total drug determination was 0.9974.

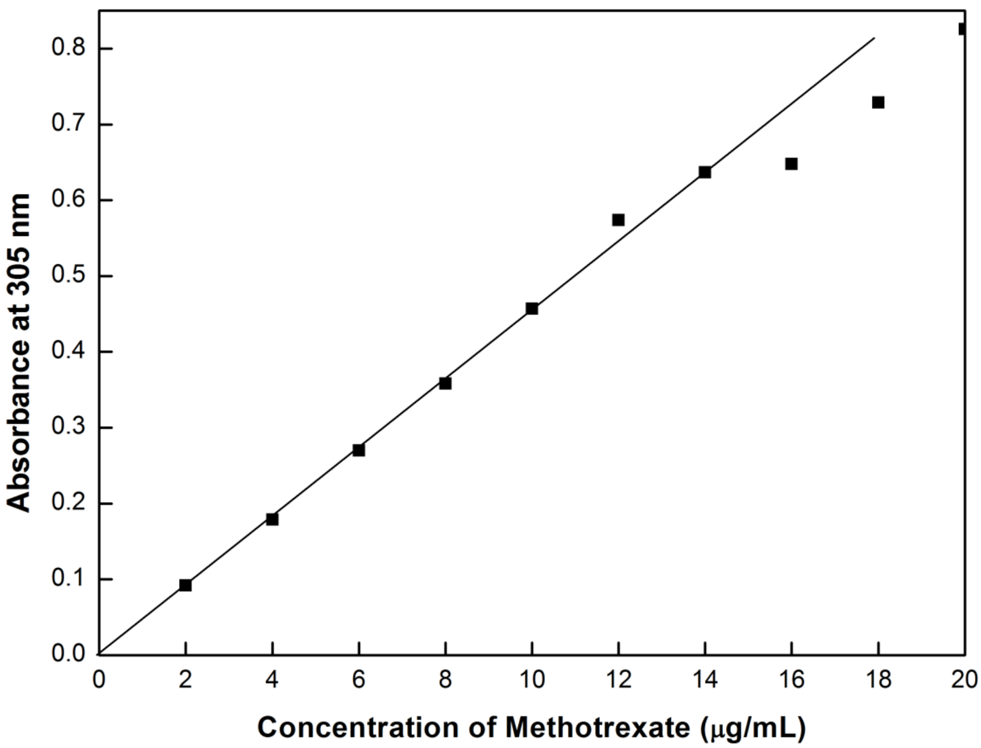

Figure A2. Calibration curve of methotrexate for total drug determination.

3) Calibration curve of methotrexate for free drug determination

The standard solutions were made in PBS (pH 7.4) and absorbance was recorded at 303 nm (Jaroslaw Ciekot *et al.* 2012; Cristina Magalhaes Santos *et al.* 2013). The correlation coefficient for calibration curve of free drug determination was 0.9999.

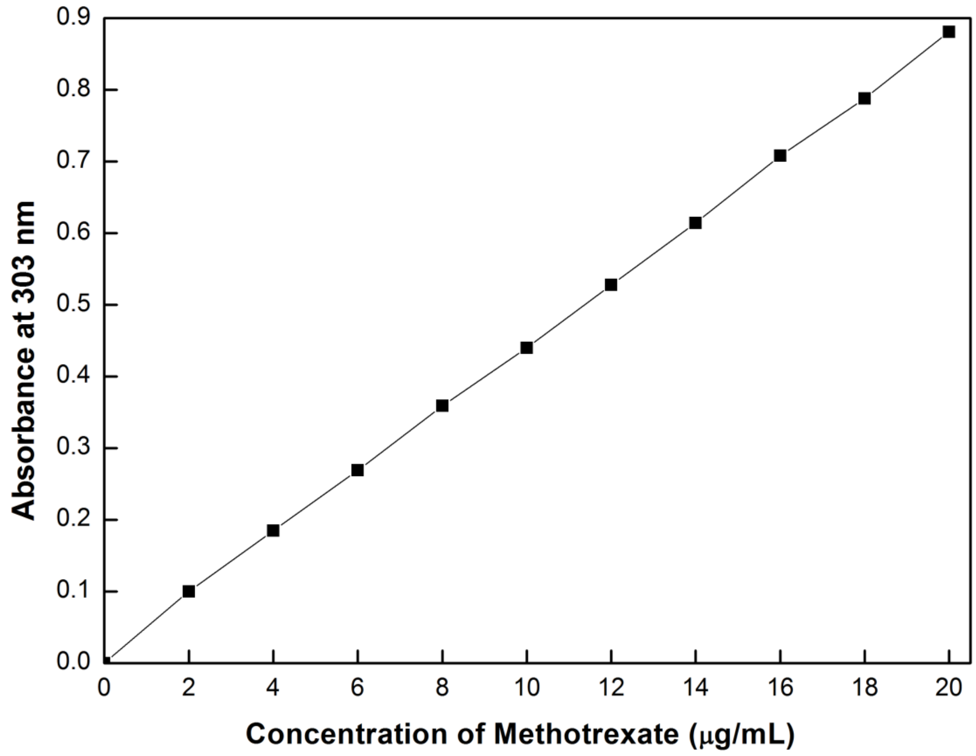

Figure A3. Calibration curve of methotrexate for free drug determination.

List of Publications

1) **Naik, K.** and Kowshik, M. Anti–quorum sensing activity of AgCl–TiO_2 nanoparticles with potential use as active food packaging material. J. Appl. Microbiol. (2014) 117:972–983. **(Impact factor 2.386)**

2) **Naik, K.** and Kowshik, M. Anti–biofilm efficacy of low temperature processed AgCl–TiO_2 nanocomposite coating. Mater. Sci. Eng. C (2014) 34:62–68. **(Impact factor 3.076)**

3) **Naik, K.**, Chatterjee, A., Prakash, H. and Kowshik, M. Mesoporous TiO_2 nanoparticles containing Ag ion with excellent antimicrobial activity at remarkable low silver concentrations. J. Biomed. Nanotechnol. (2013) 9:664–673. **(Impact factor 7.578)**

4) Kowshik, M., Desai, V. and **Naik, K**. Functionalization of silver–titanium dioxide nanoparticles, a novel strategy for enhancement of antimicrobial activity. Proceedings of Green Nanotechnology (2012) 53–61.

5) **Naik, K.,** Srivastava, P., Deshmukh, K., Shaik, Md. M. and Kowshik, M. Nanomaterial–based approaches for prevention of biofilm–associated infections on medical devices and implants. J. Nanosci. Nanotechnol. **(Accepted for publication)**

6) **Naik, K.,** Chandran, G., Rajashekaran, R., Waigaonkar, S. and Kowshik, M. Mechanical properties, biological behaviour and drug release capability of nano TiO_2–Hap–Alginate composite scaffolds for potential applications as bone implant materials. **(Communicated for publication)**

List of Conferences

1) **Kshipra Naik** and Meenal Kowshik (2013) Silver embedded titanium dioxide nanoparticle films as efficient inhibitors of biofilm formation. Poster presented at Nanomedicine 2013, Barcelona, Spain, 11–12 April 2013**,** organized by Select Biosciences. This poster was given the **Best Poster Award sponsored by ePosters.net–The Online Journal of Scientific Posters.**

2) **Kshipra Naik** and Meenal Kowshik (2012) Mesoporous Ag–TiO_2 nanoparticles with excellent antimicrobial activity. Oral Presentation at UGC Sponsored National Seminar, Nanomaterials: Synthesis, Characterization and Applications during 2nd and 3rd February, 2012, organized by Department of Chemistry, Smt. Parvatibai Chowgule College of Arts and Science, Margao–Goa.

3) **Kshipra Naik** and Meenal Kowshik (2012) Anti–Biofilm Efficacy of Ag–TiO_2 Nanoparticles. Poster presented at International Conference on Nanoscience and Technology (ICONSAT–2012) held in Hyderabad, India during 20–23 January, 2012.

4) **Kshipra Naik** and Meenal Kowshik (2011) Anti–Biofilm Efficacy of Ag–TiO_2 Nanoparticles against *E. coli*. Poster presented at 2nd International Conference on Advanced Nanomaterials and Nanotechnology (ICANN–2011), December 8–10, 2011, organized jointly by the Department of Physics and centre for Nanotechnology, Indian Institute of Technology Guwahati, India.

5) **Kshipra Naik,** Priyadarshini Parakh, Halan Prakash and Meenal Kowshik (2011) Low Ag Doped TiO_2 Nanoparticles with excellent Antimicrobial activity without the need of photoactivation. Poster presented at "Nanostech 2011–National Symposium on Nanoscience and Technology" held during 1–2 September 2011, organised by Nirmala College, Muvattupuzha, Ernakulam Dist., Kerala.

List of Workshops

1) European School on Nanoscience and Nanotechnologies (ESONN) training programme–Session 2014 held during 24th August–13th September, 2014 at Grenoble, France, organized by CEFIPRA in collaboration with Joseph Fourier University, Grenoble, France.

2) Monsoon international Workshop on Green Nanotechnology from 6th to 7th August, 2013, at Bogmallo Beach Resort Hotel, Goa, organized by Sam Higginbottom Institute of Agriculture, Technology and Sciences–Deemed University, Allahabad, India in partnership with University of Missouri, Columbia City, Missouri, USA.

3) American Society for Microbiology Virtual Workshop on Scientific Writing and Publishing on 9th August, 2012, at Birla Institute of Technology and Science Pilani K K Birla Goa Campus.

4) CEP course on Advanced Analytical Techniques from 26th to 29th March, 2012, at IIT Bombay.

5) National Workshop on Bioinformatics from 2nd to 4th April, 2010, at Birla Institute of Technology and Science Pilani K K Birla Goa Campus, Goa, organized by Supercomputing Facility for Bioinformatics and Computational Biology (SCFBIO), IIT Delhi in association with Symbionts, Department of Biological Sciences, BITS Pilani K K Birla Goa Campus.

Brief Biography of the Candidate

Ms. Naik Kshipra Sudhakar was born on 29th August 1985 in Pune, Maharashtra. She received her Bachelor's degree in Science in the field of Microbiology and Vocational Biotechnology from Pune University. She received her Master's degree in Science in Microbiology from Pune University in 2009. Successively, she cleared the CSIR National Eligibility Test (NET) securing 0228th rank, which is a national level entrance examination in India for postgraduate candidates to qualify for university level teaching jobs in India and/or admission to Ph.D. research programs. Subsequently, she joined Birla Institute of Technology and Science, Pilani K K Birla Goa Campus for pursuing Ph.D. in Nanobiotechnology. She was a recipient of CSIR fellowship from January 2010 to January 2015 (09/919(0008)/2010–EMR–1).

She was awarded travel grant by DST, India (Commitment letter no.: SR/ITS/00127/2013–2014), ICMR, India (Sanction no.: 3/2/TG–37/HRD–2013) and DBT, India (Proposal code: DBT/CTEP/02/201300084) for presenting a poster at Nanomedicine 2013, Barcelona, Spain, 11–12 April 2013. She won the Best Poster Presentation Award for her poster titled "Silver Embedded Titanium Dioxide Nanoparticle Films as Efficient Inhibitors of Biofilm Formation" She was a recipient of 2014 Cefipra–Esonn Fellowship for participation in the European School on Nanoscience and Nanotechnologies (ESONN) training programme in collaboration with Joseph Fourier University, Grenoble–Session 2014, held during August 24–September 13, 2014 at Grenoble, France. She has published three research papers in International Journals.

Brief Biography of the Supervisor

Prof. Meenal Kowshik received her M. Sc. in Microbiology from Goa University in 1997. She worked on the biological synthesis of metallic and metal sulfide nanoparticles using yeasts at Agarkar Research Institute, and obtained her Ph.D. degree from Pune University (1999–2003). Subsequently, she joined Birla Institute of Technology and Science, Pilani K K Birla Goa Campus, and is currently working as Associate Professor in the Department of Biological Sciences. Her research interests include studies on biofunctionalization of silver based nanocomposites for antimicrobial applications; synthesis of biocompatible nanomaterials for tissue engineering; application of nanomaterials in molecular biology research; interactions of nanomaterials and microorganisms with respect to nanomaterial synthesis as well as toxicity, with special emphasis on halophilic archaebacteria. She has received research grants from Department of Science and technology for two projects and from the Ministry of Earth Sciences. She has been a co–investigator on four other projects sanctioned by the agencies; Department of Biotechnology, DRDO and UGC. She has published 29 research papers in International and National journals of repute; has 3 patents to her credit and has delivered several invited talks at International and National conferences.